



Universitat Autònoma de Barcelona

ADVERTIMENT. L'accés als continguts d'aquesta tesi queda condicionat a l'acceptació de les condicions d'ús establertes per la següent llicència Creative Commons:  http://cat.creativecommons.org/?page_id=184

ADVERTENCIA. El acceso a los contenidos de esta tesis queda condicionado a la aceptación de las condiciones de uso establecidas por la siguiente licencia Creative Commons:  <http://es.creativecommons.org/blog/licencias/>

WARNING. The access to the contents of this doctoral thesis it is limited to the acceptance of the use conditions set by the following Creative Commons license:  <https://creativecommons.org/licenses/?lang=en>



**Universitat Autònoma
de Barcelona**

**ALGINATE AND SILK FIBROIN BASED TECHNOLOGIES
FOR BIOSENSING**

Augusto Márquez Maqueda

Doctoral Thesis

PhD in Chemistry

Supervised by:

Dr. Xavier Muñoz Berbel

Dr. Carlos Domínguez Horna

Tutored by:

Dr. Julián Alonso Chamorro

Departament de Química

Facultat de Ciències

2020

The present thesis, entitled “**Alginate and Silk Fibroin based Technologies for Biosensing**”, is submitted by Augusto Márquez Maqueda as a partial fulfilment of the requirements for the Doctor of Philosophy degree in Chemistry.

This thesis was carried out at the Institute of Microelectronics of Barcelona (IMB-CNM, CSIC), in the Group of Chemical Transducers (GTQ), under the supervision of Dr. Xavier Muñoz Berbel and Dr. Carlos Domínguez Horna.

This thesis was supported by the Spanish R & D National Program (MEC Project TEC2014-54449-C3-1-R) and by the MICINN for the award of a research studentship within the FPI program (BES-2015-072946).

With the approval of:

Dr. Xavier Muñoz Berbel
(Director)

Dr. Carlos Domínguez Horna
(Director)

Dr. Julián Alonso Chamorro
(Tutor)

Augusto Márquez Márquez
(Author)



CSIC
CONSEJO SUPERIOR DE INVESTIGACIONES CIENTÍFICAS



Agradecimientos

Son muchas las personas a las que he de agradecer el hecho de haber podido realizar esta tesis. Algunas contribuyeron a ello hace tanto tiempo que ni ellas, ni siquiera yo, nos acordamos ya. Es por ello que trataré de hacer un recorrido por los más recientes, sin desmerecer todos aquellos que me han enseñado durante mi vida.

En primer lugar, quiero agradecer a mis directores, Carlos Domínguez y Xavier Muñoz, por brindarme la oportunidad de pasar estos últimos cuatro años en el CNM y dotarme de todos los recursos necesarios, tanto materiales como intelectuales, para ir avanzando en el trabajo y poder compartirlo además en muchos congresos internacionales. Está de más decirlo, pero por supuesto que nada de lo que continúa en estas páginas hubiese sido posible sin vosotros.

He de agradecer también al Grupo de Transductores Químicos en su conjunto por su colaboración, por su contribución y por sus recomendaciones en los seminarios de grupo. En especial me gustaría agradecer a Juan Manuel Ríos, a Alfredo Cadarso y a Pablo Giménez por guiarme cuando comencé en el laboratorio. Por otro lado, también me gustaría agradecer a Tobias Ackermann el tiempo compartido estos años. Ha sido un referente constante durante mi tesis y de él he aprendido bastante más de lo que se pueda imaginar.

Me gustaría agradecer a Gonzalo Guirado su buena disposición para colaborar y las contribuciones científicas que han surgido de ello.

I also would like to thank Fiorenzo Omenetto for his kind reception at his Silklab in Tufts University and Moliria Dos Santos as well for the interesting collaboration we carried out together during those four months.

Le doy las gracias a todos mis compañeros, con los que he pasado momentos inolvidables tanto en el centro como fuera de él. Por suerte son

muchos, ellos lo saben, y no tiene sentido enumerarlos aquí. Habéis sido el apoyo fundamental durante todos estos años, así como yo también espero haber sido parte del vuestro. Algunos han marchado ya del CNM y, el día que me toque a mí, sé que lo haré con buenos amigos, con los que cuentas para siempre por muy lejos que estés.

Aunque hayan pasado más de seis años, me gustaría agradecer a Juan A. Anta la oportunidad que me dio para unirme a su grupo de investigación de *Nanostructured Solar Cells* en la Universidad Pablo de Olavide, donde comenzó toda mi andadura científica y donde pude realizar mi TFG y TFM.

A Thomas Berger. Creo que nunca podré agradecerte lo suficiente el tiempo que dedicaste a enseñarme casi todo lo que sé, desde el día en que entré por primera vez en el laboratorio de Juan hasta el día que me marché de Salzburgo. Este trabajo tiene mucho de ti.

Me gustaría dedicar este trabajo a mi familia y amigos. Cada vez que he pasado por Carmona, Sevilla, Zahara, Badajoz o a Madrid he encontrado ese cariño incondicional y ese respiro necesario.

Y gracias a ti Abril, por convencerme para venir, por escucharme y por consultarme, por ser mi apoyo y por sentir que soy el tuyo. Vendrán nuevos retos, y aquí estaremos.

Contents

List of Abbreviations, Units and Symbols	i
List of Tables and Figures	iv
Summary	viii
Resumen	xii
1. Motivation	1
2. Introduction	4
3. Fundamentals	25
4. Objectives	45
5. Materials and Methods	47
6. Results	69
6.1 Electrodepositable Alginate Membranes for Amperometric Glucose Biosensing	70
6.2. Alginate Membrane Integration in POC Device for Glucose and Lactate Determination.....	88
6.3. Silk-Fibroin Micro-Capillary Pads for Glucose Determination in Whole Blood	104
6.4. Silk Bio-Cladding Fiber Optics Biosensor for Glucose Detection in Whole Blood	118
6.5. Photo-Electro-Enzymatic Glucose Biosensor using dithienylethene derivatives as Reusable mediators	131
6.6. Light-Renewable Enzymatic Silk Biosensors Incorporating Diarylethene Mediators For Continuous Glucose Monitoring	143
7. General Discussion.....	155
8. Conclusions	161
9. Future Scope.....	163
10. Bibliography	168

List of Abbreviations, Units and Symbols

Abbreviations

ABTS	2,2'-azino-bis (3-ethylbenzothiazoline-6-sulfonic acid)
ATR	Attenuated total reflectance
CV	Cyclic voltammetry, Coefficient of variation
DET	Direct electron transfer
DNA	Deoxyribonucleic acid
DTE	1,2-bis (5-carboxy-2-methylthien-3-yl) cyclopentene
DTEc	Closed DTE
DTEo	Open DTE
e-beam	Electron beam
ELISA	Enzyme-linked immunosorbent assay
FBS	Fetal bovine serum
FOCS	Fiber optics chemical and biochemical sensors
FTIR	Fourier transformed infrared
GOx	Glucose oxidase
HRP	Horseradish peroxidase
IMB-CNM	Instituto de Microelectrónica de Barcelona – Centro Nacional de Microelectrónica
IUPAC	International Union of Pure and Applied Chemistry
LOC	Lab on chip
LOD	Limit of detection
LOx	Lactate oxidase
NP	Nanoparticle
PBS	Phosphate buffer saline
PDMS	Polydimethylsiloxane
PECVD	Plasma enhanced chemical vapour deposition
PMMA	Poly(methyl methacrylate)
POC	Point of Care

PSA	Pressure sensitive adhesive
RI	Refractive index
SEM	Scanning electron microscopy
SF	Silk Fibroin
SPGE	Screen-printed gold electrodes
T, A, R	Transmittance, Absorbance, Reflectance (Optics)
TMB	3,3',5,5'-Tetramethylbenzidine
UV	Ultraviolet
WE, CE, RE	Working, Counter and Reference electrode

Units

A	Ampere
Å	Angstrom
C	Coulomb
°C	Celsius degree
g	Gram
K	Kelvin degree
L	Litre
m	Metre
min	minutes
psi	Pound per square inch
s	Second
V	Volt
W	Watt

Symbols

c	Concentration (M)
E	Potential (V)
ϵ	Molar attenuation coefficient ($M^{-1} \text{ cm}^{-1}$)

F	Faraday constant (96485 C mol ⁻¹)
h	Plank's constant (6,62 kg m ² s ⁻¹)
i	Current intensity (A)
l	Length (m)
λ	Wavelength (nm)
m	Mass (g)
M	Molar (mol L ⁻¹)
n	Number of electrons, number of samples
Q	Electric charge (C)
R	Gas Constant (8,31 J K ⁻¹ mol ⁻¹)
t	Time (s)
T	Temperature (°C)

List of Tables and Figures

Table 1.1. Number of millions of people with diabetes worldwide	3
Figure 2.1. Typical scheme for biosensors classification	5
Figure 2.2. Summary of enzymatic glucose oxidation mechanisms	9
Table 2.1. List of biopolymers used in biosensing applications	15
Figure 2.3. Alginate molecular structure and electrodeposition process	17
Figure 2.4. Silk molecular structure and applications.....	20
Figure 2.5. Smartphone-based colorimetric biosensors.....	23
Figure 2.6. Smartphone-based electrochemical biosensors.....	24
Figure 3.1. Basic process for the oxidation of silicon	26
Figure 3.2. Photolithography steps	28
Figure 3.3. Electron beam physical vapour deposition scheme.....	29
Figure 3.4. Plasma enhanced chemical vapour deposition scheme.....	30
Figure 3.5. Sequential steps of a photolithography process followed by an etching or a lift-off step	31
Figure 3.6. SF patterning by casting	32
Figure 3.7. SF nanoimprinting processes	33
Figure 3.8. ArF excimer laser photolithography process to form high-resolution SF micropatterns	34
Figure 3.9. Scheme of SF e-beam lithography process	35
Figure 3.10. Open and closed forms of dithienylethene basic structure.....	36
Figure 3.11. Two and three electrodes electrochemical cells.....	40
Figure 3.12. Cyclic Voltammetry.....	41
Figure 3.13. Electromagnetic spectrum.....	42
Figure 3.14. Molecular electronic transitions from lower to higher energetic.....	43
Figure 5.1. Steps for microelectrodes fabrication from a silicon wafer.....	52
Figure 5.2. Three main parts of the electrodeposition setup.....	53
Figure 5.3. Ag and Cl electrodeposition on the Pt to fabricate a pseudo-reference Pt/Ag/AgCl electrode.....	54
Figure 5.4. PMMA structure for whole blood analysis.....	55

Figure 5.5. Gate for real sample addition.....	56
Figure 5.6. Picture of the potentiostat fabricated in collaboration with ICAS group of IMB-CNM.....	57
Figure 5.7. Cross section scheme of the biosensor for different steps of the alginate hydrogel electrodeposition.....	58
Figure 5.8. Instantaneous response of the biosensor to the addition of analytes....	60
Figure 5.9. Extraction process of SF from Bombyx mori cocoons.....	62
Figure 5.10. Schemes of the setup for SF films measurement and cartridge layers and assembly.....	64
Figure 5.11. Picture of optical fiber measurement setup.....	65
Figure 6.1.1. Aspect of alginate hydrogels applying different currents and electrodeposition times.....	74
Figure 6.1.2. Top and profile images of the biosensor comprising the transducer and the alginate electrodeposited film.....	75
Figure 6.1.3. Optimization of alginate thickness.....	75
Figure 6.1.4. Diffusion limitation by the hydrogel.....	76
Figure 6.1.5. $[\text{Fe}(\text{CN})_6]^{3-} / [\text{Fe}(\text{CN})_6]^{4-}$ diffusion in alginate hydrogel.....	77
Figure 6.1.6. Alginate stability in MES-NaOH and Imidazole-HCl buffers.....	78
Figure 6.1.7. Study of biofouling effect on the transducer by whole blood.....	79
Figure 6.1.8. Amperometric response dependence on enzyme concentration in gel.....	80
Figure 6.1.9. Cyclic voltammeteries of the biosensor in presence of glucose.....	81
Figure 6.1.10. Amperometric response of biosensors to glucose.....	82
Figure 6.1.11. Life-time enhancement for biosensors with trapped enzymes in the hydrogel.....	83
Figure 6.1.12. Electrode reusability in consecutive analysis.....	84
Figure 6.1.13. Interfering species effect in biosensor response.....	85
Figure 6.1.14. Biosensor response to different glucose concentrations in human plasma and human whole blood.....	86
Figure 6.2.1. Main parts of the smartphone-based POC device.....	93
Figure 6.2.2. Electrodeposition, detection and chamber cleaning protocol.....	94
Figure 6.2.3. Disaggregation of alginate membranes by PBS.....	94

Figure 6.2.4. Response of the biosensor to the addition of different concentrations of glucose or lactate in FBS.....	96
Figure 6.2.5. Cyclic detection with the same device alternating glucose and lactate.....	97
Figure 6.2.6. Cross-talk effect absence.....	98
Figure 6.2.7. Electrodeposition and measurement modes of the POC device and lactate and glucose calibration in spiked whole blood samples.....	100
Figure 6.2.8. Glucose and lactate monitoring in streptozotocin-induced diabetic mice	102
Figure 6.3.1. SF material characterization.....	108
Figure 6.3.2. Scheme of the resulted functionalized SF layer and enzymatic reaction for glucose determination.....	109
Figure 6.3.3. Colorimetric response of doped SF pads to glucose.....	110
Figure 6.3.4. ATR-IR and Raman spectra of SF and SF with ABTS before and after the reaction with glucose.....	111
Figure 6.3.5. Spectroelectrochemistry results of the glucose detection reaction within the SF matrix.....	112
Figure 6.3.6. Sensitivity and linearity optimization of the biosensor response.....	113
Figure 6.3.7. Absorbance spectra average change of functionalized SF after glucose addition.....	113
Figure 6.3.8. Biosensor life-time.....	114
Figure 6.3.9. Glucose determination in whole blood samples.....	115
Figure 6.3.10. Glucose determination by image analysis.....	116
Figure 6.4.1. Silk bio-cladding FOCS architecture and performance.....	122
Figure 6.4.2. Optimization of FOCS transduction mechanism.....	124
Figure 6.4.3. Optimization of the PMMA-SF FOCS measurement protocol.....	126
Figure 6.4.4. Glucose determination in buffer using PMMA-SF optical fibers.....	127
Figure 6.4.5. Glucose determination in blood using PMMA-SF optical fibers.....	129
Figure 6.5.1. DTE solubility in water enhancement.....	135
Figure 6.5.2. Enzymatic coupling to DTE.....	136
Figure 6.5.3. HRP specificity for closed DTE.....	137

Figure 6.5.4. Irreversibility of UV-Vis spectrum through consecutive reaction cycles.....	138
Figure 6.5.5. IR study of DTE enzymatic catalysis.....	139
Figure 6.5.6. Proposed reaction scheme for DTE.....	140
Figure 6.6.1. SF doping process with DTE.....	147
Figure 6.6.2. SF films doped with DTE.....	148
Figure 6.6.3. Glucose detection using patterned SF films doped with DTE, GOx and HRP.....	150
Figure 6.6.4. PMMA-SF optical fiber doped with DTE.....	151
Figure 6.6.5. Glucose cyclic detection with DTE doped PMMA-SF optical fibers	153
Results Discussion Table	160
Figure 9.1. SF stamping process using PDMS moulds.....	164
Figure 9.2. SF waveguides fabrication.....	165
Figure 9.3. SF patterning by e-beam.....	166

Summary

Due to the impact of diabetes as a worldwide disease and the expected increment in the number of people affected in the following years, especially in underdeveloped countries, there is a need for the production of precise and long-life glucose biosensors to be implemented in simple, low-cost, robust, miniaturized and portable point of care (POC) systems.

In that sense, this thesis proposes the use of biomaterials of natural origin, such as alginate and silk fibroin (SF) from brown algae (*Phaeophyceae* class) and silkworm (*Bombyx mori*) respectively, and their combination with microfabrication technologies for the production of the new generation of POC devices. Both biomaterials present excellent biocompatibility for enzyme and mediators immobilization, without disrupting their structure or functionality, and unique properties for biosensing.

Electrodepositable alginate hydrogels are used in this thesis in the production of regenerable electrochemical lab on chip (LOC) structures with the advantages of being able to select the analyte to be detected in situ and enabling the re-use of the transducer for multiple measurements. To this aim, enzymatically-doped alginate hydrogels are electrodeposited on platinum electrodes for the electrochemical detection of glucose or lactate. The detection of these molecules is achieved by the entrapment of glucose oxidase (GOx) or lactate oxidase (LOx) and horseradish peroxidase (HRP) in the hydrogel during the electrodeposition process. When a sample with glucose or lactate interacts with the gel, a chain reaction begins with the oxidation of those molecules by the action of the respective oxidase and ends with the oxidation of 3,3',5,5'-Tetramethylbenzidine (TMB), a typical peroxidase substrate that is finally detected amperometrically by reduction at the electrode surface. The electrodeposition process is fast, repetitive, restricted to the working electrode area and dependent on the electrodeposition time, which confers a complete control of the biocatalytic membrane. With the same electrodeposition conditions, the obtained membrane is identical to the previous one, not requiring additional recalibrations of the system. Additionally, the hydrogel can be removed easily by incubation with calcium-chelating solutions, allowing the electrochemical transducer to be reused consecutively to analyze different samples independently. The employed platinum electrodes, fabricated with great reproducibility in the Clean Room of the IMB-CNM using planar technology, provide the system with high precision, reproducibility in the measurements and stability. Thanks to the use of fast prototyping techniques, those electrodes are encapsulated in poly(methyl methacrylate) (PMMA),

structures to better drive both the liquid hydrogel precursor, the fluids to be analyzed and finally the cleaning buffer. As a benefit, alginate demonstrated to filter whole blood, avoiding a possible biofouling effect of the electrodes and enabling direct measurement of these samples.

In a second part, the use of SF in the development of optical biosensors is discussed, especially because to its known excellent optical properties (high transparency and refractive index (RI)), high processability and long-term stability of biomacromolecules. Unlike alginate hydrogels, when SF is processed, the result consists of a very poorly hydrated matrix that presents crystalline features given by the high conformational order of the amino acid chain. This fact allows the entrapment and protection of enzymes and mediators, which retain their biological or chromogenic activity for long time periods without requiring special storage conditions (i.e. room temperature). SF, extracted from the chrysalis of silkworms, is maintained in the form of an aqueous solution. At that time, it is doped with GOx, HRP and 2,2'-azino-bis (3-ethylbenzothiazoline-6-sulfonic acid) (ABTS) and applied on polystyrene surfaces to obtain thin films. These films, with the help of a small microfluidic PMMA structure, filter blood samples and change color proportionally to the present amount of glucose, thus enabling glucose detection in whole blood samples. This color change can be measured spectroscopically, by imaging or direct visual inspection.

Additionally to the thin films, the doped SF solution has also been used to dip coat PMMA filaments, resulting in an optical fiber in which the SF layer forms the cladding and the PMMA filament the core. Immersion of these optical fibers in samples with glucose, or even whole blood, also causes the color change of the SF cladding proportionally to the amount of glucose present in the sample, which can be therefore detected spectroscopically.

The use of ABTS as a colorimetric mediator permits only a single measurement with the SF-based optical biosensor. Therefore, the use of a photoelectrochromic molecule, 1,2-bis (5-carboxy-2-methylthien-3-yl) cyclopentene (DTE) as redox mediator, which could be re-generated by irradiation at a specific wavelength, has been studied. Photoelectrochromic materials change their color if a stimulus is applied in the form of electromagnetic radiation or if their oxidation state is changed. This color change is due to isomeric fluctuations of the molecule produced by these stimuli. For example, the DTE turns purple when it is irradiated with 300 nm ultraviolet (UV) light (closed form) and

Summary

lose the color if it is irradiated with visible light or if it oxidized (open form). It has been shown that the closed form of DTE can be oxidized by peroxidase in the presence of H_2O_2 , losing therefore its purple color. This effect allows the development of a glucose biosensor (by coupling GOx to HRP) that is activated by a pulse of UV light and, once the measurement of glucose by color loss is concluded, can be reactivated with another UV light pulse.

Finally, the different advantages of both systems, electrodeposited alginate hydrogels (reusability and adaptability) and SF (reusability and long-term stability of the biomolecules) are compared in a general discussion. Additionally, a final chapter is included with proposals about the future scope in the development of SF-based biosensors.

Resumen

Debido al fuerte impacto de la diabetes como enfermedad de extensión mundial y a las perspectivas de incremento en el número de personas afectadas durante los próximos años, especialmente en países subdesarrollados, existe una gran necesidad de producción de sistemas de detección y cuantificación de glucosa, que puedan ser implementados en dispositivos portables robustos, miniaturizados, de bajo coste y larga duración, tipo *Point of Care* (POC).

En ese sentido, en esta tesis se propone el uso de biomateriales de origen natural, como el alginato y la fibroína de seda, procedentes del alga parda (clase *Phaeophyceae*) y del gusano de seda (*Bombyx mori*) respectivamente, y su combinación con tecnologías de microfabricación para la producción de una nueva generación de dispositivos POC. Ambos materiales presentan una excelente biocompatibilidad para inmovilizar enzimas y mediadores sin afectar su estructura ni funcionalidad.

El alginato se utiliza en forma de hidrogel electrodepositado sobre electrodos de platino para la generación de biosensores electroquímicos de glucosa y, adicionalmente, de lactato. La detección de dichas moléculas se consigue por el atrapamiento de glucosa oxidasa o lactato oxidasa y peroxidasa en el hidrogel durante el proceso de electrodeposición. Cuando una muestra con glucosa o lactato entra en contacto con el gel, se inicia una reacción en cadena que comienza con la oxidación de dichas moléculas mediante la acción de la respectiva oxidasa y termina con la oxidación de 3,3',5,5'-Tetrametilbencidina (TMB), un sustrato típico de la peroxidasa que es finalmente detectado de manera amperométrica por reducción en la superficie del electrodo. El rápido proceso de electrodeposición, así como la fácil eliminación del hidrogel una vez realizado el análisis, permite la reutilización del transductor electroquímico de manera consecutiva para analizar diferentes muestras independientemente. Manteniendo las condiciones de electrodeposición, las membranas de alginato obtenidas son idénticas entre sí, evitando la necesidad de recalibrar el sistema. Los electrodos de platino empleados, fabricados con gran reproducibilidad en la Sala Blanca del IMB-CNM mediante tecnología planar, dotan de precisión y estabilidad al sistema. Adicionalmente, gracias al uso de técnicas de prototipado rápido, dichos electrodos se encapsulan en estructuras de polimetilmetacrilato (PMMA) para canalizar mejor, tanto el precursor líquido del hidrogel, como los fluidos a analizar y por último el tampón de limpieza. Como valor añadido, el alginato permite filtrar muestras de sangre, por lo que la superficie

metálica del electrodo no se ve afectada por elementos en la muestra que pudiese adsorberse sobre la misma.

En una segunda parte, se discute el uso de fibroína de seda para su uso en biosensores ópticos, debido especialmente a sus excelentes propiedades ópticas (transparencia y elevado índice de refracción), su versatilidad para ser procesada y a la estabilidad que aporta a biomoléculas inmovilizadas. Al contrario que los hidrogeles de alginato, cuando la fibroína es procesada, el resultado final consiste en una matriz muy poco hidratada que presenta características cristalinas dada la alta ordenación interna de la cadena de aminoácidos que conforman dicho polipéptido. Este hecho permite el atrapamiento y protección de enzimas y mediadores, que conservan su actividad biológica o cromogénica durante largos periodos de tiempo sin requerir condiciones de almacenamiento especiales. La fibroína de seda, extraída de la crisálida de gusanos de seda, se presenta en forma de solución acuosa. Estas soluciones se dopan con glucosa oxidasa, peroxidasa y 2,2'-azino-bis (ácido 3-etilbenzotiazolina-6-sulfónico) (ABTS) y se dispensan sobre superficies de poliestireno para obtener películas finas. Estas películas, con la ayuda de una pequeña estructura de PMMA, filtran muestras de sangre y cambian de color de manera proporcional a la cantidad de glucosa que contienen. Dicho cambio de color puede medirse por espectroscopía o directamente mediante un análisis de imagen.

De manera adicional a la fabricación de películas finas, la solución de fibroína dopada también se ha empleado para recubrir filamentos de PMMA, dando lugar a una fibra óptica donde la capa de fibroína forma el revestimiento o *cladding* y el filamento de PMMA el núcleo de propagación o *core*. La inmersión de dichas fibras ópticas en muestras con glucosa provoca el cambio de color del *cladding* de fibroína de seda de manera proporcional a la cantidad de glucosa presente de la muestra y que es medido espectroscópicamente.

El empleo de ABTS como mediador colorimétrico en la determinación de glucosa permite una sola medida con el biosensor óptico basado en seda. Por tanto, se ha estudiado el uso de una molécula fotoelectrocromática, el 1,2-bis (5-carboxi-2-metilien-3-il) ciclopenteno (DTE), como sustrato de la peroxidasa. Los materiales fotoelectrocromáticos cambian su color si se le aplica un estímulo en forma de radiación electromagnética o si se cambia su estado de oxidación. Este cambio de color se debe a cambios de isomerización de la molécula producidos por dichos estímulos. Por ejemplo, el DTE

adquiere un color violeta (la molécula “se cierra”) cuando es irradiado con luz UV de 300 nm y vuelve a decolorarse (la molécula “se abre”) si se irradia con luz visible o si se oxida. En este sentido, se ha demostrado que el DTE cerrado puede ser oxidado por la peroxidasa en presencia de H_2O_2 , perdiendo su color. Este efecto ha permitido el desarrollo de un biosensor de glucosa (acoplando la glucosa oxidasa a la peroxidasa) que se activa mediante un pulso de luz UV y que, una vez concluida la medida de glucosa por pérdida de color, puede volver a activarse con otro pulso de luz UV.

Finalmente, las diferentes ventajas que presentan ambos sistemas, tanto el basado en alginato (reusabilidad y adaptabilidad) como el basado en seda (reusabilidad y larga duración) son puestas en valor y comparadas en una discusión general. Asimismo, se incluye un capítulo final con propuestas acerca de la posible continuidad en el desarrollo de biosensores basados en seda.

1. Motivation

1. Motivation

Diabetes mellitus is a chronic condition affecting more than 400 million of people worldwide by 2017¹ and characterized by a deregulation of glucose homeostasis system leading to abnormally high levels of glucose in blood (i.e. hyperglycaemia). The cause of this pathology varies depending on the origin of the deregulation, being three main factors identified and classified in diabetes types. Type-I diabetes is being caused by an autoimmune reaction, where the body's immune system attacks and destroys the insulin-producing beta cells in the pancreas. The insulin is a vital hormone that induces the uptake of glucose from the bloodstream into the body's cells, therefore the elimination of beta cells leads to the previously commented hyperglycaemic state. In Type-II diabetes, responsible of 90 % of all reported cases², a kind of insulin-resistance is generated by the cells, who do not respond to the secreted insulin and the glucose uptake does not occur. Finally, gestational diabetes is usually a transient condition during pregnancy where the pregnant woman experiences some resistance to insulin activity. However, the control of such condition is very important it increases the probability of developing type 2 diabetes both for the mother and the children.³

If non-treated, the persistent high levels of glucose in blood can cause generalized vascular damage affecting the heart, eyes, kidneys and nerves. Diabetes is also one of the leading causes of lower limb-amputation due to blood circulation deterioration. Besides these long-term secondary effects of the chronic disease, there is also a number of acute complications like hypoglycaemia, diabetic ketoacidosis, hyperglycaemic hyperosmolar state, hyperglycaemic diabetic coma, seizures or loss of consciousness and infections.

Diabetes is well known of being a global issue that kills, disables and strikes people indistinctly the region where they live, their age or their socioeconomic level. It is among the top 10 causes of death worldwide and, in addition to the other non-communicable diseases (NCDs), i.e. cardiovascular, cancer and respiratory, is responsible of the 80% of premature NCD deaths.⁴ Diabetes also presents the challenge of being undiagnosed in the 30-80 % of cases, especially in poor developed areas⁵ where it is expected to grow significantly more than in developed regions (**Table 1.1**). The lack of diabetes detection or an inappropriate control of the pathology leads to a faster appearance of the mentioned secondary affections that, at the same time, requires more healthcare investment to be treated. For this reason, it is fundamental to develop strategies for diabetes detection and monitoring that can be extended globally in terms of cost, simplicity and local technical ability.

Region	2017	2045	Increment (%)
Western Pacific	159	183	15
Europe	58	67	16
North America and Caribbean	46	62	35
South and Central America	26	42	62
Middle East and North Africa	39	67	72
South and East Asia	82	151	84
Africa	16	41	156
World	425	629	48

Table 1.1. Number of millions of people with diabetes worldwide and per region in 2017 and 2045 (20 – 70 years). Data obtained from International Diabetes Foundation Atlas.¹

2. Introduction

This chapter presents the state of the art and fundamental knowledge in order to frame the later presented results. In a first approach, glucose biosensors historical development and updated state of the art are discussed, focusing on electrochemical and optical biosensors, and extended those areas intimately related to this thesis. Secondly, due to the undeniable role of alginate hydrogel and SF matrix in the dissertation, a description of these biomaterials properties and applications is included. Finally, the scientific fundamentals ruling the type of developed biosensors are summarized.

1. Biosensors

As it was mentioned in the summary, the aim of the presented thesis is the development of long-live and low-cost biosensors and point-of-care devices for the monitoring of diabetic patients based on biomaterials and alternative sensing strategies enabling reusability and regeneration of the sensors.

A biosensor is defined as, following the International Union of Pure and Applied Chemistry (IUPAC) recommendations,⁶ “a device that uses specific biochemical reactions mediated by isolated enzymes, immunosystems, tissues, organelles or whole cells to detect chemical compounds usually by electrical, thermal or optical signals”.

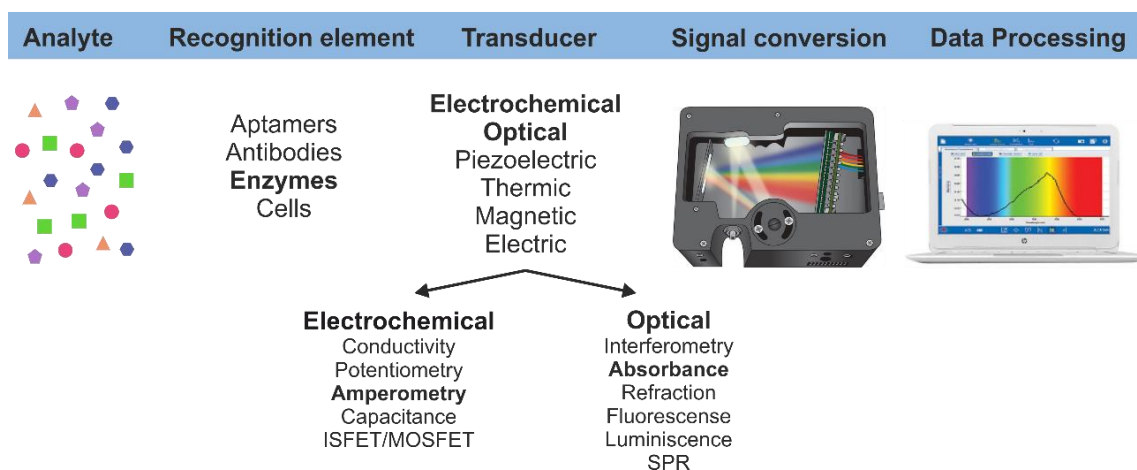


Figure 2.1. Typical scheme for biosensors classification. Highlighted the used types of recognition elements and signal transducers. As an example of signal conversion, a spectrophotometer converts the incoming light into digital signals that can be processed and represented by a dedicated software.

Biosensors are therefore composed, with simplicity, by three differentiated entities (**Figure 2.1**): i) recognition elements, ii) physicochemical transducers and iii) data amplification and evaluation components (treatment and display). Usually, the recognition element and the physicochemical transducer serves as classification guideline. By the type of recognition element, the biosensors classification fits the IUPAC’s definition, perhaps completed by aptamers and more recent DNazymes,⁷ nanozymes⁸ and nanobodies.⁹ Nevertheless, it is more common to classify biosensors depending on the employed signal transduction, which usually are electrochemical, electric, optical, thermal, piezoelectric or magnetic. As in this thesis the analytical

2. Introduction

example is based mainly on glucose and, secondarily, on lactate detection (both enzymatically), the introduction will be focus on the most employed biosensors for that purpose, distinguishing between electrochemical and optical glucose biosensors.

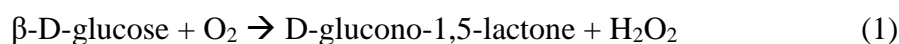
1.1. Electrochemical enzymatic biosensor

In case of electrochemical enzymatic biosensors, there are many cases of application depending on the employed electrochemical technique. For instance, there have been reported potentiometric enzymatic biosensors for urea detection based on the immobilization of urease on polyethylenimine films¹⁰ or impedimetric enzymatic biosensors based on the immobilization of catalase for H₂O₂¹¹ determination or GOx for glucose quantification.¹² Among the wide variety of electrochemical biosensors depending on the detection mechanism, in this thesis the focus will be on those dedicated to enzymatic amperometric sensing.

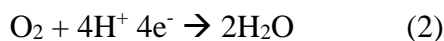
First Generation of Amperometric Glucose Biosensor

The first milestone in enzymatic biosensing occurred in 1962, when Clark and Lyons introduced the concept of glucose enzyme electrode¹³ and, since then, the successive improvements in this sensing science have led to renewed classifications.

At that time, those scientists managed to immobilize GOx in a semipermeable membrane and measured therefore the oxygen consumption by the enzymatic reaction:



This oxygen concentration drop in the patients' samples was detected amperometrically by the application of a negative potential in a platinum electrode (-0.6 V vs Ag/AgCl), in order to reduce the remaining oxygen:



Immediately, a first drawback stands out: the likely difference in the oxygen blood tension between samples. Updike and Hicks¹⁴ proposed the combination of two electrodes system, one bare and the other covered with the GOx, for a differential O₂ measurement instead of a total one.

Nevertheless, in a very short time lapse a new strategy for glucose determination, derived from the previously described, was developed. It was in 1973, when Guibault and Lubrano¹⁵ proposed the anodic detection of H₂O₂ (by-product) instead of the cathodic

detection of oxygen (cosubstrate). The H_2O_2 tracking instead of oxygen consumption eliminated the problem of basal concentrations of the analyte and facilitated the integration of biosensors in miniaturized systems. However, the detection potential for H_2O_2 (+0.6 V vs. Ag/AgCl) is liable to oxidize endogenous molecules in biological samples such as ascorbic acid, uric acid or creatinine and common drugs like salicylic acid or acetaminophen. The solution given to this problem was, at first, the use of selective membranes over the working electrode to permit the diffusion of H_2O_2 and, at the same time, avoid the electrochemical interaction of interfering molecules. Good examples of these membranes are electropolymerized films like polypyrrole,¹⁶ which entrapped the GOx nearby the electrode and serves as a size-exclusion layer, or negatively charged ionomers like Nafion,¹⁷ useful to avoid the interaction of negatively charged species.

Later on, the functionalization of the electrode surface with redox molecules also demonstrated to be useful to enhance the H_2O_2 electrocatalysis by tuning its redox potential to the potential window between 0 V to - 0.2 V vs Ag/AgCl. Ferric-ferrocyanide (also known as Prussian blue) modified electrodes,¹⁸ for instance, lower the H_2O_2 detection potential to -0.1 V vs Ag/AgCl and metallized carbon transducers, with rhodium¹⁹ or ruthenium,²⁰ also situated the H_2O_2 redox potential around 0 V vs Ag/AgCl. The key of the potential detection reduction is the specific interaction of the H_2O_2 with the metal layer. Initially, a shallow metal oxide layer is reduced by the enzymatically generated H_2O_2 , being later electrochemically oxidized giving a proportional anodic current.

Second Generation of Glucose Biosensors

At every first-generation glucose biosensor there is an underlying problem, which is the oxygen availability in the analytic environment, as it may become a stoichiometric limiting element in the reaction (1). This problem is known as “oxygen deficit” and was initially solved by modulating the glucose/oxygen ratio nearby the electrode with the help of diffusion barriers such as the already described membranes above.^{21,22}

Nevertheless, a revolutionary idea arose during the 1980s,²³ consisting of the substitution of oxygen by non-physiological electrochemical mediators and ushered a new generation (named second) of glucose biosensors. The advantageous use of GOx is accompanied by the limitation that suppose the position of its catalytic unit (the flavin adenine dinucleotide, or FAD, redox center). This coenzyme is imbedded in the

2. Introduction

polypeptide three-dimensional structure of the enzyme, what supposes a steric hindrance for a direct electron transfer (DET) from the enzyme to the electrode surface.

There is a wide range of molecules that fulfil the requirements to be used as mediators (e.g. ferricyanide, ferrocene, quinine, thionine, methylene blue, ruthenium or osmium complexes, etc.).²⁴ They should have a low and pH independent redox potential, to avoid electrochemical interferences. They also should react fast with enzyme after the glucose oxidation to avoid the oxygen competition. Probably, the samples to be analysed are aqueous (blood, serum, plasma, sweat, saliva), so the insolubility of the mediators is also required in order to minimize their loss through the medium.

A distinct way for electron transfer from the enzyme to the electrode is providing electrical connection between them by a conductive mesh (wired enzymes). This was demonstrated to be possible by Heller et al., who used poly(vinylpyridine)²⁵ or poly(vinylimidazole)²⁶ to link osmium complexes in a flexible hydrophilic polymer structure. The redox polymers can penetrate into the enzyme's structure, at the time that immobilize it over the transducer, disposing a conductive net that connects the catalytic centre with the electrode surface.

Alternatively, instead of modifying the electrode, GOx can be itself modified by covalent bonding of electrochemical species to the amino acids sequence. A good example was the bonding of ferrocene-monocarboxylic acid to lysine by carbodimide.²⁷ This strategy resulted in the straight oxidation of the FAD at the electrode due to the redox shell formed around the enzyme.

Third Generation of Glucose Biosensors

Technological advances are often helped by systems simplification so a logical ultimate evolution of enzymatic biosensors is the removal of any redox mediator and reduce the sensor to the enzyme and electrode direct interaction. Furthermore, a straight interaction would lead to the glucose detection at the redox potential of the GOx (-0.5 V vs. Ag/AgCl),²⁸ keeping away interfering molecules signals. Nevertheless, considering the spatial separation and the steric impedance, the DET between the enzymatic catalytic center (donor) and the electrode surface (acceptor) results challenging. The best strategy to achieve a DET has been the use of materials that would eventually conduct the electrons such as carbon nanotubes,²⁹ nano-structured metal oxide layers,²⁸ ionic liquids,³⁰ reduced graphene oxide/PAMAM-silver nanoparticles (NPs),³¹ reduced

graphene oxide-multiwalled carbon nanotubes³² or graphene-polyethyleneimine-AuNPs hybrids.³³ Nevertheless, the demonstration of the DET is not trivial and sometimes, like in the use of tetrathiafulvalene-tetracyanoquinodimethane (TTF-TCNQ), some authors claims that the electron transfer is indeed mediated by redox implication of the material,³⁴ behaving then like a second-generation biosensor.

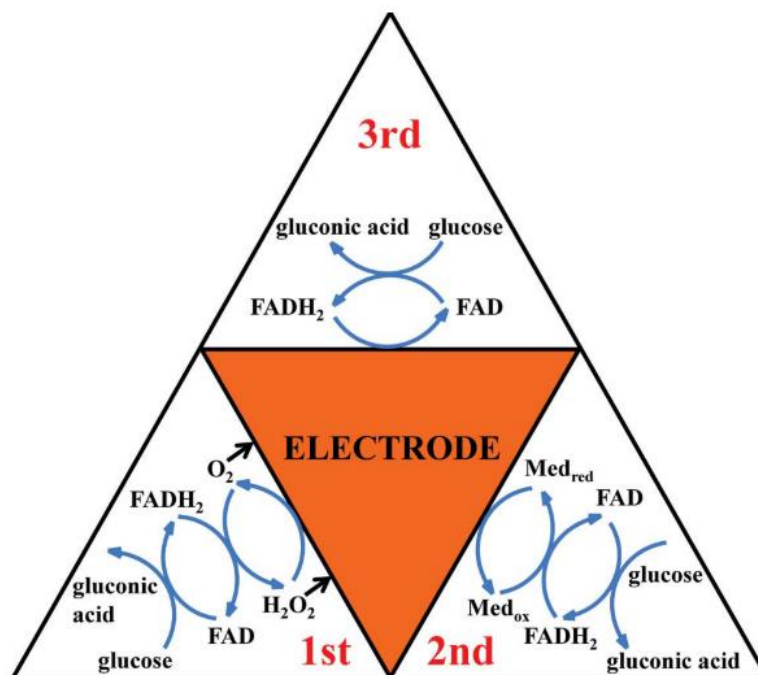


Figure 2.2. Summary of enzymatic glucose oxidation mechanisms, presented as the first, second and third generation sensors.³⁵

From the three main types of enzymatic electrochemical biosensors (**Figure 2.2**), in this thesis, a special second-generation type is developed which employs electrodepositable alginate membranes as matrix for glucose detection and quantification. In this type of sensor, the GOx catalytic activity is coupled to the HRP activity for TMB oxidation. The oxidized TMB is reduced electrochemically at the working electrode and the registered current is proportional to the initial amount of glucose present in the samples.

1.2. Optical enzymatic biosensor

Besides electrochemical, optical are also one of the most explored types of biosensor. Likewise electrochemical biosensors, there is a vast optical biosensors classification depending on the physicochemical induced change by the analyte and the

2. Introduction

used transducer. Some examples are based on analytes that induce RI changes transduced by photonic crystals,³⁶ optical resonators,³⁷ integrated optics (planar waveguides)³⁸ and optical fibers directly (label-free) or via a receptor (e.g. attached antibodies). Alternatively to RI changes, in colorimetric biosensors, an absorbance change (consequence of chromogenic molecules redox changes, aggregation changes of NPs, etc.) is measured at a certain wavelength. In this thesis, the colorimetric approach will be studied in two configurations: planar substrate and optical fiber coating.

Colorimetric biosensors

Colorimetric detection and semi-quantitative colorimetric analysis of substances is a very old transduction strategy that can be simply described as the measurement of a color change of a substance or material induced by the direct or indirect interaction with the target analyte. In case of colorimetric biosensors, enzymes have been always the quintessential recognition element for analysis, especially the HRP as it can catalyse the color change of several molecules with a high extinction coefficient in presence of H₂O₂ (e.g. TMB, ABTS, OPD, homovanillic acid) or the chemoluminescence of others (e.g. luminol). Although HRP use is widely extended nowadays, another enzyme, alkaline phosphatase, was responsible for one of the most important advances in biochemistry and molecular biology ever. In 1971,³⁹ it was published the first enzyme-linked immunosorbent assay (ELISA). Covalently bonded to a specific antibody, the enzyme helps to identify the presence of viruses, bacteria, antigens, and any antibody-recognizable molecule. This discovery replaced the used of radioimmunosorbent techniques, where the antigens were labelled to isotopes, for obvious reasons. The best commercial example of ELISA-type test is the prevalent pregnancy test, developed in the 1980s decade.⁴⁰

The use of enzymes in colorimetric biosensors is not only limited to ELISA applications. An interesting application is, for example, the enzyme acetylcholinesterase encapsulation with fluorescent indicators in liposomes that serves as a barrier for specific analytes detection.⁴¹ If the analyte is present in the sample (e.g. pesticides), it crosses the lipid membrane through a selective membrane porin, inactivates the enzyme and provokes a fluorescence signal decay. This enzyme has also been used in the fabrication of inkjet printed colorimetric biosensors for paraoxon and aflatoxin B1 detection.⁴²

Alternatively, there are also biosensors that do not incorporate enzymes to the detection strategy, as the color change is given by other circumstances. This is the case

of DNA aptamers-NPs systems, where NPs are functionalized with oligonucleotides that specifically recognize and binds a certain analyte. The bonding leads to a multi-structure formation, combining functionalized NPs with analytes. Changing the salinity of the sample, the aggregation of these complexes is induced while the non-conjugated aptamers-functionalized NPs remains in suspension.⁴³ Different aggregation states of metal NPs can result in distinctive color changes.⁴⁴ This strategy has permitted the colorimetric bio-detection of heavy metals^{45,46} (Ag^+ , Pb^{2+} , Hg^{2+}) or antibiotics⁴⁷ (oxytetracycline).

Another interesting example of bio-nano structures application in biosensing is the proposed by Miranda et al. for the colorimetric detection of bacteria using AuNPs- β -galactosidase composites.⁴⁸ The enzymatic activity, initially suppressed by electrostatic AuNPs bonding, is recovered when bacteria bind the AuNPs, releasing the enzymes and providing an amplified readout by a chromogenic substrate catalysis. AuNPs have also been combined with deoxyribozyme (DNAzymes), specially for Cu^{2+} , Zn^{2+} or Pb^{2+} detection.⁴⁹ A DNAzyme is a sequence or strand of oligonucleotides capable of performing a specific chemical reaction. In this type of sensor, the DNAzyme strand is combined with a substrate strand. In presence of the analyte of interest, the enzyme carries out the hydrolytic cleavage of the substrate strand. As the substrate strand contains, in the edges, complementary sequences to aptamers already attached to the AuNPs, the chain cleavage impedes the aggregation. On the contrary, in the absence of analyte, the substrate strand remains unaltered, bridging the NPs and provoking a color change by aggregation.

In case of glucose analysis, the use of GOx enzyme is essential to induce a colorimetric change. Commonly, the H_2O_2 produced by the GOx in the glucose oxidation to glucono delta-lactone is coupled to the HRP that would eventually catalyse the color change of a chromophore.⁵⁰ In the last decade, there have been many studies proposing the substitution of HRP by NPs capable of mimic its catalytic function (nanozymes). Examples of these materials are poly(diallyldimethylammonium chloride) coated Fe_3O_4 NPs,⁵¹ C_{60} -carboxyfullerenes,⁵² $(\text{Mg-Ni-Cu})\text{Fe}_2\text{O}_4$ composites,⁵³ porphyrin-functionalized NiO ⁵⁴ or ceria⁵⁵ NPs or Pt nanoclusters.⁵⁶ In contrast, few studies have demonstrated the glucose oxidation specific capability of inorganic materials. Recently, Zhang et al. have published the use of BSA functionalized Au NPs as dual catalytic (GOx and peroxidase) entities, being capable of the direct color change of a mediator in presence of glucose.⁵⁷ Wang et al. have also published the use of NiPd hollow NPs for

2. Introduction

their “triple-enzyme mimetic activity” (catalase, peroxidase and oxidase) also for direct glucose detection applications.⁵⁸ Nevertheless, the main drawback of these systems is the poor specificity of these composites, as they also oxidizes other monosaccharides like fructose and even disaccharides as maltose, sucrose and lactose.

Unlike other analytes, the colorimetric detection of glucose in patients have always been limited by the type of samples. For an accurate monitoring, the best human fluid to measure glucose levels is blood. Obviously, the direct colorimetric detection of glucose in whole blood presents the enormous drawback of the intense red color of the presented haemoglobin. To overcome this, previous blood treatment need to be carried out (centrifugation, filtering) or other human fluids are analyzed like urine,⁵⁹ sweat or tears.⁶⁰

In the presented thesis, a SF matrix doped with electrochromic mediators and enzymes has been used for the filtering and glucose determination in whole blood samples.

Optic Fiber biosensor

An alternative strategy to whole blood samples pre-treatment or the change of human fluid (specially the last one because analytical substitution of blood may be not plausible for many biomarkers) is a change in the light interaction with the sample. It has been shown how, normally, samples are measured in transmittance (when a liquid absorbance is measured in a cuvette) or in reflectance (when a substrate color change is followed spectroscopically or by image analysis).

In a fiber optic biosensor, the light travels through the confining material and interacts with the light in a softer way. There are many types of optical fibers biosensors depending, precisely, on the nature of the interaction with the sample. Good examples are those based on gratings (fiber Bragg gratings, tilted fiber Bragg gratings, long-period fiber gratings) based on interferometry (all-fiber interferometers, Fabry-Pérot interferometers) based on resonances (surface plasmon resonance, localized surface plasmon resonance, lossy mode resonance), among others.

Optical fibers biosensors presents several advantages that make them very suitable for biosensing applications.⁶¹ Optical fibers are usually made of polymers (e.g. PMMA) or silica, materials with a high biocompatible profile. This composition also gives them flexibility, reduced size and low weight, what are ideal advantages additionally to their

inexpensive cost. The low reactivity of these materials makes them highly resistant to hazardous media and, at the same time, immune to electromagnetic interferences.

Actually, all these possibilities offered by optical fiber biosensors have recently enhanced that some researchers refers to all these applications as “lab on fiber” technology,⁶² reminding the “lab on a chip” concept. Depending on the geometrical configuration, lab on fiber devices are classified in lab on tip, lab around fiber or even lab in fiber, when hollow fibers are used and inner-functionalized.

Some optical fiber biosensors have been reported for glucose detection and quantification. Tierney et al. published the use of a functionalized hydrogel in the tip of an optical fiber.⁶³ The hydrogel was covalently modified with 3-phenylboronic acid and dimethylaminopropylacrylamide and the glucose concentration was measured interferometrically by a glucose-induced swelling (linking those molecules). In a similar way, Wang et al. have proposed the fabrication of a partially oxidized dextran doped with GOx layer by layer constructed structure at the tip of an optical fiber.⁶⁴ The present GOx catalyse the glucose present in the sample, producing gluconic acid. The local pH change provokes the hydrogel swelling. Alternatively, Srivastava et al. proposed the use of a U-shaped optical fiber biosensor functionalized with Au NPs covalently bonded to GOx, being the glucose concentration determined by localized surface plasmon resonance.⁶⁵ There are also other reported examples based on medium color changes⁶⁶ or RI differences.⁶⁷

In this thesis, the fabrication of PMMA core fibers coated with a doped SF cladding in a lab on tip and lab around fiber configuration is described for the detection and quantification of glucose. The color change of the SF cladding is proportional to the amount of glucose present in the samples and is therefore measured spectroscopically.

2. Biosensors functionalization: use of natural biomaterials

One of the most critical step in a biosensor fabrication is the immobilization of the biorecognition element. Many strategies have been developed for this purpose, presenting some advantages and disadvantages.⁶⁸ For instance, physisorption on an electrode or

2. Introduction

optical fiber is the simplest way to biofunctionalize a surface but, at the same time, the biomolecules are poorly attached and very exposed so suffer from deactivation in a short time. A stronger way to bond the enzymes to a surface is covalently, using linking agents like carbodiimides to bond carboxylic groups of a surface to amino groups present in the biomolecule. Nevertheless, the biomolecules are still unprotected against external agents that induce their deactivation (pH changes, heat, light irradiation, etc.). A different alternative like cross-linking can provide a protective material by bonding the enzymes within a matrix such as glutaraldehyde. The main drawback of this strategy is that the biomolecules still suffer deactivation due to conformational changes or chemical alterations in the active site. Immobilization by affinity is a very powerful technique as it is capable of immobilize the biomolecules at a specific binding site and with a specific orientation, so the activity loss through immobilization is negligible. However, the process may require structural modification of the biomolecules (i.e. the amino acids sequence of an enzyme), hindering the biosensor functionalization. Alternatively, entrapment has been considered an accurate immobilization strategy as it combine its simplicity with its biocompatibility. Consists, basically, in the biomolecules immobilization within a three-dimensional matrix without a direct chemical bonding. Furthermore, compatible biomaterials like polysaccharides or proteins can be used for such a purpose, creating an appropriate environment for biomolecules activity maintenance.

A biomaterial can be defined from two different perspectives. It is consider a biomaterial any organic or inorganic compound specifically design for, or applied to, the compatible interaction with bio-entities such as cells or tissues, commonly for a biomedical purpose. In accordance with the latter, the IUPAC defines a biomaterial as: “Material exploited in contact with living tissues, organisms or microorganisms.”⁶⁹ However, it is also extended in the scientific literature the use of biomaterial definition for those compounds with a natural origin that are also used for different purposes, not necessarily related to the structural support role that normally play in biomedical applications. In this case, they can be also named biopolymers. Because of their renewable and great availability, these materials have been used (among other fields) in

large and diverse biosensing applications (**Table 2.1**). In this thesis, alginate hydrogel from brown algae *Macrocystis pyrifera* and SF from *Bombyx mori* cocoons are employed in electrochemical and optical biosensors development, respectively.

Biopolymer	Origin	Biosensor
Cellulose, Nanocellulose, Nitrocellulose	Cell wall of green plants, cotton fibres, genetically modified bacteria	Catechol, ⁷⁰ Cu ²⁺ , ⁷¹ <i>E. coli</i> O157:H7, ⁷² immunoglobulin G, ⁷³ lactate ⁷⁴
Polylactic acid	Fermented starch	Streptavidin, ⁷⁵ glucose, ⁷⁶ DNA, ⁷⁷ creatinine ⁷⁸
Chitin/Chitosan	Arthropods exoskeleton Cell wall of yeast Shellfish	Glucose, ⁷⁹⁻⁸¹ ethanol, ⁸² cholesterol, ⁸³ DNA, ⁸⁴ pH, ⁸⁵ pesticides, ⁸⁶ urea ⁸⁷
Starch	Potato, wheat, maize, rice, etc...	Paraoxon, ⁸⁸ H ₂ O ₂ , ^{89,90} O ₂ , ⁹¹
Collagen	Connective tissues	H ₂ O ₂ , ⁹² cancer cells, ⁹³ tropomyosin, ⁹⁴ deoxynivalenol, zearalenone and Aflatoxin B1 ⁹⁵
Hyaluronic acid	Rooster comb, vitreous body	BSA, ⁹⁶ D-sorbitol ⁹⁷

Table 2.1. List of biopolymers used in biosensing applications, as a passive matrix or as an active element of the biosensor.

2.1. Alginate

Alginate is a natural occurring anionic copolymer composed by homopolymeric blocks of (1-4)-linked β -D-mannuronate (M) and α -L-guluronate (G) residues (**Figure 2.3a**). It is typically extracted from brown algae (*Laminaria hyperborea*, *Laminaria digitata*, *Laminaria japonica*, *Ascophyllum nodosum* and *Macrocystis pyrifera*)⁹⁸ by a method already patented in 1936.⁹⁹ Alternatively, alginate can be produced in bacteria (*Azotobacter* and *Pseudomonas*) in a well know anabolic pathway,¹⁰⁰ facilitating the

2. Introduction

production of high-controlled alginate chemical structures and physiological properties. Moreover, new alginates with unique and tailor-made properties are generated by the genetic modification of alginate producing bacteria. The G-blocks of alginate participate in the intermolecular cross-linking reaction by the presence of divalent cations such as Ca^{2+} ,¹⁰¹ forming a hydrogel. This cation addition can be by simply mixing the alginate with a calcium-salt solution (e.g. CaCl_2).

However, the direct mixture with cross-linking solutions leads to a poorly controlled aggregation of alginate chains. More sophisticated strategies like the induced Ca^{2+} liberation by progressive dissolution of calcium particles by changes in the environment conditions (e.g. CaCO_3 dissolution by pH change) permit to obtain more homogeneous gels, with a certain geometry and in a concrete location (e.g. electrode) (**Figure 2.3b**).¹⁰²

Due to its biocompatibility, low toxicity, relatively low-cost and induced gelation in soft-reaction conditions (low temperature, aqueous solution, neutral pH, etc.), alginate hydrogels have been used in different biomedical applications like drug delivering,¹⁰³ wound dressing,¹⁰⁴ cell culture¹⁰⁵ and tissue regeneration.¹⁰⁶

In case of biosensors development, there are several examples of alginate hydrogel applications. Electrochemical biosensors for the detection of trichloroacetic acid¹⁰⁷ or glucose,¹⁰⁸ the evaluation of the antioxidant capability of microorganisms¹⁰⁹ and the 3D culture growth tracking,¹¹⁰ for instance, have been developed. Also optical biosensors (e.g. lactate sensing),¹¹¹ fluorescence biosensors (e.g. bacteria detection),¹¹² bioluminescence biosensors (e.g. endocrine-disruptive chemicals detection)¹¹³ or even calorimetric biosensors (e.g. creatinine quantification)¹¹⁴ have been reported recently.

Alginate hydrogel, as a soft matrix, can be disaggregate by the presence of chelating agents that bind the cross-linking cations (e.g. phosphate ions). This fact is exploited in the presented thesis to develop a tuneable and regenerable biosensor for the amperometric detection of glucose and lactate in whole blood samples.

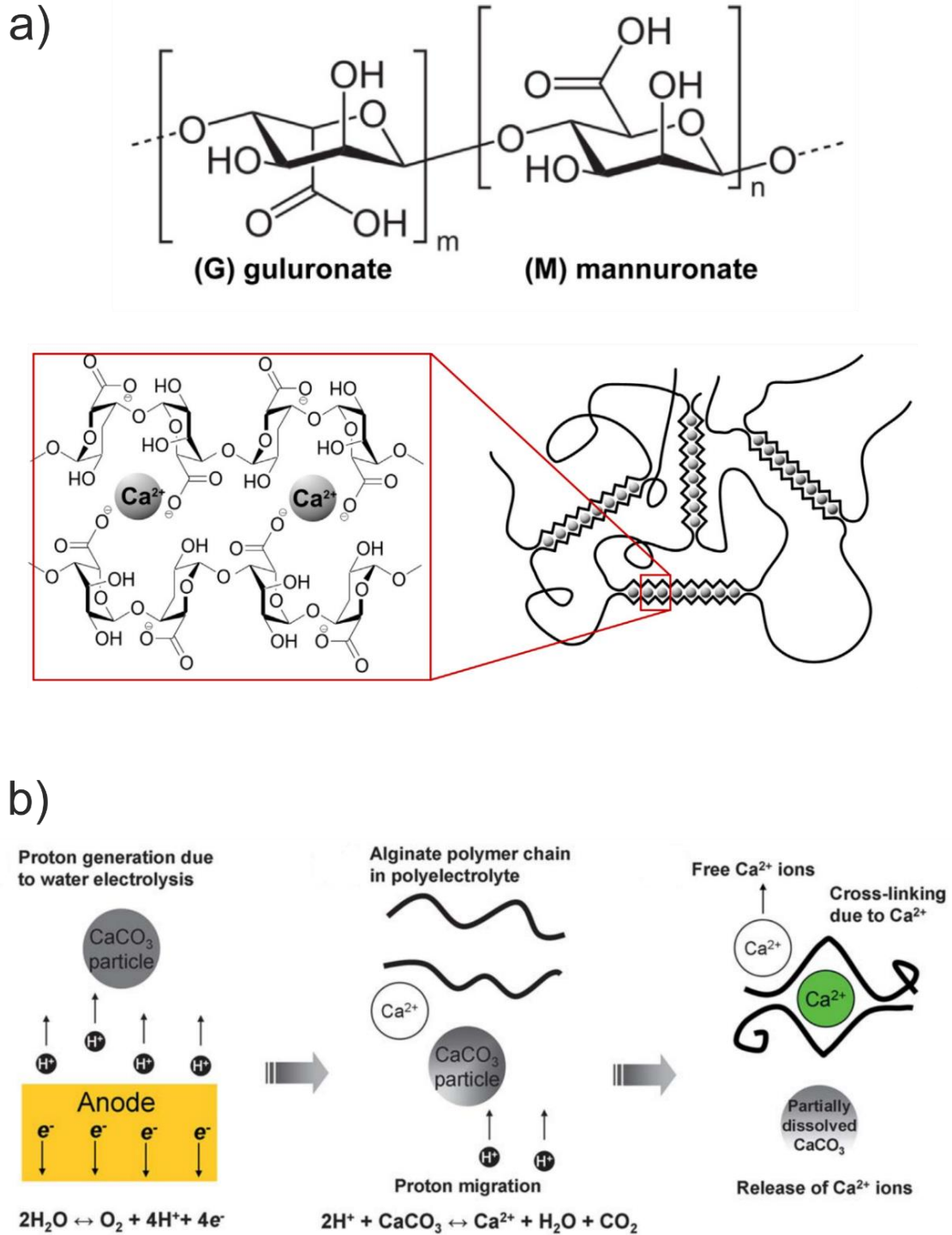


Figure 2.3. Alginate molecular structure and electrodeposition process. a) Structure of alginate, composed by the monomers guluronate (G) and mannuronate (M) and the cross-linking reaction induced by Ca²⁺ in the so-called egg-box model.¹⁰¹ b) One of the alternative mechanisms of controlled alginate cross-linking by induced dissolution of CaCO₃ particles by a local acidification nearby an electrode by anodization and water splitting into H⁺ and O₂.

2.2. Silk Fibroin

Silk are naturally occurring protein polymers produced by a wide variety of worms and spiders.¹¹⁵ As a fibrous protein, it is characterized of being composed by a highly repetitive primary amino acids sequence that leads to a significant homogeneity in the secondary structure. Due to their biological function, for instance as a spider web for prey capture or as a cocoon for silkworm metamorphosis, these fibered proteins usually exhibits interesting mechanical properties. Silk fibers are composed of two main proteins: fibroin (SF) and sericin. While SF is the inner core of the fibers, responsible of silk mechanical properties, sericin actuates as a glue-like proteins, joining adjacent fibers. Silk extracted from *Bombyx mori* (silkworm) has been employed during centuries as a fiber for textiles, fishing, etc... In the last decade, there has been a silk reinvention, especially for SF in the field of biomedicine¹¹⁶ due to its extraordinary properties: mechanical resistance, biocompatibility and biodegradability.

SF consists of a light (L) and a heavy (H) chain (**Figure 2.4a**) linked by a single disulphide bond at the C-terminus of H-chain, forming an H-L complex. Another component of SF is a glycoprotein P25, which attached by non-covalent interactions to the covalently bonded heavy and light chain complex.¹¹⁷ H-chains (Mw \approx 391 kDa) form β -sheet domains in the crystallization process that serve as the main structural component, responsible of the good mechanical properties of the material. The polypeptide sequence is quite simple,¹¹⁸ mainly composed by glycine (43 – 46%), alanine (25 – 30%) and serine (12%), which are some of the simplest amino acid. Additionally, tyrosine is also present (5%), giving some reactivity to the material, which is reported to be poorly reactive in any case. Other amino acids are also present, but in less than a 2% (valine, aspartic acid...).

The H-chain composition is very regular: 12 hydrophobic domains with repetitive amino acids sequence interspersed with 11 hydrophilic domains with non-repetitive amino acids sequence.¹¹⁹ The repetitive domains are capable of reassembly themselves in very ordered β -sheet conformations via intra- and intermolecular forces (hydrogen bonds, van der Waals, hydrophobic interactions) (**Figure 2.4b**). These β -sheet structures confers crystallinity to the annealed SF, while the non-repetitive domains (mainly composed by acidic or charged amino acids like glutamic acid, aspartic acid, arginine and lysine) form the amorphous structure of the SF matrix.

Following a relatively simple extraction process, explained more in detail lately, SF can be extracted from the silkworm cocoons obtaining an aqueous solution of the protein, which is stable up to 60 days at 4° C before gelification. Depending on the treatment, the SF can be mechanized into different structures, from the macro to the nanoscale (**Figure 2.4c**). It can be casted to generate thin films, electrospinned to build fibered matrices, freeze dried to fabricate sponges, dropped in methanol solutions to synthesize microspheres and physically cross-linked to obtain hydrogels.

It is of vital importance for the SF applicability to biosensors development that the precursor to all of this SF based structures is an aqueous solution, because it can be doped with elements that would suffer inactivation in other types of solvents (e.g. organic solvents). Thus, by simply dissolution in the aqueous SF precursor, complex biomacromolecules such as enzymes, antibodies, growth factors, etc... can be immobilized, maintaining their functions and endow the material with specific functionalities for long time-periods.¹²⁰

The type of given structure is intimately related to the desired function of the material, and is the key for the vast amount of applications in which the SF has been used. For example, SF films can be used as a biocompatible and biodegradable substrate for electronics¹²¹ but can also be patterned by soft lithography¹²² or photolithography¹²³ for biophotonic applications. SF electrospinned fibered matrices, tubes, sponges and hydrogels have demonstrated to be of interest in 3D cellular growth and, therefore in tissue regeneration applications while SF microspheres can be applied in drug delivery applications (**Figure 2.4c**).

Beyond biomedical applications, SF has also been applied in sensing fields. Some examples are electrochemical biosensors for alcohol,¹²⁴ glucose,¹²⁵ bisphenol A¹²⁶ or pesticides.¹²⁷ Also colorimetric biosensors based on SF for antigen-antibody detections have been reported recently.¹²⁸

In this thesis, SF has been used as a matrix component for stable immobilization of enzymes and mediators, presenting an active role in the biosensing mechanisms in some cases. The functionalized SF has been employed as a colorimetric biosensor for glucose detection in whole blood samples both for disposable but also regenerable colorimetric biosensors. SF has been isolated from *Bombyx mori* cocoons and disposed as thin films and also as fiber optic cladding after their biodeposition.

2. Introduction

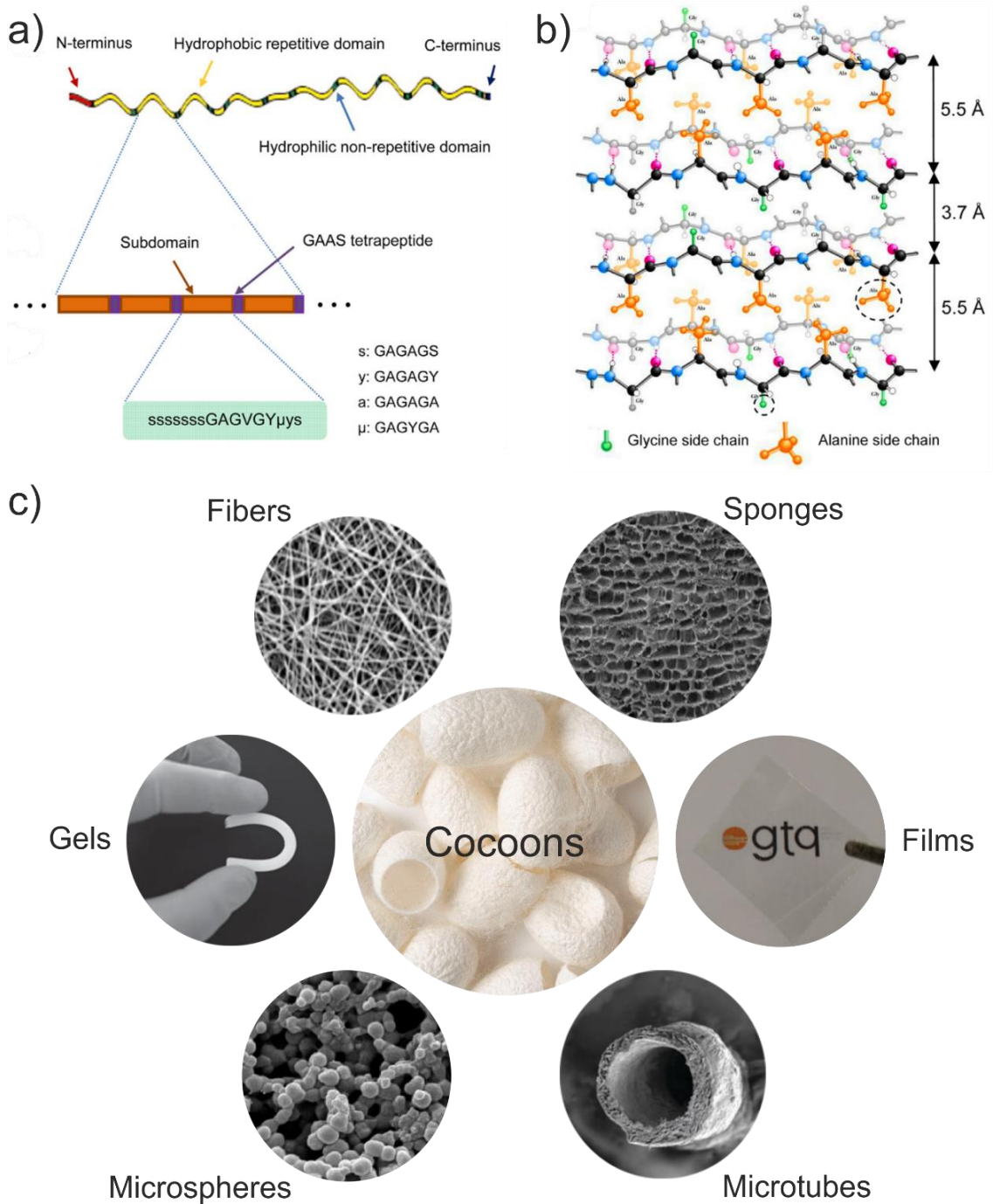


Figure 2.4. Silk molecular structure and applications. a) Hydrophobic repetitive and hydrophilic non-repetitive domains alternation in H-chain of SF and b) SF accepted stacking for β -sheet domains, facing one sheet projecting methyl groups of alanine side chain to another sheet exposing hydrogen atoms from glycine side chain.¹²⁹ c) Representation of the wide SF mechanization possibilities into electrospun fibers,¹³⁰ freeze dried sponges,¹³¹ casted films, microtubes,¹³² microspheres¹³³ or gels.¹³⁴

3. Applied biosensors – Point of Care Testing devices

Diagnosis and monitoring of human conditions is changing in the last years regarding the used instrumentation and the place where they are carried out. Both are intimately related since the miniaturization and underselling of technological platforms (microelectronics, microfluidics, cameras, etc...) is enhancing the fabrication of POC devices, which expands the possibility of performing health tests at patients' home, i.e. homecare. In developed countries, chronic patients monitoring represents a double advantage since increases their live standards of chronic patients while reducing the healthcare costs associated to their control. Meanwhile, this possibility also leads the way for diseases diagnosis in underdeveloped regions, where the access to expensive instrumentation and experienced technicians is limited.

The implementation of POC devices presents additional advantages in comparison to traditional benchtop laboratory methods, such as the reduction of diagnosis time and the low consumption of energy and reagents. The extensive use of smartphones in the last decade all over the world has made the use of POC gone one step further, situating these devices as the principal and versatile interface between the user and the specific test platform. Furthermore, the smartphone can actuate not only providing the control over additional instruments (e.g. potentiostats), powering them and receiving and processing data (i.e. dedicated software) but also as active detection systems (e.g. standard integrated cameras).

Human fluids susceptible for POC analysis are blood (including plasma and serum), sweat, urine and tears. Blood is maybe the most reliable sample for analysis due to the relatively high amount of biomarkers in reasonable concentrations present in this fluid. There are several ways of blood analysis using a POC device. The electrochemical test is maybe the preferential one as it has been implemented for decades in the well-known glucometer by the use of disposable test strips. Beyond glucose, electrochemical and paper-based biosensors have been widely used for detecting ions, metabolites, proteins and nucleic acids.^{135–137}

Other reported detection methods in POC blood testing alternative to the classical electrochemical ones are the brightfield, the colorimetric and the fluorescence tests. The simple working principle of brightfield technology facilitates the adaptation to POC devices. The sample is irradiated with white light from the bottom and the contrasts generate by the sample in the light transmission is associated to different parameters, as

2. Introduction

the cell confluence for instance.¹³⁸ CD4¹³⁹ and sperms¹⁴⁰ cells have been demonstrated to be detectable and quantified by this method using a smartphone and a relative simple and miniaturized setup composed of light sources and lenses, supported by a dedicated software.

Colorimetric tests are also quite extended for their application in POC. Normally, the color change is induced by a biochemical assay, involving chromogenic molecules immobilized on a substrate. Integration of CMOS image sensors and optical gratings in combination with a spectrum processing technique permitted the development of colorimetric smartphone-based POC devices for distinct purposes.¹⁴¹ Good examples are the rapid detection (in less than 15 min) of Ebola virus in serum samples,¹⁴² the colorimetric quantification of blood haematocrits (LOD = 0.1 %) ¹⁴³ or even the test for HIV and *Treponema pallidum* infections determination.¹⁴⁴

In case of fluorescence tests, the high sensitivity and strong specificity that offers the method enhance its use in antibodies and nucleic acids detection in blood. A good example of its application in smartphone-based POC is the proposed for the influenza A (H1N1) virus.¹⁴⁵

In case of glucose detection with smartphone-based POC devices, there are many cases of application based in colorimetric systems.^{146–151} For example wearable microfluidic devices for the quantification of hydronium ions, glucose and lactate in sweat have been developed recently (**Figure 2.5a**).¹⁵² Also, very recently, the inoculation of oxygen-sensitive polymer dots together with GOx permitted the monitoring of glucose in vivo (**Figure 2.5b**).¹⁵³ In a different approach, a dermal tattoo biosensor for the colorimetric detection of pH, glucose and albumin have been described (**Figure 2.5c**).¹⁵⁴ The ultralong phosphorescence lifetime of the polymer dots permitted to monitor the subcutaneous glucose by optical images capture.

In case of electrochemical glucose biosensors supported on smartphone interfaces, the number of reported works is reduced in comparison to colorimetric as it needs the assistance of an external potentiostat and, in addition, there are numerous commercial kits available for that purpose (glucometers) that employ disposable test strips. Nevertheless, some contributions have been published recently based on this system (**Figure 2.6**).^{155,156}

In this thesis, we propose the combination of the developed amperometric glucose biosensor with a smartphone-based platform that includes a potentiostat developed by collaborators. Additionally, the colorimetric detection of glucose based on SF was also based on image analysis of the color change of the material. All these results are in accordance with the state of the art works mentioned above.

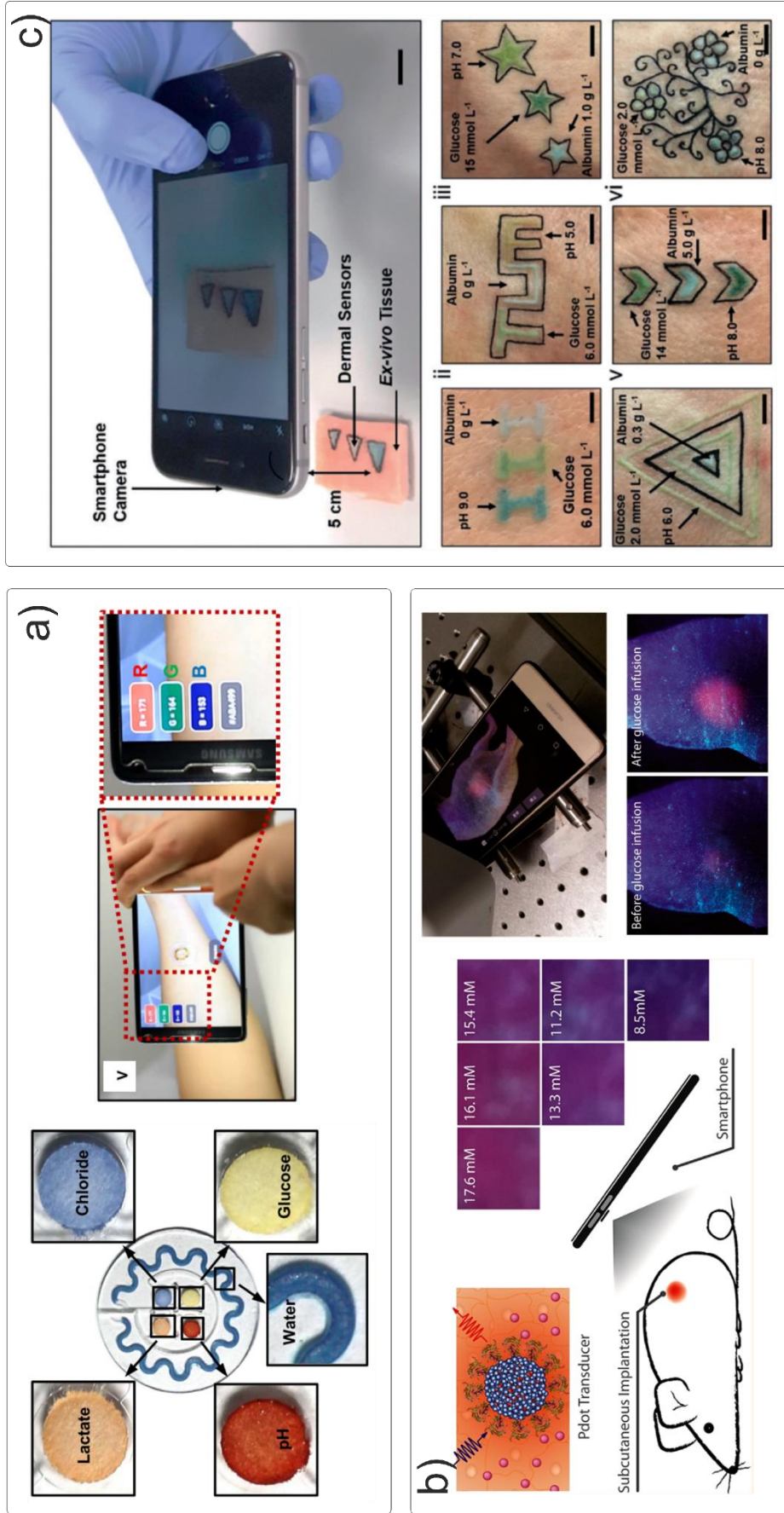


Figure 2.5. Smartphone-based colorimetric biosensors. a) A wearable microfluidic device for multianalyte colorimetric detection in sweat.¹⁵² b) Polymer-dot with high phosphorescence for wireless glucose detection in vivo.¹⁵³ c) Dermal tattoo biosensors for colorimetric detection of pH, albumin and glucose.¹⁵⁴ In all the represented systems, the color or phosphorescence changes are measured by smartphone-based systems through image acquisition and dedicated analysis.

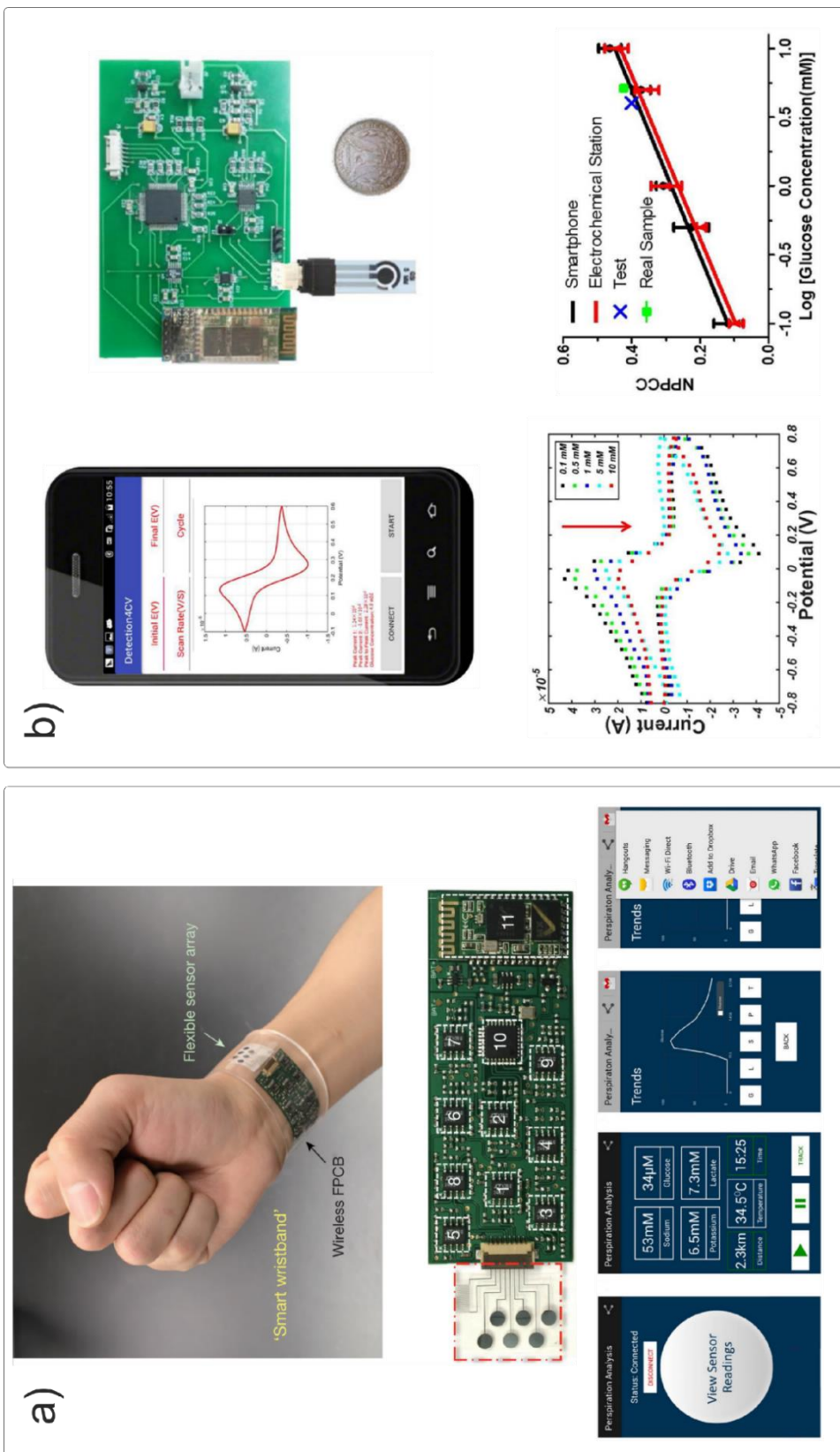


Figure 2.6. Smartphone-based electrochemical biosensors. a) Fully integrated wearable biosensor array for multiplexed analyte detection. A picture of the sensor array (red dashed box) connected to the integrated circuit components (white dashed boxes) is shown. The device is connected via Bluetooth to a smartphone, where the data is processed and shown to the user.¹⁵⁵ b) Glucose detection using an external potentiostat in a smartphone-based system. A real-time cyclic voltammery is depicted in the smartphone associating the voltammogram peaks values to glucose concentrations. The performance of the system is comparable to the used electrochemical station.¹⁵⁶

3. Fundamentals

This chapter highlights the basic information related to the technology involved in fabrication of the employed electrochemical transducers for the alginate-based biosensor. Furthermore, the state of the art of SF processing is discussed in order to link the available technology with future work with this material. The principles of photoelectrochromic compounds behaviour are described and the fundamentals of the employed techniques for measuring and characterize the electrochemical and optical biosensors.

1. Silicon Technologies

Among the great number of Si-based planar fabrication technologies available in the Clean Room of IMB-CNM, in this thesis only some of them have been used for the fabrication of the electrochemical transducers. In this section, the concepts behind these fabrication steps will be exposed with the objective to clarify aspects not included in the methodology section.

In silicon technologies, the initial substrate is a silicon wafer, which is processed and patterned to obtain the final product of chip. In general terms, microfabrication processes can be additive (when adding a new material to the wafer) or subtractive (when removing part of the material already present in the wafer). The most relevant processes used in the fabrication of the current electrochemical chip are described below.

Thermal oxidation: Thermal oxidation is an additive process where a thin silicon oxide layer is produced on the silicon wafer. The exposition of the silicon wafer to high temperatures in presence of oxygen or water vapour (**Figure 3.1**) produces the formation of a SiO_2 layer that grows spontaneously on the native Si following the Deal-Groove model¹⁵⁷ in a self-limiting process where the wafer gains volume by the incorporation of O_2 . The thickness and properties of the layer depends on the thermal deposition conditions (temperature, time, etc.).

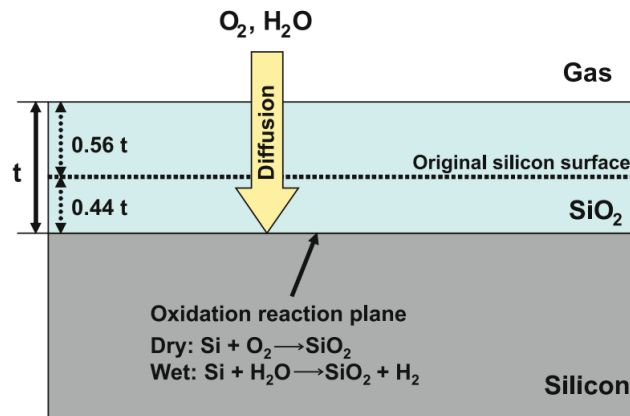


Figure 3.1. Basic process for the oxidation of silicon.¹⁵⁷

The generation of the SiO_2 layer as a first step is widely extended among the clean room processes due to its properties as electrical insulator layer, its high chemical stability, the enhancement of photoresist spin coating homogeneity and additional functions, for example, for the excellent optical properties of silicon oxide in photonics

(UV-Vis transparency, high RI). Thanks to the hydrophilic properties of this layer, in opposition to the more hydrophobic silicon wafer, thermal oxidation is a common process previous to other additive microfabrication steps, e.g. spin coating.

In our process, thermal oxidation was the first step in the clean room to generate an isolating layer on the Si wafer to avoid the short circuit of the electrodes, and between the electrodes and the Si semiconductor substrate.

Spin Coating: This additive technique consists of the deposition of material on the wafer and spinning at a constant speed to produce a homogenous layer of photoresist. It permits to set the thickness of the layer by controlling the spin speed, which also depends on the viscosity of the material. The control over the photoresist thickness is critical for the following steps, as it fixes the depth of the revealed patterns. This is the case of polymer nanoimprinting techniques, where the developed photoresist serves as a master to structure a material (e.g. SF).

Photolithography: Photolithography is a subtractive process where a pre-deposited photoresist layer is partially removed to generate a pattern on the wafer surface. The photolithographic patterning involves (i) the deposition of the photoresist, (ii) the exposure of specific areas to UV radiation and (iii) the partial removal of the resist with a suitable developer (**Figure 3.2**). As previously exposed, the deposition is normally performed by spin coating. Once deposited in the suitable thickness, the photoresist is cured (if needed) at a certain temperature and irradiated using a previously designed photo-mask. The photo-mask permits to irradiate selected areas of the wafer thus producing the desired pattern. Depending on the response to the irradiation, the photoresist are classified in positive or negative. In a positive photoresist, the irradiated area is eliminated after developing, while in a negative photoresist the radiation activates a photo-initiator that induces polymerization thus, the irradiated regions are those that remain after the developing step. The developers are chemical substances, normally specific organic solvents that can dissolve and eliminate the non-polymerized photoresist.

The irradiation energy to be used depends on the photoresist characteristics and of the desired patterns resolution. Common commercial photoresists used in IMB-CNM clean room like HiPR and OiR (positive) or SU-8, AZ and polyamides (negative) are cured using the so called g, h and i lines, that uses a Hg lamp as irradiation source, filtered

3. Fundamentals

to give 436, 405 and 365 nm wavelength respectively. However, these lines have a critical dimension (CD) of $\sim 1 \mu\text{m}$, which is the minimum feature size given by:

$$CD = k_1 \frac{\lambda}{NA}$$

where k_1 is a coefficient that encapsulates process-related factors, λ is the irradiation wavelength and NA is the numerical aperture.

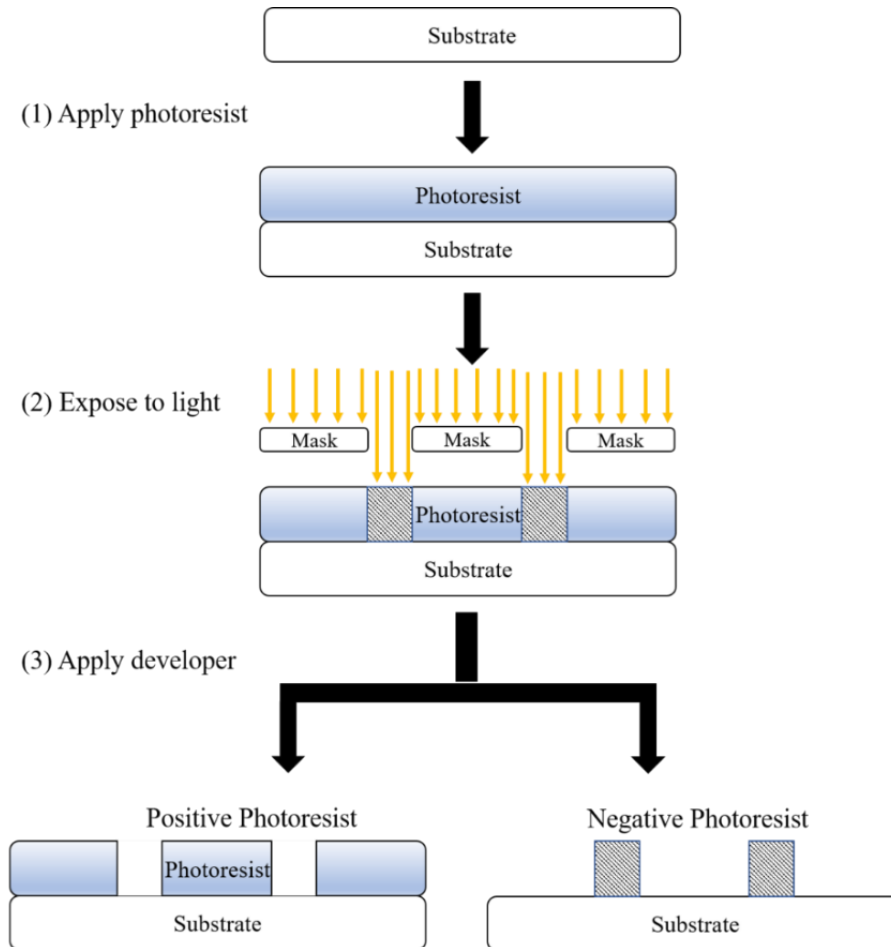


Figure 3.2. Photolithography steps, using a mask for the developing of positive or negative photoresists on a substrate.¹⁵⁸

There are different strategies to reduce the CD, like the use of *steppers* (*step-and-repeat camera*) systems that reduce the mask-irradiating pattern by the use of lenses to collimate, focus and reduce the light pattern before it arrives to the photoresist layer. Alternatively, the reduction of the irradiation wavelength also permits the reduction of the CD. For this purpose, KrF (248 nm) or ArF (193 nm) lasers can be used, although the

limit of air absorption (185 nm) is very close, so slightly more improvements can be achieved by photolithography. To reach lower resolutions, electrons or ions should be used as irradiation due to the low λ associated to these particles, given by:

$$\lambda = \frac{h}{\sqrt{mE/2}}$$

where h is the Plank's constant, m is the particle's mass and E is the particle's energy. Although the resolution can reach values below 50 nm, these techniques are mask-less as the electron or ion beam needs to scan the surface, what extends the process duration.

Once the photoresist patterns are revealed, some areas of the SiO₂ surface are exposed. Then, additive (depositions) or subtractive (etchings) steps can be carried out. In our case, the photoresist was used to define the area of the electrodes, connection and pads.

Electron-beam physical vapour deposition (EBPVD): By this additive method, a target of the desired material to be deposited is bombarded in a high vacuum chamber with an electron beam (e-beam), generating a vapour phase of sublimated material that is deposited on the substrate. After the deposition, the photoresist is dissolved with an adequate solvent and only the metal directly deposit on the SiO₂ layer remains. This combination of photoresist development, metal deposition and photoresist dissolution is called *lift-off* process and is extensively used for localized metal deposition, as they present difficulties to be etched from the surface directly (**Figure 3.3**). In the presented case, metal layers of Ti and Pt are deposited by EBPVD.

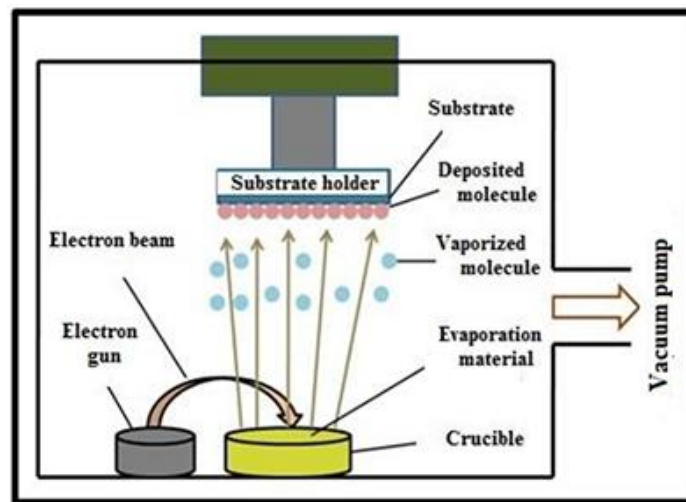


Figure 3.3. Electron beam physical vapour deposition scheme.¹⁵⁹

3. Fundamentals

Plasma enhanced chemical vapour deposition (PECVD): In PECVD, the wafers are introduced in a chamber with a relatively low temperature (usually below 400 °C) and low pressure (around 1 Torr). Then, some precursor gases are injected in the chamber and the reaction takes place, helped by the extra energy intake given by the plasma generation (**Figure 3.4**). In this additive process, the layer thickness can be controlled through the power of the discharge, the temperature and the pressure applied.

In this case, a second layer of SiO₂ (passivation layer) was deposited by PECVD to protect the deposited metal layers. For SiO₂ deposition different gas sources can be used:

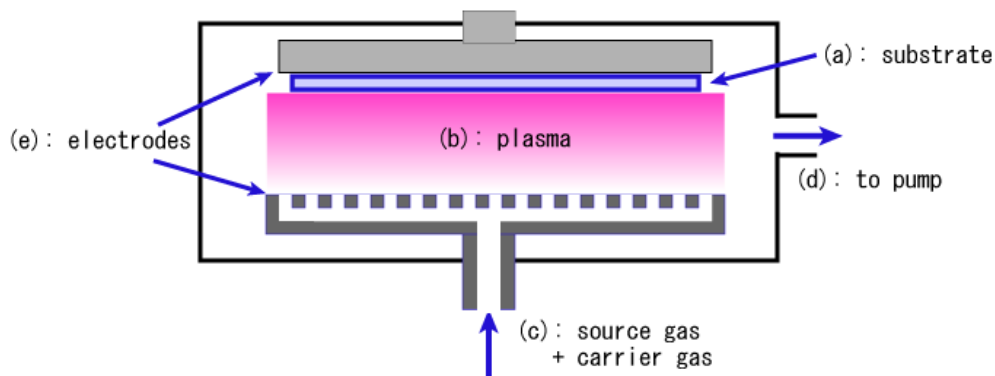
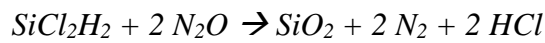
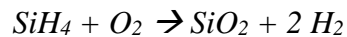


Figure 3.4. Plasma enhanced chemical vapour deposition scheme.

Wet etching: Wet etching is a subtractive process where a specific material is attacked by chemical substances that dissolve it without any damage on the other exposed components. The wet etching depends, therefore, on the materials exposed in the surface of the wafer and the possibility of formulate suitable reactants.

In this case, wet etching is used to selectively remove part of the previous SiO₂ deposited passivation layer. To this end, a second photolithography step is carried out, similar to the first one, developing the same areas of photoresist over the second deposited SiO₂ layer. At this moment, instead of the lift-off process performed before, a wet etching of the exposed SiO₂ is done, eliminating all the SiO₂ until the metal electrodes beneath it are exposed (**Figure 3.5**). To dissolve SiO₂, hydrofluoric acid mixtures are employed.

Finally, the photoresist can be removed with a suitable developer *stripper* (basic formulated solutions that etch away the irradiated resists).

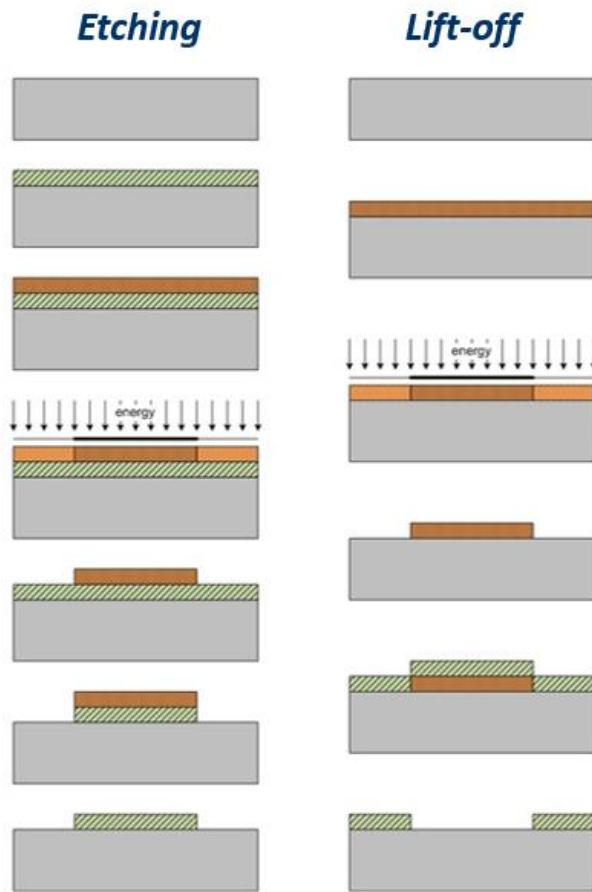


Figure 3.5. Sequential steps of a photolithography process followed by an etching or a lift-off step. While in etching process the photoresist is applied to protect some areas from chemical attack, in lift-off the photoresist helps to detached material from non-desired areas.

2. Silk Technologies

SF, obtained from silkworm cocoons and employed in aqueous solutions, has demonstrated to be compatible with Clean Room processing either direct or to indirect micro-/nano-patterning techniques. The most commonly techniques used for processing SF will be detailed below.

The simplest way to structure the SF is indirectly, by casting the aqueous solution onto previously designed masters. A master is a mould containing the patterns to be transferred to the SF layer. In the case of SF, it is deposited on the master, dried, annealed

3. Fundamentals

for crystallization and peeled off from the master. In an example proposed by Omenetto et al. in 2008,¹⁶⁰ the masters were fabricated by a lift-off process using PMMA as sacrificial layer, e-beam lithography to burn the PMMA and exposed substrate, e-beam evaporation to deposit a layer of Cr and acetone to dissolve the remaining PMMA and detach the Cr above it. The result was a periodical disposition of Cr nanocylinders on the substrate. The obtained SF films incorporated, negatively, the patterns from the master with accuracy (**Figure 3.6**).

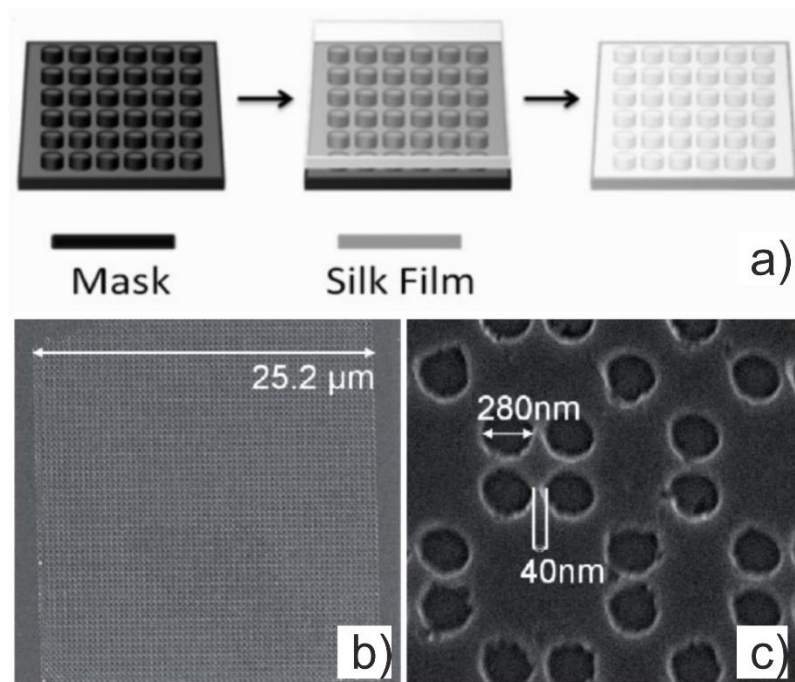


Figure 3.6. SF patterning by casting. a) Schematic procedure for the SF casting process. b) SEM image of the surface of a SF film with a periodic square pattern of air holes. c) SEM detail of a non-periodic decoration motif of air holes “printed” in a SF film. Images adapted from *Nano- and Micropatterning of Optically Transparent, Mechanically Robust, Biocompatible Silk Fibroin Films*.¹⁶⁰

A second approach to SF patterning, also indirect, is based on a rapid nanoimprinting of previously casted flat SF films. Nanoimprinting is a microfabrication technique where the patterns in a mould, this time of nanometric sizes, are transferred to the layer of interest after a short contact of both structures at a suitable temperature and pressure. Using again a previously designed and fabricated master, in 2010, Omenetto et al. demonstrated two ways of SF nanoimprinting (**Figure 3.7**).¹²² The SF glass-transition temperature depends on the adsorbed moisture of the films. For films prepared at ambient

humidity (~35%), the transition occurs at 100 °C, while for water saturated films the transition occurs at 25 °C. In those conditions, by applying a pressure of 50 psi with the master over a SF deposited on a glass slide, the master patterns were transferred to the film.

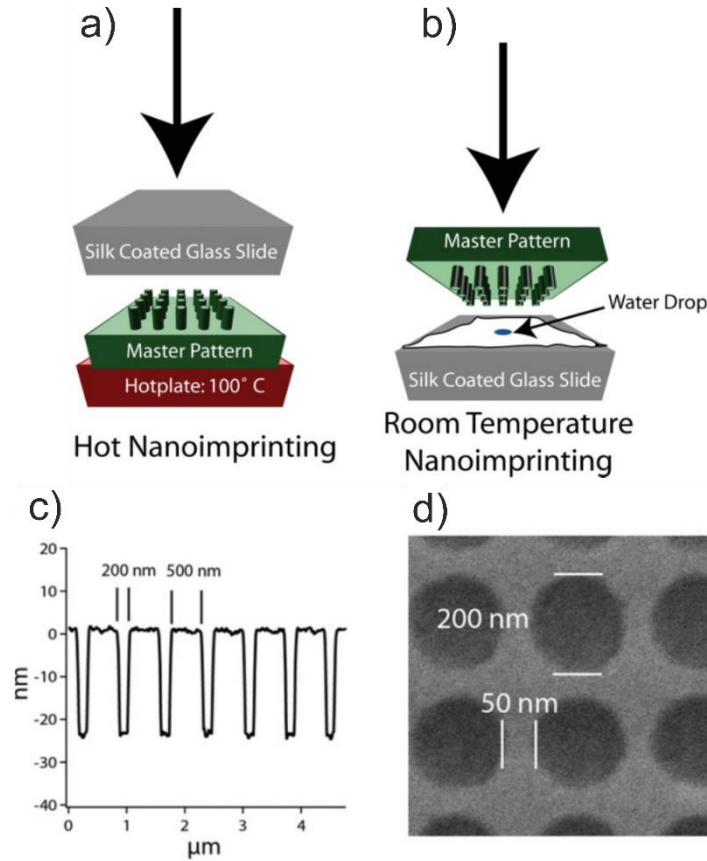


Figure 3.7. SF nanoimprinting processes: a) hot embossing and b) room-temperature embossing. c) Cross section of a periodic pattern imprinted in silk with 200 nm holes separated by 700 nm. d) SEM image of a silk film imprinted with a periodic array of 200 nm diameter, 30 nm height Cr nanocylinders separated by 250 nm. Images adapted from *Rapid Nanoimprinting of Silk fibroin Films for Biophotonic Applications*.¹²²

Photolithography has been also used in the patterning of SF layers. Conventional UV-lithography (light sources between 320 and 500 nm) cannot be directly used to pattern SF films but needs a chemical modification of the polypeptide chain, i.e. a photo-initiator. It was reported in 2013 by Yavadalli et al. a method to bond the 2-isocyanatoethyl methacrylate molecule to SF to yield a photocrosslinkable fibroin negative photoresist (FPP).¹⁶¹ Although good resolutions were obtained, the main disadvantage presented by

3. Fundamentals

the chemical modification is the use of organic solvents such as 1,1,1,3,3,3-hexafluoro-2-propanol (HFIP) due to the insolubility in water of the FPP. This fact, together with the direct exposure of FPP to UV light to provoke the crosslinking, limits seriously the incorporation of biomolecules such as antibodies or enzymes without losing their activity.

Alternatively, SF can be directly patterned by photo-lithography if using more energetic radiation at lower wavelengths. This possibility was explored by Kim et al., who reported in 2016 the use of annealed SF as positive photoresist employing a deep UV (DUV) source (ArF excimer laser) of 193 nm wavelength.¹²³ At this wavelength, as every polypeptide, SF shows great absorption. Actually, Fourier transformed infrared (FTIR) measurements of irradiated areas reveal a decrease in amides signals, what indicates a peptide bonding breakage. The irradiated areas can be removed by a simple water-washing step while the non-irradiated remain (**Figure 3.8**). Thus, the DUV photolithography of SF exhibits a perfect compatibility with biomolecules immobilization, as the patterning process does not disrupt their functionality.

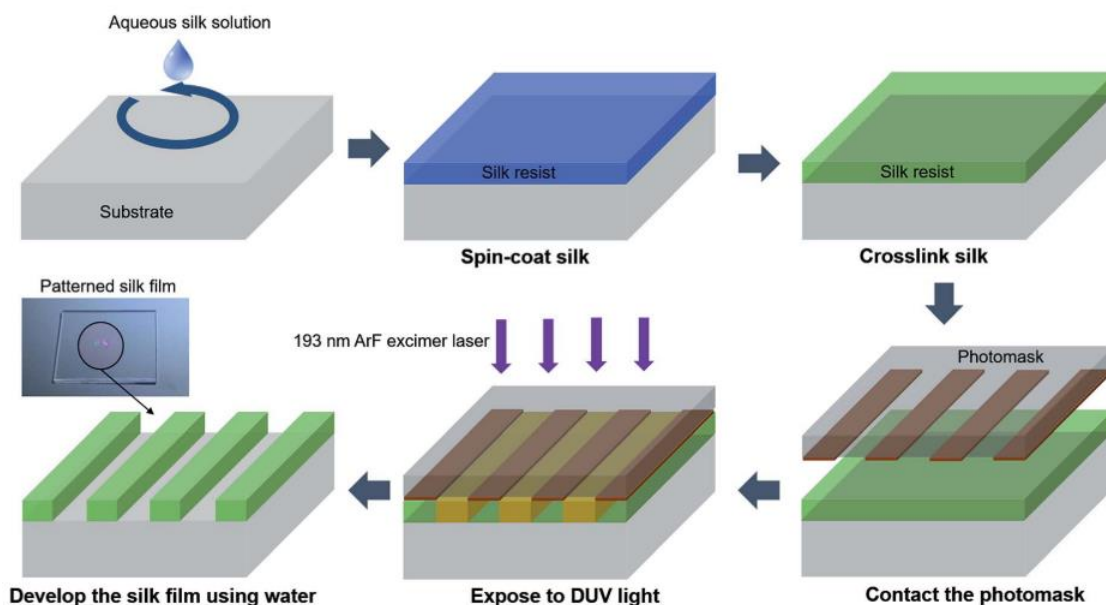


Figure 3.8. ArF excimer laser photolithography process to form high-resolution SF micropatterns. No photoinitiator material was used here, and water was the only chemical involved in this process. Images adapted from *Eco-friendly photolithography using water-developable pure silk fibroin*.¹²³

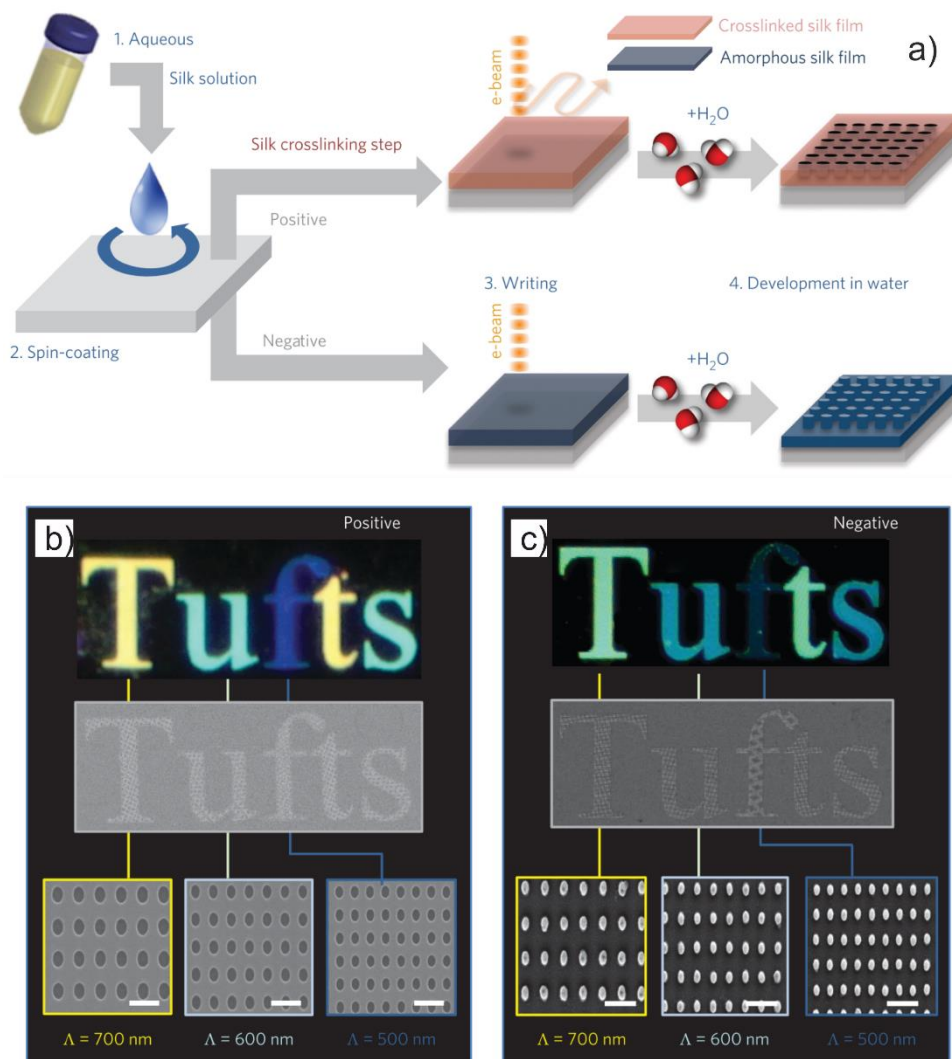


Figure 3.9. Scheme of SF e-beam lithography process (a). For positive resist work the film is crosslinked, but for negative resist, this step is skipped and the film is left in its uncrosslinked state. E-beam exposure on selected areas either crosslinks or de-crosslinks SF molecules. Water can then be used to wash away the water-soluble (uncrosslinked) areas. b, c) Dark-field and electron microscopy images of silk nanostructures generated on positive (b) and negative (c) resist. Each character is composed of a two-dimensional photonic crystal with different lattice constants (200-nm-diameter holes with centre- to-centre spacing of 500, 600 and 700 nm, as shown in the insets), thereby presenting different structural colours. Scale bars, 1 μm . Images adapted from *All-water-based electron-beam lithography using silk as a resist*.¹⁶²

Another strategy for direct patterning of non-modified SF is e-beam lithography. It was reported in 2014 by Omenetto et al. the use of spin coated SF both as negative or positive resist (**Figure 3.9**).¹⁶² If it is not annealed, the SF can be employed as negative

3. Fundamentals

resist using low e-beam doses ($\sim 2250 \mu\text{C cm}^{-2}$), what provokes the crosslinking of the material. After a final washing step with water, the irradiated areas remains while the still soluble non-annealed SF is dissolved (negative-like resist). Alternatively, the SF can be first annealed and then exposed to the e-beam. In this case, higher doses are needed ($\sim 25000 \mu\text{C cm}^{-2}$) to provoke the rupture of peptide bonds of SF. Finally, after a washing step, the irradiated areas are removed from the film (positive-like resist).

The direct e-beam lithography presents as main advantages the no need of chemical modifications of SF and the use of water as developer, thus maintaining an all water-based process. Additionally, especially when used as a positive resist where the final SF structure is not exposed to the e-beam, biological dopants such as antibodies or enzymes can be included in the SF matrix without further disruption during the processing.

Although e-beam offers very highly resolvable patterns and versatility for patterning arbitrary shapes, the technique results slow (consists of a SF substrate screening with the beam) and expensive (prolonged use of electron source filaments like tungsten shorten their lifetime).

3. Photo-electrochromic Molecules

In the search of novel enzymatic mediators, a class of molecules named photoelectrochromics are evaluated in the present thesis as substrates for the HRP with the intention of designing a photo-induced and photo-regenerable optical biosensor capable to measure multiple times and monitoring the analyte of interest.

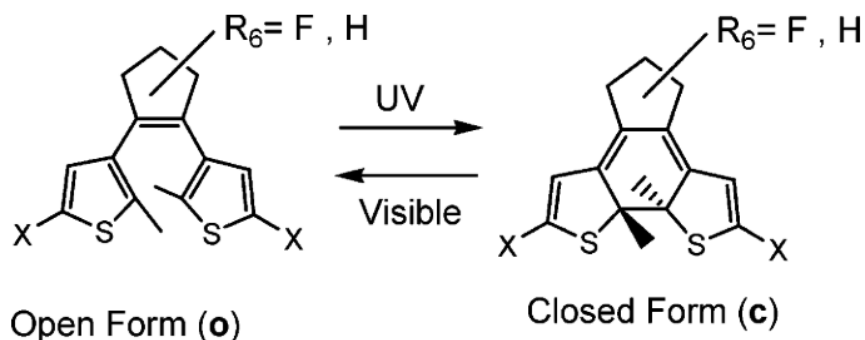


Figure 3.10. Open and closed forms of dithienylethene basic structure. Adapted from *Understanding Electrochromic Processes Initiated by Dithienylcyclopentene Cation-Radicals*.¹⁶³

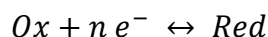
Photoelectrochromic molecules are characterized of being single molecular units that can undergo reversible isomerization by applying external stimuli such as light or electricity.¹⁶⁴ The compound color change is due to the large gap change between the highest occupied molecular orbital (HOMO) and the lowest unoccupied molecular orbital (LUMO) resulting from this UV-induced isomerization.

From the different photochromic families (spiropyrans, azobenzenes, photochromic quinones, etc.), dithienylethene are promising. First, because they show both photo- and electrochromic behaviour and second, due to the many substituents that can be introduced in the basic structure (**Figure 3.10**), what modulate the redox potential of the molecule until coupling with that of the redox molecule of interest.¹⁶³ Following this fact, the one that includes carboxylic substitutions, named DTE, is studied as enzymatic mediator due to the adequate redox potential and also because of its incremented solubility in water respect to the other substituted dithienylethenes.

4. Electrochemical Transduction Principles

Electrochemistry is the part of science dedicated to the study of chemical changes provoked by the transient of an electric current and, vice versa, the production of electrical energy by chemical reactions. Actually, it is a wide experimental area where many different phenomena are studied: metal corrosion, electrochromic displays, batteries, fuel cells or, as it is the case of this thesis, electroanalytical sensors.

Any electrochemical reaction of chemical species at the interface of an electrode with an electrolyte can be represented as:



where the species are either oxidized or reduced. The concentration of the oxidized [Ox] and reduced [Red] states of the species are in equilibrium with the cell potential E (V), following the Nernst equation:

$$E = E^{0'} + \frac{RT}{nF} \ln \frac{[Ox]}{[Red]}$$

3. Fundamentals

being E^0 the standard potential of the species (V), R the gas constant ($8.314 \text{ J mol}^{-1} \text{ K}^{-1}$), T the temperature (K), n the number of electrons involved in the reaction, and F the Faraday constant (96485 C mol^{-1}).

Electrochemical reactions are usually studied in the so-called electrochemical cells, where two or more electrodes are placed and the transport of charge across the interface between the electrode (electronic conductor or semiconductor) and an ionic conductor (electrolyte) occurs. The reaction takes place in the *working electrode* (WE) while the *reference electrode* (RE) is built of phases with a constant composition to maintain their potential fixed and serve as a standard (e.g. hydrogen electrode, saturated calomel electrode or silver-silver chloride electrode). A difference between the electrodes potential can be introduced by means of an external power supply (e.g. by a potentiostat). This variation can generate a current flow in the external circuit, because electrons cross the electrode/electrolyte interface as the reactions occur. In an electrochemical reaction, the relationship between the transient charge and the amount of product generated is ruled by *Faraday's law*:

$$m = \frac{QM}{nF}$$

where m is the mass of the generate specie at the electrode (g), Q is the electric charge passed through the electrode (C) and M is the molar mass of the substance (g mol^{-1}).

There is a distinction among faradaic and non-faradaic electrochemical processes, being the *faradaic* those in which the electron transfer through the interface provoke an oxidation or reduction while in the *non-faradaic* no-charge transfer reaction occurs but some events of absorption-desorption can be induced.

Respect to the type of cell, there is also a distinction between *galvanic* and *electrolytic* cells. While in the first, the current is generated by spontaneous reactions in the electrodes (converting chemical energy into electrical energy) in the second the reactions are induced by the application of an external voltage. Galvanic cells are composed essentially by an anode and a cathode while electrolytic cells commonly incorporated also the reference electrode for a better control of the applied potential difference. Reductions occur in the cathode (electrons cross the interface from the electrode to species in solution) and oxidations occur in the anode (electrons cross the

interface from species in solution to the electrode). The cathode and anode can be, alternatively, the working and the counter electrodes.

The reaction rate of an electrochemical reaction is given by:

$$i (A) = \frac{dQ (C)}{dt (s)}$$

$$\frac{Q (C)}{nF (C \text{ mol}^{-1})} = N (\text{mol electrolyzed})$$

being i the registered current in coulombs per second (A).

$$\text{Rate (mol s}^{-1}\text{)} = \frac{dN}{dt} = \frac{i}{nF}$$

Therefore, the reaction rate is directly proportional to the registered current in the working electrode. As electrochemical reactions are heterogeneous, taking place at the electrode-electrolyte interface, the reaction rate is usually described in reference to the electrode area:

$$\text{Rate (mol s}^{-1} \text{ cm}^{-2}\text{)} = \frac{i}{nFA} = \frac{j}{nF}$$

where j is the current density (in A cm⁻²).

In any electrode reaction, the reaction rate or current density is affected by several parameters such as:

- Mass transfer (from the bulk of solution to the electrode surface).
- Electron transfer at the interface.
- Chemical reactions happening before or after the electron transfer.
- Other events: Adsorption, desorption, electrodepositions, etc...

Every one of these events supposes an electrical resistance to the system that contributes to the cell resistance R .

In the electrochemical cell, a two-electrode configuration (WE – RE) is valid if the passage current is low (of the order of 1 nA) as well as the cell resistance R since these small currents- resistances do not affect the potential of the reference electrode. If the case of study implies different characteristics, a three-electrode cell is preferable. The current is, in this case, flowing between the working and the *auxiliary* or *counter electrode* (CE),

3. Fundamentals

whose electrochemical properties must not affect the behaviour of the electrode of interest (**Figure 3.11**).

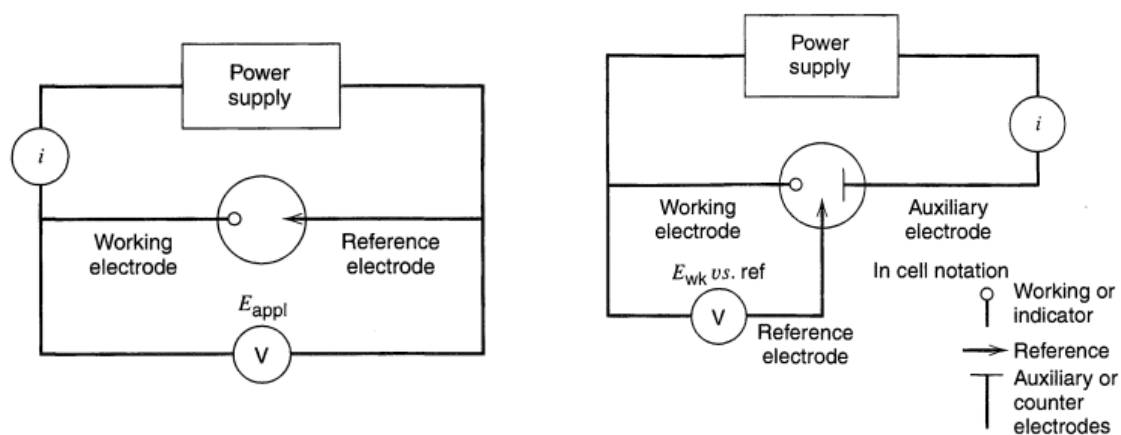


Figure 3.11. Two electrodes (left) and three electrodes (right) electrochemical cells. Adapted from *Electrochemical Methods. Fundamentals and applications*.¹⁶⁵

Cyclic voltammetry

Cyclic voltammetry is one of the most common electrochemical techniques in the study of electrochemical systems. In a cyclic voltammetry (CV), a variable potential (E) is applied between the WE and the RE while the response current is measured (i) between the WE and the CE. Calling the Nernst equation, if a potential $E = E^{0'} \approx E_{1/2}$ is applied to a solution of an oxidized compound (Ox), this will be reduced until balancing the concentration of oxidized and reduce molecules $[\text{Ox}] = [\text{Red}]$. At the same time, during the potential sweep characteristic of CVs, the ratio of $[\text{Ox}]/[\text{Red}]$ molecules in solution close to the electrode changes in accordance to the Nernst equation.

In a CV, as the potential is scanned anodically (from lower to higher values) from A to D (**Figure 3.12**), the reduced compound is oxidized completely near the electrode. At point C, where the anodic peak is observed, the current depends on the delivery of additional reduced compound to the electrode from the bulk solution. The amount of oxidized compound nearby the electrode is increasing with the scan, increasing therefore the diffusion layer, what slows down the diffusion of reduced molecules. This is why the current decreases as the scan continues, from C to D:

$$I = n F J(c_X)$$

where J is the analyte flow to the electrode, which is a function of the analyte concentration (c_X). The process is carried out inversely, from D to G, provoking reduction of the previously oxidized molecules.

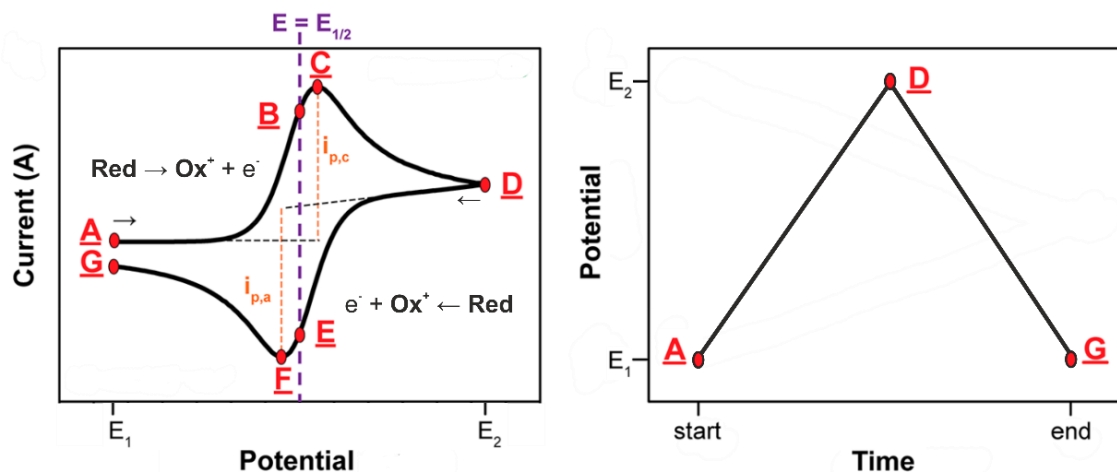


Figure 3.12. Cyclic Voltammetry. Typical “duck” shape of a cyclic voltammetry (left) of a reversible specie by applying a sweep potential from A to D and back to G (right). Adapted from *A Practical Beginner’s Guide to Cyclic Voltammetry*.¹⁶⁶

At points B and E, the concentration of oxidized and reduced compound at the electrode surface is the same, following the Nernst equation: $E = E_{1/2}$. This value corresponds to the half-wave potential between the anodic (C) and cathodic (F) peaks and provides a straightforward way to estimate the E^0 for a reversible electron transfer.¹⁶⁶

Amperometry

In an amperometric measurement, the applied potential between the working and the reference electrode is set at a fixed value, while the electric current is measured between the working and the counter electrode over time. Amperometry is an interesting analytical technique because it is possible to correlate the registered current density j with the presence of a certain analyte nearby the electrode by the oxidation or reduction of the latter at a suitable applied potential. The potential needed to provoke the oxidation ($E > E_{1/2}$) or reduction ($E < E_{1/2}$) of those molecules is usually obtained by CV studies of the analyte in the medium of analysis.

5. Optical Spectroscopy

In any spectroscopic technique, the interaction between an electromagnetic radiation (**Figure 3.13**) and the interrogated sample is studied, usually due to the specific extinction/emission by substances from the sample. Extinction mechanisms are mostly associated to scattering, when the light/matter interaction results in the absorption and re-emission of light in all directions, or absorption processes, when the light, after being absorbed by the molecule, is mostly internally attenuated, e.g. as thermal energy. This absorption can be detected directly or indirectly (by secondary emissions from the material). It is one of the broadest characterization techniques, as it employs (from more to less energetic) gamma rays, X-rays, ultraviolet, visible, infrared, microwave and radio waves irradiation, depending on the nature of the sample and the sought information.

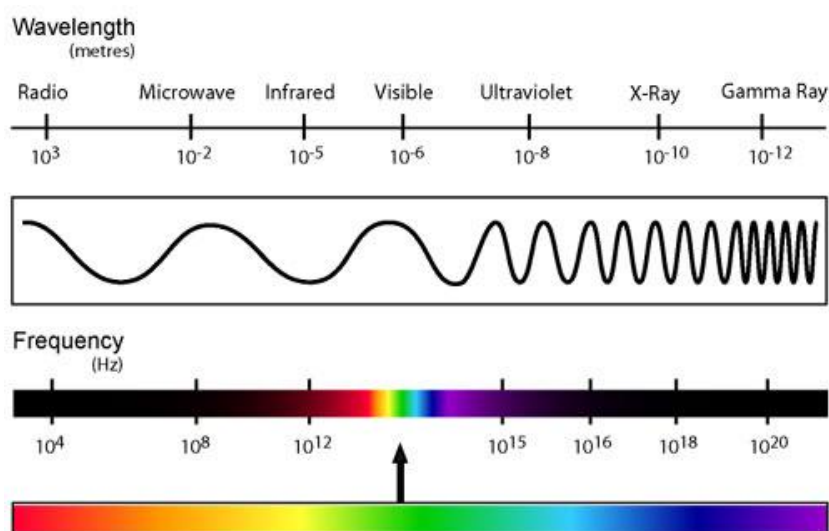


Figure 13. Electromagnetic spectrum.

UV-Vis spectroscopy

UV-Vis spectroscopy refers to the evaluation of the electromagnetic radiation in the wavelength range between 280 and 800 nm, which corresponds to the range detectable by the bare eye (i.e. the eye has receptors sensitive to the radiation in this range). For this reason, molecules susceptible to be interrogated by this technique are colored (capable to absorb light at a selective wavelength) or dispersing (able to scatter light).

Molecules that contain either bonding or non-bonding electrons can absorb UV-Vis irradiation by exciting these electrons to higher anti-bonding molecular orbitals. As a rule,

energetically favoured electron promotion will be from the highest occupied molecular orbital (HOMO) to the lowest unoccupied molecular orbital (LUMO). In the energetic range of UV-Vis radiation, only $n\text{-}\pi^*$ and $\pi\text{-}\pi^*$ transitions are permitted (**Figure 3.14a**).

While in atoms the electronic transitions result in very narrow absorbance bands at very characteristic wavelengths (spectral lines), in molecules vibrational and rotational energy levels are superimposed on the electronic energy levels (**Figure 3.14b**). Therefore, the absorption bands are broadened as many transitions with different energies can occur.¹⁶⁷

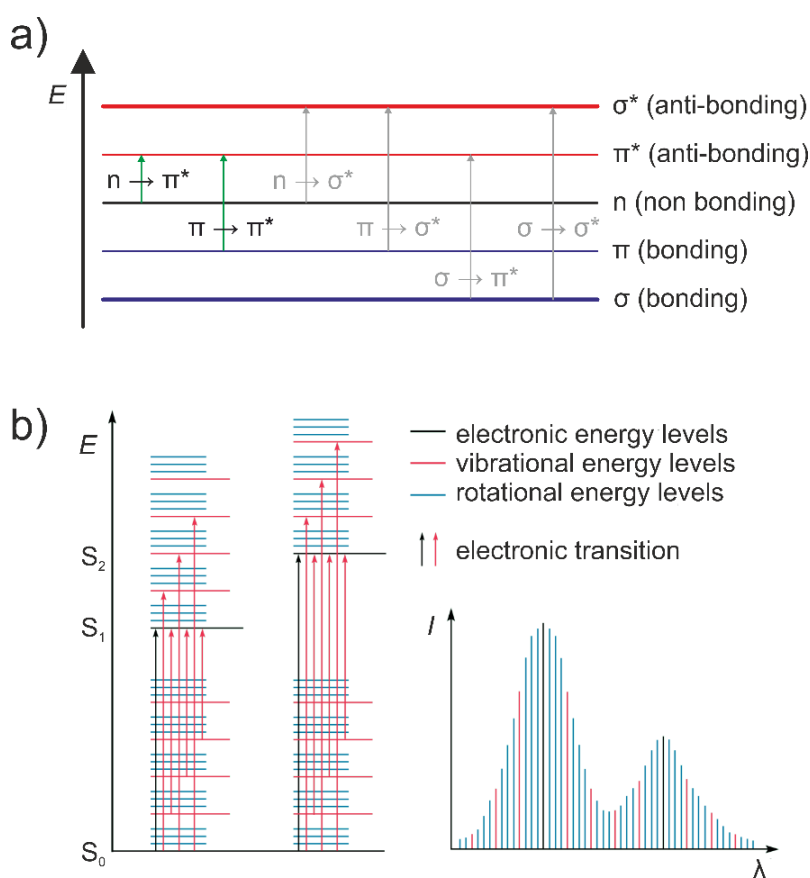


Figure 3.14. Molecular electronic transitions from lower to higher energetic (a). In black, those permitted for visible light irradiation. Absorbance spectrum association to electronic transition and associated vibrational and rotational levels (b). Adapted from *Fundamentals of UV-Visible spectroscopy*.¹⁶⁷

If the electronic transition is energetically possible to happen, some of the incident radiation on the sample will be absorbed as the electrons promote to a more energetic orbital. Therefore, there is a difference in the intensity between the incident and the

3. Fundamentals

measured irradiation from the sample. The amount of light absorbed is expressed as transmittance (T) or absorbance (A):

$$T = \frac{I}{I_0}$$

$$A = -\log T$$

where I_0 is the incident light intensity and I is the transmitted or reflected light after the interaction with the sample.

The Beer-Lambert law relates the absorbance of a sample with the concentration of a specie at a certain wavelength:

$$A = \varepsilon l c$$

where ε is the molar attenuation coefficient of absorptivity ($\text{M}^{-1} \text{cm}^{-1}$) of the sought specie, l is the optical path length (cm) and c is the concentration of the specie (M). Maintaining the structure of the measured sample unaltered (constant l) and being ε specific for a certain analyte at a certain wavelength, it is possible to correlate absorbance value at that wavelength with the concentration of the analyte.

4. Objectives

In this chapter, the main objectives of this thesis are exposed.

4. Objectives

The main objective of the present thesis is the development of long-life enzymatic biosensors based on the use of biomaterials of natural origin, i.e. alginate and silk-fibroin, as main components of the biocatalytic membrane. The hypothesis behind this thesis is that biomaterials, due to their composition and water content, may provide a more physiological environment to biomacromolecules, e.g. enzymes, increasing their stability and the durability of the biosensor. To achieve this ambitious aim, the following specific objectives have been envisioned:

1. Production of alginate hydrogels and SF biocatalytic membranes with size-exclusion capacity for glucose biosensing in whole blood samples.
2. Production of a reversible electrodeposition-removal protocol, and point-of-care system, based on alginate hydrogels for the in situ selection of the analyte of interest.
3. Integration of enzymatically-doped SF layers in the production of glucose test strips and optical fiber-based biosensors for quantitative determination of glucose concentration.
4. Development of new enzymatic photo-electrochromic mediators and their application in the development of reversible optical biosensors.

5. Materials and Methods

This chapter contents a summary of used reagents and employed instrumentation, techniques and processes that, being essential for the present thesis development, do not suppose an intrinsic innovation of the state of the art and/or are shared among the different results chapters. Therefore, they are here included in pursuit of clarifying the basis of the previously presented results avoiding redundancy.

1. List of Reagents and Materials

All chemicals used in this thesis are grouped in the following list. All of them were used as received without additional purification protocols, unless it stated. Aqueous solutions were always prepared using de-ionized water with a resistivity of 2 M Ω cm.

2-(N-morpholino)ethanesulfonic acid hydrate (MES hydrate, Sigma Aldrich, ≥ 99 %)

3,3',5,5'-Tetramethylbenzidine (TMB, Sigma Aldrich, ≥ 98 %)

Acetic acid (Sigma Aldrich, ACS reagent, ≥ 99.7 %)

Alginic acid sodium salt (Sigma Aldrich)

Calcium carbonate (CaCO_3 , Panreac, ≥ 98.5 %)

Calcium chloride (CaCl_2 , Sigma Aldrich, ≥ 93 %)

Citric acid anhydrous (Panreac, 99.5 %)

D-(+)-Glucose (Sigma Aldrich, ≥ 99.5 %)

Dimethyl sulphoxide (DMSO, Panreac, 99.5 %)

Disodium phosphate (Na_2HPO_4 , Panreac, ACS reagent, ≥ 99 %)

Ethanol absolute (Panreac, ≥ 99.5 %)

Fetal bovine serum (FBS, Capricorn Scientific).

Glucose oxidase from *Aspergillus niger* (GOx, Sigma Aldrich, Type X-S, lyophilized powder, 100-250 units mg^{-1})

Hydrochloric acid (HCl, Panreac, ACS reagent, 37 %)

Hydrogen peroxidase from horseradish (HRP, Sigma Aldrich, Type VI-A, essentially salt-free lyophilized powder, 250-330 units mg^{-1})

Hydrogen peroxide (H_2O_2 , Sigma Aldrich, 30% in H_2O)

Imidazole (Panreac, ACS reagent, 99 %)

L-(+)-tartaric acid (Fluka, ≥ 99 %)

Lactate oxidase from *Pediococcus* sp. (LOx, Sigma Aldrich, lyophilized powder, ≥ 20 units mg^{-1})

Lithium bromide (LiBr, Sigma Aldrich, $\geq 99\%$)

Monopotassium phosphate (KH_2PO_4 , Fluka, ACS reagent, $\geq 99.5\%$)

Nitric acid (HNO_3 , Sigma Aldrich, $\geq 69\%$)

Potassium chloride (KCl, Fluka, $\geq 99\%$)

Potassium ferricyanide ($\text{K}_3[\text{Fe}(\text{CN})_6]$, Panreac, ACS reagent, $\geq 99\%$)

Potassium ferrocyanide ($\text{K}_4[\text{Fe}(\text{CN})_6]$, Sigma Aldrich, ACS Reagent, $\geq 98.5\%$)

Potassium hydroxide (KOH, Sigma Aldrich, $\geq 86\%$)

Rhodamine 6G (Sigma Aldrich)

Silver nitrate (AgNO_3 , Sigma Aldrich, $\geq 99\%$)

Sodium L-lactate (Sigma Aldrich, $\sim 98\%$)

Sodium acetate anhydrous (Panreac, ACS reagent, 99%)

Sodium carbonate (Na_2CO_3 , Sigma Aldrich, $\geq 99.5\%$)

Sodium chloride (NaCl, Sigma Aldrich, ACS reagent, $\geq 99\%$)

Sodium hydroxide (NaOH, Sigma Aldrich, $\geq 98\%$)

Sulfuric acid (H_2SO_4 , Panreac, 96%)

Tetramethylammonium hydroxide solution (TBAOH, Sigma Aldrich, 1 M in methanol)

Trisodium citrate dihydrate (Sigma Aldrich, USP testing specifications)

Additional reagents and materials are detailed below:

Phosphate buffered Saline (PBS) solution contained NaCl (8 g L^{-1}), KCl (0.2 g L^{-1}), Na_2HPO_4 (1.42 g L^{-1}) and KH_2PO_4 (0.24 g L^{-1}).

TMB 50 mM stock solution was daily prepared using DMSO as solvent.

Whole blood samples were extracted from either a volunteer or C57BL/6 male mice and stored at 4°C until measurement.

Screen-printed gold electrodes (SPGEs, Dropsens, 220BT) with a Au working and counter electrodes and Ag pseudo-reference electrode were purchased from Dropsens.

Polydimethylsiloxane (PDMS) was purchased from Sylgard. PDMS preparation was performed following the instruction of the supplier and cured at 80°C for 20 minutes. PDMS patterning was performed by laser ablation.

PMMA foils of different thicknesses were purchased from Goodfellow and clear polyester double-sided adhesive tape from ARcare. The adhesive is MA-93 acrylic medical grade, also known as pressure sensitive adhesive (PSA).

2. Alginate

2.1. Equipment for biosensing

2.1.1. Electrochemical measurements

For electrochemical measurements of the SPGEs, a Dropsens μ STAT8000 potentiostat controlled with Dropview 8400 software was used. For silicon chip electrodes, an Autolab electrochemical workstation (PGSTAT-100 potentiostat - galvanostat, Ecochemie, Utrecht, The Netherlands) controlled using a PC with NOVA software was used.

Electrodepositions of Ag and chlorination were performed using a Keithley 2430 1 kW pulse Source Measure Unit and a Watson Marlow peristaltic pump to maintain a constant flow of the reactants.

In case of DTE electrochemical analysis, cyclic voltammetry experiments were performed using a BioLogic potentiostat (VSP100) controlled with EC-Lab V9.51 software. The measurements were performed in a conical electrochemical cell using a glassy carbon disk ($\phi=0.5$ cm) as a working electrode, Pt wire as a counter electrode and Saturated Calomel Electrode as reference electrode. $2.5 \cdot 10^{-3}$ M DTE solutions were prepared in 0.01 M PBS aqueous solution (pH 7).

2.2. Alginate characterization techniques.

2.2.1. Profilometry

For profilometry measurements, an optical profilometer pL μ 2300 from Sensofar controlled with PL μ Confocal Imaging Profiler was used.

2.2.2. Imaging

The images of alginate hydrogels and PMMA constructions were acquired with a digital microscope camera DigiMicro 2.0 Scale.

2.3. Fabrication and Prototyping

In the following paragraphs, the processes, technologies and protocols employed in the fabrication of each component of the final prototype are described in detail.

2.3.1. Silicon chips – microfabrication technology

Silicon chips were manufactured through thin-film microfabrication technologies in the Clean Room facilities at IMB-CNM. This manufacturing strategy provided high precision, stability, durability and reproducibility of the components, and possibility to scale for mass production. Electrochemical transducers were produced with this technology, which enable the use of these electrodes many times thanks to its stability and durability, without losing activity. The design of the chip included four rectangular platinum electrodes corresponding to the working (WE; two working electrodes), reference (RE) and counter electrodes (CE), this last one with a larger area to avoid charge transfer limitations. The electrodes in the chip were connected to independent pads of big size to facilitate the external connection to the potentiostat through spring-loaded connectors.

The four electrode silicon chips were fabricated through a well established lift-off process (**Figure 5.1**), by a protocol previously described by our group and in collaboration with Dr. Pablo Giménez and Dr. Angel Merlos.¹⁶⁸ Briefly, a silicon wafer was exposed to thermal oxidation to obtain a first SiO₂ layer of 1000 nm. Afterwards, a photoresist was spread over the oxidized wafer by spin coating and cured by UV irradiation developing only the SiO₂ areas for metal covering. Two metal layers were subsequently deposited by e-beam evaporation, namely a 25 nm layer of Ti to enhance the adhesion of Pt, and the Pt layer of 150 nm. The photoresist was then removed by immersion in acetone and, therefore, the metal over it (lift-off), while the metal directly deposited on the wafer remained, comprising the electrodes, connections and pads.

A subsequent step for electrodes protection was performed consisting of a first 600-700 nm SiO₂ deposition by PECVD, which covered the electrodes. After that, a layer of photoresist was spread, cured and developed, allowing the wet etching of an

area over the metal using buffered hydrofluoric acid solution. These steps avoided the direct exposure to the solution of the edges of the electrodes, increasing their robustness and durability. In the end, the excess of photoresist was removed with acetone.

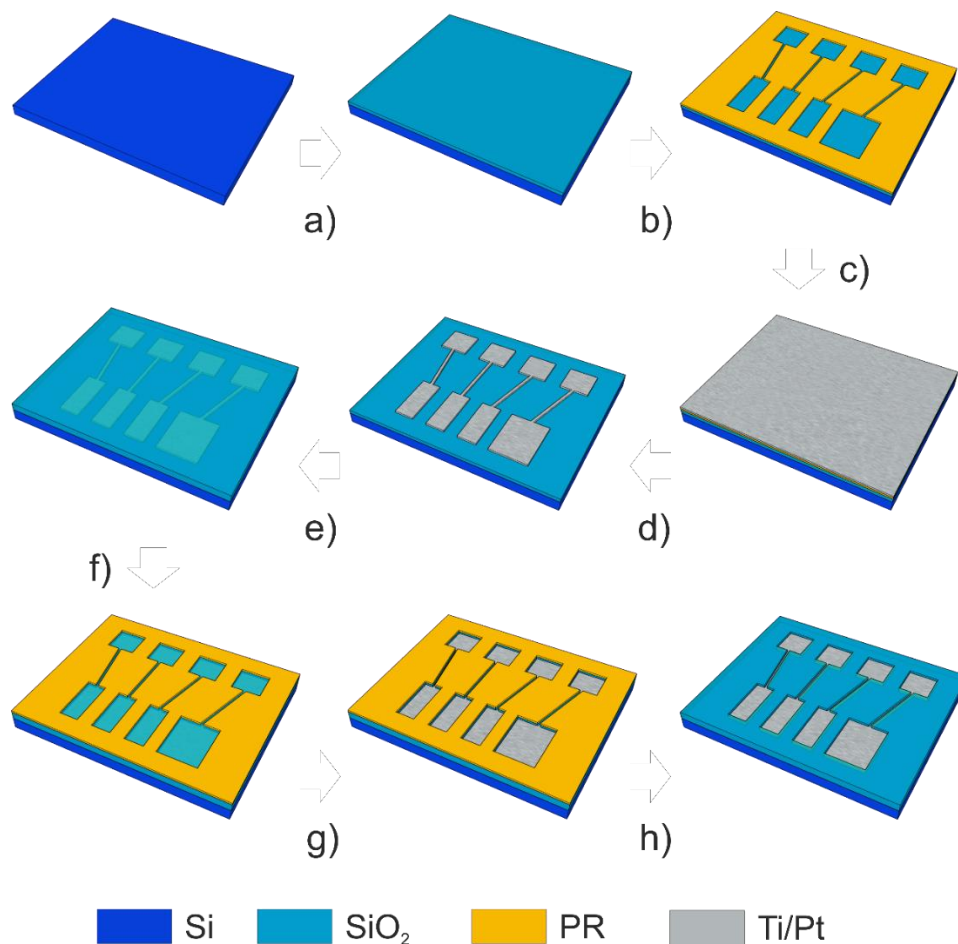


Figure 5.1. Steps for microelectrodes fabrication from a silicon wafer. a) The shallow Si is oxidized thermally to form a SiO₂ layer. b) A layer of photoresist is spin coated over the SiO₂ and the electrodes pattern is revealed. c) A first layer of Ti and a second layer of Pt are deposited by e-beam evaporation. d) The photoresist is dissolved using acetone and the metals over it are detached (lift-off). e) A passivation layer of SiO₂ is deposited by PECVD and f) the photoresist pattern is revealed again over it. g) The exposed SiO₂ is attacked by HF and h) the remaining photoresist is removed. The layers thicknesses are not in scale.

Ag/AgCl reference electrode

The reference electrode in the silicon chip was modified to provide with a stable potential for long times. With this aim, the following electrodeposition/chlorination protocol¹⁶⁹ was used to produce a Ag/AgCl pseudo reference electrode. Before Ag

electrodeposition, the electrode was cleaned with 96 % ethanol, 6 M H₂SO₄ and finally immersed in 50 mM KOH and 25 % H₂O₂ solution for 15 min to eliminate any contamination of the surface. The silicon chip was then introduced in an electrodeposition chamber (Figure 5.2) containing a second silicon chip in front of the previous one and separated at a distance of 1 mm to make the electrodeposition process more homogeneous. The electrodeposition of the Ag layer was done galvanostatically while a constant flow of tartaric acid and AgNO₃ solution was passed through the chamber. After Ag deposition, the Ag layer was partially chloritized, also galvanostatically, with a solution of KCl and HCl passing through the chamber.

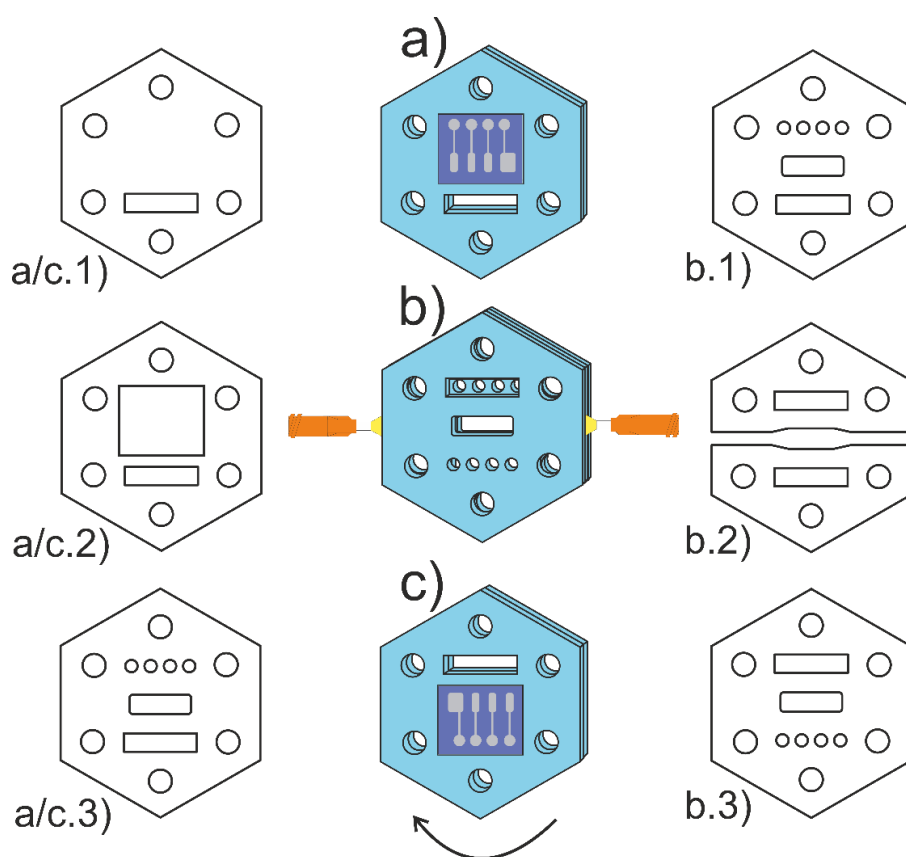


Figure 5.2. Three main parts of the electrodeposition setup: a) Chip 1 holder piece, b) chamber and channel piece and c) chip 2 holder piece. Notice that piece b) would be mounted over piece a) and piece c) over piece b) after flip it 180°. A PDMS layer with the exact shape of a/c.3) for a-b and b-c junctions must be included to avoid any liquid leakage. From a/c.1) to a/c.2) represents the scheme of the PMMA layers that conform pieces a) and c) while from b.1) to b.3) represents the scheme of the PMMA layers that conform piece b). Employed thicknesses are: 0.5 mm for a/c.2, a/c.3, b.1 and b.3; 1 mm for b.2 and 2 mm for a/c.1.

Obtained reference potential was comparable to those supplied by commercial reference electrodes, i.e. external reference (Orion 92-02-00, Thermo Fisher Scientific Inc., Beverly USA). The potential shift between the commercial and the fabricated Ag/AgCl electrode was only of 25 mV while the shift, in case of using the bare Pt electrode as reference, was situated at 180 mV (**Figure 5.3**).

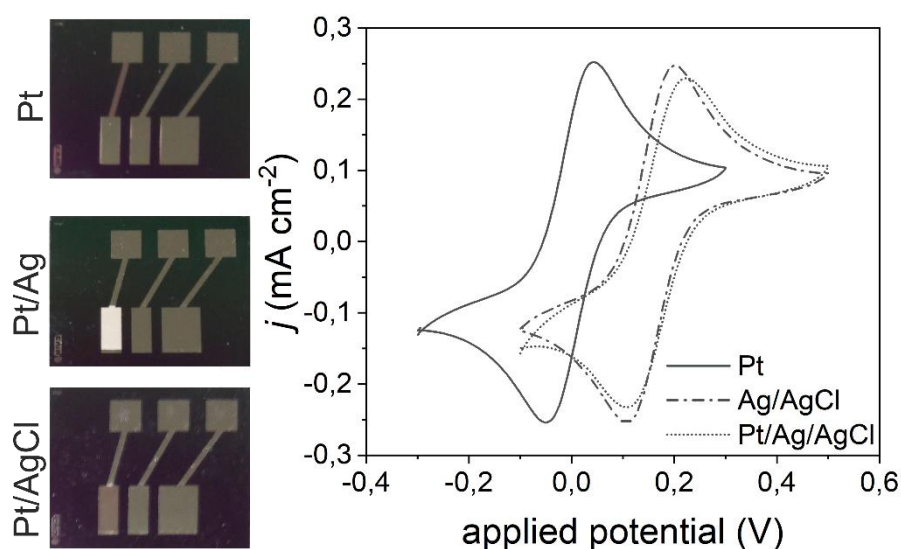


Figure 5.3. Ag and Cl electrodeposition on the Pt to fabricate a pseudo-reference Pt/Ag/AgCl electrode, and comparison with a commercial glass Ag/AgCl reference electrode.

The integrated pseudo-reference electrode demonstrated long-term stability and durability, supplying the same potential over time at least for 2 months, values that were completely comparable to the commercial one.

2.3.2. Microfluidic elements – Fast prototyping

Microfluidic elements were manufactured in the polymers PMMA and PDMS. The patterning and processing of the polymers was done using an Epilog Mini 24 Laser by CO₂ laser ablation. For the designs, Corel Draw X7 software was used. The patterning of PMMA foils was used to construct, layer by layer, a device with the silicon chip footprint and microfluidic channels and connections for (i) fluid management, (ii) stable and robust electrode packaging and (iii) the isolation of the pad connectors.

The construction of the microfluidic structure resulted from the assembling of three parts, namely I) the base, III) the microfluidic part and V) the cover (**Figure 5.4**).

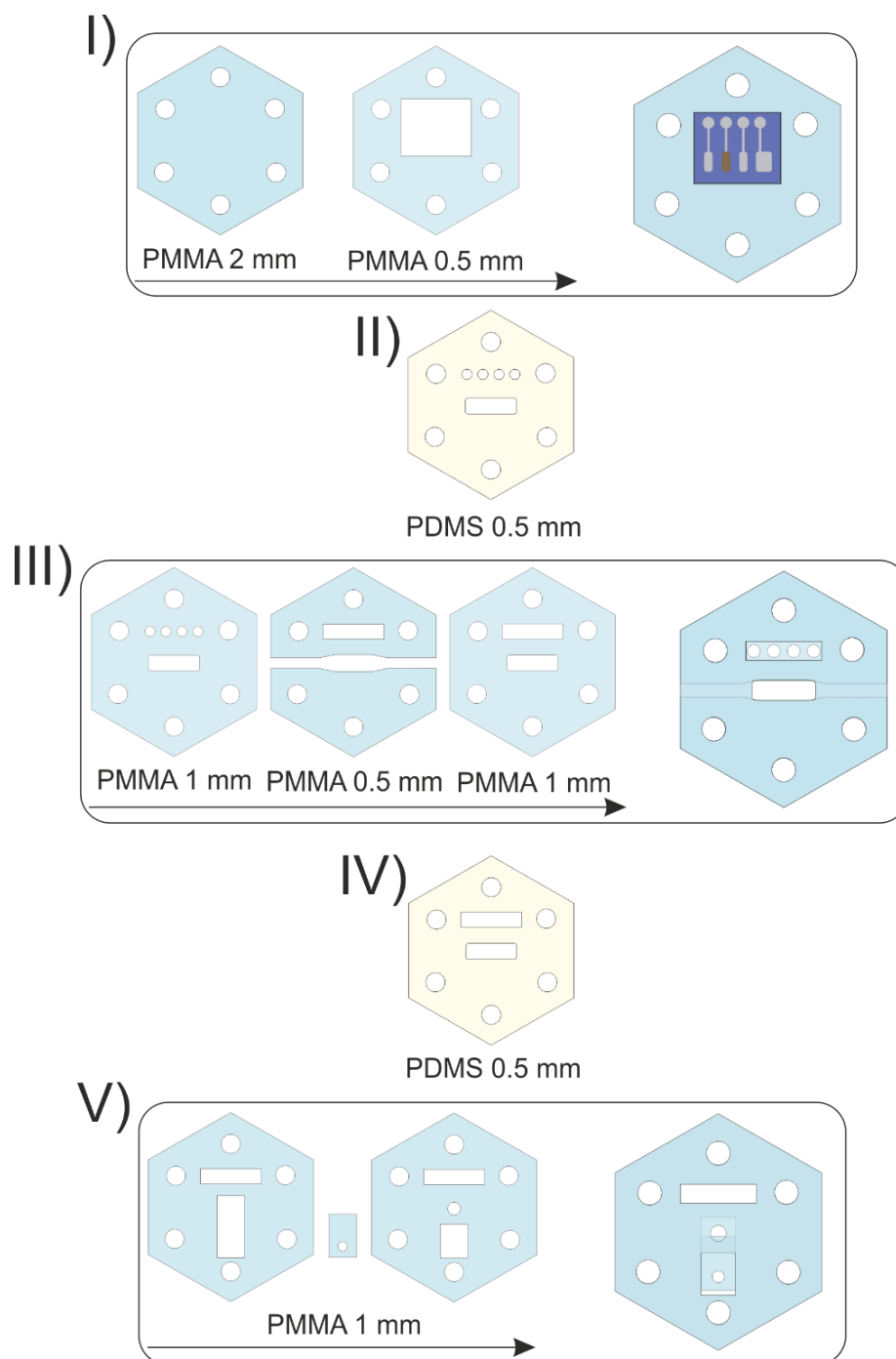


Figure 5.4. PMMA structure for whole blood analysis. Three PMMA blocks conform the device: I) electrodes holder, III) channel chamber and V) top with access for real samples. Between the blocks, PDMS pieces II) and IV) are included to prevent any leakage. Finally, the structure is closed with screws and the electrodes are contacted by spring-loaded connectors.

Each one of these parts was composed of two or more PMMA layers bonded through PSA. The base contained two PMMA layers, a 0.5 mm PMMA layer patterned

5. Materials and Methods

with the chip footprint to stably immobilize the silicon piece, and a 2 mm layer used as support. Over the base, the microfluidic part contained all the microfluidic elements for liquid management. This part was composed of three PMMA layers: the intermediate layer (1 mm thick) comprising the channels and the measurement chamber, and two adjacent layers (0.5 mm thick each) sealing the channels but not the measurement chamber. Finally, the cover was positioned over the microfluidic part to seal the system. This part included a movable PMMA element with a small aperture for opening-closing the access to the measurement chamber. This element enabled a dual filling mechanism of the measurement chamber. On the one hand, when closed, the measurement chamber could be filled through the fluidic inlet without leakage (**Figure 5.5**). When opened, it allowed the introduction of small sample volumes directly to the measurement chamber and the transducers, avoiding dead volumes and enabling to work with small sample volumes. This second operation mechanism was of particular interest in the case of blood samples, where, for practical applications, the sample volume was restricted to a blood drop of few μL .

The three parts were finally assembled using screws and PDMS layers as junctions to avoid fluid leakage (layer II and IV in **Figure 5.4**). Two fluidic connections were introduced and bonded to the fluidic channels corresponding to the fluidic inlet and outlet of the device. The fluidic connections were sealed with epoxy resist.

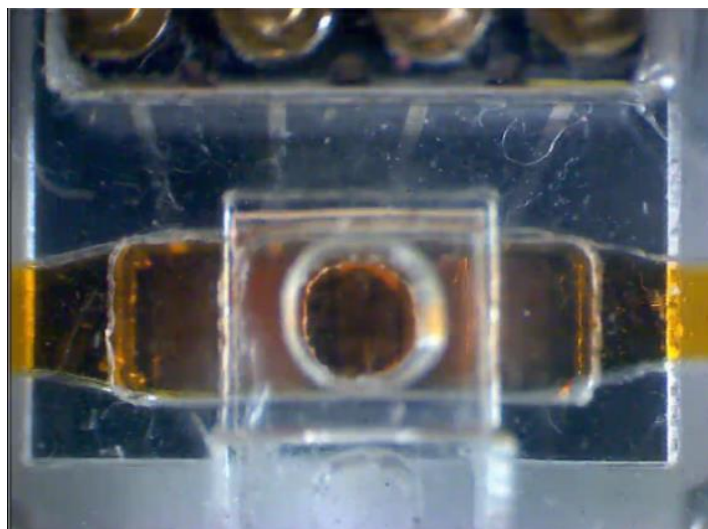


Figure 5.5. Gate for real sample addition. Photograph of the closed access to the chamber while a colored aqueous solution is flowing through.

2.3.3. Smartphone-interfaced μ Potentiostat

A custom made potentiostat was developed resembling that described in our previous publication¹⁷⁰ (**Figure 5.6**). It was designed to execute the following basic functions: (i) to operate the sensor in potentiostatic mode, (ii) to read the transduced signal, (iii) to convert it into the digital domain and (iv) to provide the data link through USB on-the-go protocol. In this way, bidirectional data transmission and powering of the system was provided avoiding the use of batteries.



Figure 5.6. Picture of the potentiostat fabricated in collaboration with ICAS group of IMB-CNM.¹⁷⁰

All these functions were implemented adding few discrete electrical components to the LOC, and ensuring the low cost, small size, simplicity and lightweight of the POC system. The minimalistic electronic design only required one standard microcontroller (ATMega32U4), two operational amplifiers (AD4692), resistors and capacitors. The combination of all these components implemented an analog-to-digital delta-sigma converter with tuneable read-out range between 1nA to 100 μ A. The potentiostatic system enabled two operation modes, namely chronoamperometry, used for analyte detection, and cyclic voltammetry, this required for membrane electrodeposition. In both cases, the potential voltage was programmed between +/- 1.65 V. In the cyclic voltammetry mode, the scan rate was adjusted between 2 to 200mV/s.

2.3.4. Electrodeposition of alginate hydrogels

Electrodeposition of calcium alginate hydrogels was optimized by considering the magnitude of the applied current and the duration of the electrodeposition step. The

5. Materials and Methods

proposed mechanism¹⁰² consists of the rupture of CaCO_3 particles due to the protons generated by water electrolysis and the subsequent cross-linking reaction between different alginate molecules by Ca^{2+} ions (**Figure 5.7**).

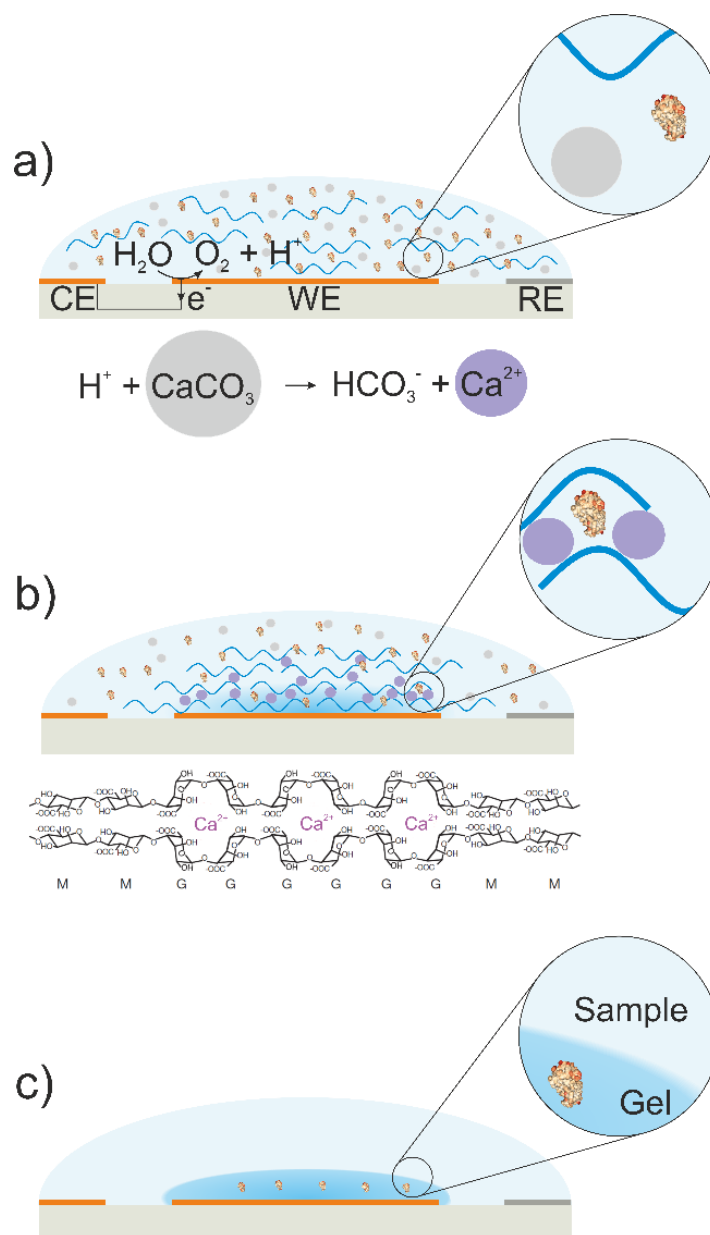
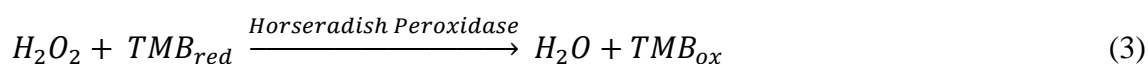
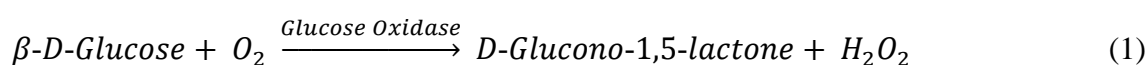


Figure 5.7. Cross section scheme of the biosensor for different steps of the alginate hydrogel electrodeposition: a) A solution containing sodium alginate (blue curly lines), CaCO_3 and enzymes of interest is dropped over the transducer and an anodizing current of $100 \mu\text{A}$ is applied to the working electrode to liberate protons that dissolve the CaCO_3 particles. b) The released Ca^{2+} cations react with the alginate monomers in a cross-link reaction among the G-blocks of this copolymer. c) When the hydrogel is formed, the transducer is rinsed with distilled water to discard the precursor. Finally, only the hydrogel remains attached to the working electrode, retaining the enzymes.

The precursor composition was fixed at 1 % w/v of sodium alginate, 0.5 % w/v of CaCO₃ and different enzyme concentrations (only HRP in case of H₂O₂ biosensor and HRP-GOx in case of glucose biosensor). According to bibliography¹⁷¹, the random distribution of the two enzymes within the hydrogel should not affect the performance of the biosensor.

2.4. Glucose and lactate determination

The selected enzymes for the development of the biosensors, i.e. GOx (1), LOx (2) and HRP (3), catalyse the following reactions:



The oxidized form of TMB (TMB_{ox}) was reduced electrochemically on the working electrode of the biosensor, recording a negative current. The intensity of this negative current was proportional to the initial quantity of H₂O₂ present in the sample. This hydrogen peroxide concentration could be produced by a second enzyme, e.g. GOx or LOx. In this second scenario, the negative current would be directly proportional to either the glucose (in the case of GOx) or the lactate (by LOx) concentration in the medium. The detection potential *versus* Ag pseudo-reference electrode was selected from a cyclic voltammetry of TMB and set at 0.1 V (below the reduction potential).

For drop measurements in the preliminary characterization of alginate sensing membranes, 50 μL droplets (including sample, buffer and mediator) were deposited on the biosensors ensuring the complete coverage of the three electrodes. In the case of real samples (plasma and whole blood), 40 μL of sample were mixed with 2 μL of 50 mM TMB and 8 μL of glucose solution in water at different concentrations yielding to different final glucose concentrations. Due to diffusion limitations, 2 minutes were established as incubation time prior to measurement to ensure the stability of the recorded signal. For direct H₂O₂ measurement, the reaction rate was so fast that incubation was not necessary.

5. Materials and Methods

In case of PMMA prototype, a constant current was recorded while the buffer was flowing through the chamber without analyte. Then, when a known concentration of the analyte of interest was added into the measurement chamber, a fall in the current was registered (**Figure 5.8**).

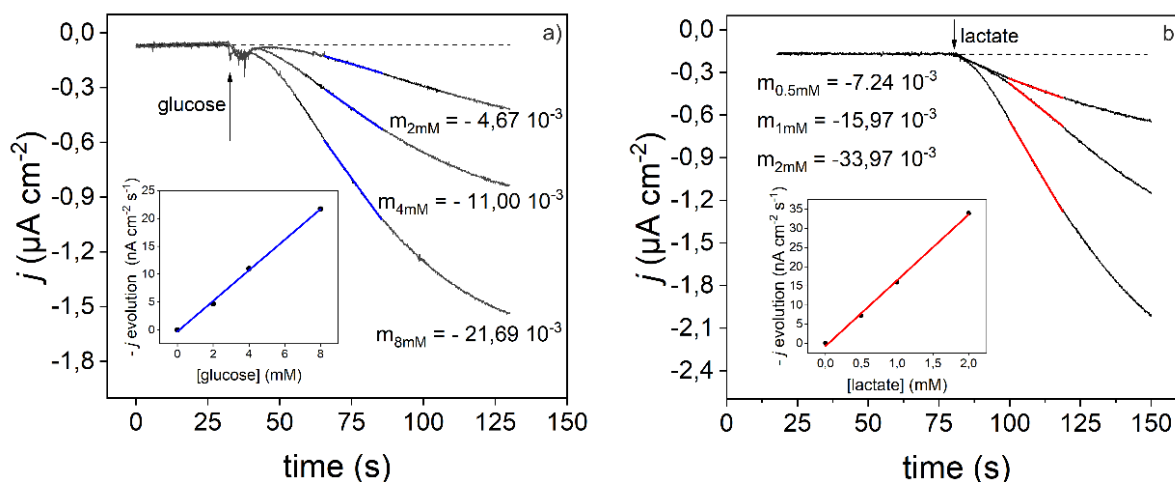


Figure 5.8. Instantaneous response of the biosensor to the addition of analytes: glucose (a) or lactate (b). The registered negative current is product of the reduction previously oxidized TMB and therefore proportional to the amount of analyte present in the sample. Medium: 200 mM MES-NaOH pH 7, 145 mM KCl, 100 mM CaCl_2 and 2 mM TMB. Applied potential: 0.1 V vs. pseudo reference Ag/AgCl electrode.

In the case of fetal bovine serum (FBS), whole blood analysis and real samples, the open-close access to the measurement chamber was used in order to minimize the sample volume. With the current design, the system required a volume between 30 and 50 μL per assay.

In the calibration with FBS and whole blood, the samples were spiked with glucose and lactate to adapt the final concentration to the ranges of interest. In the case of real samples from diabetic and control mice, plasma was obtained after blood centrifugation (10000 g, 5 min, room temperature). Glucose and lactate concentrations in these real samples were measured in the POC system and the results were compared to those determined at the Servei de Bioquímica Clínica

Veterinària of the Universitat Autònoma de Barcelona with an Automated Clinical Chemistry Analyzer (Olympus AU480) by enzymatic-based assays.

2.4.1. Diabetes induction and blood samples processing

C57BL/6 male mice (8-10 weeks) were randomly assigned to the control (vehicle) (n=6) or diabetic group (n=6). Mice were housed in a temperature- and light-controlled room with free access to water and normal chow diet. Diabetes was induced in fasted mice by intraperitoneal injection of streptozotocin (STZ) (50 mg/kg/day) (Sigma-Aldrich, Madrid, Spain) for 5 consecutive days, whereas animals in the control group received vehicle (0.1 M sodium citrate buffer, pH 4.5). After 21 days, the presence of diabetes was established by the presence of plasma glucose levels higher than 250 mg/dl. Mice were sacrificed 8 weeks later and the blood was used for plasmatic determination of glucose and lactate by specific enzymatic-based assays following manufacturer's instructions. All animal procedures were performed in agreement with the European guidelines (2010/63/EU) and approved by the University of Barcelona Local Ethical Committee.

3. Silk Fibroin

3.1. Purification and Processing

3.1.1. Extraction

For the SF extraction (**Figure 5.9**), cocoons of *Bombyx mori*, obtained from silkworms reared in the sericulture facilities of the Instituto Murciano de Investigación y Desarrollo Agrario y Alimentario (IMIDA, Murcia, Spain), were chopped in 4 or 5 pieces and boiled in 0.02 M Na₂CO₃ for 30 min to remove the glue-like sericin proteins. Then, raw fibroin was rinsed thoroughly with water and dried at room temperature for 3 days. The extracted fibroin was dissolved in 9.3 M LiBr for 3 h at 60 °C to generate a 20 % w/v solution that was dialyzed against distilled water for 3 days (Snakeskin Dialysis Tubing 3.5 kDa MWCO, Thermo Scientific, USA) with total water exchanges resulting in a 7-8% w/v fibroin solution.

3.1.2. Silk Fibroin films fabrication

Pure or doped (e.g. with enzymes and/or redox mediators) SF was casted onto Petri dishes and dried overnight. Once dried, the films were water annealed at 800 mbar

5. Materials and Methods

atmosphere and 45°C, in a chamber with high humidity content. With this strategy, SF crystallized producing thin (< 20µm), stable, robust, mechanically resistant and highly transparent layers.

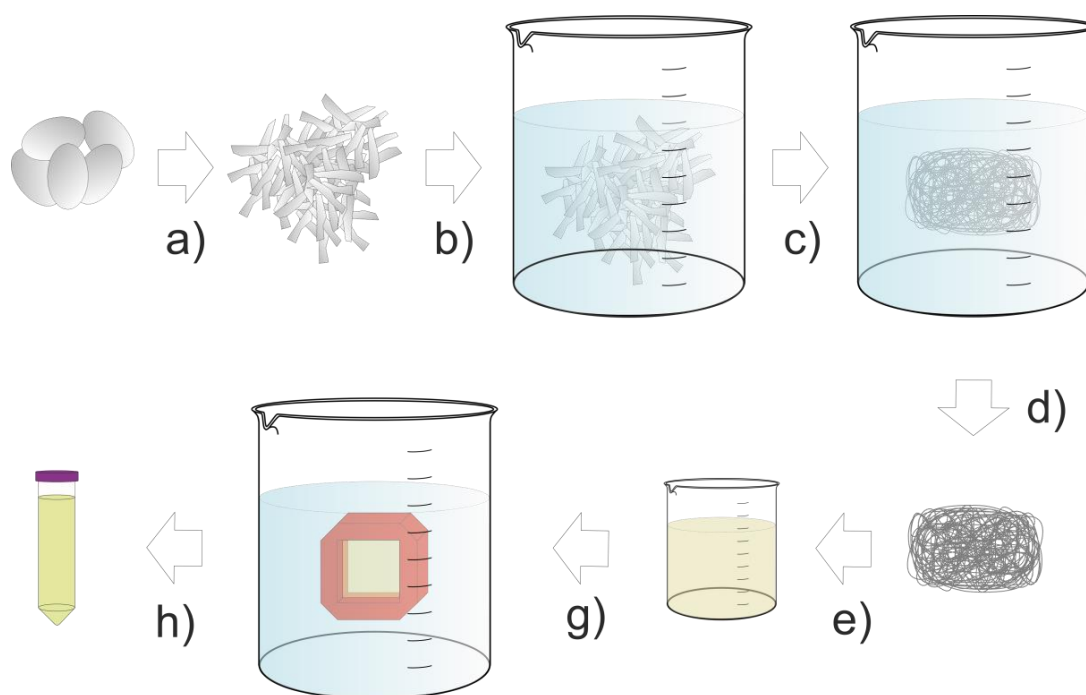


Figure 5.9. Extraction process of SF from *Bombyx mori* cocoons. The whole cocoons are a) chopped into pieces and b) boiled in NaCO_3 solution to dissolve and remove the sericin by c) consecutive rinsing steps. The obtained fibroin fibers are d) dried and e) dissolved in saturated LiBr solution. Finally, the SF solution in LiBr is g) dialyzed against distilled water to obtain an h) aqueous solution of 7% w/v of SF.

3.1.3. PMMA filaments dip coating with doped Silk Fibroin

PMMA transparent fibers of 1.75 mm (Sigma Aldrich, HIRMA PMMA 3D Printing) were cut by CO_2 laser ablation using an Epilog mini 24 instrument controlled by Corel Draw software.

The previously purified 7-8 % w/v SF solution was concentrated to 10% w/v by water evaporation, maintaining the solution in a 3.5 kDa dialysis tube within a dry atmosphere and controlling the weight loss. When concentrated, the solution was doped with a variety of compounds. For PMMA filament interaction with the SF cladding, the SF solution was doped with 0.1 mM Rhodamine 6G. For the

disposable optical fiber glucose biosensor, SF was doped with HRP, GOx and ABTS at a final concentration of 2, 3 and 5 % w/w respectively. In case of the photoregenerable glucose biosensor, instead of ABTS, the SF was doped with DTE.

Using a linear actuator (Firgelli L12) controlled by Elegoo Uno® board and Arduino Software®, the PMMA filaments were dip coated with the doped SF at 0.6 mm s⁻¹ speed. When dried, the SF coated PMMA filaments were exposed to 800 mbar atmosphere at 45 ° C with high humidity content to provoke the water annealing of the SF cladding.

3.2. Equipment for biosensing

3.2.1. Spectroelectrochemical measurements

A SPELEC (Dropsens) apparatus controlled by DROPVIEW SPELEC Software (Dropsens) was used to measure simultaneously cyclic voltammeteries and absorbance spectra of functionalized 4 mm diameter SF pads. To this end, SF pads were positioned on the working electrode of transparent poly(3,4-ethylenedioxythiophene) polystyrene sulfonate (PEDOT:PSS) electrodes purchased from Dropsens.

3.2.2. UV-Vis Spectroscopy

Cuvette Setup for UV-Vis spectroscopy

For the UV-Vis measurements, a cuvette setup from Ocean Optics was used. This setup consisted of a cuvette holder with three optical fiber connectors, two positioned at 180° for transmittance measurements and another at 90° for determination of fluorescence and/or scattering. In this thesis, only the first one was used. Two optical fibers were connected to cuvette. The first one (1 mm core) was used as light input and coupled to the light source, either a deuterium-halogen (DH-2000-BAL, Mikropack) or an halogen (HL-2000-FHSA, Ocean Optics) lamp, depending on the experiment. The second optical fiber (600 μm core) was used to guide the light from the cuvette to the detector, i.e. a Qe65 Pro Spectrometer controlled by OceanView software (both from Ocean Optics).

Additionally, in DTE analysis a 300 nm LED (M300F2, Thorlabs) was situated on the top of the cuvette and used to close the molecule.

During the experiment, the setup was maintained at every moment in darkness to prevent any interference from environmental light over the compound. For the absorbance spectra acquisition, the cuvette was only irradiated at the time of the measurement.

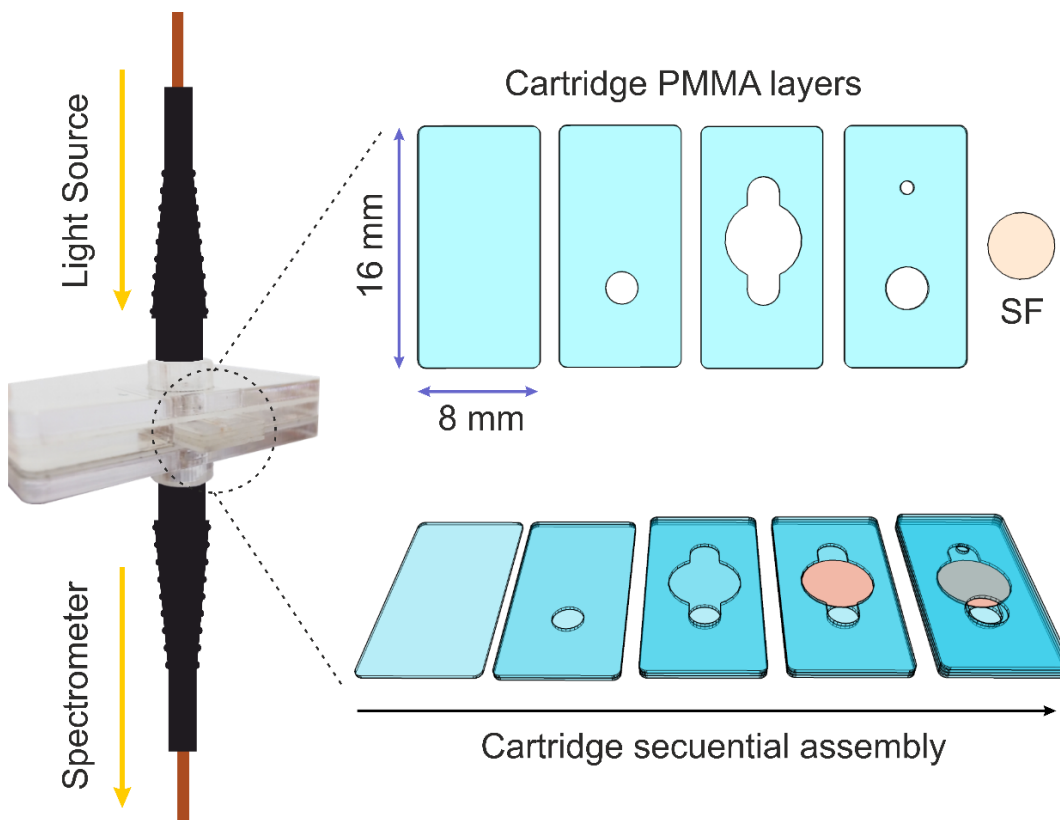


Figure 5.10. Schemes of the setup for SF films measurement (left) and cartridge layers and assembly (right). The first layer serves as a base. The second layer includes a hole to form a sample reservoir. The third layer structure fixes the SF pad and connect to the sample reservoir to facilitate the contact between the fluid and the pad. Finally, the fourth layer closes the system, leaving one access for sample loading and another, smaller, for air escape.

Silk Films measurement

A homemade setup was manufactured and assembled with the aim to characterize this particular type of sample. The setup, illustrated in **Figure 5.10**, consisted of a homemade PMMA holder containing two connectors for optical fibers perfectly aligned and separated 2 mm. A 50 μm SMA optical fibers (Thorlabs) was coupled to each connector being the top one connected to the light source, i.e. a deuterium-halogen lamp (Ocean

Optics), and the bottom one to a QEPro spectrometer (Ocean Optics). In between the two optical fibers, in the 2 mm space, a sample cartridge containing the SF film was inserted for characterization. The architecture of the sample cartridge, consisting of 4 PMMA layer of 0.5 mm thickness, joined by PSA layers is shown also in **Figure 5.10**, and described below.

PMMA-SF optic fibers measurements.

In transmission measurements, the SF is aligned to two commercial glass fibers of 600 μm (light inlet from the halogen lamp) and 200 μm (light outlet to the spectrometer). The fibers are fixed to mobile platforms controlled by micromanipulators, for a better alignment. In case of reflection measurements, the doped SF coated PMMA filaments are connected to a reflection probe (Ocean Optics, QR600-7-UV-125F) with a PDMS adapter (**Figure 5.11**). The incoming halogen light is coupled into the structure while the reflected light is guided to the spectrometer (Ocean Optics, USB2000+UV-VIS) controlled by OceanView software (Ocean Optics).

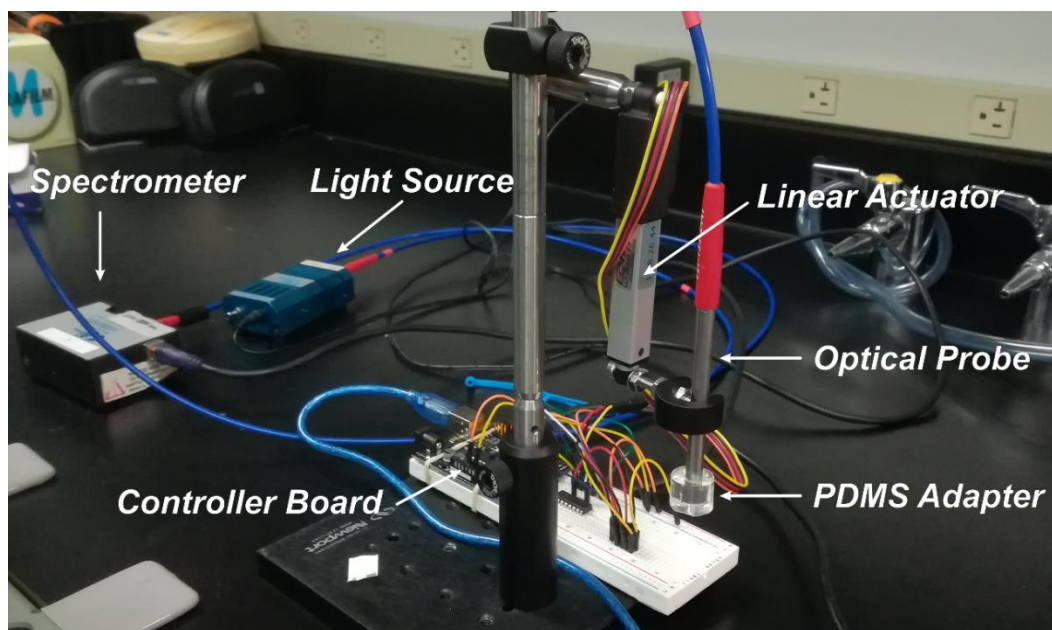


Figure 5.11. Picture of optical fiber measurement setup. The optical fiber is coupled to the optical probe by a flexible PDMS adapter. The optical probe vertical position depends on a linear actuator controlled by a controller board. This optical probe is connected to both the light source and the spectrometer, where the absorbance changes of the SF cladding are recorded. In case of PMMA filaments coating, they are attached directly to the linear actuator, which moves vertically to immerse and emerge the filament from the precursor.

To close the DTE present in the SF cladding, the optical fibers were irradiated manually with a 300 nm UV lamp (UVP – 8W model UVLMS-38) controlling the absorbance increment at 530 nm by the spectrometer. In a similar way to the dip coatings, the probe was attached to a linear actuator in order to control the immersion speed (0.6 mm s^{-1}) and the time that the optical fibers were maintained in the solutions (8 s).

3.2.3. Image analysis

Pictures of the SF functionalized pads were acquired with DigiMicro 2.0 Scale analyzed by public domain ImageJ software. An average value of RGB (red, blue, green) was obtained from the pixels that comprises the selected area of the picture (i.e. SF pads).

3.2.4. Spectral microscopy

For the spectral image analysis, an Olympus Inverted microscope, equipped with a halogen lamp (Olympus, U-LH100L-3) as light source and coupled to a multispectral camera (CRI Nuance EX) controlled by the Nuance 3.0.2 software was used to acquire and unmix the maps in different spectral components. The represented absorbance was given by the software by comparison of a reference area light emission (non UV-irradiated silk) and the area to be analyzed (UV-irradiated silk).

3.3. Silk Fibroin Characterization Techniques

3.3.1. Attenuated Total Reflectance – Fourier Transformed Infrared Spectroscopy (ATR-FTIR)

FTIR was performed using a Platinum ATR from Bruker that contains a diamond crystal to measure ATR. Spectra were obtained by averaging 54 scans at a resolution of 4 cm^{-1} and were represented as $-\log(R/R_0)$, where R and R_0 are the reflectance values corresponding to the single beam spectra recorded for sample and reference. Reference was measured by simple exposition of the prism to air while the sample measurement was carried out by pressing the sample against the diamond prism.

For DTE analysis, the measurements were performed using FTIR Tensor 27 Bruker spectrophotometer, and a Specac's Golden Gate accessory for the ATR measurements. OPUS 5.5 software was used for monitoring the IR spectra. The IR spectra were registered in solid state for better resolution, hence the solvent of the samples were evaporated using a N_2 flow at room temperature.

3.3.2. X-Ray Diffraction (XRD) Analysis

XRD patterns were obtained with a Materials Research Diffractometer (MRD) from Malvern PANalytical. The diffractometer had an horizontal omega-2theta goniometer (320 mm radius) in a four-circle geometry and worked with a ceramic X-ray tube with Cu K α anode ($\lambda=1.540598 \text{ \AA}$). The detector used was a Pixcel, a fast X-ray detector based on Medipix2 technology.

Additional components were:

Incident optics: Parabolic Mirror, divergent slit $1/4^\circ$, Mask 2 mm, Soller slits 0.04 rad , Ni Filter (0.02 mm).

Diffracted optics: Pixcel (detector), antiscatter 7.5 mm.

The measurements were done using the scanning mode of the detector. Measurement conditions: 2theta range= $10\text{-}50^\circ$, step size= 0.03° , and counting time (time per step) = 500s.

3.3.3. Thermogravimetric Analysis (TGA)

For TGA, a Netzsch STA 449F1 instrument controlled by Netzsch software was used. Samples 5 mg of SF were deposited in a Al_2O_3 crucible and heated up from RT to $700 \text{ }^\circ\text{C}$ in a ramp of $10 \text{ }^\circ\text{C min}^{-1}$ while the loss of mass was registered.

3.3.4. SEM

Polymeric and SF samples were first coated with gold by sputtering using an Emitech SC7620 sputter coater and imaged using a Zeiss EVO MA10 SEM (EHT = 8 keV, WD = 7.5 mm, SE detector).

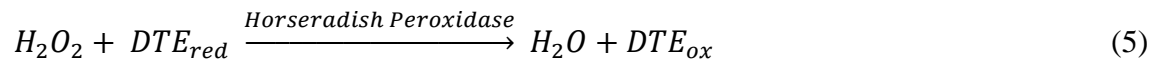
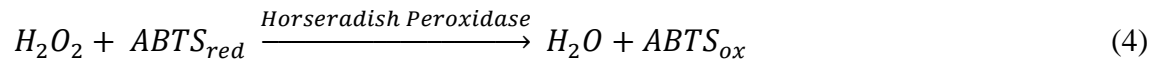
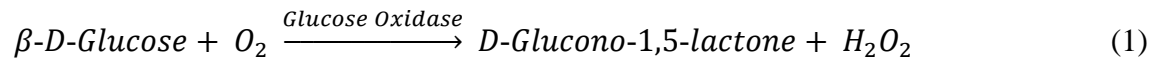
3.3.5. Raman

Raman spectra of the samples were collected on a RAMII Bruker spectrometer equipped with a Ge detector using liquid nitrogen as the coolant and a Nd:YAG laser emitting at 1064 nm. The laser light power was 1000 mW. A back-scattering configuration was used. An average of 1024 scans was performed at a resolution of 4 cm^{-1} over a range from $4000 \text{ to } 400 \text{ cm}^{-1}$.

3.4. Glucose determination

The selected enzymes for the development of the biosensors, i.e. GOx (1) and HRP (4, 5), catalyse the following reactions:

5. Materials and Methods



The absorbance spectrum of the doped SF material, either as a thin film or as a PMMA fiber cladding, is compared before and after the reaction with a glucose container sample. The increment (in case of ABTS) or decrease (in case of DTE) of the absorbance band is related to the amount of glucose present in the sample,

6. Results

In this chapter, a detailed exposition of the obtained results is exposed. A number of six sections are included ordered chronologically. The first two sections are related to the development of a glucose electrochemical biosensor based on alginate membranes for glucose and lactate determination while sections 3, 4 and 6 describes the use of SF in glucose optical biosensors development. Section 5, preliminary to the study exposed in section 6, describes the novel use of a photoelectrochromic molecule as enzymatic mediator for the HRP.

6.1 Electrodepositable Alginate Membranes for Amperometric Glucose Biosensing

Abstract

Simple and disposable POC systems are usually the best solution for chronic patients to get a rapid diagnosis in home care context. However, their main drawback relies on the poor reliability derived from the low stability of the bio-recognition elements and low quality of the transducers. In the current chapter, we study the use of electrodeposited calcium alginate hydrogels as a biocompatible matrix in the development of enzymatic amperometric biosensors for whole blood analysis, to enhance the enzymes stability and to protect the transducer from biofouling. The alginate electrodeposition involves the controlled Ca^{2+} release, so the gel thickness can be modulated. In the biosensor, HRP and GOx were electrodeposited within the hydrogel and the activity of the bi-enzymatic system was analyzed chronoamperometrically using TMB as the mediator. Besides enzyme entrapment, the obtained gels protected the transducer from biofouling, enabling the reuse of the transducer after hydrogel removal and re-electrodeposition. The biosensors showed good analytical characteristics to glucose determination in whole blood samples, discriminating among healthy and hyperglycemic samples, with good sensitivity ($-0.27 \mu\text{A cm}^{-2} \text{mM}^{-1}$), low LOD (126 μM) and long lineal range (2 to 12 mM).

This chapter contents results previously published in:

Congresses:

Enzymatic biosensors based on electrodeposited alginate hydrogels. A. Márquez-Maqueda, J.M. Ríos-Gallardo, N. Vigués, F. Pujol, M. Díaz-González, J. Mas, C. Jiménez-Jorquera, C. Domínguez, X. Muñoz-Berbel, *Procedia Engineering*. 2016, 168, 622-625, (As a Poster contribution at Eurosensors 2016, Budapest, Hungary; Oral Contribution at MNE 2016, Vienna, Austria and Oral Contribution at XXI Transfrontier Meeting Sensors and Biosensors 2016, Barcelona, Spain).

Journals:

Electrodepositable alginate membranes for enzymatic sensors: An amperometric glucose biosensor for whole blood analysys. A. Márquez, C. Jiménez-Jorquera, C. Domínguez, X. Muñoz-Berbel, *Biosens. Bioelectron.* 2017, 97, 136

1. Introduction

The development of simple and low-cost methods based on biosensors for the detection of biomarkers is nowadays one of the main challenges in analytical science¹⁷²¹⁷³ as an alternative to sophisticated benchtop instruments like high performance liquid chromatography or mass-spectrometry, among others. In the field of clinical analysis, as well as environmental monitoring and food industry, amperometric biosensors are a first choice for the simplicity, low-cost and robustness of amperometric transducers, the portability and low energetic requirements of amperometric instrumentation and the sensitivity and selectivity of biological molecules (e.g. enzymes) commonly used as recognition elements.¹⁷⁴ A very representative case of success is the glucometer with test strips, where all these advantages are exploited in the best-selling biosensor ever. However, the lack of accuracy of these systems is still a motive of concern.¹⁷⁵¹⁷⁶¹⁷⁷ First concerns are technological, due to the low accuracy of the fabrication protocols that affect measurements reliability and reproducibility. Even more important is biosensor dysfunction, resulting from the high sensitivity of enzymes to the environmental factors and the immobilization protocol that may affect their activity.¹⁷⁸ Enzyme immobilization is thus a critical process in biosensors development for two reasons: (i) can disrupt the enzyme activity but, at the same time, (ii) can maintain the structural integrity of the enzymes for longer times, once immobilized. Classical immobilization protocols such as physisorption, covalent bonding or cross-linking rely on poor stability of the biomolecule in the sensor surface or loss of activity due to steric hindrance or reaction with amino acids from the active site.¹⁷⁹ Entrapment on biocompatible matrices, emerges as an auspicious alternative for (i) enabling the immobilization of high amount of biocomponent in a 3D architecture, (ii) avoiding orientation problems or inactivation of the biomolecule for reaction with the recognition or active centres, (iii) providing a wet environment (hydrogels) to improve biomolecules stability and (iv) acting as a diffusion barrier that minimizes the poisoning of the electrode and allows working with complex real samples without pre-treatments (waste water, milk, blood, etc.). In this sense, alginate hydrogels have positioned as one of the most promising biocompatible matrices for enabling biomolecules entrapment at very soft experimental conditions, i.e. room

temperature and pH 7. The advantage of alginate is that this linear copolymer, combining (1,4)-linked β -D-mannuronic acid (M) and α -L-guluronic acid (G), spontaneously cross-links in presence of divalent cations (e.g. Ca^{2+}) without requiring temperature or irradiation and therefore, without compromising the integrity and activity of the biomolecule.¹⁸⁰ Calcium ions may be directly added to alginate solution or in situ generated,¹⁸¹ which provide these membranes with high versatility. These excellent gelling conditions have been exploited in the entrapment of enzymes¹⁸²¹⁸³¹⁸⁴ and cells,¹⁸⁵¹⁸⁶ as well as in tissue engineering¹⁸⁷ and drug delivery.⁹⁸ Recently, it has been described the use of alginate membranes in the entrapment of enzymes or cells for biosensors development¹⁸⁴¹⁸⁸¹⁸³. However, electrodepositable alginate hydrogels have never been applied to biosensors development for glucose analysis in whole blood samples.

In the present chapter, electrodepositable calcium alginate enzymatic membranes are employed in the development of a glucose biosensor for whole blood samples by entrapment of GOx and HRP (GOx/HRP cascade reaction)¹⁸⁹ using SPGEs as electrochemical transducer. Enzyme electrodeposition is performed at soft reaction conditions (i.e. room temperature, pH 7) and does not compromise enzyme integrity or activity. The electrodeposition of the matrix presents three more advantages: localized membrane deposition, reproducibility and reusability of the transducer by elimination and in situ re-electrodeposition (refreshing) of the enzymatic membrane. Patternability is achieved because the matrix grows only over the working electrode surface. Furthermore, applying a constant current is enough to growth the matrix, so defining its intensity and duration is enough to obtain a reproducible process. The matrix can be easily re-dissolved after the detection using Ca^{2+} quelating agents such as PBS or citrate buffers (low reactive solutions), and the same electrode can be re-used for a next matrix synthesis and analyte detection only performing a fast electrochemical cleaning between measurements. Electrodeposited alginate matrix characteristics, mediator diffusion through the matrix, transducer protection and amperometric response of the biosensor to glucose from buffer, plasma and whole blood samples are discussed in this chapter.

2. Results and discussion

2.1. Optimization of electrodeposition process

The physico-chemical properties of the hydrogel depended on the electrodeposition conditions. The characteristics of the obtained hydrogels were analyzed under several conditions: duration of the electrodeposition step (from 30 to 180 s) and applied current (from 50 to 150 μA). **Figure 6.1.1** shows the aspect of the alginate hydrogel under these conditions. The electrodeposition current affected the consistency of the hydrogel. More consistent and rigid gels were obtained when applying higher currents due to the higher number of cross-linking events taking place. Electrodeposition currents around above 100 μA provided stable and consistent hydrogels suitable for enzymatic membranes development.

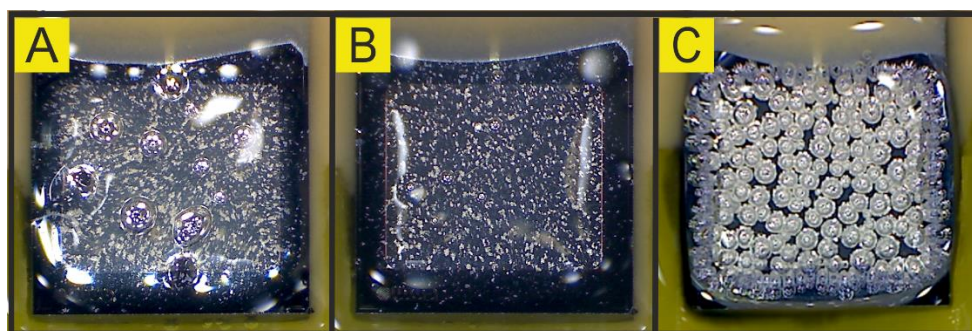


Figure 6.1.1. Aspect of alginate hydrogels applying different currents and electrodeposition times between the WE and CE: A) 1 mA cm^{-2} for 120 s (A), 2 mA cm^{-2} for 90 s (B) and 3 mA cm^{-2} for 60 s (C). Longer times provoke big bubbles accumulation even applying low currents (A) while large currents provoke small bubbles accumulation, even at short times (C). Gel precursor: Sodium alginate 1 % w/v and CaCO_3 0.5 % w/v. Current applied between a Pt WE (0.05 cm^2) and a Pt CE electrode using a Ag/AgCl electrode as RE.

The duration of the electrodeposition step, on the other hand, showed high correlation with the presence of bubbles in the final gel. The bubbles formation was associated to the co-generation of O_2 during electrodeposition. Electrodeposition times above 90 s were discarded for producing high amounts of bubbles, even when applying low currents. The presence of bubbles made heterogeneous membranes that detached from the electrode surface. Below 90 s of electrodeposition, homogenous, transparent and stable hydrogels with restricted area of electrodeposition were obtained on the working

electrode. For SPGEs, alginate was electrodeposited at 0.795 mA cm^{-2} during 90 s obtaining transparent and bubble-free hydrogels (**Figure 6.1.2**).

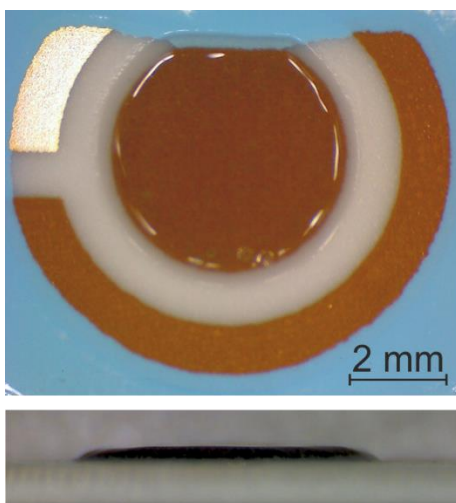


Figure 6.1.2. Top and profile images of the biosensor comprising the transducer and the alginate electrodeposited film. Electrodeposition conditions: 90 s and 0.795 mA cm^{-2} . Gel precursor: Sodium alginate 1 % w/v and CaCO_3 0.5 % w/v.

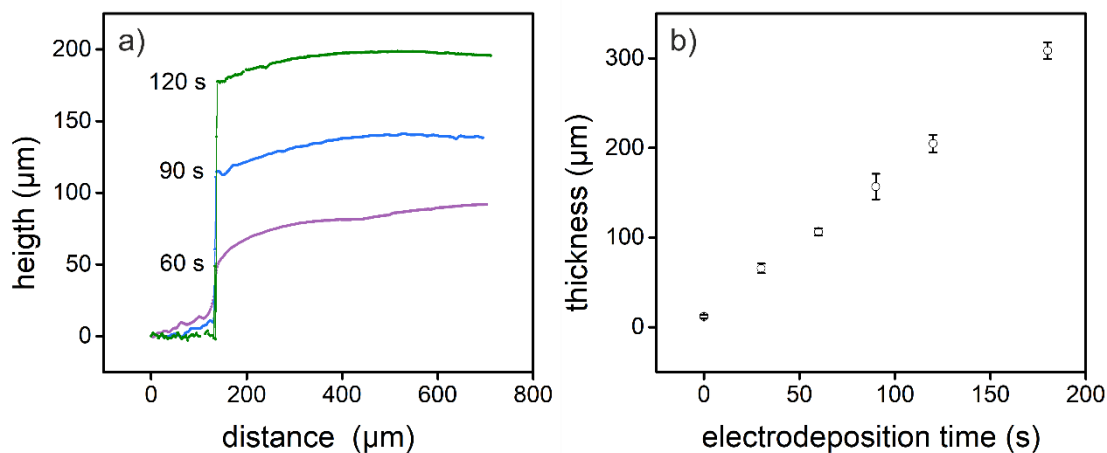


Figure 6.1.3. Optimization of alginate thickness. a) Hydrogel thickness dependence on the electrodeposition time, measured by profilometry. b) Profiles of three alginate gels, deposited with different electrodeposition times ($n=5$). Gel precursor: Sodium alginate 1 % w/v and CaCO_3 0.5 % w/v. Applied current between the WE and CE: 0.795 mA cm^{-2} .

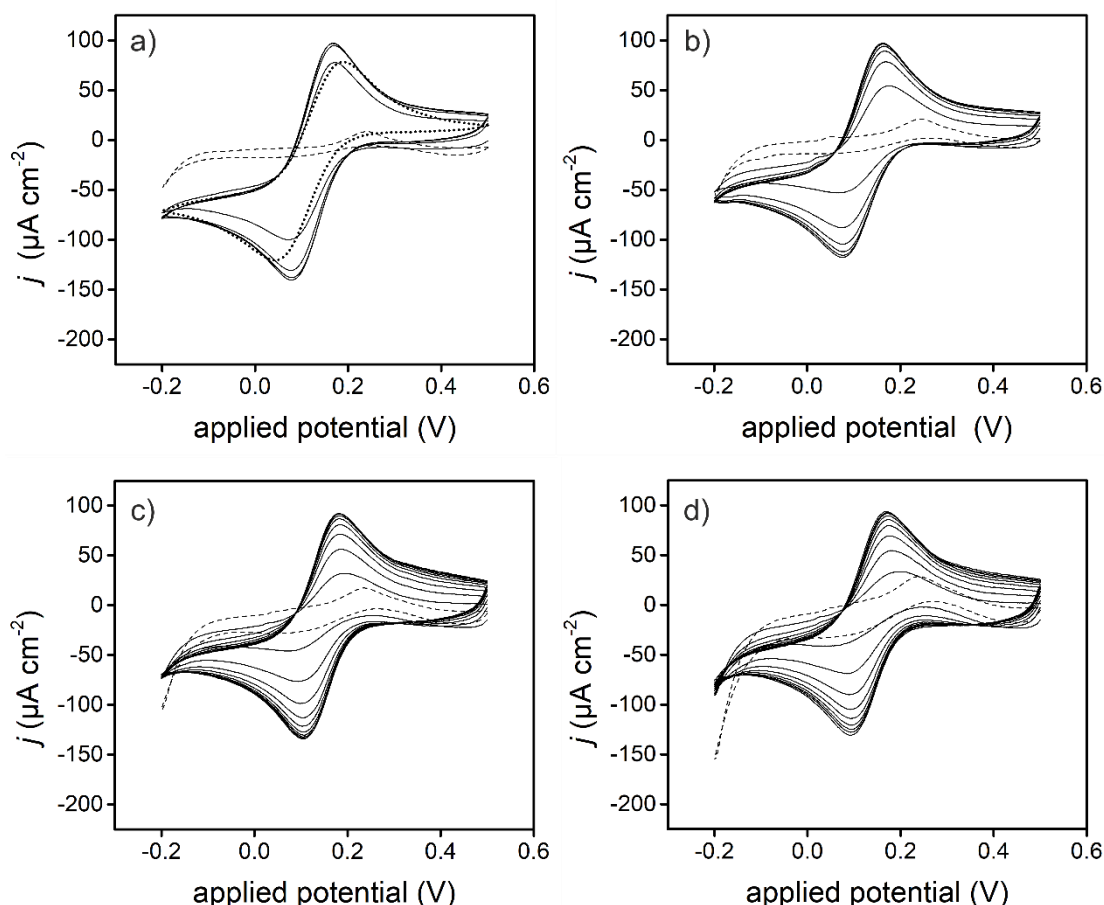


Figure 6.1.4. Diffusion limitation by the hydrogel. Hydrogels electrodeposited applying 0.795 mA cm^{-2} during a) 30 s, b) 60 s, c) 90 s and d) 120 were immersed in a buffer solution containing $1 \text{ mM K}_3[\text{Fe}(\text{CN})_6]$ and successive cyclic voltammeteries were recorded obtaining different saturation responses of the $[\text{Fe}(\text{CN})_6]^{3-} / [\text{Fe}(\text{CN})_6]^{4-}$ redox peaks. Dashed line represent a cyclic voltammetry with no $\text{K}_3[\text{Fe}(\text{CN})_6]$. Medium: MES-NaOH (0.2 M , pH 7), 0.145 M KCl , 0.01 M CaCl_2 and $1 \text{ mM K}_3[\text{Fe}(\text{CN})_6]$. Scan rate: 50 mV s^{-1} .

The thickness of the hydrogel (**Figure 6.1.3**), and consequently the electrodeposition time, also affected the diffusion of analytes (and mediators) through the membrane. The diffusion of ferricyanide molecules (1 mM solution) for hydrogels electrodeposited during 30, 60, 90 and 120 s was evaluated by cyclic voltammetry. Results are illustrated in **Figure 6.1.4**. Diffusion rate was determined by monitoring the increment of the intensity of the redox peaks of ferricyanide in consecutive cyclic voltammeteries with electrodes covered with hydrogels of different electrodeposition times. Under the same experimental conditions, diffusion rate showed correlation with the electrodeposition time (and thickness) of the hydrogel, being smaller for hydrogels

electrodeposited during longer times (**Figure 6.1.5**). This diffusion restriction associated to the thickness of the membrane should be taken into consideration when incubation times of the samples in the biosensor were calculated.

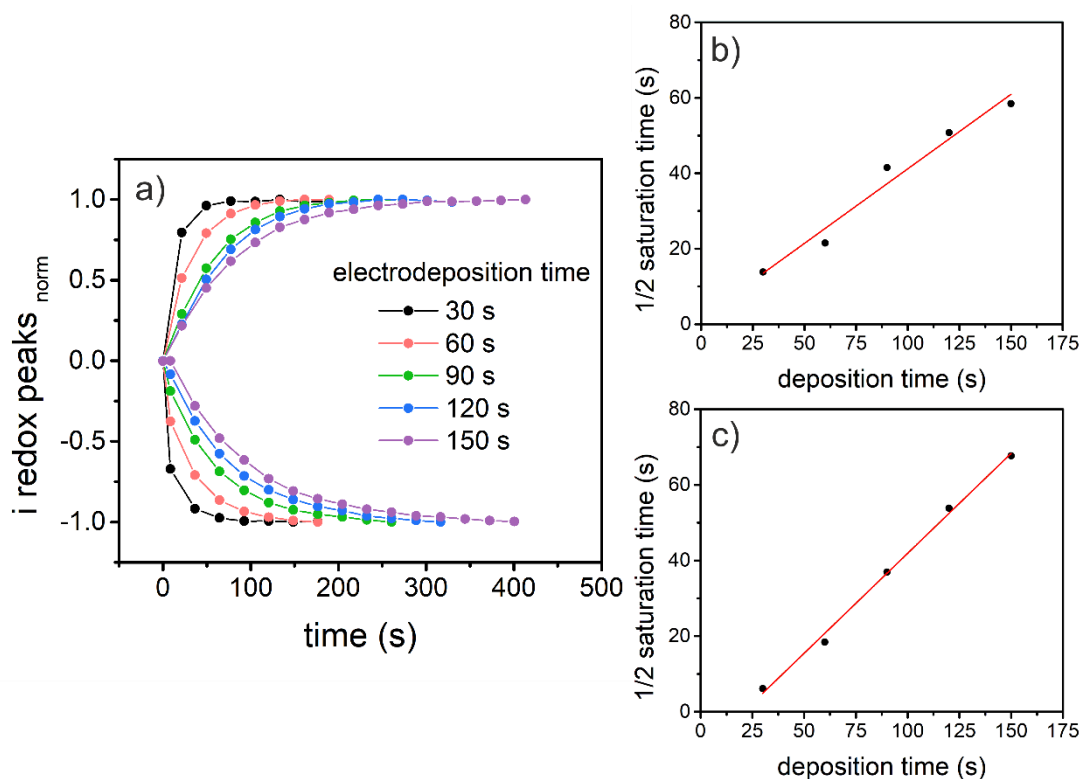


Figure 6.1.5. $[\text{Fe}(\text{CN})_6]^{3-}/[\text{Fe}(\text{CN})_6]^{4-}$ diffusion in alginate hydrogel. a) Normalized saturation of redox peaks current values of $[\text{Fe}(\text{CN})_6]^{3-} / [\text{Fe}(\text{CN})_6]^{4-}$ for chips covered with alginate hydrogels of electrodeposition times (extracted from cyclic voltammeteries in Figure 4). b) Anodic and c) cathodic redox peaks current saturation time dependence on the electrodeposition time of the hydrogel (thickness). Medium: MES-NaOH (0.2 M, pH 7), 0.145 M KCl, 0.01 M CaCl_2 and 1 mM $\text{K}_3[\text{Fe}(\text{CN})_6]$.

2.2. Hydrogel Stability

Alginate hydrogels are sensitive to cation chelating agents, which disaggregate them with facility. The stability of alginate hydrogels to contact with buffers of different compositions was evaluated. PBS and citrate buffers, containing Ca^{2+} chelating agents, disaggregated the gel after less than 10 minutes, whereas alginate hydrogels remained stables in Imidazol-HCl and MES-NaOH buffers (**Figure 6.1.6**). MES-NaOH (0.2 M, pH 7), in combination with 0.145 M KCl (to emulate physiological samples saline

6. Results

concentration) and 0.01 M CaCl₂ (to maintain the gel cohesion), was chosen for electrochemical measurements. PBS, on the other hand, was used to clean the electrodes between successive electrodepositions and for biosensor refreshing.

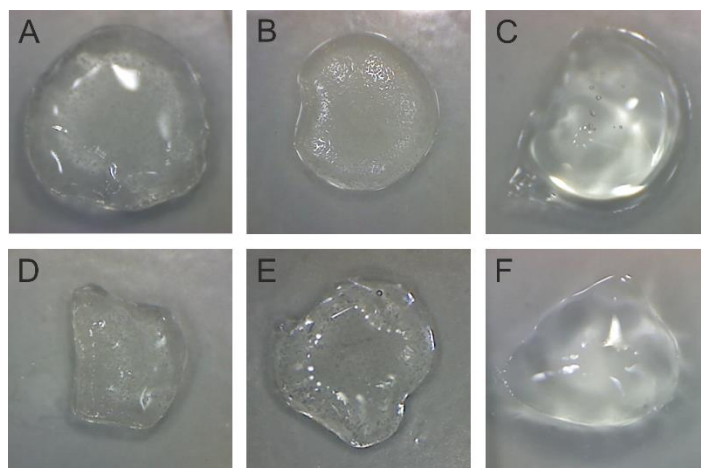


Figure 6.1.6. Alginate stability in MES-NaOH and Imidazole-HCl buffers. Pictures of gels maintained in MES-NaOH (0.5 M, pH 7) (A-C) and Imidazole-HCl (0.2 M, pH 6) (D-F) just after electrodeposition (A, D), after 24 h (B, E) and after 48 h (C, F).

2.3. Protection of the transducer from biofouling

In the analysis of biological samples, molecules and cells susceptible to be adsorbed on the transducer surface are widely present so biofouling becomes an issue.¹⁹⁰ The use of membranes has been the ordinary strategy to avoid transducer dysfunction. In the case of alginate hydrogels, the enzymatic membrane may have the dual function as biocompatible support for the enzyme and as size-exclusion barrier avoiding cell and molecule diffusion to the transducer surface. To evaluate this second function, cyclic voltammeteries of the bare electrode (uncovered) and the electrode protected with an alginate membrane (covered) were compared when measuring whole blood samples containing 1 mM K₃[Fe(CN)₆]. It is clear from **Figure 6.1.7** that redox peaks (**Figure 6.1.7a and 6.1.7b**) current density were much smaller when the electrode was not covered, probably due to a dramatic reduction of the active area of the electrode associated to biofouling. The filtering capacity of alginate hydrogels could be observed by naked eye. When a drop of blood is added to a gel matrix and washed several times

with water, it was appreciated how the liquid pass through the gel but the red cells remain in the edge of the membrane.

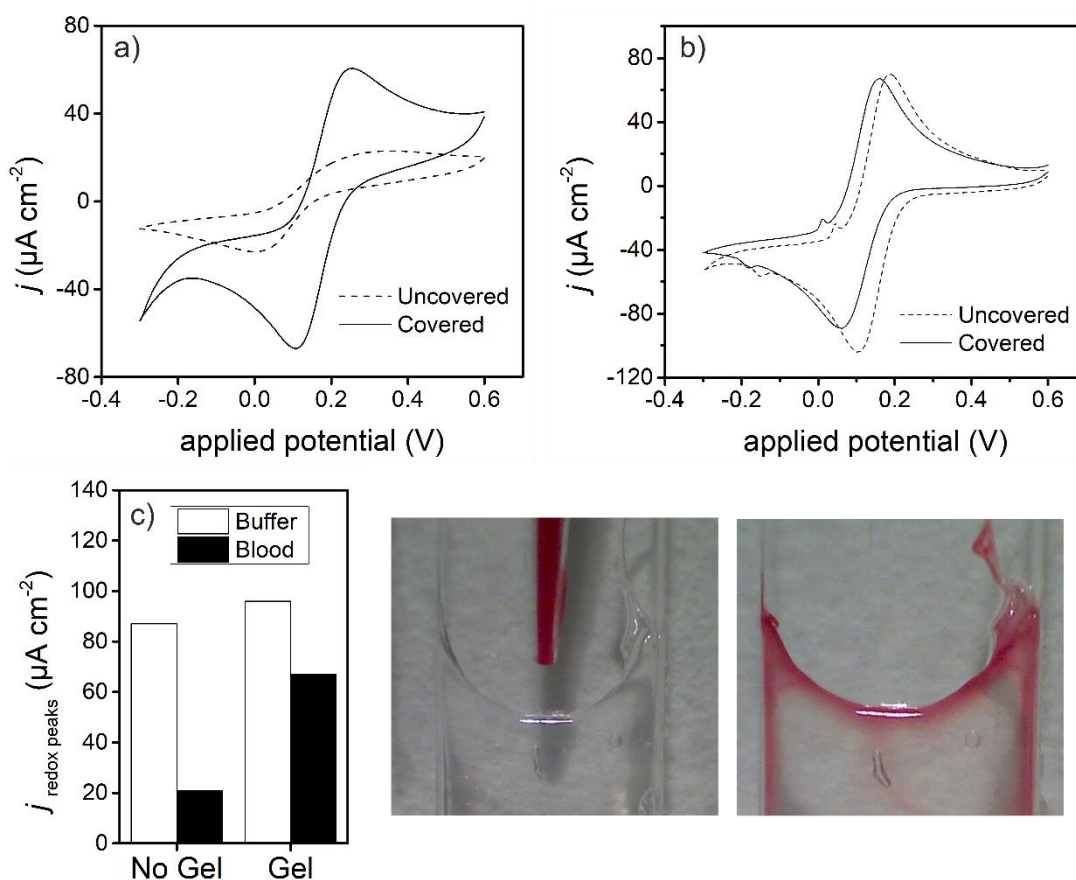


Figure 6.1.7. Study of biofouling effect on the transducer. Cyclic voltammeteries obtained for: a) whole blood samples and b) buffer samples with 1mM $\text{K}_3[\text{Fe}(\text{CN})_6]$ with the working electrode covered with alginate hydrogel and uncovered. c) Comparison of current values for the redox peaks for 1mM ferricyanide with and without alginate covering on the WE. The pictures show the capability of alginate hydrogel to retain blood cells. Buffer: MES-NaOH (0.2 M, pH 7), 0.145 M KCl, 0.01 M CaCl_2 .

2.4. Optimization of enzyme and mediator content

In the development of a biosensor, the composition of the enzymatic membrane and the concentration of enzymes and mediator should be adapted to the requirements of the final application. Since this biosensor is based on the coupled activity of HRP and GOx, the relative concentration of these enzymes should also be considered. To avoid HRP inactivation by the exposition to high H_2O_2 concentrations,¹⁹¹ a HRP/GOx molar ratio

6. Results

around 8 was established, according to bibliography.¹⁹² Maintaining this ratio, enzyme concentrations between 5 to 100 $\mu\text{g mL}^{-1}$ GOx were evaluated (**Figure 6.1.8**). Optimal conditions providing with a clear Michaelis-Menten behaviour, good sensitivity and linear range were obtained for concentrations of HRP and GOx of 11 $\mu\text{g mL}^{-1}$ and 5 $\mu\text{g mL}^{-1}$ respectively. Under these conditions, we could assume that the biosensor response decayed for enzyme-substrate saturation and not because of an electron transfer or diffusion limitation at the transducer surface.¹⁹³

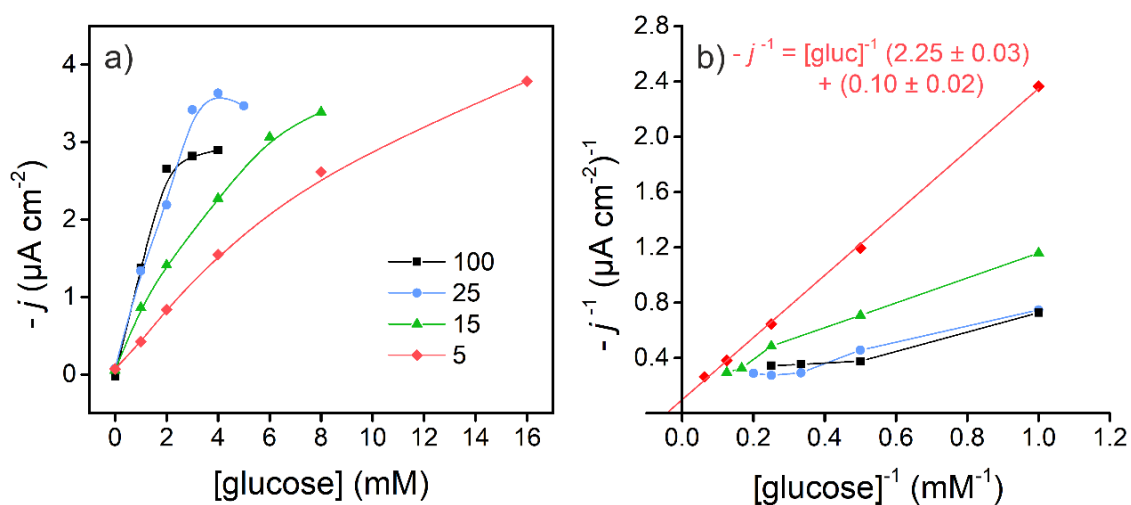


Figure 6.1.8. Amperometric response dependence on enzyme concentration in gel. a) Calibrations curves for glucose with different concentrations of GOx ($\mu\text{g/ml}$) in alginate gel precursor. b) Lineweaver-Burk plots for the different curves in a).

In the case of the mediator, TMB was chosen for presenting a low detection potential (0.1 V vs. Ag pseudo-reference), far from potential interfering molecules (e.g. ascorbic acid). TMB is oxidized in presence of glucose using the bi-enzymatic system of GOx and HRP. The oxidized TMB is then reduced at the WE and the registered current is proportional to the amount of glucose present. In **figure 6.1.9** it is evident how the anodic current decreases while the cathodic current increases when this reaction takes place.

The concentration of mediator influenced the lineal range of the biosensor and had to be optimized. Two TMB concentrations were compared, 0.5 and 2 mM, by enzymatic membranes containing optimal concentrations and ratio of enzymes (**Figure 6.1.10**). Biosensors with 0.5 mM TMB presented good sensitivity (0.36 ± 0.00 $\mu\text{A cm}^{-2} \text{mM}^{-1}$)

and LOD (11.31 μM) but a short linear range between 0 and 4 mM ($R^2 = 0.999$). The increase of TMB to 2 mM, nevertheless, expanded the linear range from 2 to 12 mM ($R^2 = 0.993$), enabling to distinguish between healthy (3.8 and 6.5 mM) and hyperglycemic subjects (> 7 mM) with sensitivity ($0.32 \pm 0.02 \text{ } \mu\text{A cm}^{-2} \text{ mM}^{-1}$) and without compromising the detection capacity of the system (LOD = 270 μM). A TMB concentration of 2 mM was thus selected for biosensor development.

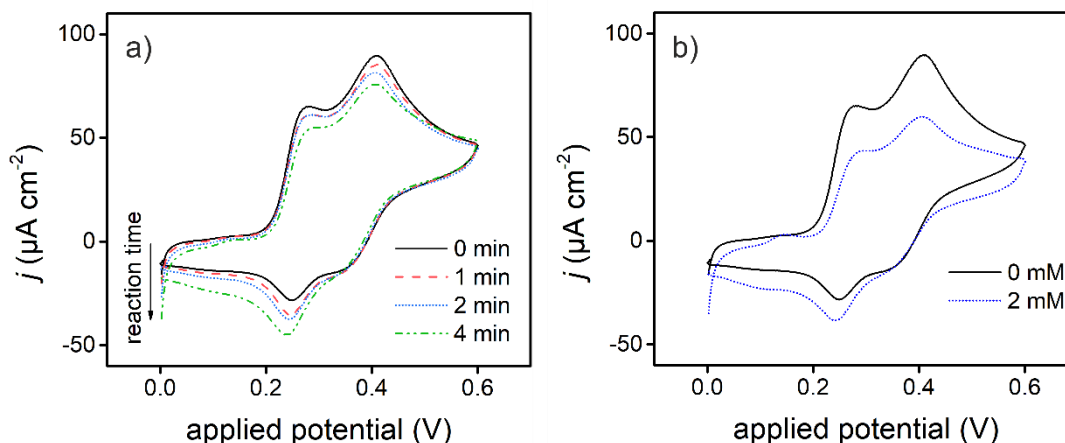


Figure 6.1.9. Cyclic voltammeteries of the biosensor in presence of glucose. a) 1 mM glucose, at different times from the glucose addition and b) 0 mM and 2 mM after 2 min of the glucose addition. The decrease of the anodic peaks current and increase of cathodic peaks current is appreciable. Medium: MES-NaOH (0.2 M, pH 7), 0.145 M KCl, 0.01 M CaCl_2 and 0.5 mM TMB. Scan rate: 50 mV s^{-1} .

There is no response of the biosensor when one of the two enzymes is not present in the alginate matrix neither with both enzymes present but in absence of glucose (inset **Figure 6.1.10a**).

The biosensor response was compared to a reference biosensor (same transducer) with the enzymes free in solution and without alginate electrodeposition (**Figure 6.1.10c**). It is remarkably a higher sensitivity ($0.74 \pm 0.03 \text{ } \mu\text{A cm}^{-2} \text{ mM}^{-1}$) without hydrogel for glucose calibrations in buffer.

2.5. Enzymatic stability within alginate hydrogels

The conditions nearby the transducer when the anodization is occurring may affect the activity of the enzymes, not only because of direct charge transference but also because of regional pH changes to acidic values.¹⁹⁴ However, previous studies report that

6. Results

the hypothetical pH shift is restrained by the buffering effect of CaCO_3 ,¹⁰² remaining above pH 6 even close to the transducer when CaCO_3 is present at 0.5 w/v % and a current of 0.6 mA cm^{-2} is applied (0.795 mA cm^{-2} in this study).

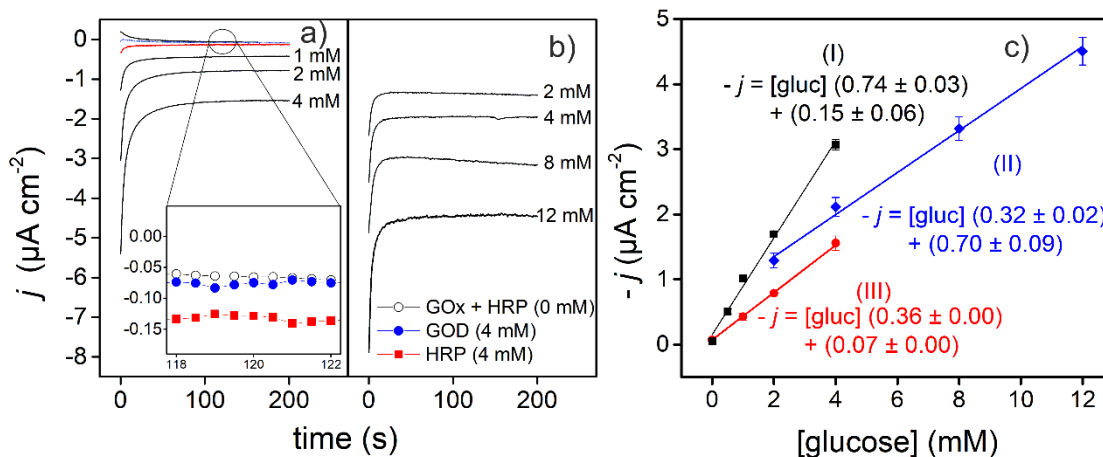


Figure 6.1.10. Amperometric response of biosensors to glucose using two concentrations of TMB as mediator a) 0.5 mM (from 0 to 4 mM glucose) and b) 2mM (from 2 to 12 mM glucose). Negative control responses are included (4 mM glucose), where only one of the enzymes is present (inset in a)). c) Calibration curve for glucose: (I) Biosensor without alginate membrane and 0.5 mM TMB, (II) With alginate membrane and 2 mM of TMB and (III) With alginate membrane and 0.5 mM of TMB ($n=6$). Medium: MES-NaOH (0.2 M, pH 7), 0.145 M KCl, 0.01 M CaCl_2 , TMB (0.5 mM or 2 mM). Detection potential: 0.1 V vs. Ag pseudo-reference electrode.

The stability of the enzymes in the alginate matrix over time was evaluated and compared with enzymes adsorbed on the electrode surface. The enhanced sensitivity commented above remained constant for 15 days, decreasing to 50 % of initial activity in one month. Comparative studies with adsorbed enzymes revealed a decrease in a 50 % of the sensitivity only one day after the biosensor fabrication (**Figure 6.1.11**).

2.6. Reusability and repeatability of the biosensor

In closed systems (e.g. LOCs), where the sensing compartment is not accessible, electrodeposition becomes a great advantage, as it allows to introduce a liquid precursor and to immobilize the hydrogel with the recognition element only over the electrochemical transducer, just by a simple anodization step. Furthermore, if this

membrane is degradable, several electrodeposition events can be performed, using fresh or different recognition elements each time and expanding the transducer lifetime. In the case of alginate, it is even easier since, as already exposed, it may be dissolved using simple calcium chelating solutions such as PBS. The re-usability limitation is then due to the transducer stability and not to the recognition part (this can be regenerated when required). The re-usability of the transducer was thus evaluated by electrodepositing alginate membranes and removal with PBS. Concretely, the removal protocol included addition of PBS and electrochemical activation by cyclic voltammeteries in 0.5 M H₂SO₄ (5 cycles; 0 and 1.5 V vs. Ag pseudo-reference electrode). As shown in **Figure 6.1.12**, eight consecutive calibration curves of glucose were performed using the same transducer and refreshing the alginate matrix. The slope of the linear calibration (sensitivity) decreases only a 10 % between the 1st and the 8th calibration. This result demonstrated the reusability of the system and their potential application in closed systems such as Lab-on-a-chip architectures.

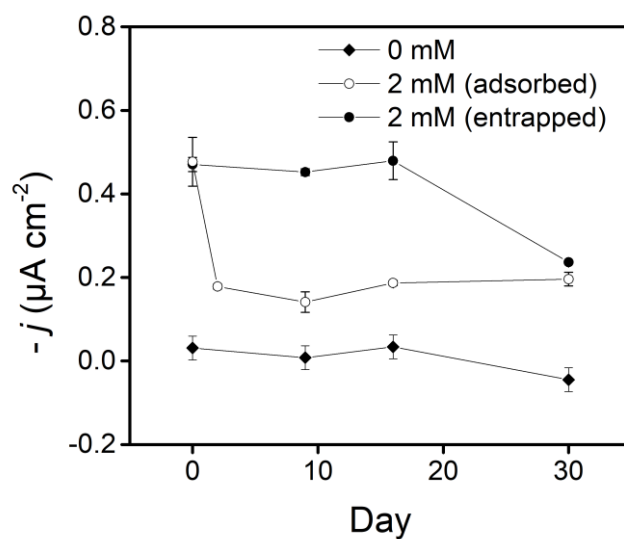


Figure 6.1.11. Life-time for two biosensors, with the enzymes adsorbed on the electrode or trapped in the hydrogel (n = 3). The biosensors were stored at 4° C. Biosensors with alginate hydrogel also in humid environment to avoid alginate drying. Medium: MES-NaOH (0.2 M, pH 7), 0.145 M KCl, 0.01 M CaCl₂, 0.5 mM TMB.

2.7. Interference test

Common blood interfering substances such as salicylic acid (SA), acetaminophen (AP), creatinine (CN), uric acid (UA) and ascorbic acid (AA) may have positive or negative contribution to the amperometric signal obtained with the presented biosensor. In this context, the maximum common concentration of these molecules in blood (Medscape) is added to the buffer solution and, both in absence (0 mM glucose) and presence (4 mM glucose), the current response at 0.1 V vs. Ag pseudo-reference electrode are measured.

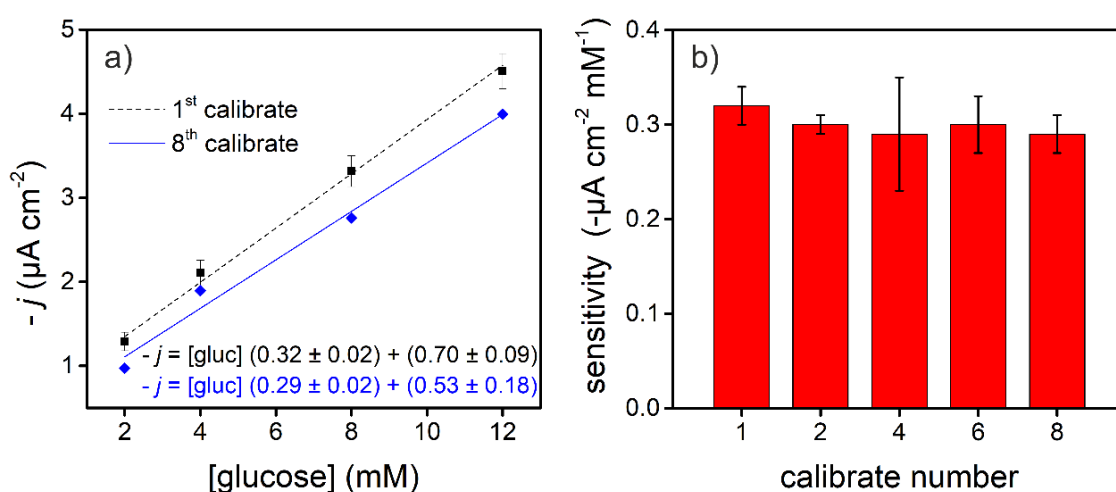


Figure 6.1.12. Electrode reusability in consecutive analysis. Calibration curves for glucose using the same transducer and successive alginate hydrogel electrodeposition steps with HRP-GOx. Medium: MES-NaOH (0.2 M, pH 7), 0.145 M KCl, 0.01 M CaCl₂, 2 mM TMB. The chip was washed with PBS between calibrations to remove the alginate matrix and afterwards cleaned electrochemically with 5 cyclic voltammeteries between 0 and 1.5 V in 0.5 M H₂SO₄. Scan rate: 100 mV s⁻¹, n=5.

As shown in **Figure 6.1.13**, there are not significant differences in the biosensors response due to the presence of these interfering species (Kruskal-Wallis and Dunn's multiple comparison tests, $P < 0.05$), except in case of ascorbic acid. In this case, at 0.5 mM TMB, almost no current was registered. This molecule is well known as antioxidant, so the provoked interference is related to the reduction of the previously oxidized TMB in the GOx-HRP cascade reaction. This problem was resolved with an increment of TMB from 0.5 to 2 mM. Then, a normal response to glucose was register due to the molar

excess of TMB respect AA (2 mM and 0.15 mM respectively). This result is very important in order to establish the proper conditions to proceed blood samples where the AA is present.

2.8. Biosensor response with whole blood samples

With the optimized biosensor we proceed to measure human samples of plasma and whole blood, directly (health) and spiked (pre-diabetic and diabetic) to comply with the hyperglycaemic conditions. Real blood samples required a re-optimization of the enzymes concentration to adapt the response of the biosensor, lower in this case due to matrix effects, to the glucose concentration.

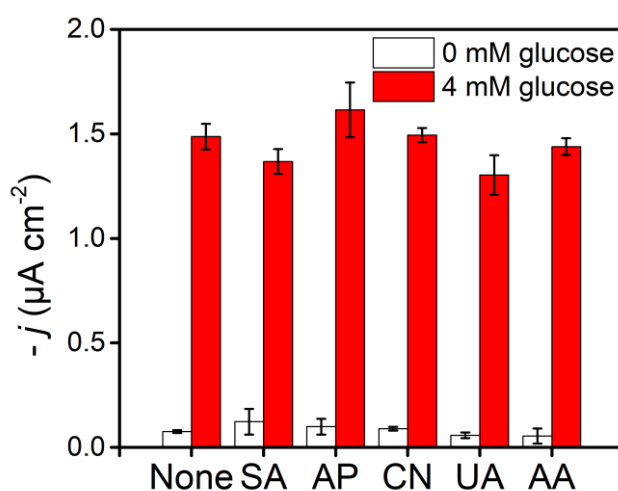


Figure 6.1.13. Amperometric current density responses of the biosensor in presence of interfering species: None (no interfering species), SA (0.75 mM), AP (0.35 mM), CN (0.25 mM), UA (0.5 mM) and AA (0.15 mM). Medium: MES-NaOH (0.2 M, pH 7), 0.145 M KCl, 0.01 M CaCl₂, TMB (0.5 mM or 2 mM in case of AA) (n = 3). Detection potential: 0.1 V vs. Ag pseudo-reference electrode.

A proper calibration with real samples required HRP and GOx concentrations of 55 $\mu\text{g mL}^{-1}$ and 25 $\mu\text{g mL}^{-1}$ respectively, maintaining the TMB concentration at 2mM. As shown in **Figure 6.1.14**, good linear responses were then obtained both in plasma ($R^2 = 0.995$) and whole blood ($R^2 = 0.996$). It is remarkable that the sensitivity and the LOD is similar in both cases (whole blood and plasma), concluding that the presence of cells did not interfere the obtained results and confirming the good performance of the alginate matrix as size-exclusion barrier, in contrast to the response to spiked samples of a

6. Results

reference biosensor (enzymes in solution and no hydrogel membrane protecting the transducer) where the sensitivity is very low in case of plasma and negligible in case of whole blood (dashed lines in **Figure 6.1.14**).

With this design of membrane, it was possible to distinguish between healthy, pre-diabetic and diabetic patients with high precision in a single, fast and sensitive assay.

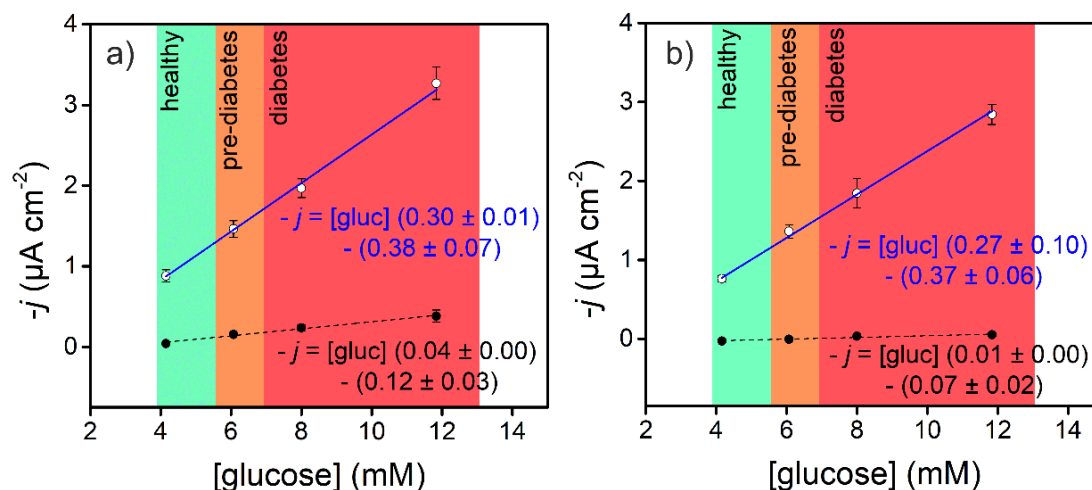


Figure 6.1.14. Calibration curves of biosensor to different glucose concentrations in a) human plasma and b) human whole blood (n= 6). Dashed line represent the response of a biosensors with same amount of enzymes in suspension but no alginate membrane on the WE. Mediator: 2 mM 3,3',5,5'-tetramethylbenzidine. Detection potential: 0.1 V vs. Ag pseudo-reference electrode. Stabilization time of the chronoamperometry: 3 min.

3. Conclusions

A simple, reusable and easily-fabricated biosensor for glucose detection in whole blood samples was developed using electrodeposited calcium alginate as enzymatic membrane. The geometrical selective electrodeposition of the hydrogel, besides the possibility of immobilize different enzyme types or concentrations, makes the fabrication very reproducible and adaptable to different samples. Furthermore, the hydrogel is easily re-dissolved with common buffers (PBS, citrate, among others) so it is possible to reuse the same electrochemical transducer for successive enzyme immobilization steps and analytes detection. This easy removing and deposition of new membranes lead to costs and time saves, since no extra calibration is needed. The alginate also demonstrates to be a good barrier protecting the electrodes from biofouling, which permits a reliable measure

of whole blood glucose concentration, and also capable of maintaining the enzyme activity longer times than other simple fabrication method such as adsorption. In fact, it is critical to use this protective membrane in case of real samples analysis (plasma and whole blood) as almost no response is obtained with bare transducers. Good sensitivity of the biosensor was achieved, for buffer, plasma and whole blood measurements, modulating the enzymatic content of the membrane and the mediator concentration, making it possible to distinguish normal from hyperglycemic glucose concentrations.

6.2. Alginate Membrane Integration in POC Device for Glucose and Lactate Determination

Abstract

At the POC, on-side clinical testing allows fast biomarkers determination even in resource-limited environments. Current POC systems rely on tests selective to a single analyte or complex multiplexed systems with important portability and performance limitations. Hence, there is a need for handheld POC devices enabling the detection of multiple analytes with accuracy and simplicity. Here we present a reconfigurable smartphone-interfaced electrochemical LOC with two working electrodes for dual analyte determination enabling biomarkers' selection in situ and on-demand. Biomarkers selection was achieved by the use of electrodepositable alginate hydrogels. Alginate membranes containing either GOx or LOx were selectively electrodeposited on the surface of each working electrode in around 4 min, completing sample measurement in less than 1 min. Glucose and lactate determination was performed simultaneously and without cross-talk in buffer, FBS and whole blood samples, the latter being possible by the filtration capacity of the hydrogels. At optimal conditions, glucose and lactate were determined in a wide linear range (0 -12 mM and 0 – 5 mM, respectively) and with high sensitivities (0.24 and 0.54 $\mu\text{A cm}^{-2} \text{mM}^{-1}$, respectively), which allowed monitoring of Type-1 diabetic patients with a simple dual analysis system. After the measurement, membranes were removed by disaggregation with the calcium-chelator PBS. At this point, new membranes could be electrodeposited, this time being selective to the same or another analyte. This conferred the system with on-demand biomarkers' selection capacity. The versatility and flexibility of the current architecture is expected to impact in POC analysis in applications ranging from homecare to sanitary emergencies.

This chapter contents results previously published in:

Congresses:

Portable and Miniaturized Lab on a Chip with Regenerable Membrane for Sanitary Emergencies. Augusto Márquez, Joan Aymerich, Pablo Giménez-Gómez Michele Dei, Francesc Serra-Graells, Cecilia Jiménez-Jorquera, Carlos Domínguez and Xavier Muñoz-Berbel, *Proceedings*. 2017, 1, 736. (Oral Contribution at the 5th International Symposium of Sensor Science, Barcelona, Spain).

Journals:

Reconfigurable multiplexed point of Care System for monitoring type 1 diabetes patients. A. Márquez, J. Aymerich, M. Dei, R. Rodríguez-Rodríguez, M. Vázquez-Carrera, J. Pizarro-Delgado, P. Giménez-Gómez, Á. Merlos, L. Terés, F. Serra-Graells, C. Jiménez-Jorquera, C. Domínguez, X. Muñoz-Berbel, *Biosens. Bioelectron.* 2019, 136, 38.

Acknowledgements:

The used μ -potentiostat and smartphone-based application were designed and developed by J. Aymerich and M. Dei.

Biochemical analysis of mice samples were done by R. Rodríguez-Rodríguez and M. Vázquez-Carrera.

Electrodes array chips were designed by P. Giménez-Gómez and Á. Merlos and fabricated in the Clean Room of the IMB-CNM.

1. Introduction

POC systems have impacted in clinical diagnosis for enabling diagnostic tests out of central medical laboratories and near the side of patient care.^{195,196,197} Their advantages include low-cost, simplicity, portability, miniaturization and minimal user intervention, which make them ideal to operate in resources-limited environments such as developing countries, the bedside of the patient or at home.¹⁹⁸ From the 80s, many POC tests for fast and accurate on-side determination of glucose,¹⁹⁹ lipids,²⁰⁰ glycohemoglobin (HbA1c),²⁰¹ hepatitis C virus (HCV),²⁰² immunodeficiency virus (HIV),²⁰³ influenza,²⁰⁴ urinalysis,²⁰⁵ hematology,²⁰⁶ several types of cancer,^{207,208,209,207} pregnancy²¹⁰ or prothrombin²¹¹ have been produced and commercialized, mostly based on lateral flow test or immunoassays.^{212,213}

Main limitations of current POC systems rely on the poor versatility and adaptability of the tests. That is, most POC systems are restricted to a single analyte and the application to another one requires the almost complete redesign of the test and/or the device. This is quite limiting since, in many cases, an appropriate diagnosis or treatment monitoring requires clinical evidences from more than one analyte.²¹⁴ This is the case of type 1 diabetes mellitus, a global life-threatening pathology with an incidence rate per annum of 3.4%.²¹⁵ Analysis of early metabolic changes during the development and progression of diabetes is crucial to the management of the disease. Among these changes, determination of circulating lactate, in addition to glycaemia, has been reported to be a helpful predictor of poorly regulated type 1 diabetes mellitus.²¹⁶ In addition, recent reports on antidiabetic drugs have revealed novel mechanisms of action involving substantial changes on lactate and related metabolites.^{217,218} Therefore, monitoring both glucose and lactate lead, not only for an early detection of diabetes, but also shed light on novel targets and signalling pathways regulating the disease.

Multiplexed systems may solve this problem by providing a way to determine multiple analytes from a single specimen.^{219,220} Currently, they consist of combinations of individual tests spatially or regionally separated from the others by spots,²²¹ wells,²²² independent channels (channel networks)²²³ or electrodes (electrode arrays).²²⁴ Each spot, well, channel or electrode is functionalized to

recognize one analyte and this selectivity cannot be modified over time. Since each detection area/element is operated individually, multiplexed systems normally require complex and bulky instruments difficult to operate out of the laboratory. The few portable multiplexed systems, also known as multiplexed POC,²²⁰ are mostly single use and present limited multiplexing capacities and poor versatility. Some devices based on microelectrode arrays have been already developed for the simultaneous determination of glucose and lactate in rat brain samples^{225,226} or in serum²²⁷. In the case of brain analysis, the systems used glutaraldehyde as cross-linker for covalent bio-functionalization of the transducer. The final biosensor was thus application-specific, could not be adapted to other analytes, and required high enzyme concentrations between (10 mg/mL of GOx and 20 mg/mL of LOx, respectively). The system designed to measure serum samples still required high enzyme concentrations (30 mg/mL of GOx and 10 mg/mL of LOx, respectively) and, although very sensitive, presented a very short lineal range, which was very far from a real application.

In an attempt to solve this open issue, a cost-effective, miniaturized, portable and smartphone-interfaced POC system has been developed, which provides multi-analyte determination in whole blood and in situ selection of the analyte on-demand. Analyte selection is achieved by means of electro-addressable and selective alginate hydrogel membranes. Alginate electrodeposition is achieved by acidic dissociation of calcium carbonate particles.¹⁰² That is, water splitting produces the local acidification of the medium and calcium release near the working electrode. This process leads to the formation of alginate hydrogels on the working electrode, with spatial resolution and thickness control.²²⁸ The presence of selective recognition biomolecules, e.g. enzymes, in the alginate precursor solution enables the generation of selective bio-recognition membranes in situ^{228,229} and the selection of the analyte on-demand. Alginate membranes present additional advantages such as long-term stability of the biomolecules and filtering capacity, enabling the measurement in whole blood samples without additional separation steps, and requiring small enzymes concentrations (around 0.5 mg/mL)²²⁸. These membranes, moreover, disaggregate at room temperature when immersed in a solution containing a calcium chelator solution, e.g. PBS. After that, the membrane can be re-generated and the removal/re-generation process can be

repeated multiple times. This confers the LOC with high versatility and adaptability, since the re-generated membrane can contain the same or another biorecognition element, enabling the determination of multiple analytes with the same simple and miniaturized system.

This smartphone-based POC present, therefore, (i) high-versatility, adaptability and capacity for whole blood analysis by the use of electrodeposable alginate hydrogels as selective membranes; (ii) durability, sensitivity and accuracy in the measurement by incorporating silicon-based micro-electrodes obtained by microfabrication technologies; and (iii) simplicity, portability and lightweight by combining a simple microfluidic architecture on PMMA and PDMS with a minimalistic μ -Potentiostat controlled and powered by the smartphone (without the need of external batteries). The performance of the reconfigurable multiplexed POC system is here evaluated in the identification of Type-I diabetic patients through the measurement of glucose and lactate.

2. Results

2.1. POC system

The smartphone-based POC was designed and fabricated differentiating three main parts (**Figure 6.2.1**), namely i) the silicon chip for amperometric measurements, ii) the microfluidic structure for fluid management and chip packaging, and iii) the smartphone-interfaced μ Potentiostat, designed and manufactured with discrete elements to control measurement. Each component fabrication is described in *Materials and Methods* section.

2.2. In situ production and re-generation of alginate membranes

The element conferring selectivity, versatility and reversibility to the smartphone-interfaced POC system was the electrodeposable alginate hydrogel used as biocatalytic membrane by incorporation of enzymes. The in situ generation and removal of the alginate membrane was based on an already reported protocol,¹⁰² explained in detail in *Materials and Methods*, and adapted to the LOC architecture.

The protocol to demonstrate the versatility and adaptability of the POC system is illustrated in **Figure 6.2.2**. First, the empty chamber containing the four electrodes for

amperometric measurements (**Figure 6.2.2a**) was filled with the alginate hydrogel precursor solution containing GOx and HRP (**Figure 6.2.2b**). After applying an electrodeposition potential of 1.4 V vs. Ag/AgCl pseudo-reference for 90 s (**Figure 6.2.2c**) and rinsing with distilled water to remove the excess material a biocatalytic membrane selective to glucose was generated on the first WE surface (**Figure 6.2.2d**). In a similar process (**Figure 6.2.2e, 6.2.2f**), a membrane selective to lactate was electrodeposited over the second WE, by the substitution of GOx by LOx in the second injected precursor.

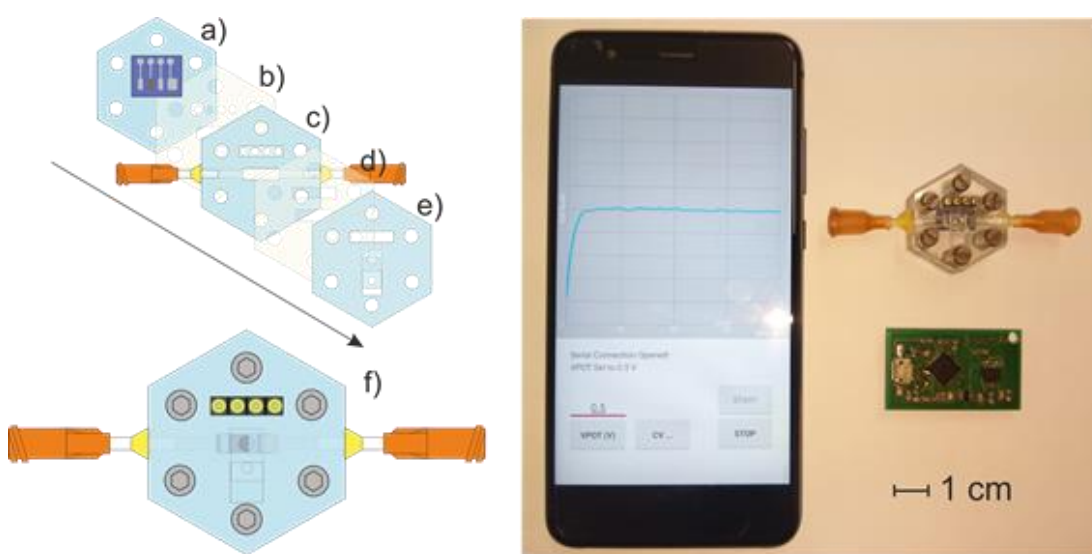


Figure 6.2.1. Main parts of the smartphone-based POC device depicted in assembly order from bottom to top (a-e). PMMA made pieces (a, c and e) represent the base (holding the silicon based electrodes array), channel-chamber and cover parts respectively. PDMS layers (b and d) are introduced among the channel-chamber and the other two pieces to avoid any leakage. On the bottom (f), the whole device from a top view. On the right side, a picture of the three independent elements for the measurement: mobile phone with the controlling application, PMMA-PDMS device and μ Potentiostat circuit.

At this point, the introduction of a glucose containing solution first (**Figure 6.2.2g**) and a lactate containing solution afterwards (**Figure 6.2.2h**), produced the selective oxidation of the analyte and hence the mediator (TMB), which changed from uncoloured to blue as can be appreciated in the respective membranes.

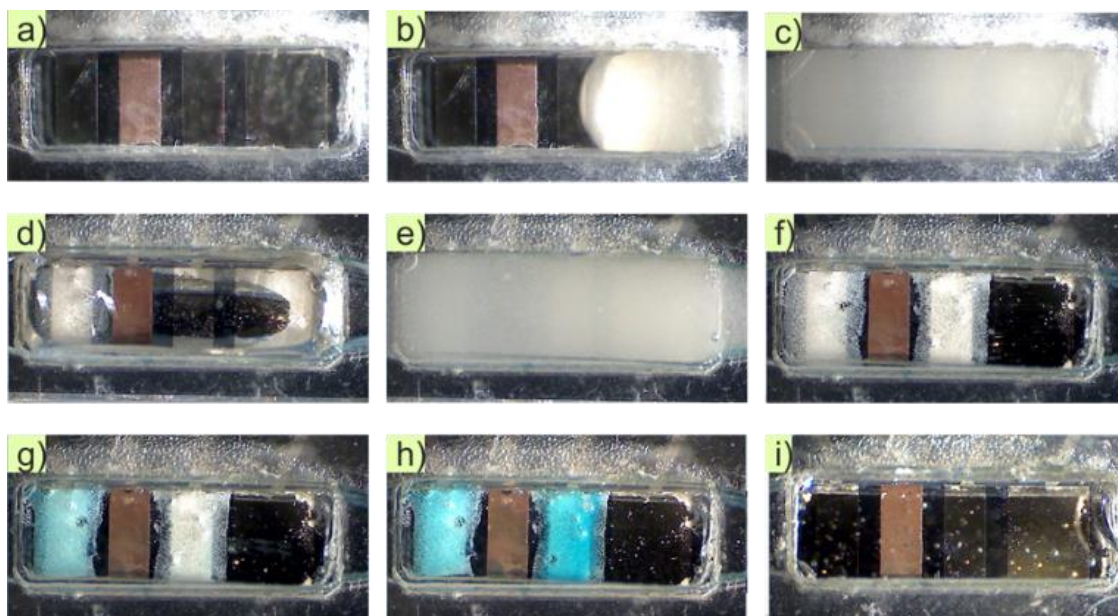


Figure 6.2.2. Electrodeposition, detection and chamber cleaning protocol. Top view of closed chamber with a four electrodes chip: a) empty, b) chamber filled with alginate precursor for glucose detection 1, c) hydrogel electrodeposition, d) chamber rinsing to eliminate first precursor excess, e) chamber filled with alginate precursor for lactate detection, f) chamber rinsing to eliminate second precursor excess, g) colour change result of the reaction that occurs in the membrane with glucose, h) colour change result of the reaction that occurs in the membrane with lactate. Finally, the chamber is washed with PBS to dissolve the membranes.

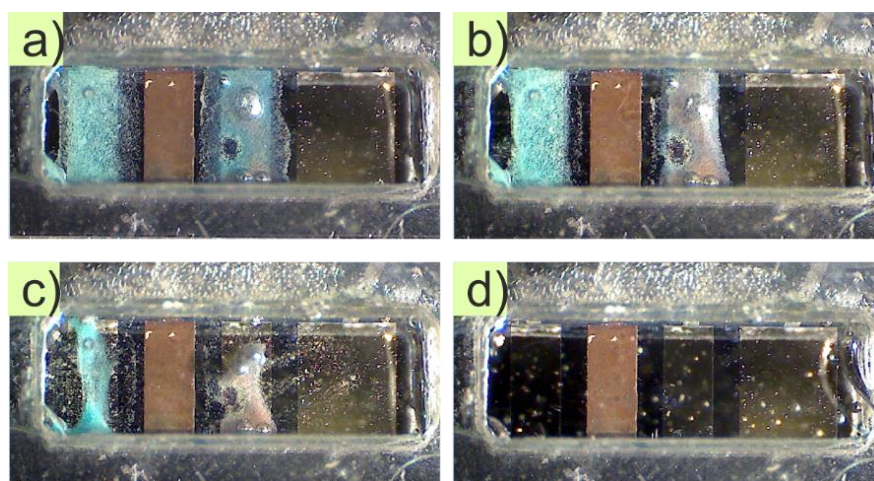


Figure 6.2.3. Disaggregation of alginate membranes by PBS after the co-detection of glucose and lactate in a MES buffered solution.

The oxidized TMB concentration, proportional to the analytes, was determined amperometrically at 0.1 V vs pseudo Ag/AgCl, the reduction potential of the TMB. The

biocatalytic membranes were then removed by injection of a PBS solution (**Figure 6.2.3**), and could be re-generated afterwards following the same protocol and enabling in situ selection of biomarkers on demand.

2.3. Simultaneous determination of multiple analytes and cross-talk analysis in serum samples

In the sequential determination of multiple analytes with the smartphone-interfaced POC system, glucose and lactate were selected as biomarkers for their interest in identification and monitoring of type 1 diabetes patients. In both cases, the biosensor response was maximized in separate prior to the calibration in FBS to guarantee optimal measurement conditions. By adjusting the concentration of enzyme in the biocatalytic membrane, it was possible to adapt the linear response of the biosensor to the analyte level in real samples. Concretely, HRP content in the precursor solution was fixed to 15 activity units mL⁻¹ and the content of GOx and LOx was increased until reaching maximum amperometric response for the largest analyte concentration of interest²²⁸ (i.e. 10 mM glucose and 5 mM lactate in case of human samples and 70 mM glucose and 10 mM lactate in case of mice). According to this, the optimal GOx and LOx concentrations were set at 2 and 10 activity units ml⁻¹ and 0.2 and 5 activity units ml⁻¹, respectively. The results for the two optimizations were in agreement with the maximum current density allowed by the amperometric system since in both cases reached a value close to 4 μA cm⁻².

Under optimal condition, the glucose biosensor presented a sensitivity of 0.33 μA cm⁻² mM⁻¹ and a LOD of 0.18 mM while the lactate biosensor has a S of 0.78 μA cm⁻² mM⁻¹ and a LOD of 0.12 mM (raw data for electrochemical measurements is plotted in **Figure 6.2.4**). LOD was determined considering the 3 sigma method (three times the standard deviation of the blank).

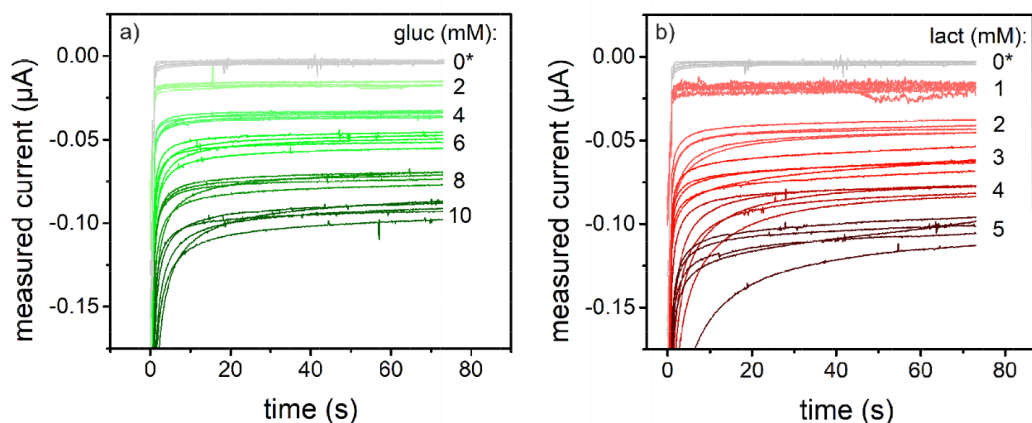


Figure 6.2.4. Response of the biosensor to the addition of different concentrations of glucose (a) or lactate (b) in FBS. The registered negative current is product of the reduction previously oxidized TMB and therefore proportional to the amount of analyte present in the sample. Working electrode surface: 0.025 cm^2 .

After biosensor optimization, several detection cycles combining glucose and lactate determinations were carried out to validate the biosensors (**Figure 6.2.5**) and to demonstrate the absence of cross-talk between measurements of glucose (**Figure 6.2.5a-c**) and lactate (**Figure 6.2.5d-f**). A detection cycle comprised i) biocatalytic membrane generation, ii) rinsing, iii) detection of the analyte and iv) membrane removal with PBS, as detailed previously. In each cycle, a single analyte concentration was determined. The replicas for a single biomarker concentration were, therefore, obtained from three independent membranes subsequently formed and removed. In the glucose determination (**Figure 6.2.5a, 6.2.5b**), good repeatability in the generated membranes was observed in the whole linear range with variation coefficients (CV) below 18.5 % in all cases.

The calibration curve also presented good responses with a linear range from 0 to 12 mM ($R^2 = 0.99$) that ensured an accurate determination of the analyte in the range of interest. Due to the high repeatability of the membranes and the durability and stability of the micro-fabricated electrodes, it was not necessary to recalibrate the system between measurements, simplifying the assay and improving the performance of the whole POC system. It is important to note that after the removal of the membrane the amperometric system lost the capacity to respond to glucose

as shown in **Figure 6.2.5c**, although maintaining their activity and not requiring re-activation.

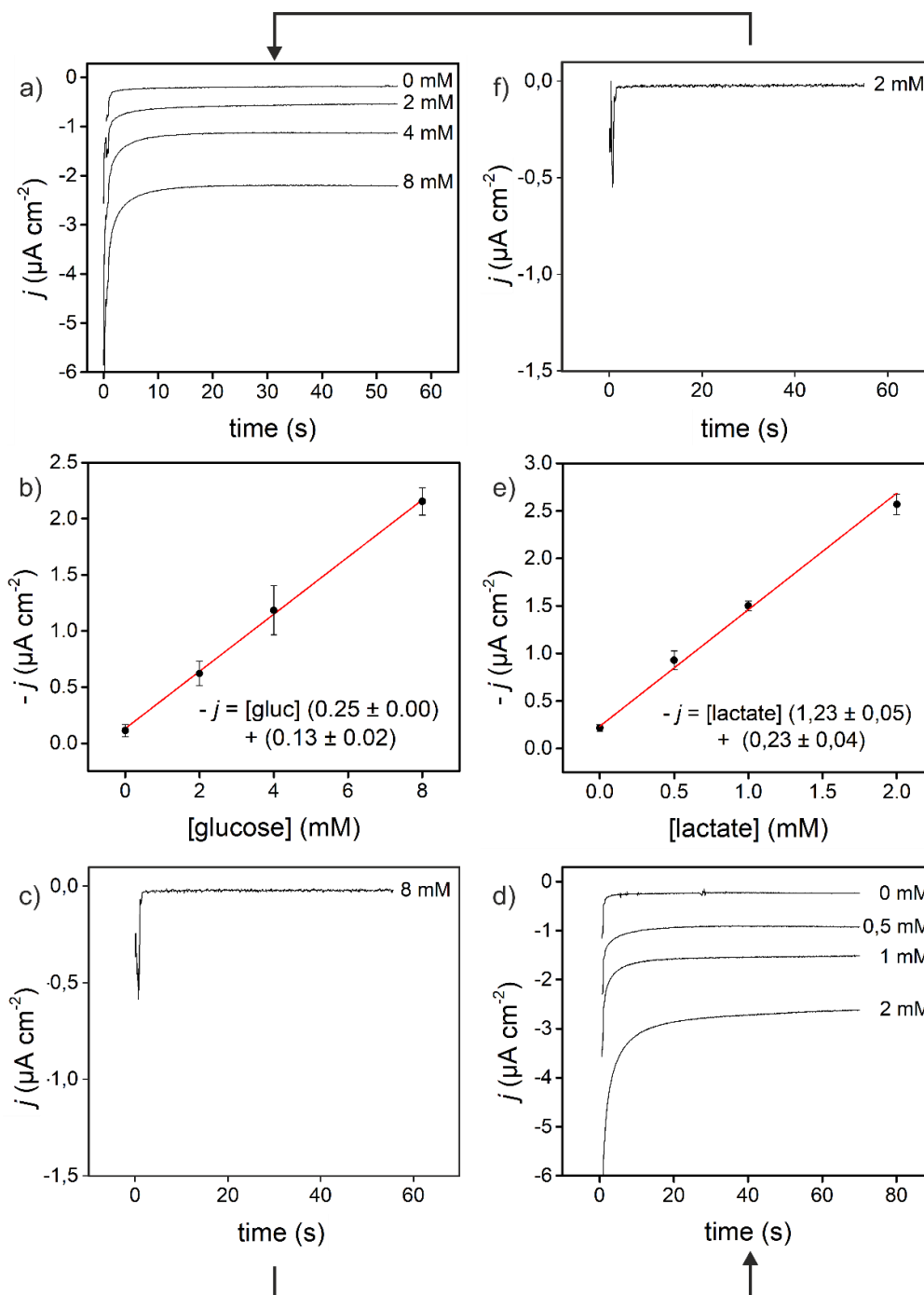


Figure 6.2.5. Cyclic detection with the same device alternating glucose and lactate. Amperometric response to different glucose (a) or lactate (d) concentrations and calibration curves of the stable current signals for glucose (b) or lactate (e). Amperometric response to 8 mM glucose (c) and 2 mM lactate (f) using a bare transducer after cleaning the biosensor chamber with PBS. Medium: 200 mM MES-NaOH pH 7 buffer, 145 mM KCl, 100 mM CaCl_2 and 2 mM TMB, $n=5$.

6. Results

This fact demonstrated that the removal of the membrane was complete and that it was not memory effect of the membrane between consecutively generated membranes, which not interfere subsequent measurements.

Similarly, lactate determination provided repetitive values from individually generated and removed membranes (**Figure 6.2.5d, 6.2.5e**), with good repeatability and CV below 10.7 % in any case, as well as a good calibration curve with large linear range from 0 to 2 mM ($R^2 = 0.99$). As before, the amperometric response to lactate in absence of a functionalized alginate membrane was negligible (**Figure 6.2.5f**) and, therefore, the memory effect was negligible.

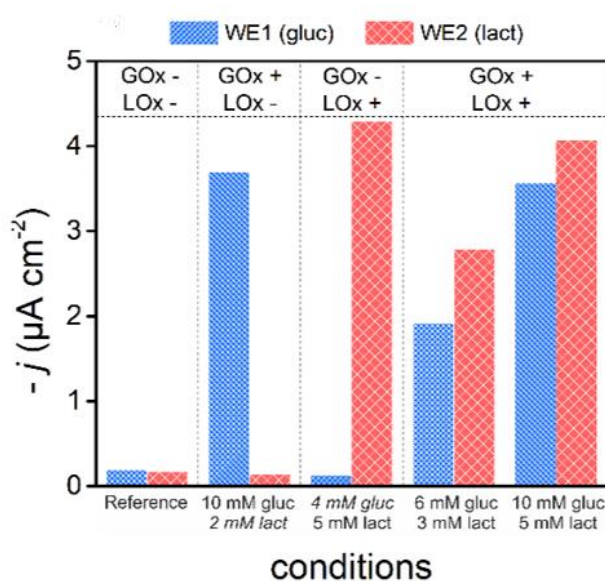


Figure 6.2.6. Cross-talk effect absence. Response to glucose and lactate when GOx or LOx are present or absent in the gel precursor. Only when both enzymes are present in the respective hydrogel, two signals are obtained proportionally to glucose and lactate concentrations (WE1 and WE2 respectively). When any of the enzymes is not present (or both) the signal for the specific analyte is negligible. FBS had an initial content of 2 mM lactate and 4 mM glucose. TMB stock solution is added to the samples to a final TMB concentration of 2 mM prior to detection.

When the electrodeposited membranes lacked of the necessary enzymes for the detection of one of the analytes (**Figure 6.2.6**), the amperometric system lost the capacity to respond to that, regardless the concentration of analyte in the sample. In addition, when both enzymes are present in the respective hydrogel, two signals were obtained, being

proportional to the glucose and lactate concentrations and comparable to the previous results from individual calibrations. Thus, the measurement of glucose did not interfere lactate determination, and vice versa. This fact demonstrated that it was not cross talk between consecutively generated membranes or among the two working electrodes during the same measurement.

2.4. Whole blood sample analysis

In the case of blood, samples were introduced to the POC system through the aperture present in the top piece of the microfluidic architecture to minimize sample consumption and dead volumes. The top aperture was closed during the precursor injection, electrodeposition, precursor recovery and chamber rinsing (**Figure 6.2.7a**). The pressure provided by the screws together with the PDMS layers avoided any leakage from the chamber during all these processes. The aperture was opened for whole blood analysis, which enable the introduction of the sample directly on top of the biosensor (**Figure 6.2.7b**). Once the signal was recorded, the gate was closed again and the chamber was washed with PBS first and finally with water for sample and membrane removal.

The alginate membrane was demonstrated to act not only as retention matrix for enzymes immobilization but also as a size-exclusion filter, enabling the retention of the cell fraction of the blood and minimizing biofouling.²²⁸ Additionally, the biosensor selectively responded to glucose without significant contribution in the electrochemical signal by interfering molecules such as salicylic acid, acetaminophen, creatinine, uric acid or ascorbic acid, commonly present in real samples.²²⁸ This is of particular interest in the analysis of complex samples, e.g. whole blood.

This capacity was employed in the present work in the determination of glucose and lactate in whole blood samples without additional separation or purification steps. Blood samples were spiked with glucose doses emulating real situations of healthy persons, pre-diabetic and diabetic patients. When compared to analyte detection in buffer solutions, the sensitivity of both glucose and lactate decreased significantly with whole blood (**Figure 6.2.7c, 6.2.7d**). Concretely, it was reduced a 27 % (S in whole blood =

6. Results

$0.24 \mu\text{A cm}^{-2} \text{mM}^{-1}$) for glucose and a 31% (S in whole blood = $0.54 \mu\text{A cm}^{-2} \text{mM}^{-1}$) for lactate, mostly attributed to matrix effects. On the contrary, the LODs did not change in any case.

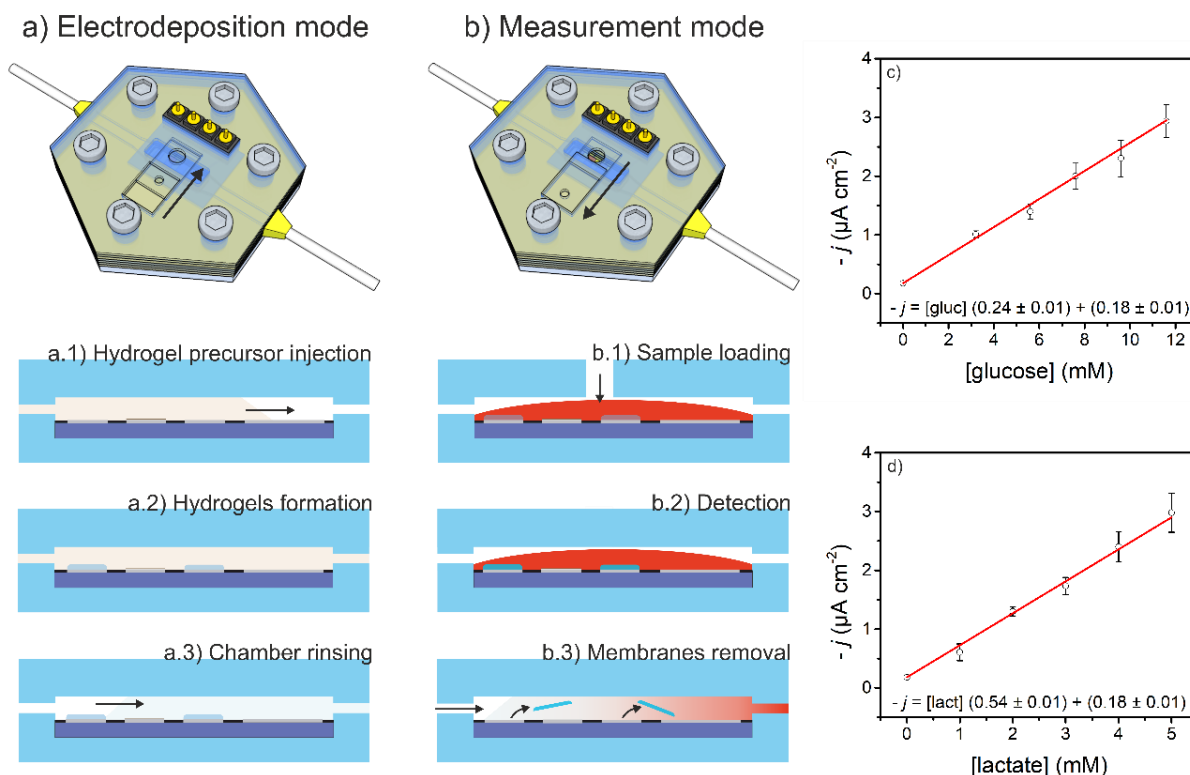


Figure 6.2.7. Electrodeposition and measurement modes of the POC device and lactate and glucose calibration in spiked whole blood samples. PMMA-PDMS construction including the open-closed system for the top block. In the electrodeposition mode a), the gate remains closed, while the alginate membrane is electrodeposited. For real sample analysis b), the gate is open and a drop of blood is added. Once the measurement is finished, the gate is closed again and the chamber is cleaned with PBS. Calibrations of spiked blood samples are depicted in c) for glucose and d) for lactate ($n=5$). Used blood had an initial content of 2 mM lactate and 4 mM glucose. TMB stock solution is added to the samples to a final TMB concentration of 2 mM prior to detection.

In terms of linear range, the biosensors presented larger linear ranges for glucose (from 0 to 12 mM) and lactate (from 0 to 5 mM), which allowed to distinguish between healthy and unhealthy levels of analyte. That is, glucose levels between 4 and 5 mM were considered normal, from 6 to 8 mM risky and over 8 mM were clearly related to diabetic

condition. Similarly, lactate levels may be indicative of many pathological states. For example, below 1 mM may be normal and over 2 mM were related to sepsis.²³⁰ Regarding diabetic patients, which was the case of study, lactate concentration between 5 and 7 mM were considered normal and below 4 mM pathological or indicative of type 1 diabetes.

Finally, the system maintained the high repeatability of the biocatalytic membranes, with CV below 20 %, which allowed analyte determination without constant recalibration of the system.

In conclusion, the current smartphone-interfaced POC system enabled on-demand selection of target molecules and multiple analyte determination in whole blood samples by in situ production/removal of biocatalytic membranes based on alginate hydrogels.

2.5. Real sample analysis and type 1 diabetes diagnosis

STZ-induced diabetic mice displayed fasting plasma glucose levels 5 times higher than the control group (**Figure 6.2.8a**) with a substantial reduction in plasma lactate concentrations (**Figure 6.2.8c**) with both methods. Results from the reconfigurable multiplexed POC system were in perfect agreement with the standard method. This was clear when evaluating the quantile-quantile (Q-Q) plots presented in **Figure 6.2.8b** and **6.2.8d** and corresponding to the comparison of the standard method with the POC system in the determination of glucose and lactate, respectively. As show, both plots presented good linearity ($R^2=0.99$) and comparable results, with a slope magnitude of 1 and y-intercept of 0.

Regarding the clinical relevance of the results, these data were in line with a previous report in which STZ-induced diabetic mice showed hyperglycaemia with a concomitant falling in circulating lactate levels.²¹⁷ Interestingly, treatment of these mice with metformin reduced glycaemia and restored lactate levels via direct stimulation of major glycolytic enzymes.²¹⁷ The authors of this study concluded that activation of glycolysis contributes to the hypoglycaemic effect of this drug. These findings might imply that type 1 diabetic patients with low lactate levels would benefit from the treatment with drugs, such as metformin, that stimulate glycolysis. In agreement with this, it has been recently reported that metformin improves insulin sensitivity in youth with type 1

6. Results

diabetes mellitus.²³¹ It would be interesting to study whether the improvement in the control of the disease in type 1 diabetic patients correlates with the restoration of lactate levels following metformin treatment.

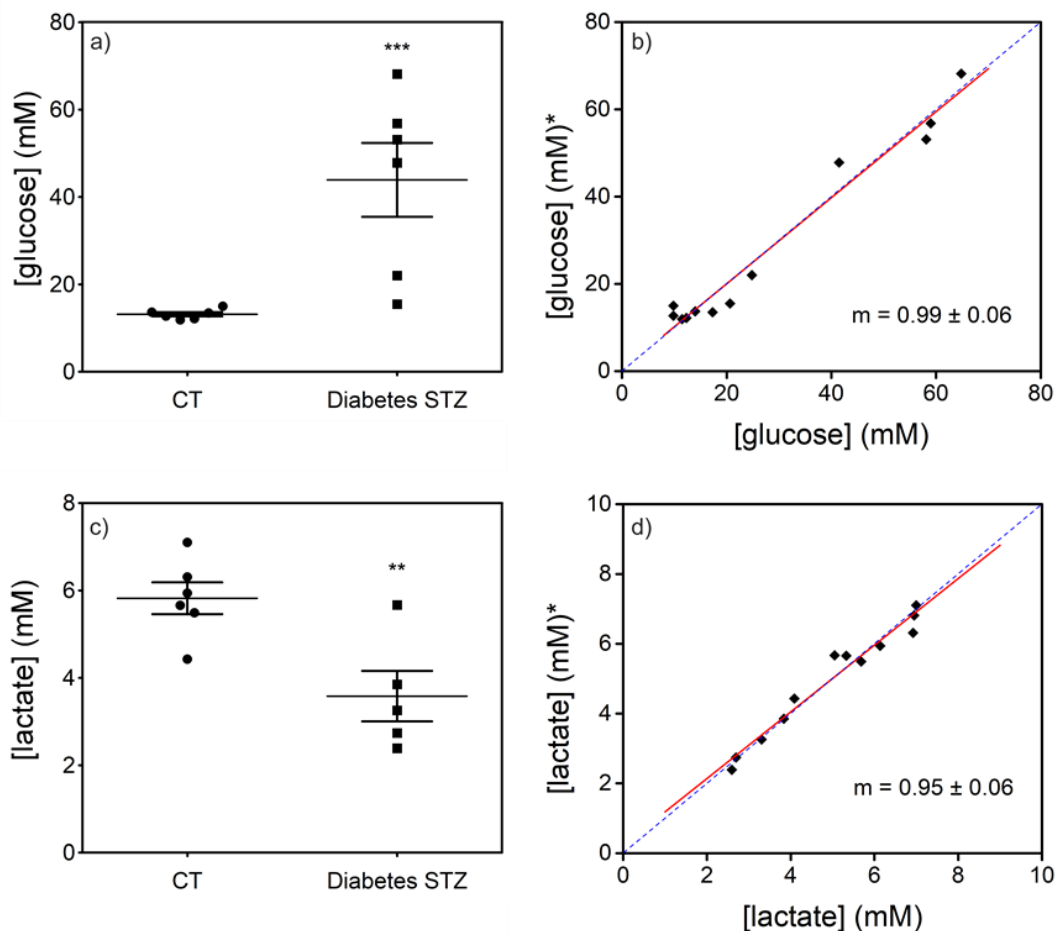


Figure 6.2.8. Glucose and lactate monitoring in streptozotocin-induced diabetic mice. Plasma glucose a) and lactate c) in control and streptozotocin-induced diabetic mice. Glycaemia was significantly increased in diabetic mice whereas plasma lactate concentration was decreased compared to control non-diabetic mice. Data are expressed as mean \pm SEM (n=5-6). **P<0.01, ***P<0.001 vs CT group (t-test). In b) and d), results obtained with the Automated Clinical Chemistry Analyzer Olympus AU480 (*) in the determination of glucose and lactate were compared to the ones obtained with the device.

3. Conclusions

A reconfigurable multiplexed POC system enabling in situ selection and electrochemical determination of multiple analytes in blood samples is developed and applied to the identification of type 1 diabetic patients through simultaneous

determination of glucose and lactate. The use of electrodepositable alginate hydrogels as biocatalytic membranes confer the system with operational flexibility, enabling in situ generation of membranes and selection of the analyte on demand, and capacity to measure in whole blood samples by the size-exclusion filtering capacity of the gels. The POC system is precise and repetitive by the use of silicon-chips, but also miniaturized, portable and low weight by the combination of costless polymer-based microfluidic structures and a dedicated μ potentiostat, controlled and powered by the smartphone. Glucose and lactate are thus determined rapidly and simply without cross-talk and in the range for type 1 diabetes control. The high portability of the complete system, together with the analytical versatility of the alginate membranes and the reusability of the electrodes due to the membrane protection qualifies this prototype to be used in healthcare centres and at home, but also in resource-limited environments such as in any location where a health emergency is taking place.

6.3. Silk-Fibroin Micro-Capillary Pads for Glucose Determination in Whole Blood

Abstract

In the search of new biomaterials for biosensing applications, SF from *Bombyx mori* appears as promising platform for photonic biosensing where other materials, such as paper, find limitations. Besides its notable optical properties (high transparency in the visible and high RI), SF has demonstrated to be an optimal matrix for biomolecules immobilization (drugs, antibodies, enzymes), maintaining their biofunctionality unaltered through time. The biocompatible immobilization of GOx, HRP and ABTS within the SF matrix leads to the conformation of a colorless transparent material that responds to the presence of glucose changing to deep purple. The reaction involves the tyrosine residues from the SF, becoming the matrix also an active component of the biosensor, tripling the absorbance signal of the ABTS radical. The integration of the doped SF within a PMMA structure allows blood filtration, decreasing the important interference from hemoglobin, and capillary pumping of plasma through the silk pad. After bio-reaction in whole blood samples, direct image analysis of the SF color change with inexpensive instruments or even by visual inspection.

This chapter contents results previously/to be published in:

Congresses:

Silk fibroin based nanophotonic crystal for biosensing. Augusto Márquez, E. Baquedano, P.A. Postigo, Salvador D. Aznar-Cervantes, J. L. Cenis, Carlos Domínguez and Xavier Muñoz-Berbel. (As Poster Contribution at MNE 2017, Braga, Portugal)

Silk Fibroin Pads for Whole Blood Glucose Determination. Augusto Márquez, Salvador D. Aznar-Cervantes, J. L. Cenis, Carlos Domínguez and Xavier Muñoz-Berbel, *Proceedings*. 2018, 2, 886. (As Poster Contribution at Eurosensors 2018, Graz, Austria)

Journals:

Silk-Fibroin Micro-Capillary Pads for Glucose Determination in Whole Blood. Augusto Márquez, Molíria V. Santos, Gonzalo Guirado, Salvador D. Aznar-Cervantes, Jose Luis Cenis, Carlos Domínguez, Silvia H. Santagneli, Fiorenzo G. Omenetto, Xavier Muñoz-Berbel, (*To be submitted*).

1. Introduction

Photonic based POC devices are conceived to transfer medical test from central laboratories to the place of patients' care. The flagship of POC devices is paper-based lateral flow assay, where the paper¹⁹⁶ pumps the liquid through the system by capillarity and the device provides the result after few minutes and without user's intervention. Albeit simple and low cost, most of LFAs are restricted to either yes/no or subjective and interpretable results. The reasons for that are: the opacity of cellulose papers, which limits the optical path to few microns, too short to perform absorbance measurements; and the ageing of the paper matrix, which discolor over time and produces color inhomogeneity at the readout zone. Alternatives based on nanocellulose papers, e.g. nanofibrillated papers²³² or bacterial cellulose,²³³ and synthetic microfluidic papers in cyclic olefin copolymer (COP)²³⁴ or off-stoichiometry-thiol-ene (OSTE),²³⁵ have been already produced overcoming some of previous limitations. However, the low transparency and variability of nanocellulose papers²³⁶ and the need for organic solvents in the processing of synthetic papers²³⁷, which may compromise biomolecules integrity and activity, limits their widespread implementation to POC.

In the pursuit of new materials for POC, SF from *Bombyx mori* has positioned as a real alternative to paper in the development of optical/photonic sensors. SF is a natural protein fiber with chemical and thermal stability,²³⁸ mechanical robustness,²³⁹ biocompatibility²⁴⁰ and controllable biodegradability.²⁴¹ Natural SF fibers can be degummed, dissolved in water²⁴² and regenerated to a number of morphologies, including sponges, hydrogels, tubes, composites, microspheres or thin films. These matrices serve most notably as surgical sutures (e.g. SOFSILK™), carriers for drug delivery²⁴³ and scaffolds for tissue engineering,²⁴⁴ although also used as flexible interfacial components in electronic and photonic devices, such as edible food sensors²⁴⁵ and organic light-emitting transistors.²⁴⁶ Taking advantage of the excellent optical properties of SF (i.e. RI of 1.54²⁴⁷, and full transparent in the visible range), bi- and three-dimensional optical components based on silk films have been already produced. These include diffractive patterns,¹⁶⁰ holograms,²⁴⁸ optical grating,¹²² waveguides²⁴⁹ and photonic crystals.²⁵⁰ Since SF films are obtained by crystallization at soft conditions (i.e. room temperature and vacuum), bio-macromolecules such as cells, antibiotics, monoclonal antibodies and peptides²⁵¹ can be incorporated in the bulk of the SF matrix, while preserving their structure and function^{252,253}.

Regarding the latter, in this chapter it is reported how SF films doped with enzymes and chromogenic redox mediators are used in the production of colorimetric silk-based LFAs, presenting cell-exclusion capacity and capillarity, for quantitative and sensitive determination of glucose in whole blood samples.

2. Results

2.1. Silk Fibroin films characterization

Transparent SF films of 10 μm thick were obtained after vacuum crystallization of aqueous solutions of SF at the experimental conditions detailed in ²⁴². These films presented high light transmittance in the visible range, always above 90% (**Figure 6.3.1a**), with some absorption below 300 nm. The crystallization protocol was completely green and water-based, and allowed the incorporation of water-soluble bio-molecules in the SF matrix while preserving their structure and function. The GOx and peroxidase (HRP), and the redox mediator ABTS were incorporated in the SF films for glucose determination. SF membranes doped with these biomolecules presented an additional absorption band at 420 nm associated to HRP absorption (**Figure 6.3.1a**). No one of these bands interfered in the colorimetric detection of glucose in whole blood.

The doping bio-molecules slightly modified the structure and properties of the SF layers. The transition from amorphous to crystalline structure of the SF has been widely studied by infrared spectroscopy²⁵⁴²⁵⁵¹²³ and is essentially attributed to changes in the β -sheet contribution to the amide I band (1600-1700 cm^{-1}). While the non-annealed SF present an amide I band centered around 1640 cm^{-1} , assigned to random-coil structures, in the annealed samples the band peak shifts to 1620 cm^{-1} (**Figure 6.3.1b**), which is attributed to β -sheet conformations. Additional β -sheet signal is recorded at 1700 cm^{-1} likewise a higher relative contribution of tyrosine side chain in the amide II at 1514 cm^{-1} , related to the packing of the β -sheet crystals.²⁵⁶ All these evidences of β -sheet formation are still present, but diminished, in the presence of HRP and GOx.

In accordance to previous X-ray diffraction studies,²⁵⁷ the SF films reported in this chapter showed diffraction peaks corresponding to the α -helix structure at 11.95° (lattice spacing, $d = 0.740$ nm) and 24.02° (0.370 nm), and to the β -sheet structure at 16.71° (0.530 nm), 20.34° (0.436 nm), 24.49° (0.363 nm), 30.90° (0.289 nm) and 34.59° (0.259 nm) (**Figure 6.3.1c**). Addition of enzymes into the SF matrix caused a remarkable change in the diffraction profile, especially in the α -helix peaks that almost disappeared. This

6. Results

change may be attributed to the entrapment of water-soluble enzymes in the hydrophilic α -helix regions, which produce a partial loss of crystallinity. Unfortunately, it was not possible to identify additional diffraction peaks associated to the presence of enzymes, suggesting that they either did not crystallize inside the SF film or produced a signal too weak to be detected.

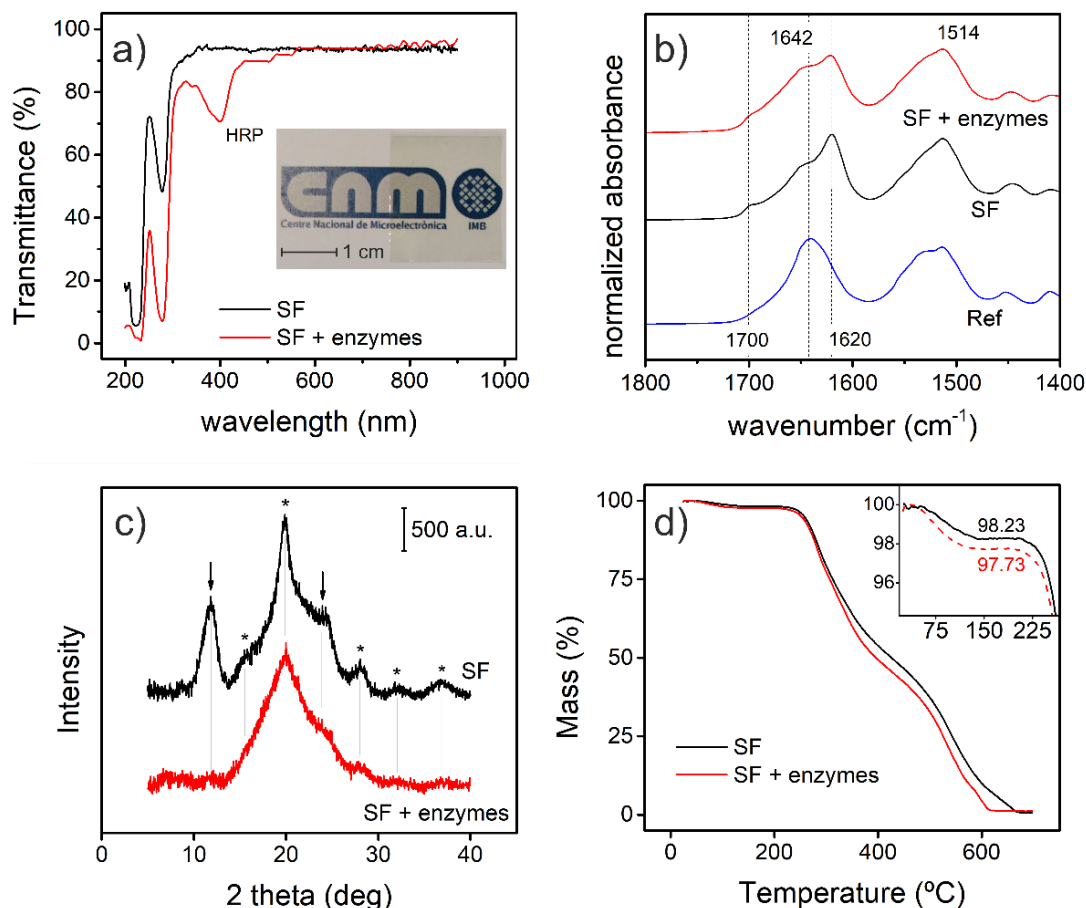


Figure 6.3.1. SF material characterization. a) UV-Vis-NIR transmittance spectra, b) ATR-FTIR spectra, c) X-Ray diffraction patterns and d) thermogravimetric analysis of 100 % w/v SF layers and SF layers doped with 4 % w/w GOx and 6 % w/w HRP. In figure a, a picture of a SF film corresponding to the red spectrum is shown. In figure b, the reference spectrum refers to a non-annealed SF film.

The presence of the biomolecules also modified the thermo-gravimetric records. SF films containing enzymes maintained a higher water content after vacuum annealing (around 1% in weight) and became slightly less resistant to temperature, presenting a faster degradation profile by the lower thermal stability of biomolecules (**Figure 1d**). Nevertheless, this stability loss did not compromise the performance of the biosensor.

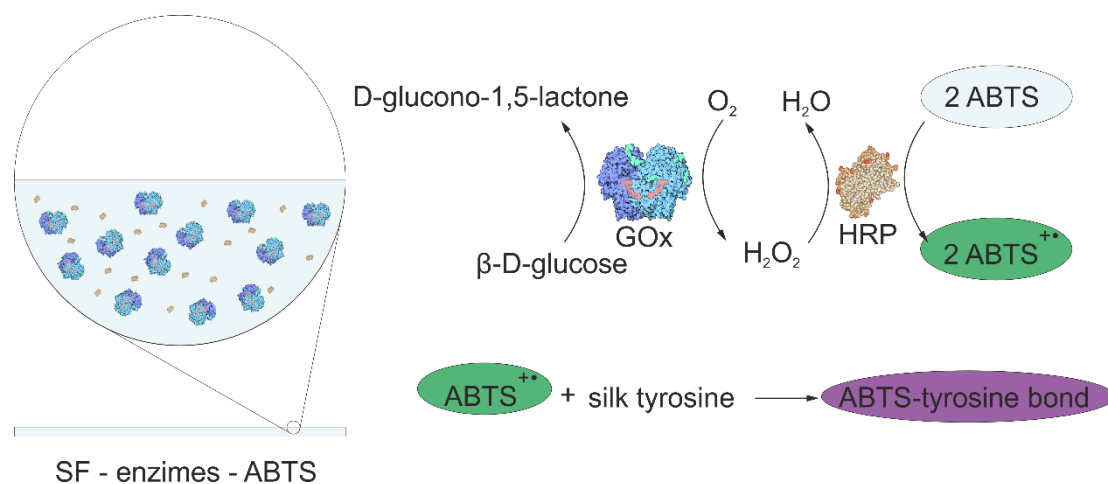


Figure 6.3.2. Scheme of the resulted functionalized SF layer and enzymatic reaction for glucose determination.

2.2. Biosensor principle: ABTS radical generation and self-reaction with the SF matrix

In a functional point of view, the incorporation of GOx, HRP and ABTS into the SF matrix confer it with sensitivity to glucose molecules. Importantly, SF was not only the support material where the bioassay took place, but it had an active role in the biosensing protocol that enhanced sensitivity. It is illustrated in **Figure 6.3.2**, where bio-functionalized SF films responded to glucose through a conventional cascade enzymatic reaction where the redox mediator ABTS was finally oxidized to its green radical ion form (**Figure 6.3.3a**, ii). In a second step, ABTS radicals reacted with the tyrosine amino acids of the SF matrix to produce a purple SF-ABTS compound, which presented a high molar absorption coefficient and absorption bands at 545 nm that doubled in magnitude the most intense absorbance band of ABTS radical at the same glucose concentration (**Figure 6.3.3a**, iii to v). The production of SF-ABTS complexes required 10 min for completion (**Figure 6.3.3b**) but even after 5 min, its absorbance magnitude was higher than ABTS.

The ABTS radical reaction with the SF tyrosine was first monitored by ATR-IR measurements. Several ABTS vibration signals that appeared in the SF films after the molecule integration either diminished or disappeared after the reaction with glucose (**Figure 6.3.4a**): 1120 cm^{-1} , corresponding to the aliphatic amine of the ABTS, and 1027 cm^{-1} of the C-H in plane bending of the tyrosine carbon that binds the ABTS nitrogen of the aliphatic amine.

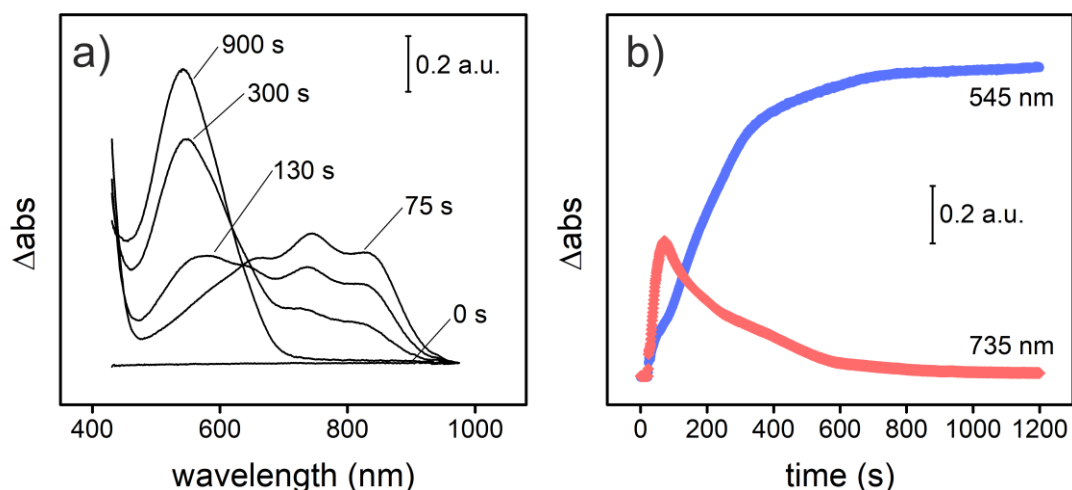


Figure 6.3.3. Colorimetric response of doped SF pads to glucose. a) Absorbance spectrum i) before and ii) 75, iii) 130, iv) 300 and v) 900 s after the functionalized SF is soaked by capillary pumping with a 12 mM glucose PBS solution. b) Absorbance spectra kinetics evolution for the soluble ABTS radical (745 nm) and the bonded ABTS to tyrosine residues (545 nm) of the SF.

The 882 cm^{-1} vibration that disappeared may correspond to the para-substitution benzene of the tyrosine, which had three substitutions after the reaction (due to the new bonding to the ABTS). Secondly, a Raman analysis revealed the clear appearance of new signals at 1200 , 1300 and 1350 cm^{-1} (related to C-C aliphatic symmetric stretching vibrations) and 1540 cm^{-1} (related to N=N symmetric stretching vibrations) and also a signal loss at 1610 cm^{-1} (related to C-N symmetric stretching vibrations) of the functionalized SF films after the reaction with glucose (**Figure 6.3.4b**). These vibrations, that reveals changes in the carbon and nitrogen bonds that bridge the cyclic moieties of the ABTS molecule, are in agreement with the proposed mechanism by Åkerström et al.,²⁵⁸ in which tyrosine amino acids demonstrated to react with ABTS radicals by reduction and covalent binding.

The irreversibility of the reaction was demonstrated by spectroelectrochemical measurements, where the ABTS lost its redox capacity after the molecule breakage and bonding to the tyrosine residues of SF (**Figure 6.3.5**). The doped SF was placed over a three-electrode chip in a closed chamber filled with PBS. Before the addition of glucose, ABTS radical absorbance spectrum appeared and disappeared depending on the applied potential (by cyclic voltammetry) (**Figure 6.3.5a, 6.3.5b**). After the addition of 12 mM glucose to the chamber, the absorbance spectrum was, firstly, a combination of ABTS

radical and ABTS-Tyrosine at the same time as the faradaic currents in the cyclic voltammetry decreased (**Figure 6.3.5c, 6.3.5d**). Finally, 900 s after the glucose addition, the absorbance spectrum corresponded only to the ABTS-Tyrosine structure and was independent on the applied voltage, while the faradaic currents in the cyclic voltammetry were negligible (**Figure 6.3.5e, 6.3.5f**).

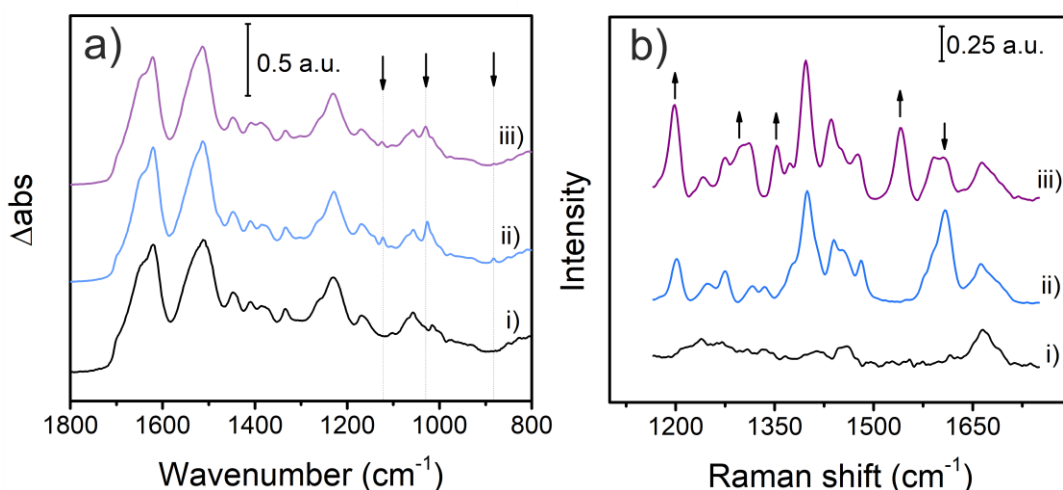


Figure 6.3.4. ATR-IR and Raman spectra of SF and SF with ABTS before and after the reaction with glucose. a) ATR-IR and b) Raman spectra i) annealed SF, and SF with 6 % w/w ABTS ii) before and iii) after the reaction with 12 mM glucose PBS buffer. Samples with ABTS also contained 3 % w/w HRP and 2 % w/w GOx.

Optimization of SF biocatalytic membranes entailed changes in the concentration of enzymes and mediators entrapped in the SF matrix to reach maximum sensitivity without modifying the wide linear response of the biosensor (from 0 to 12 mM glucose). The HRP:GOx relation was set at 3:2 w/w to avoid funnel effects in the enzymatic cascade reaction. GOx and ABTS concentrations were evaluated in the range between 0.5 and 3 % (w/w) and 3 and 9 % (w/w), respectively. Maximum sensitivity (**Figure 6.3.6a**) with high linearity (**Figure 6.3.6b**) was obtained at the highest concentrations of both enzymes and mediator, with the cost of reducing drastically the linear range. In opposition, below 6 % w/w ABTS, the relation between glucose and redox mediator was sub-stoichiometric and it was not possible to obtain a linear response of the sensor, particularly at low concentrations of enzyme. Above 6 % w/w ABTS, a 2% w/w GOx provided enough sensitivity and good linearity, while maintaining the wide linear range. These conditions were set as optimal for the SF biosensor.

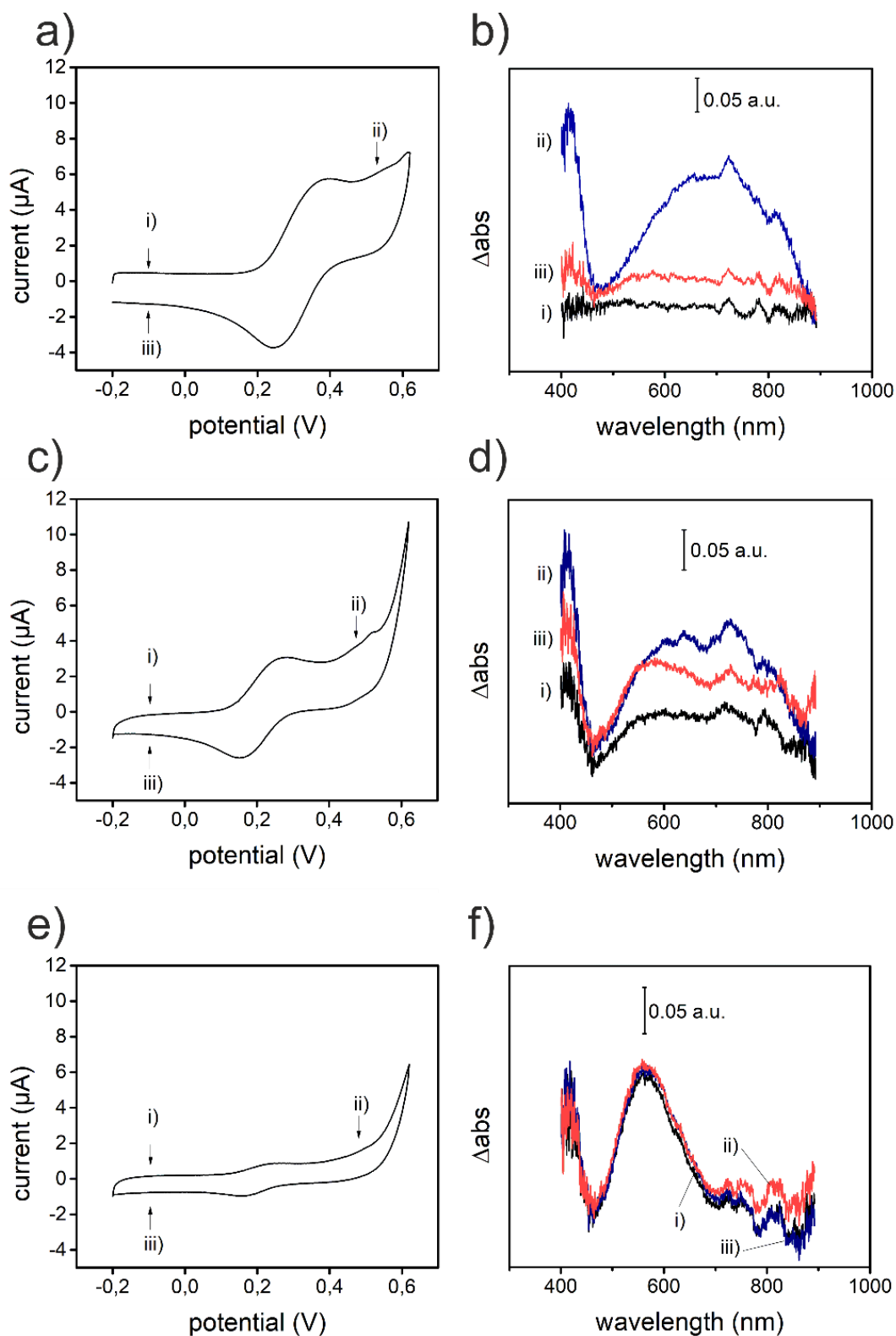


Figure 6.3.5. Spectroelectrochemistry results of the glucose detection reaction within the SF matrix. Cyclic voltammeteries and simultaneous absorbance spectra at indicated applied potentials for SF pads a-b) before and c-d) 90 s and e-f) 900 s after addition of 12 mM glucose solution.

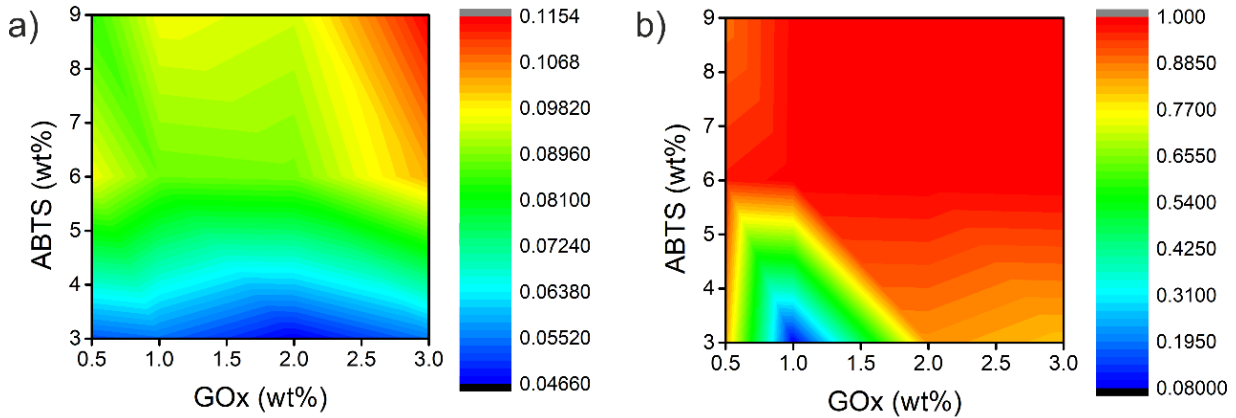


Figure 6.3.6. Sensitivity and linearity optimization of the biosensor response. a) Sensitivity (abs (a.u) mM⁻¹) and b) linearity (R²) of the response of the biosensor depending on the % wt of ABTS and GOx respect to the SF content of the pads (HRP is always in a 3:2 w/w relation to GOx).

Absorbance changes associated to the production of ABTS radicals after short reaction times (1 min) were too small to distinguish between hypoglycemic (4 mM glucose), pre-diabetic (8 mM) and diabetic (12 mM) patients (**Figure 6.3.7a**). In opposition, the formation of the SF-ABTS complex after 10 min of reaction produce a substantial change in the absorbance magnitude that allowed glucose quantification in the range of interest (**Figure 6.3.7b**).

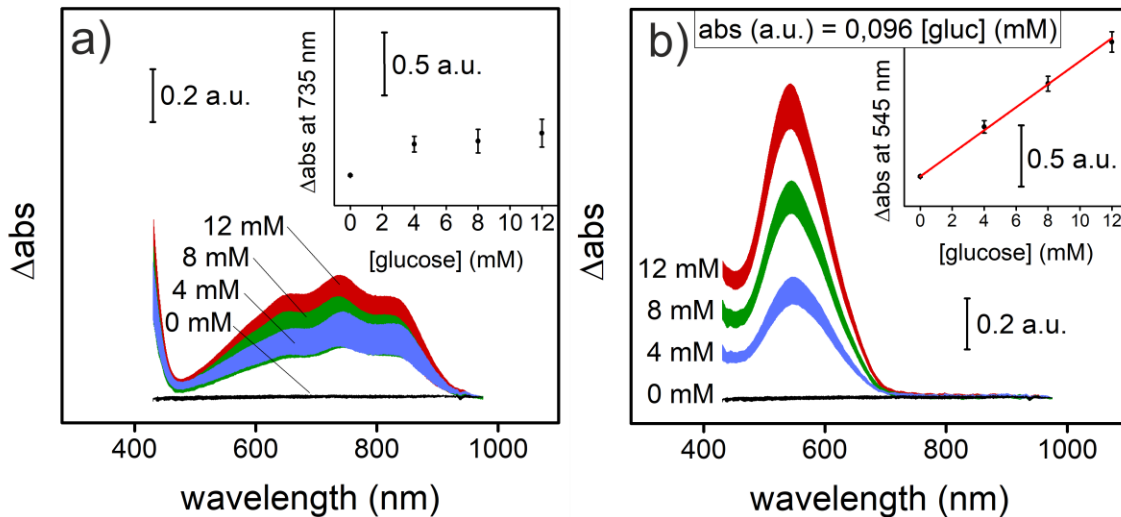


Figure 6.3.7. Absorbance spectra average of functionalized SF a) 75 s and b) 900 s after the addition of PBS solutions with different glucose concentrations (n=5). Calibration curves with absorbance values at a) 735 and b) 545 nm are depicted in the respective insets.

6. Results

Enzymes and ABTS immobilized within the SF matrix presented high stability. The biofunctionalized SF layers were stored for 40 weeks dried, at room temperature and in the dark to avoid premature light-induced ABTS oxidation. Regularly, SF pads were measured after incubation with glucose concentrations of 0, 4 and 8 mM in PBS. Along this time, functionalized SF pads maintained the same bio-catalytic activity that presented the first day of fabrication (**Figure 6.3.8**), widely surpassing the stability of most durable cellulose-based test strips in the market, which did not exceed 4 months.

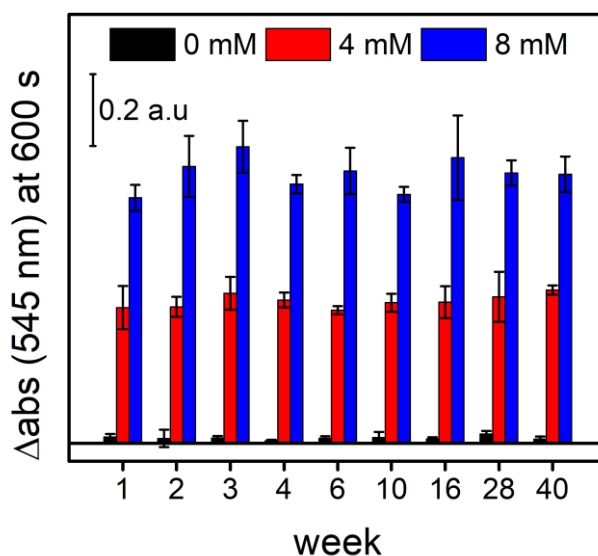


Figure 6.3.8. Durability of the biosensors represented as the average response (absorbance increment at 545 nm) of the pads to 0, 4 and 8 mM glucose PBS solution in time (n = 5).

2.3. Whole blood filtration and glucose quantification

The analysis of real samples with complex matrices such as whole blood involved dealing with a variety of interfering signals. In the case of optical detection, main interferences were due to absorption of hemoglobin. In opposition to conventional optical systems where blood is centrifuged or filtered before measurement to remove the interfering cell fraction, SF membranes presented size-exclusion filtering capacity and capillarity, which enabled direct determination of glucose in whole blood samples. Blood analysis required the fabrication of the PMMA holder illustrated in **Figure 6.3.9a-c**. The holder consisted of four layers bonded with PSA. From bottom up, it contained the base (i), a layer with a 2 mm well acting as blood reservoir (ii), a layer with the footprint of the SF pad for its correct positioning and with holes to ensure fluidic connection between layers (iii) and the top layer with two holes acting as fluidic inlet and outlet (iv).

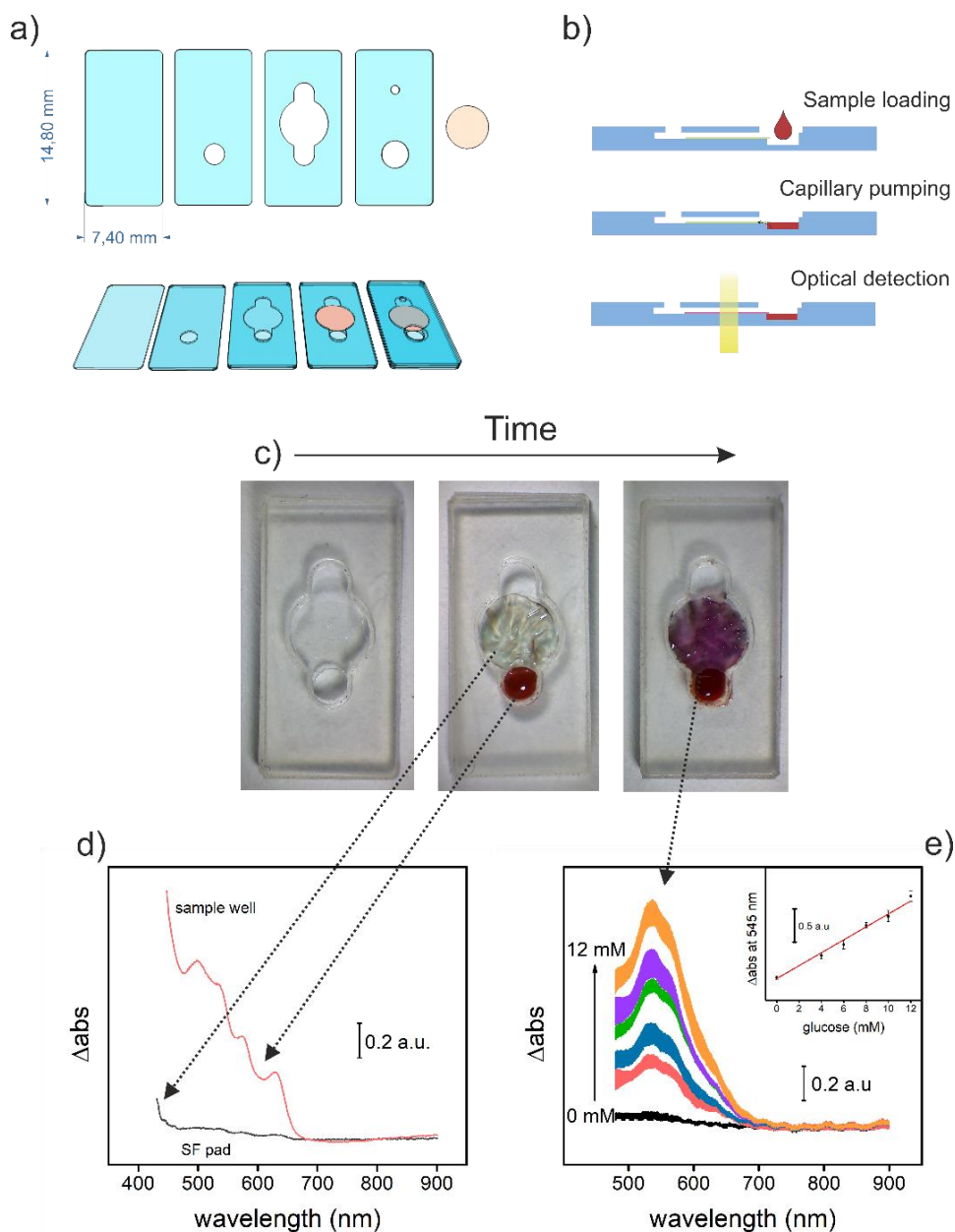


Figure 6.3.9. Glucose determination in whole blood samples. a) Scheme of the PMMA prototype for SF positioning and analyte measurement. b) Scheme of the cross-section and c) pictures from the top view of a SF pad inside the PMMA construction in the three key situations of the analysis: before blood addition, wetting by capillary pumping and after the reaction. d) Absorbance spectra of the blood charged well of the prototype and a SF pad wet by capillary pumping with whole blood. e) Absorbance spectra of the silk pads 600 s after the addition of whole blood (4 mM) and glucose spiked whole blood samples at (6, 8, 10 and 12 mM) and calibration curve using the absorbance values at 545 nm ($n=5$).

In the measurement, 4 μl of blood were loaded into the well (**Figure 6.3.9b, 6.3.9c**). The SF pad got in contact with the sample by the edge and, by capillarity, pumped the

6. Results

plasma through the SF matrix while maintaining the cell fraction into the well. The glucose present in the blood reacted with the enzymes and the mediator producing the color change of the SF pad from transparent to deep purple by the formation of the SF-ABTS complex (**Figure 6.3.9e**), which was detected optically (**Figure 6.3.9b**).

Thanks to the filtering capacity of SF pads, the interference associated to the presence of hemoglobin in red cells was widely minimized (**Figure 6.3.9d**). With this configuration, it was possible to determine glucose concentration in spiked whole blood samples with precision and sensitivity in the range from 0 to 12 mM (**Figure 6.3.9e**) using a simple broadband light source and a spectrometer.

Image analysis of SF pads was used for a more accessible and inexpensive glucose determination. SF pads after bio-recognition reaction were imaged with a conventional smartphone and analysis was performed with the free-ware *ImageJ* after separated quantification of RGB channels. A range of glucose concentrations were evaluated in PBS (**Figure 6.3.10a**) and in spiked whole blood samples (**Figure 6.3.10b**), for comparison. In both cases, color intensities for red, green and blue were in agreement to the amount of glucose present in the samples. Some differences were observed, however, in terms of sensitivity and linear range.

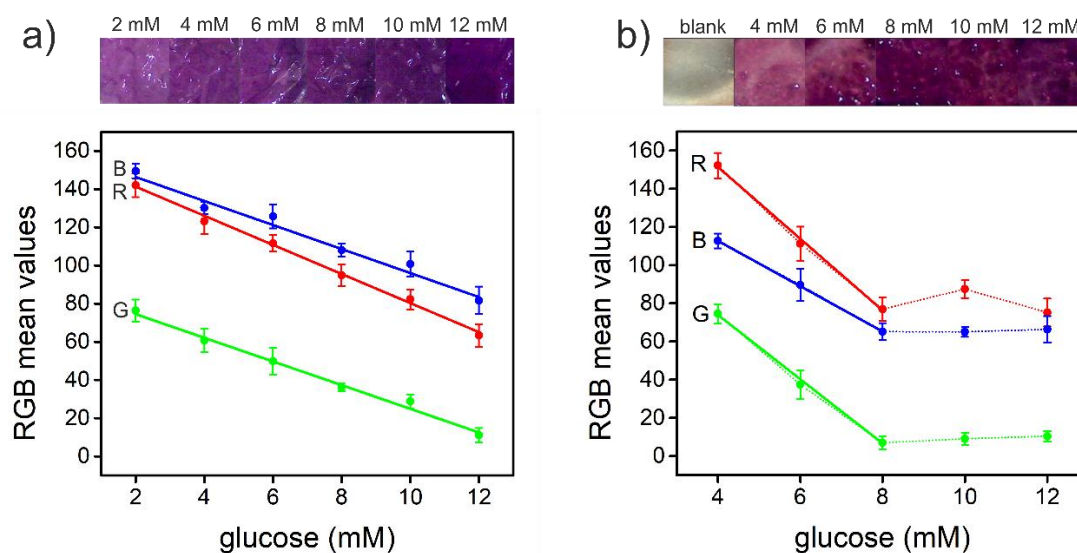


Figure 6.3.10. Glucose determination by image analysis. Quantification of different glucose concentrations in a) PBS solutions and b) whole blood samples by photographing the pads and representing the RGB contributions obtained by image analysis (n=5).

Glucose determination with SF pads in whole blood was more sensitive than in PBS, but presented a much shorter linear range up to 8 mM. This effect may be partially associated to the blood matrix. On the one hand, blood components may contribute to improve enzymatic detection. On the other hand, blood conferred some color to the SF pad that contributed to saturate the signal and reduce the linear range. Although not ideal, the range from 0 to 7 mM glucose was enough to distinguish between hypoglycemic and hyperglycemic situations in diabetic patients. SF pads presented high reproducibility with a low CV, always below 11%, which widely improved variations reported by cellulose papers, which varied from 15 to 20%.

3. Conclusions

The use of enzyme-doped SF films as a sensitive matrix for glucose detection is presented, highlighting as a novelty the capability of the material to filter whole blood samples, to pump liquids through its nanoporous matrix and to enhance glucose determination sensitivity by reaction of SF matrix components with redox mediators produced by the enzyme cascade reaction. These advantages, together with the already reported green and water-based processing, long-term stability of biomolecules and high transparency in the visible range, makes SF pads ideal for colorimetric detection of biomarkers at the POC. Glucose is here detected with precision, sensitivity and in a wide linear range enabling to distinguish from hypoglycemic and hyperglycemic states of a diabetic patient by a simple and inexpensive image analysis. As the images were taken by the camera of a smartphone, it would be possible to implement an application to correlate RGB values with the glucose concentration directly in blood. In such a case, no need of additional specific apparatus would be needed for the fast diagnosis.

6.4. Silk Bio-Cladding Fiber Optics Biosensor for Glucose Detection in Whole Blood

Abstract

At the POC, the use of fiber optics chemical and biochemical sensors (FOCS) is being extended for their simplicity, miniaturization capacity and low cost. With a normal structure consisting of shallow functionalized optical fiber cores and/or tips, FOCSs present a limited capacity to measure in coloured matrices, e.g. blood. Besides, FOCSs, as all biosensors, require better encapsulation protocols to guarantee the stability of the biomolecules used as recognition elements SF has demonstrated to be an excellent biomaterial both in optical sensing and in biomolecules encapsulation (enzymes, antibodies, drugs). The dip-coating of PMMA filaments with SF layers doped with GOx, HRP and ABTS leads to the production of PMMA-core/SF bio-cladding FOCS sensitive to glucose. In glucose biosensing, the tyrosine residues from the SF bond the ABTS radical generated by the enzymatic reaction, being the SF matrix also an active component of the biosensor. The intrinsic SF colour change together with the insolubility of the membrane due to the annealing process permits to wash it after the measurement without colour losses. Then, even strong coloured samples such as blood can be measured with low matrix interference after a final washing step.

This chapter contents results to be submitted as:

Silk Bio-Cladding Fiber Optic Biosensor for Glucose Detection in Whole Blood.

Augusto Márquez, Molíria V. Santos, Gonzalo Guirado, Salvador D. Aznar-Cervantes,
Jose Luis Cenis, Carlos Domínguez, Fiorenzo G. Omenetto, Xavier Muñoz-Berbel.

1. Introduction

Chronic patients suffer from long-lasting pathologies requiring an accurate and constant control through clinical tests of key biomarkers and medical visits. Due to the prevalence and persistence of such pathologies, expenses associated to the treatment and control of chronic patients is enormous. Only as an example, the annual spent in medical care due to patients with a chronic condition in the U.S is around 75% of the total.²⁵⁹ Current tendency to reduce healthcare expenditure and to improve the quality of life of the patients consists of translating clinical tests from clinical laboratories to the patients' home. Some examples of the so-called POC devices are the electrochemical glucose test strips or optical lateral flow assays (e.g. pregnancy) based on paper matrices, among others. Unfortunately, the technologies and biomarkers available are still limited and the development new technologies will be necessary to cover the current necessities of the society.

The use of FOCS in POC applications may be very advantageous as they offer small size and miniaturization potential, possibility of optical fibers for being implanted,^{260,261} use of harmless and contactless visible light for sample interrogation, remote sensing and low cost. FOCS are classified depending on the fiber geometry and disposition (de clad, tapered fiber, fiber bundle, bifurcated fiber bundle, U-bend, etched tip, modified end-face) and presence of recognition elements (active or doped cladding, tip active cladding)²⁶² what is related to a direct or indirect detection. Direct optical detection (based on refractive indices (RI) differences⁶⁵ or light absorbance of the sample²⁶³) is not always possible, especially in case of biosensing, when the analytes are in small concentrations and/or do not absorb visible light so they require an indirect detection by the use of recognition elements like enzymes, antibodies or oligonucleotides. The most used conformation is the core/tip functionalization of a de clad optical fiber with one of these biomolecules that can actuated as active or passive recognition elements. While in passive recognition the union of the analyte to the recognition element (oligonucleotides of a certain sequence or dedicated antibodies) provokes a measurable change in the local RI (this is de case of surface plasmon resonance FOCS),^{264,265,266} in active recognition the analyte is catalysed enzymatically.⁶⁷ In any case, biosensing with FOCS is highly limited by the colour of most biofluids of clinical interest, i.e. blood, plasma, serum or urine, and the low stability of the biomolecules used as recognition elements.

Rather than direct enzyme bonding to the fiber core, we consider an alternative strategy consisting of the coating of a naked PMMA filament that actuate as core, with an enzyme-doped material that can perform as active bio-cladding. In such a case, SF can be employed as an optimum coating material because of its extraordinary optical properties (high transparency in the visible spectrum and RI of 1.54) as well as its biocompatibility,²⁶⁷ mechanical robustness,¹²⁹ thermal stability,²⁵⁴ biodegradability,²⁶⁸ and long-term stability of biomacromolecules.¹²⁰ In fact, SF has been already explored as an optical material in the development of diffractive patterns,¹⁶⁰ gratings,²⁶⁹ holograms²⁵⁰ and waveguides²⁷⁰ although it has not been reported previously as a functional bio-cladding in an polymer optic fiber biochemical sensor.

In the present chapter, PMMA fibers are coated with doped SF to form a fiber optics with an active bio-cladding for glucose detection in whole blood samples.

2. Results

2.1. PMMA-SF optical fiber fabrication characterization

PMMA transparent filaments of 4, 3 and 2 cm, cut by CO₂ laser ablation to obtain polished edges, were coated with doped SF using a homemade dip coater, built of a linear actuator, always leaving 1 cm uncoated for optic probe coupling. Therefore, the obtained optical fibers consisted of a 1.75 mm PMMA filament core covered with a doped SF bio-cladding (**Figure 6.4.1a**) of 3, 2 and 1 cm respectively. To avoid confusion, we will refer to the length of the SF coating rather than the length of the PMMA filament. The SF bio-cladding had a homogenous thickness of ~4 μm and were in intimate contact with the PMMA filament (**Figure 6.4.1b**). The refractive indices difference (1.49 for PMMA and 1.54 for SF) enhanced light interaction with the bio-cladding, where the Rhodamine 6G dye (for characterization) or the biosensing elements (enzymes and colorimetric mediators) were immobilized, necessary for a latter detection.

Once dried, the SF was water annealed by exposition to 800 mbar water-saturated atmosphere at 45 °C overnight. This *green* protocol permitted the immobilization of organic dyes (e.g. Rhodamine 6G), colorimetric mediators (e.g. ABTS) or bio-macromolecules such as enzymes (e.g. HRP and GOx), preserving their structural integrity and activity over time.

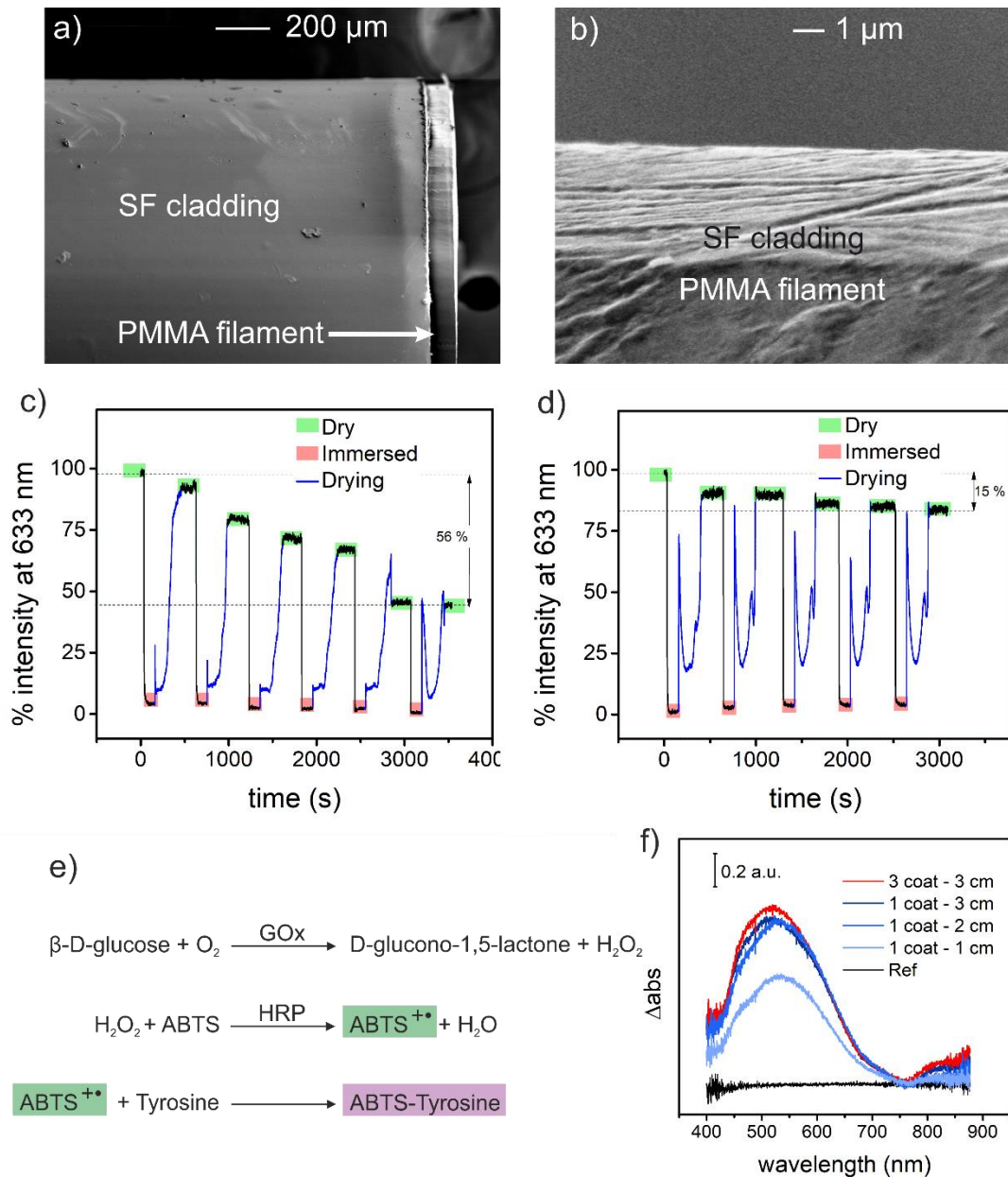


Figure 6.4.1. Silk bio-cladding FOCS architecture and performance. SEM images of the a) top view and b) cross-section of the PMMA filaments coated with the enzymes doped SF solution. Percentage of light intensity loss measured at 633 nm in reflection of a SF coated PMMA filament c) non-annealed and d) water annealed after consecutive water immersions. e) Enzymatic cascade reaction for the ABTS radical formation due to the presence of glucose. The ABTS radical is finally bonded to the tyrosine amino acids of the SF. f) Absorbance spectra obtained in reflectance from PMMA-SF optical fibers of different coated lengths and different number of doped SF coatings after the immersion in a 10 mM glucose PBS solution.

The annealing process, which has been widely reported to provoke the SF structural transition from random to β -sheet motives,²⁵⁴ was also critical to maintain the stability of the SF cladding, especially when the fibers were immersed in water, as the SF becomes insoluble when crystallized. For the sake of comparison, two optical fibers of PMMA-SF were immersed several times in water while the reflected light was measured using a coupled optical probe. The fiber with the non-annealed SF bio-cladding (**Figure 6.4.1c**) showed a constant fall, up to 56 % in the light reflected back, as a consequence of the bio-cladding loss by dissolution. On the contrary, the annealed SF bio-cladding (**Figure 6.4.1d**) demonstrated to be more stable and, despite a small decay of the 15 % of the initial light intensity, it finally became stable without any further loss. Probably, this small initial loss was due to structural changes of the SF layer upon hydration, also affecting optical parameters (e.g. the RI) as no detachment was observed.

The immobilization of GOx and HRP together with the mediator ABTS turned SF bio-cladding self-sensible to glucose molecules. Indeed, tyrosine residues of the SF were involved in the cascade reaction (**Figure 6.4.1e**) that started with the glucose oxidation by the GOx, continued with the ABTS radical formation by the HRP and finished with the ABTS radical bonding to tyrosine.²⁵⁸ In **Chapter 6.3**, it was shown how this ABTS radical capability of bonding to the SF tyrosine enhanced the system sensibility, as the absorbance of this new compound was two times higher than the free ABTS radical.

2.2. PMMA-SF optical fiber biosensor's geometry optimization

A fundamental aspect, in terms of sensibility, of the optical PMMA-SF fiber biosensor is the architecture of the FOCS. The cladding thickness and the fiber length were studied with the aim to increase the absorbance signal at 545 nm associated to the formation of the ABTS-Tyrosine compound after selective biorecognition of glucose molecules. PMMA-SF fiber optics of different lengths and bio-cladding thickness (resulting from a different number of coating steps) were immersed in a 10 mM glucose PBS solution and measured after 10 min of reaction.

While the length of the PMMA-SF fiber increased substantially (almost doubled) the measured absorbance, the bio-cladding thickness barely improved it. The increment of the fiber length involved an increase in the optical path and consequentially in the interaction points between the light from the PMMA core and the coloured SF bio-

6. Results

cladding. As a result, more molecules in the bio-cladding absorbed light before this was coupled back to the optic fiber of the probe for the measurement. Nevertheless, an increment in the bio-cladding thickness did not contribute to a higher absorbance. Based on the latter, 2 cm long coating was considered optimal for the biosensor fabrication.

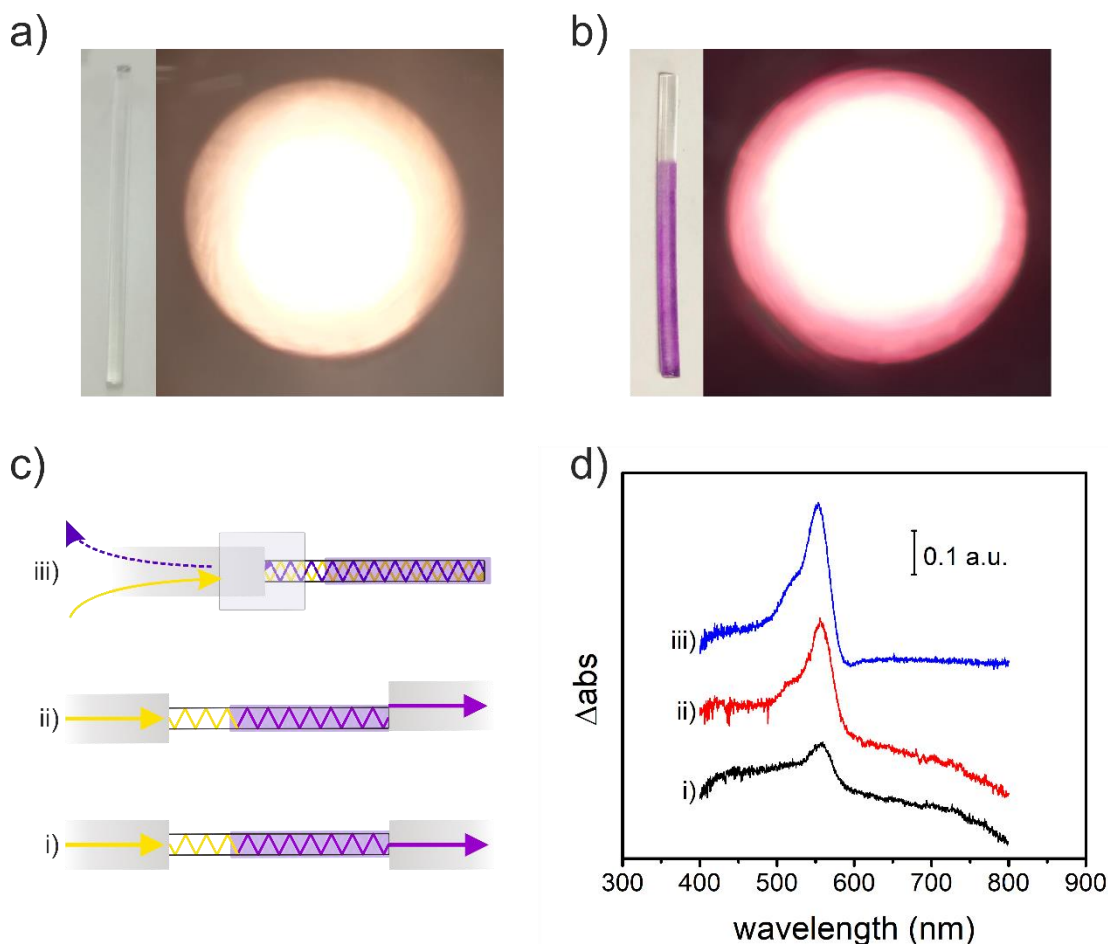


Figure 6.4.2. Optimization of FOCS transduction mechanism. Pictures of the PMMA-SF optical fibers (SF doped with enzymes and ABTS) a) before and b) after the reaction with 10 mM glucose PBS solution and the respective cross-section of the halogen light irradiated fibers. c) Measurement setup schemes: i) transmittance from the core of the optical fiber, ii) transmittance from the cladding of the optical fiber and iii) reflectance and d) respective absorbance spectra obtained from a Rhodamine 6G doped SF coated PMMA filament. Coating: 10% w/v SF solution doped with 0.1 mM Rhodamine 6G.

In the selection of the transduction mechanism for the PMMA-SF bio-cladding FOCS, it was important to consider that the colour change associated to the enzymatic recognition reaction was localized in the bio-cladding area. It is clear when could be

clearly appreciated when comparing the optical fibers before (**Figure 6.4.2a**) and after (**Figure 6.4.2b**) the immersion in a 10mM glucose PBS solution. The modes of these optical fibers reveal how the colour output was localized in the bio-cladding and barely in the core. Based on the latter, three different transduction modes were compared for the PMMA-SF FOCS: i) transmittance measurements from the core of the optical fiber, ii) transmittance measurements from the bio-cladding of the optical fiber and iii) reflectance measurements (**Figure 6.4.2c**). In transmission mode, Rhodamine 6G absorbance spectra were collected in both configurations i) and ii) (**Figure 6.4.2d**). However, more intense absorption bands were obtained when the 200 μm light input/output optic fibers were situated in front of the coloured SF bio-cladding. This result revealed two important facts. First, light transmitted along the PMMA filament partially interacted with the SF bio-cladding as the Rhodamine 6G spectrum could be appreciated even when aligning the collection optical fiber in the middle of the PMMA filament. Second, the light tended to be confined in the SF bio-cladding, as the absorbance intensity of Rhodamine 6G was higher when the collection optical fiber was aligned with the bio-cladding. This second conclusion could be understood by considering the higher RI of the SF used as bio-cladding when compared to PMMA. Reflection measurements presented higher sensitivities (in terms of absorbance) than transmission measurements. This increase in sensitivity may be understood when considering the light/bio-cladding interaction. As shown in **Figure 6.4.2c**, in the reflectance configuration the light had to cross the structure twice before being collected back at the probe, so it interacted two times with the absorbing molecules in the bio-cladding, doubling the optical path length when compared to the transmission measurement. Measurements in reflection were thus chosen instead of transmission because their highest sensitivity and repeatability.

In order to improve the reproducibility of the measurements, PMMA-SF fibers were attached to a linear actuator for a controlled immersion/emersion of the probe into the sample (**Figure 6.4.3a**). In the measurement, the PMMA-SF was immersed in a 10 mM glucose PBS while the reflected light spectra were recorded (**Figure 6.4.3b**). Two wavelength intensities were compared over time: 545 nm, corresponding to the ABTS-Tyrosine absorption band, and 850 nm used as reference since no changes due to ABTS-Tyrosine were expected (**Figure 6.4.3c**). After an important fall of the intensity of the reflected light at both wavelengths upon fiber immersion in the sample, induced by the higher RI of water (1.33) compared to the air (1), the intensity remained stable at 850 nm

6. Results

while a constant decay was detected at 545 nm due to the onset of ABTS-Tyrosine bonding. The fiber was then extracted from the solution and dried. After a drying period of 6 min, the light intensity at 850 nm recovered the initial value before immersion while it was lower at 545 nm due to the ABTS-Tyrosine absorbance.

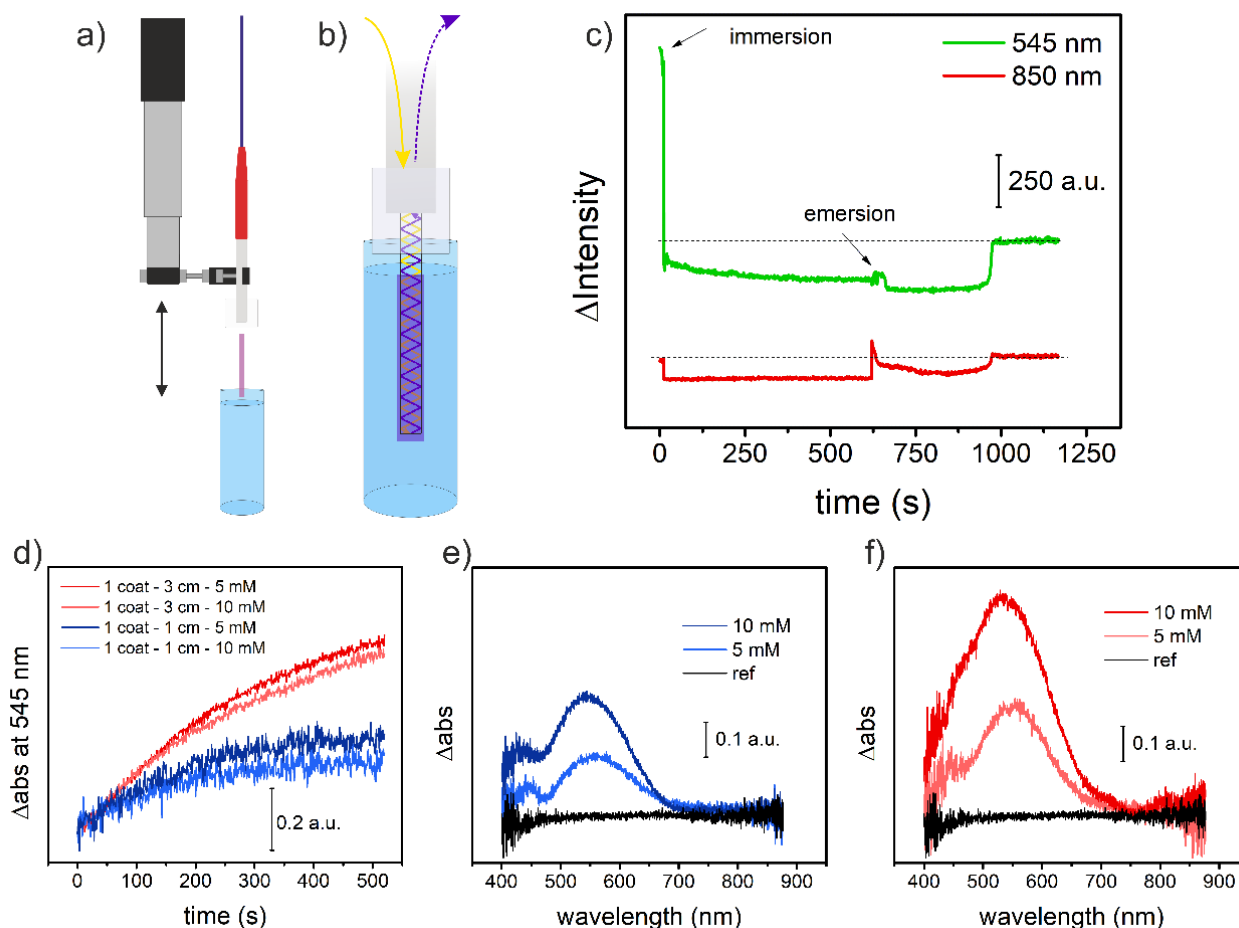


Figure 6.4.3. Optimization of the PMMA-SF FOCs measurement protocol. a) Scheme of the measurement setup using the linear actuator controlled by Arduino to move the probe coupled to the coated filaments for the immersion-emersion in the samples. b) Light pathway scheme within the PMMA filament, interacting with the doped SF cladding. c) Measured intensity at 545 and 850 nm of the reflected light from a PMMA filament coated with doped SF after the immersion-emersion in a glucose PB solution. d) Absorbance increment kinetics at 545 nm for 1 and 3 cm doped SF coated SF filaments after the immersion in 5 and 10 mM glucose PBS solutions. Absorbance spectra obtained from e) 1 cm and f) 2 cm filaments coated with doped SF after the immersion during 6 seconds in 5 and 10 mM glucose PBS solutions and dried at air.

One of the critical parameters in glucose determination was the immersion time. Since only a limited amount of ABTS could be incorporated in the SF bio-cladding, the sensitivity and measurement range of the sensor was strictly linked to the biorecognition reaction time, this time determined by the immersion time.

When the fibers were immersed in PBS solutions containing either 5 or 10 mM glucose concentrations for above 10 s, differences in absorbance could not be detected (**Figure 6.4.3d**), although they were evident when changing, for example, the length of the fiber. Despite the glucose concentration in the solutions was significantly different, the stoichiometry was uncompensated and all ABTS reacted in both cases. Reducing the immersion to 6 s, it was possible to distinguish between 5 and 10 mM glucose values (**Figure 6.4.3e**). Again, increasing the fiber length drove to a better sensibility of the biosensor (**Figure 6.4.3f**).

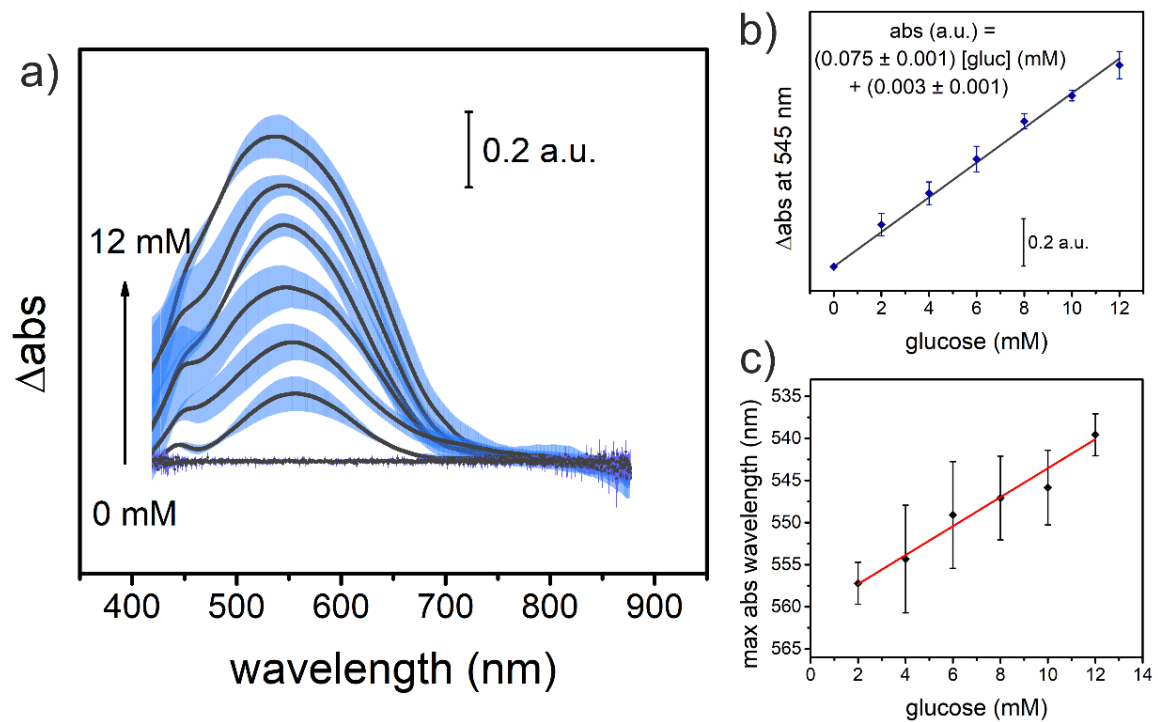


Figure 6.4.4. Glucose determination in buffer. a) Absorbance spectra average obtained after the immersion of 3 cm length filaments (coated 2 cm once with doped SF) during 6 seconds in glucose PBS solutions with different concentrations (0, 2, 4, 6, 8, 10 and 12 mM). b) Calibration curve for different glucose concentrated PBS solutions measuring the absorbance at the maximum value of the ABTS-Tyrosine absorbance band. c) Absorbance spectra peak shift average due to the increment of glucose in the PB solution. n=5.

2.3. Glucose concentration determination in PBS and whole blood samples

The optimal PMMA-SF fiber biosensor (2 cm, 1 coat of bioactive SF bio-cladding and measured in reflectance) was then calibrated using PBS solutions with different glucose concentrations (**Figure 6.4.4a**). A glucose concentration range between 0 and 12 mM was chosen in accordance with the sensing requirements for diabetic patients.²⁷¹

Good sensitivity and a CV below 7 % was obtained in the full concentrations range (**Figure 6.4.4b**). Besides, a subtle shift of the ABTS-Tyrosine absorption band to the blue direction was also detected. This shift, that may be attributed to the contribution around 400 nm embedded in the 545 nm band, was dependant also on the glucose concentration (**Figure 6.4.4c**), offering thus the possibility of using this sensor not only in dependence of the absorption intensity but also on the absorption band peak position. It may be remarked that even when presenting similar measurement range, the CV obtained when determining glucose concentration through the peak shift were much higher than when considering the absorbance intensity.

The final goal of the PMMA-SF fiber biosensor was the analysis of glucose in whole blood samples, where the SF bio-cladding was not only acting as the entrapment matrix for enzymes and mediators, and a reactive element of the biorecognition reaction, but also as a filtration element to avoid interferences from matrix components. For this purpose, different glucose quantities were added to defibrinated sheep blood and quantified afterwards (**Figure 6.4.5a**). In case of the blood analysis, the linear range was obtained between 0 and 9 mM, being the sensitivity higher compared to the calibration in PBS, which attributed to matrix effects (**Figure 6.4.5b**). The CV was not higher than 12 % in any case. The SF bio-cladding actuates well as a barrier to diminish the high blood interference still a washing step was needed to eliminate the blood adhered to the external surface of the bio-cladding before the measurement (**Figure 6.4.5c**).

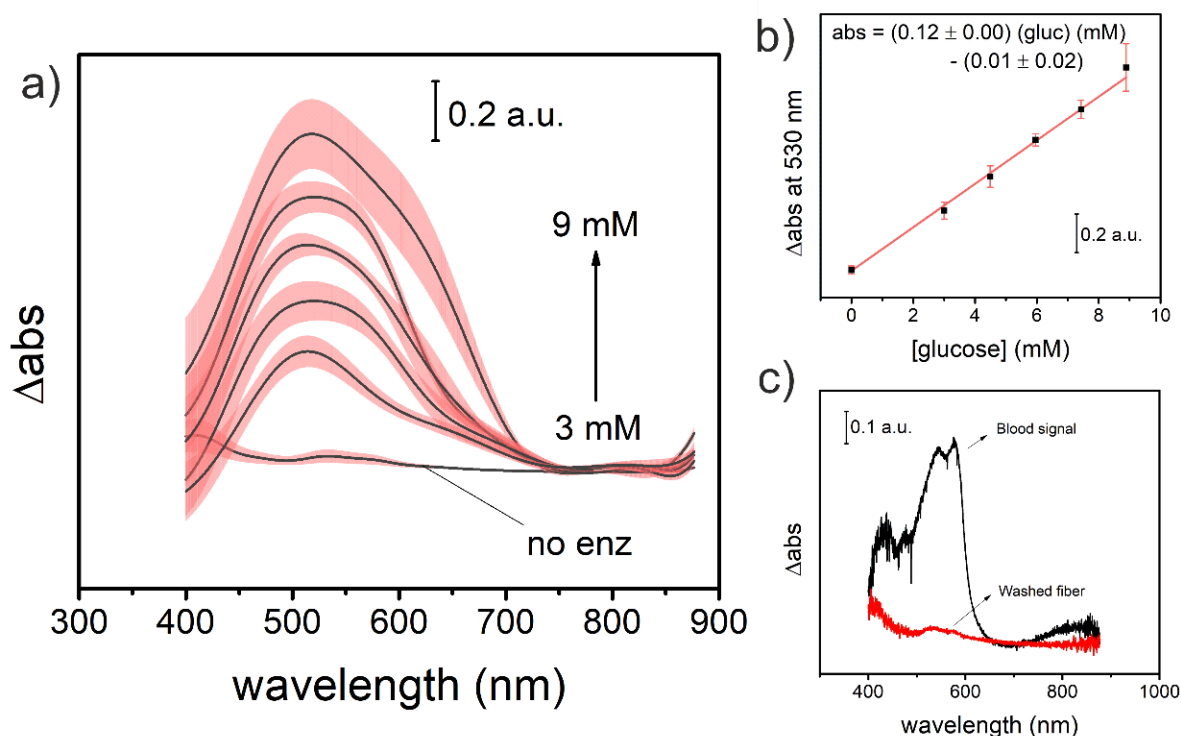


Figure 6.4.5. Glucose determination in whole blood. a) Absorbance spectra average obtained after the immersion of 3 cm length filaments (coated 2 cm once with doped SF) during 6 seconds in whole blood samples spiked with glucose (3, 4.5, 6, 7.4 and 8.9 mM) and washed in distilled water by 6 seconds immersion. b) Calibration curve for absorbance average at the maximum value of the ABTS-Tyrosine absorbance band for different glucose concentrations in spiked whole blood samples. c) Absorbance spectra obtained from a 2 cm SF coated PMMA filament after the immersion in whole blood and after washing by immersion in distilled water. $n=5$.

3. Conclusions

The fabrication of PMMA-SF optical fibers and the doping of the SF bio-cladding with GOx, HRP and ABTS permitted the detection and quantification of glucose both in PBS and whole blood samples. The length of the optical fibers (3 cm of filament and 2 cm coated), coating thickness (1 coat, 4 μm) and measurement mode (reflection) were optimized to obtain the maximum sensibility and linear range. The novelty of using of SF as bio-cladding demonstrated to be of great advantage as it was possible to immobilize enzymes, without disrupting their catalytic activity, together with a colorimetric mediator (ABTS) and carry out a fast essay for glucose quantification. Furthermore, tyrosine residues of SF reacts with the ABTS radicals, revealing a measurable signal at 545 nm

6. Results

with enhanced sensitivity, when compared to conventional ABTS peaks. The covered glucose concentration range comprehends values that fluctuate from healthy to hyperglycemic patients. The *green* annealing process, which only involves the exposition of the PMMA-SF optical fibers to a low pressure and humid atmosphere, do not disturb the immobilized molecules but made the cladding insoluble. As the SF matrix changed its colour from transparent to deep purple, product of the reaction with ABTS radical, it was possible to wash the optical fibers after the measurement of strongly coloured samples (e.g. whole blood) to remove interferences without disrupting the SF-ABTS absorbance signal.

6.5. Photo-Electro-Enzymatic Glucose Biosensor using dithienylethene derivatives as Reusable mediators

Abstract

In the development of enzymatic peroxidase-based colorimetric biosensors, the use of electrochromic mediators such as TMB or ABTS has been accepted and widely used during decades. The main drawback of these types of enzymatic substrates is the difficult recovery of the initial redox state of the molecule, which can be done electrochemically or by antioxidants addition, complicating the initially simple structure of the biosensor. Actually, those strategies are rarely followed; being the single-use and disposable biosensor configuration the most extended for this detection mechanisms. Alternatively, we propose the first reported use of a diacid dithienylethene DTE photoelectrochromic compound as a substrate of the HRP. The photoisomerization between the open (DTEo) and closed (DTEc) forms of the molecule and the respective shift in the redox potential allowed the light-induced enzymatic detection of glucose in the GOx – HRP cascade system. This fast and easy control over the enzymatic substrate availability by light pulses permits a gradually consumption and the light-regeneration of the biosensor for a number of cycles. We consider the presented results transcendent in the development of reusable and light-controlled photonic biosensing systems.

This chapter contents results to be submitted as:

Photo-Electro-Enzymatic Glucose Biosensor using dithienylethene derivatives as Reusable Mediators. Augusto Márquez, Sara Santiago, Carlos Domínguez, Xavier Muñoz-Berbel, and Gonzalo Guirado.

1. Introduction

Photoelectrochromic compounds are characteristic for undergo reversible isomerization, ruled photonically (at a certain wavelengths) and/or electrochemically (at a certain potentials), what changes the optical material properties (e.g. UV-Vis-absorbance or RI) but also the structural conformation.²⁷² This photoelectrochemical modulation of the intrinsic properties of the material enhances the application of such compounds in a wide variety of fields like smart windows and glasses,²⁷³ color-changing displays,²⁷⁴ smart cards,²⁷⁵ e-paper,²⁷⁶ computing technology (data storage),²⁷⁷ optics (active filters),²⁷⁸ etc...

These properties of photoelectrochromic compounds have been also applied in sensing. For example, recently Zou et al. have reported the use of a polyoxometalate in low cost UV radiations sensors for real-time solar UV dosimeters.²⁷⁹ Furthermore, photochromic spiropyran, integrated in PDMS, have been applied in HCl gas sensing²⁸⁰ and also inorganic composites such as Au-WO₃ or Ag-TiO₂ have been employed in H₂²⁸¹ and acetone gas²⁸² detection, respectively.

Nevertheless, photoelectrochromic compounds have never been reported useful in biosensing applications where they could play a role as colorimetric mediators in enzymatic detections, for instance. The detection of many biomarkers of interest in healthcare or professional sports (e.g. glucose, lactate, cholesterol...) can be achieved, among others strategies, by an oxidase-peroxidase cascade system in which firstly the oxidase coproduces H₂O₂ after the oxidation of the target analyte and secondly the peroxidase uses the produced H₂O₂ to oxidase the mediator. Afterwards, the mediator can be detected either electrochemically or optically (if the oxidation is accompanied by a color change).

Among different families of organic photochromic molecules (i.e. phenoxyquinones, spiropyran, azobenzenes), in the present chapter we discuss the possibility of using a dithienylethene dye (DTE) as enzymatic mediator for glucose detection. Diarylethenes are a family of thermally irreversible photoelectrochromic molecules (P-type) composed by two basic entities: aromatic thienyl groups and a hexatriene subunit.¹⁶³ DTE experiments reversible cyclization of the hexatriene skeleton by UV (closure) and visible (opening) irradiation, translated in the coloration and discoloration of the molecule, respectively. Furthermore, DTE structure is also interesting

since its highly symmetry, highly fatigue resistance and, the most important, its electrochromic behaviour, what makes the molecule both photo- and electro-chromic.²⁸³

In a first approach, the catalysis of the DTE by the HRP in presence of H₂O₂ was studied for both isomers revealing that only the closed one could be catalysed. This fact is corroborated in terms of redox potential of both isomers, being only the closed one accessible for the HRP oxidation. Secondly, the oxidation of glucose by the GOx was coupled to the HRP reaction, ending in the detection of the analyte following the enzyme induced bleaching of the DTEc.

2. Results

2.1. Sample preparation

In order to facilitate the measurements in aqueous solutions, the isolated DTE was first dissolved in acetonitrile and titrated with TBAOH to deprotonate the two carboxylic functional groups of the molecule. After the evaporation of acetonitrile, the DTE was then dissolved in PBS, revealing that the deprotonation had increased the solubility in the aqueous solution almost 4 times (**Figure 6.5.1**). This solubilisation increment was critical, as every previous electrochemical study of the compound had always been realized using acetonitrile, which is not compatible with bioassays involving enzymes. The deprotonation of the molecule provokes a shift to the blue in the main absorbance peak present in the visible spectrum (534 – 496 nm) that did not affect to the further spectroscopic studies.

2.2. HRP activity coupling to DTE catalysis

The capability of the HRP to catalyse the oxidation of the DTE was evaluated spectroscopically by consecutive cycles of UV-induced coloration and enzyme-induced bleaching of the molecule. First, a PBS solution of DTE in presence of HRP and GOx was irradiated with 300 nm UV light to close the molecule and the absorbance spectrum was measured respect to the same solution before irradiation (**Figure 6.5.2a**). Secondly, a glucose solution was mixed with the prior volume and, instantly, a spectrum was taken every 30 s to follow the absorbance decay. The same cycle was repeated 21 times (**Figure 6.5.2b**) with a full molecule recovering in terms of absorbance at 515 nm until the 16th cycle. As the glucose was in excess respect to the DTE ($2 \cdot 10^{-3} \text{ M} : 7.5 \cdot 10^{-5} \text{ M}$) and not all the DTE was

closed upon UV irradiation in each cycle, extra additions of glucose were not needed. Although in principle recovered, by increasing the number of cycles the DTE signal decreased gradually until disappearance, dismissing a possible reversibility of the DTE to the initial state. Furthermore, two more signals in the visible were detected: one transitory at 760 nm and another at 345 nm that increased its value with the consecutive cycles.

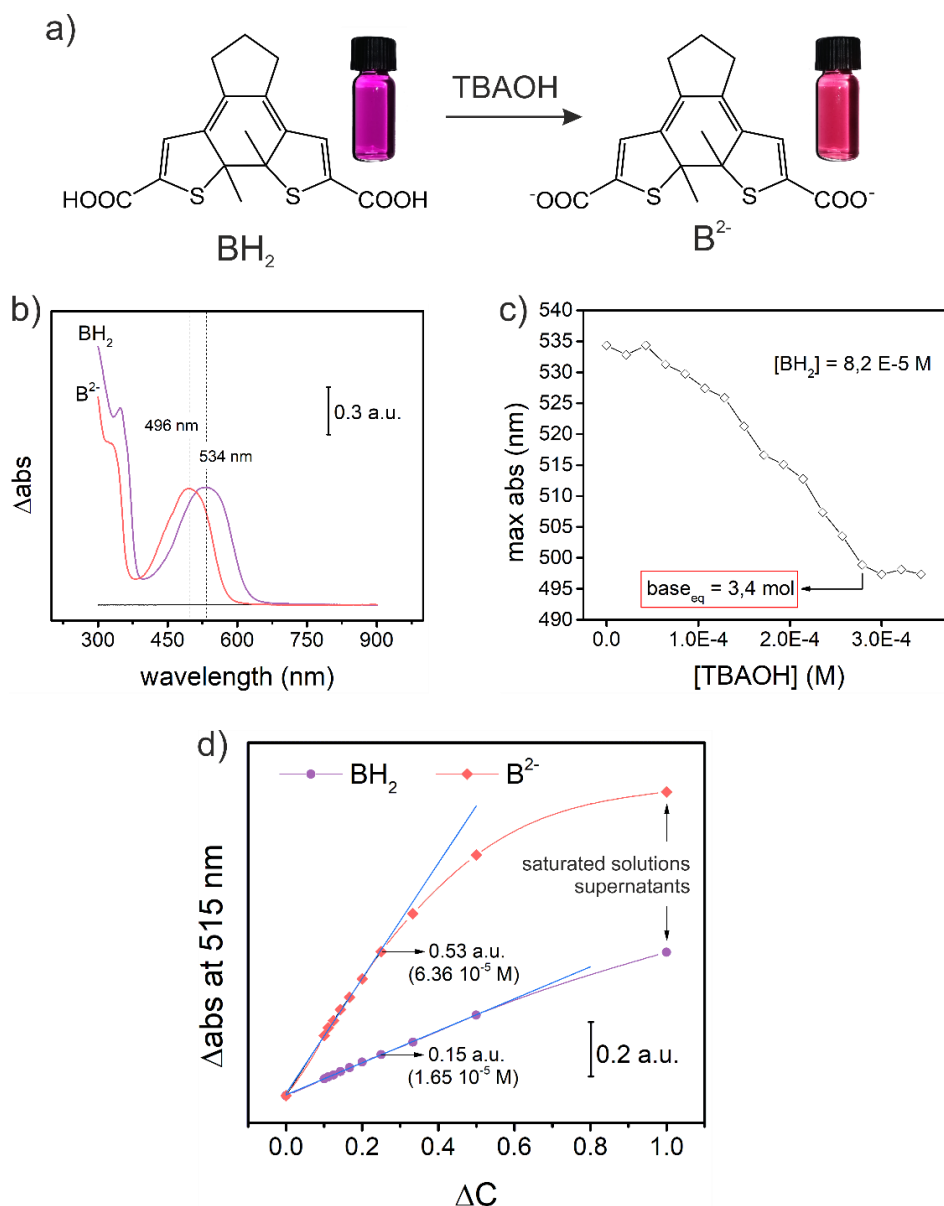


Figure 6.5.1. DTE solubility in water enhancement. a) DTE titration with TBAOH for the molecule deprotonation. b) Absorbance spectrum shift due to the deprotonation. c) Amount of TBAOH need for a full deprotonation. d) Solubility in H_2O increment of the DTE in the deprotonated form.

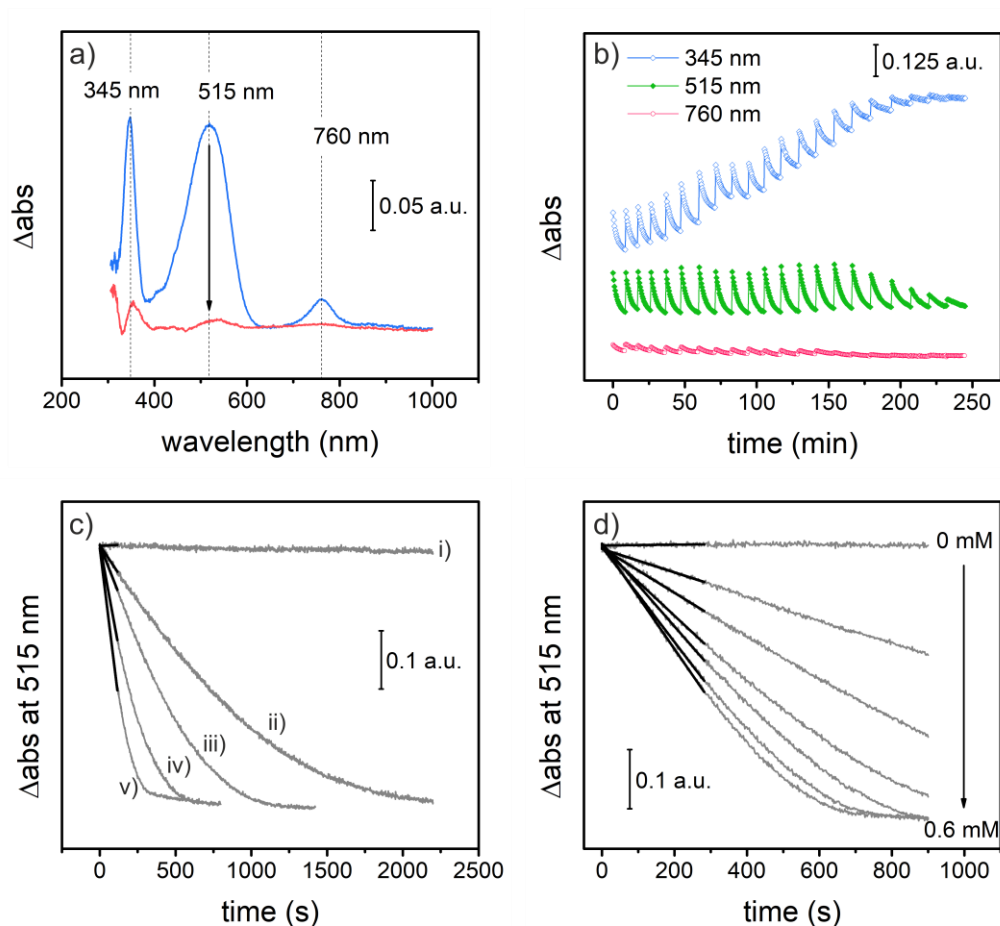


Figure 6.5.2. Enzymatic coupling to DTE. a) Absorbance spectra evolution of DTEc in PBS solution after the addition of HRP-GOx and glucose. b) Absorbance values at different wavelengths within subsequent cycles of DTE coloration upon UV irradiation and bleaching by HRP enzymatic activity. Solution: $7.5 \cdot 10^{-5}$ M DTE (B^{2-}), 0.01 M PBS, $2 \cdot 10^{-3}$ M glucose, 1 u ml^{-1} HRP and 0.67 u ml^{-1} GOx. c) DTEc (B^{2-}) bleaching by the enzymatic activity of i) 0 u ml^{-1} , ii) 0.25 u ml^{-1} , iii) 0.5 u ml^{-1} , iv) 1 u ml^{-1} and v) 2 u ml^{-1} of GOx in combination of HRP (2:3 relation) in the presence of $2 \cdot 10^{-3}$ M glucose 0.01 M PBS solution. d) DTEc (B^{2-}) bleaching by GOx-HRP system (1 and 1.5 u ml^{-1} respectively) in different glucose concentrated 0.1 M PBS solutions (from 0 to $6 \cdot 10^{-4}$ M, increments of $1 \cdot 10^{-4}$ M).

2.3. Glucose detection by GOx – HRP cascade reaction system using DTE

The catalysed bleaching of the DTE by the HRP can be exploited in biosensing applications. In order to study this possibility, the glucose oxidation by the GOx enzyme with O_2 was coupled to the peroxidase in a well-known oxidase-peroxidase cascade reaction widely employed in enzymatic sensors. In the mentioned cascade, the glucose

oxidation coproduct, H_2O_2 , is used subsequently by the HRP to oxidise usually a chromophore molecule (e.g. TMB, ABTS, DAB, etc...), that changes its color and reveals the presence of the initial glucose. By adjusting the parameters, it is possible to calibrate the enzymatic sensor to associate the color change intensity to the initial glucose quantity.

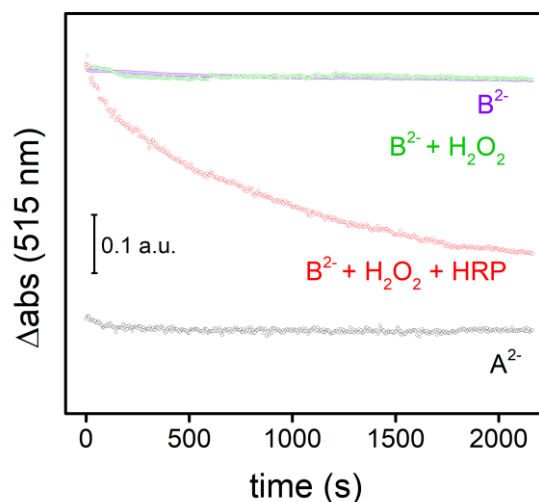


Figure 6.5.3. HRP specificity for closed DTE. Control measurement for color loss absence of closed DTE in presence of H_2O_2 and absence of HRP. Solution: $1.4 \cdot 10^{-4}$ M DTE (A^{2-} or B^{2-}), 10 mM PBS, $3 \cdot 10^{-4}$ M H_2O_2 and 1 u ml^{-1} HRP.

Based on this system, we substituted the traditional mediator by the DTE molecule. Varying the reaction parameters, the bleaching rate of DTE changed. For instance, the increment of GOx-HRP concentration in the reaction volume accelerated the discoloration of DTE (**Figure 6.5.2c**) for the same concentration of $2 \cdot 10^{-3}$ M glucose in PBS solution, denoting a clear dependence on the enzymatic activity and the possibility to couple the DTE bleaching to the oxidase-peroxidase system. The DTE is then potentially useful to detect any analyte that can be catalysed by an oxidase enzyme (e.g. glucose, lactate, cholesterol, monoamines, tryptophan, etc...) that coproduces H_2O_2 . Remarkably, there is no DTE bleaching in presence of H_2O_2 and in absence of HRP (**Figure 6.5.3**), what revealed that the DTE is not sensitive to the presence of the oxidant if the reaction is not catalysed by the peroxidase. The system also demonstrated to be dependent on the analyte concentration (**Figure 6.5.2d**) and showed clear different bleaching rates between 0 and $6 \cdot 10^{-4}$ M glucose maintaining the same amount of enzymes (1 and 1.5 u ml^{-1} of GOx and HRP respectively), what means that the system is useful not only for the detection but also for the analyte quantification.

2.4. UV-Vis spectra changes of DTE induced by consecutive detection cycles

Regarding the two additional signals that appeared in the visible spectrum during the reaction at 760 and 345 nm (**Figure 6.5.2a**), they provide useful information to figure out the reaction pathway of the system. Spectra of the 21 cycles at two different moments are depicted: just after the UV irradiation and before the next irradiation, when the spectrum was stable. After the UV irradiation, a sudden increment at 515 nm is appreciated because of the DTE closure (**Figure 6.5.4a**). When the UV irradiation was stopped, a second signal appeared at 760 nm, with some seconds of delay. Finally, both signals decreased while a signal at 345 nm remained and even increased in the subsequent cycles (**Figure 6.5.4c**). This signal was associated to a final reaction product of the catalysis of the DTEc by the HRP in presence of H_2O_2 .

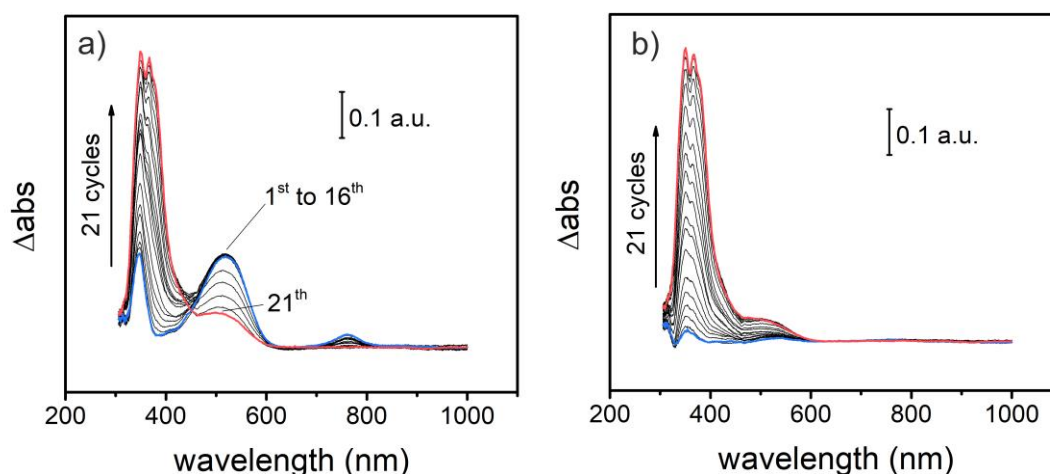


Figure 6.5.4. Irreversibility of UV-Vis spectrum through consecutive reaction cycles. a) First and b) last spectra of the subsequent 300 nm light irradiation – HRP-GOx/Glucose reaction cycles carried out in Figure 1b. Solution: $7.5 \cdot 10^{-5}$ M DTE (B^{2-}), 0.01 M PBS, $2 \cdot 10^{-3}$ M Glucose, 1 u ml^{-1} HRP and 0.67 u ml^{-1} GOx. Last spectra was taken in equilibrium.

2.5. FTIR spectroscopy

To seek more information about the product of the enzymatic reaction, IR measurements were done when all the DTE present had been catalysed (**Figure 6.5.5**). In a first comparison between the open and closed forms of DTE, it can be appreciated small changes at 1660 (O – H vibration) and 1345 cm^{-1} , having a higher absorption the DTEc compound in both cases. While the first one is attributed to a higher moisture retention from the less hydrophobic DTEc compound, the second is attributed to $-CH_3$ bending

changes related to ring closure. The IR spectrum of catalysed DTE shows remarkable differences in the C = O ($1800 - 1500 \text{ cm}^{-1}$) and C – O vibrations ($1270 - 1180 \text{ cm}^{-1}$) regions, while the intense fingerprint peaks of the cyclic structure in the $1500 - 1300 \text{ cm}^{-1}$ remain unchanged. The signal at 1720 cm^{-1} , only present in the catalysed DTE, can be associated to the C = O stretching vibration with a weakly hydrogen bonding (low degree of esterification with aromatic esters), which can belong to the dimerization of the carboxylic moieties of different DTE molecules, favoured by a charge transition intermolecule complex formation after the oxidation by the peroxidase. The signal at 1630 cm^{-1} , intense in the DTEo and DTEc is shifted to 1670 cm^{-1} in the catalysed DTE. The decay at 1630 cm^{-1} (relative to C = C stretching vibrations) can be related to lower conjugation of the structure, while the increase at 1670 cm^{-1} may be associated to C = O stretching vibrations in the conjugated DTE dimers.

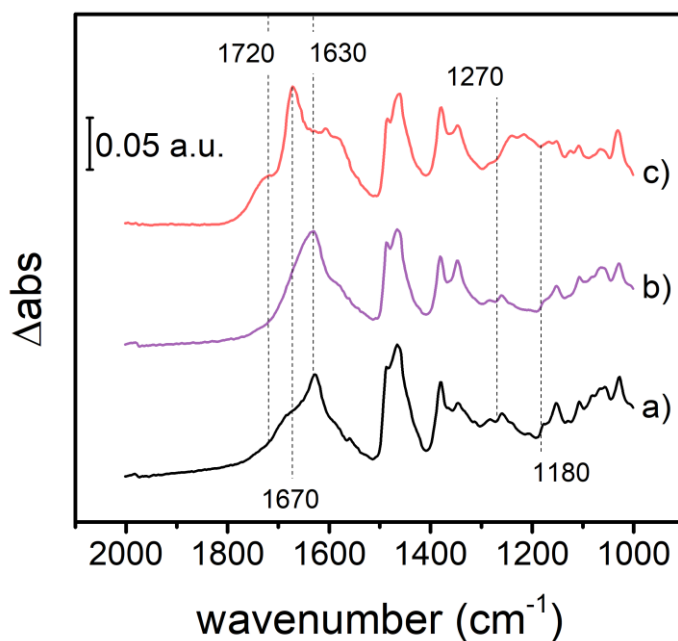


Figure 6.5.5. IR study of DTE enzymatic catalysis. IR absorbance of the a) DTEo, b) DTEc and c) DTEc after complete catalysis by HRP in presence of H_2O_2 . Medium: 0.01 M PBS, 6 u ml^{-1} HRP, $2.5 \cdot 10^{-3}$ M DTE and, in c), 0.01 M H_2O_2 .

2.6. Proposed mechanism

In presence of H_2O_2 , there is a well described oxidation transition of Fe III to Fe IV in the heme group of the enzyme²⁸⁴ (named Compound I) by direct bonding of one oxygen atom from the H_2O_2 to the Fe, liberating H_2O (1). Sequentially, the oxygen is reduced

6. Results

first to hydroxide (Compound II) (II) and finally to H_2O (III), by the uptake of 2H^+ and 2e^- from a donor (i.e. DTEc).

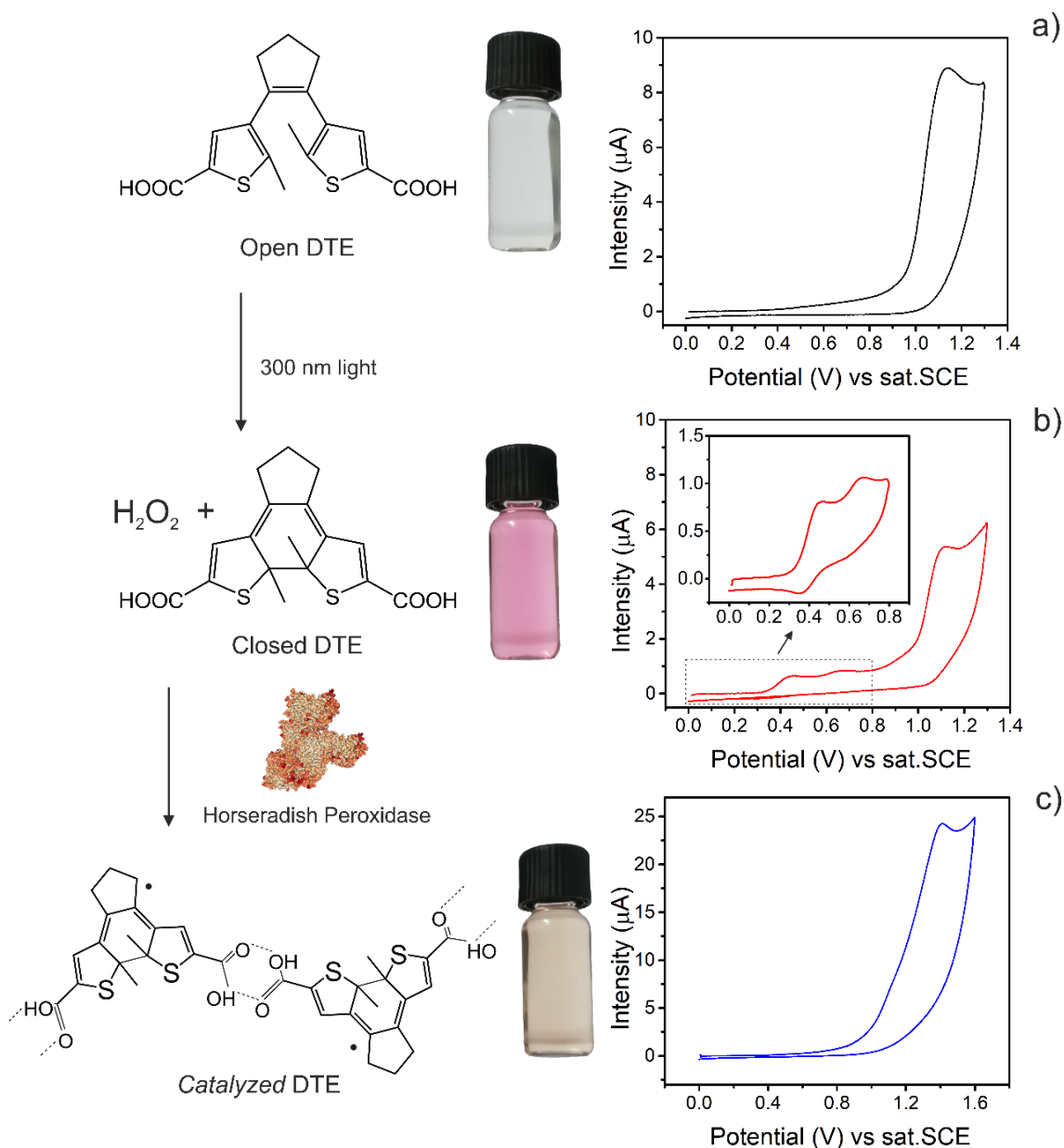
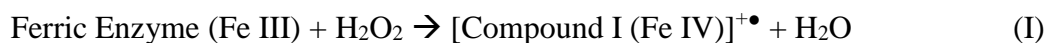


Figure 6.5.6. Proposed reaction scheme for DTE. a) The DTEo is closed by UV irradiation at 300 nm. b) In presence of glucose, GOx and HRP (or simply H_2O_2 and HRP), the closed molecule is oxidized by the last, ending in a reddish product that absorbs slightly at 410 nm. The cyclic voltammeteries of $2.5 \cdot 10^{-3}$ M DTE, measured in 0.01 M PBS, revealed that only the DTEc is accessible for HRP catalysis. Scan rate: 0.5 V s^{-1} , Working electrode: Glassy carbon, Reference electrode: Saturated Calomel, Counter Electrode: Pt.

Regarding the obtained results, the fast initial interaction of HRP with the DTE in presence of H₂O₂ provokes the appearance of a transitory signal at 760 nm wavelength, which may be related to the interaction of Compounds I and II with the DTE, and a final, and remaining signal at 345 nm wavelength, related to the radical DTEc[•]. Previous studies revealed a similar behaviour when Cu II was added to a DTE solution.²⁸⁵



The final cation radicals are prone to form charge transfer complexes, in a similar way as happens with other colorimetric mediators like TMB,²⁸⁶ ascorbate, hydroquinone²⁸⁷ and chlorpromazine.²⁸⁸ This theory is supported by the infrared spectroscopy results, where the signals related to the carboxylic moiety vibrations presented changes while the signals arising from the cyclic structure remained unchanged: dimers formation through carboxylic acid moieties is more likely than DTE degradation upon HRP oxidation.

The control on the UV irradiation time of the DTEo can modulate the amount of DTEc in the system and, therefore, the amount of available substrate for the detection reaction. The HRP ($E^0 = 0.59 \text{ V}$)²⁸⁹ can catalyse only the DTEc ($E^0 = 0.41 \text{ V}$) as the DTEo ($E^0 = 1.04 \text{ V}$) is not accessible in terms of potential²⁸⁵ (**Figure 6.5.6**).

3. Conclusions

The photoelectrochromic DTE molecule can be used as a colorimetric mediator for the HRP enzyme, which catalyse the molecule oxidation once closed by UV irradiation due to the redox potential fall respect to the open ring isomer. We demonstrate the first enzymatic reaction for biosensing that employs a photoelectrochromic molecule as colorimetric mediator. The described system is very interesting as the amount of available mediator for the reaction can be modulated by UV irradiation (DTEc) regardless the total amount of mediator present in the essay (DTEc and DTEo). This fact is interesting because permits a controlled mediator consumption in the reaction, enabling consecutive analyte detections using the same enzymes and restarting the system only by an UV pulse. Additionally, it would be possible to fabricate 2D solid structures with immobilized

6. Results

DTE using the same precursor but irradiating differentially adjoining areas. The availability of mediator for the detection would be different in those areas and would be given only by the irradiation time. The decoloration of more or less previously UV colored areas could be therefore associated to an analyte concentration in the sample in a semi-quantitative essay. The possibility of HRP enzymatic activity coupling to the molecule color change prospects the adaptation to any oxidase-peroxidase cascade system for further biomolecules detection, as it has been demonstrated for glucose.

6.6. Light-Renewable Enzymatic Silk Biosensors Incorporating Diarylethene Mediators For Continuous Glucose Monitoring

Abstract

Enzymatic biosensors based on optical transduction have been traditionally limited to single-use end-point devices due to the impossibility to restore the initial conditions of the sensor. The substitution of traditional electrochromic mediators, for example TMB or ABTS for new photoelectrochromic molecules, belonging to diarylethene family, opens the possibility of light-induction (rather than analyte-induction) of the reaction and light-recovery of the biosensor after measurement. The integration of biorecognition elements (i.e. GOx and HRP) together with the photoelectrochromic molecule DTE within a SF matrix from *Bombyx mori* leads to the conformation of a transparent and homogenous material that becomes colored by UV light irradiation and turns colourless by visible light irradiation or glucose exposure. The easy, eco-friendly and versatile manipulation of doped SF permitted the functional material disposition in films by casting or in layers by dip coating. The used protocol, based on a fast solvent evaporation, leads to the conformation of transparent films rather than hydrated gels. The SF-based functional material allowed direct glucose quantification by image analysis of exposed films or by spectroscopic determination after immersion of the material as an optical fiber bio-cladding. With this configuration, the light-mediated recovery of the initial biosensor conditions enables multiple measurements and glucose monitoring over time with a single, biocompatible and biodegradable biosensor.

This chapter contents results previously/to be published as:

Congresses:

Green chemistry based nanopatterning of bio-functionalized silk fibroin layers for reversible optical biosensing. A. Márquez, M. Procek, G. Guirado, Salvador D. Aznar-Cervantes, J.L. Cenis, , C. Domínguez, X. Muñoz-Berbel. (As Oral Contribution in MNE 2018, Copenhagen, Denmark).

Journals:

Light-Renewable Enzymatic Silk Biosensors Incorporating Diarylethene Mediators For Continous Glucose Monitoring. Augusto Márquez, Molíria V. Santos, Sara Santiago, Gonzalo Guirado, Salvador D. Aznar-Cervantes, Jose Luis Cenis, Carlos Domínguez, Fiorenzo G. Omenetto, Xavier Muñoz-Berbel, (*To be submitted*).

1. Introduction

The detection and quantification of glucose represents a crucial backbone in biosensors development given the relevant role of this analyte in fields like healthcare or food industry²⁹⁰. In the human health case, the importance of glucose monitoring is intimately related to diabetes mellitus, especially for the derived complications of this condition, e.g. renal problems or blindness. Even though, glucose regulation transcends the same as the presence of altered physiological glucose values are also found, for instance, in tumour proliferation.²⁹¹²⁹²

Albeit there are new sophisticated methods less and less invasive for glucose monitoring,²⁹³ the most extended commercial strategy is still the electrochemical detection in a drop of patient's blood, self-extracted by finger puncture. Still electrochemical glucose biosensors are well extended, there are more ways of glucose sensing reported such as fluorescence-based biosensors,²⁹⁴²⁹⁵ colorimetric detections⁶⁰²⁹⁶ or optical sensors.²⁹⁷²⁹⁸ Colorimetric biosensors are very promising for simplicity and cost, although less sensitive than other biosensors and still dealing with the presence of interfering coloured molecules in the blood/urine matrices, i.e. haemoglobin or bilirubin. They follow the same principle as electrochemical biosensors that include mediators but, in this case, the redox state change is accompanied by a color change of the material. That color change can be monitored by image analysis from a smartphone or by minimalistic spectrophotometers or photodetectors. As the pursued glucose concentrations to be detected in diabetes are relatively high (over 7 mM), the lack of sensibility in comparison with other methods is not so relevant. Additionally, strategies to minimize the interference of biological matrices in the colorimetric measurement have been already demonstrated, such as cell-fraction sieving in blood samples.^{170,228}

Biosensors employed in POC applications trend to be disposable, following the general strategy to reduce costs, and colorimetric essays are not an exception (i.e. pregnancy test). This fact occurs because most biosensors are single use since the system recovery to the initial state represents an issue (i.e. electrochemical recovery of electrochromic mediators) and it is not worth to include more components to do so, especially in disposable devices. At this point, photoelectrochromic molecules are relevant for their capability of alternating between two isomeric forms by specific wavelength irradiation. This interconversion is associated to color changes of the

material.²⁷⁴ In case of DTE, it has been demonstrated that the open-closed state of the diarylethene molecule can be also modulate electrochemically,²⁸⁵ opening the possibility of using this molecule as electrochromic mediator in enzymatic reactions. Albeit photoelectrochromic molecules and composites has already been used for sensing applications like hydrogen²⁸¹ (Au-WO₃), acetone gas²⁸² (Ag-TiO₂) or even solar UV dosage²⁷⁹ (phosphomolybdic acid – lactic acid), their use in biosensing has been limited and only one paper demonstrates their potential coupling to enzymatic reactions (Chapter 5.5).

In the search of an adequate matrix material for enzymes and photoelectrochromic molecules combinative hosting for biosensors development, SF from *Bombyx mori* appears as a suitable candidate for its extraordinary properties (biocompatible,²⁹⁹ biodegradable,³⁰⁰ transparent in the Vis-NIR spectrum, thermally resistant,³⁰¹ and capable to store biomacromolecules for long time periods without altering their structure or function). SF becomes then suitable to develop (depending on the treatment) a wide variety of materials (films, gels, fibers, sponges, tubes, spheres).³⁰²

In the presented chapter, the use of DTE as enzymatic photo-reversible mediator in the development of a glucose optical biosensor integrating both the enzymes and mediator in a SF matrix is proposed. The exclusivity of the DTE closed isomer to be catalysed by the HRP, rather than the open one, permitted to rule the biosensor by UV pulses that switched on the reaction mechanism. The use of SF favoured the co-immobilization of enzymes together with the poorly water-soluble DTE, maintaining both entities their functionality (biorecognition and photochromism, respectively) after the water annealing of the structure. The water annealing, besides maintaining biomolecules functionality, compacted the structure limiting the DTE leakage to liquid samples. Additionally to the films configuration, it is proposed the use of the doped SF as bio-cladding of polymeric optical fibers, where the SF served as functional bio-cladding of a PMMA filament (core). The light propagating in the core of the PMMA filament was efficiently coupled into the SF coating due to the evanescent field enhancement associated to the RI difference³⁰³ (1.49 and 1.54, respectively). Moreover, by annealing, the SF becomes water-insoluble so the PMMA-SF optical fiber could be soaked in liquid samples for sequential detections without material loss.

2. Results

2.1. DTE immobilization in SF

DTE was immobilized within the SF fibroin matrix following a novel protocol developed for compounds with a low or negligible solubility in H₂O (**Figure 6.6.1**). While water-soluble molecules or proteins can be directly dissolved in the aqueous SF solution, for DTE a pre-solubilisation in ethanol was needed (max. solubility $1.2 \cdot 10^{-3}$ M). The SF solution at 7 % w/v obtained from the dialysis process was meanwhile concentrated by water evaporation in a dry chamber up to 20 % w/v. The DTE dissolved in ethanol was mixed with an equivalent volume of H₂O and then added to an equivalent volume of SF 20 % w/v. The intermediate mixture of the DTE ethanol solution with water was needed as the SF would aggregate if only ethanol was added to the solution. In fact, the final mixture ($3 \cdot 10^{-4}$ M DTE and 10 % w/v SF in etOH-H₂O 1:3) was not stable for more than 2 h as the SF tended to aggregate in presence of alcohols. This precursor was casted onto polystyrene surfaces to obtain doped SF films. An enhanced evaporation of the etOH-H₂O at 60 °C was needed in order to obtain transparent films (**Figure 6.6.2a**) rather than gels. Once dried, the casted films were water annealed in a vacuum chamber at 800 mbar and 45 °C with H₂O saturated atmosphere to provoke the crystallization of the SF.

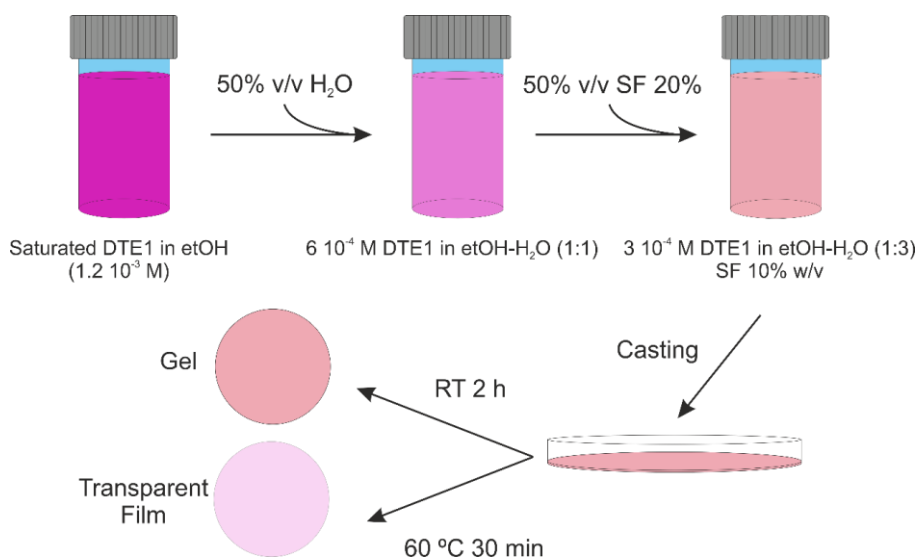


Figure 6.6.1. SF doping process with DTE. The supernatant of a saturated solution of closed DTE ($1.2 \cdot 10^{-3}$ M) in ethanol was mixed with the equivalent volume of H₂O. The 1 to 1 etOH-H₂O solution of DTE1 was then mixed with an equivalent volume of 20 % w/v of SF aqueous solution. A fast evaporation of the solvent drove to the formation of a transparent film while the incubation at room temperature carried to a gel formation.

6. Results

Despite the SF crystallization, the DTE has demonstrated to maintain its reversible isomerization capability within the SF matrices (**Figure 6.6.2a**). Furthermore, it was possible to develop color homogeneous patterns in the SF transparent films (**Figure 6.6.2b**) by selective irradiation of specific areas using masks opaque to UV light. Additionally, the control over the exposure time leads to a higher or lower DTE isomerization, what is translated in a more or less intense coloration of the transparent SF films and, therefore, in a coloration gradient by successive UV irradiation steps of different areas (**Figure 6.6.2c, 6.6.2d**). The isomerization of the DTE within the film occurs fast with the employed UV source and, after 2 min of irradiation, no further coloration is observed. On the contrary, the molecule decoloration was slow and films needed to be exposed during 24 h to ambient light to bleach the films. These kinetics of photocoloration and photobleaching are in accordance to the already reported of the molecule in solution.²⁸³

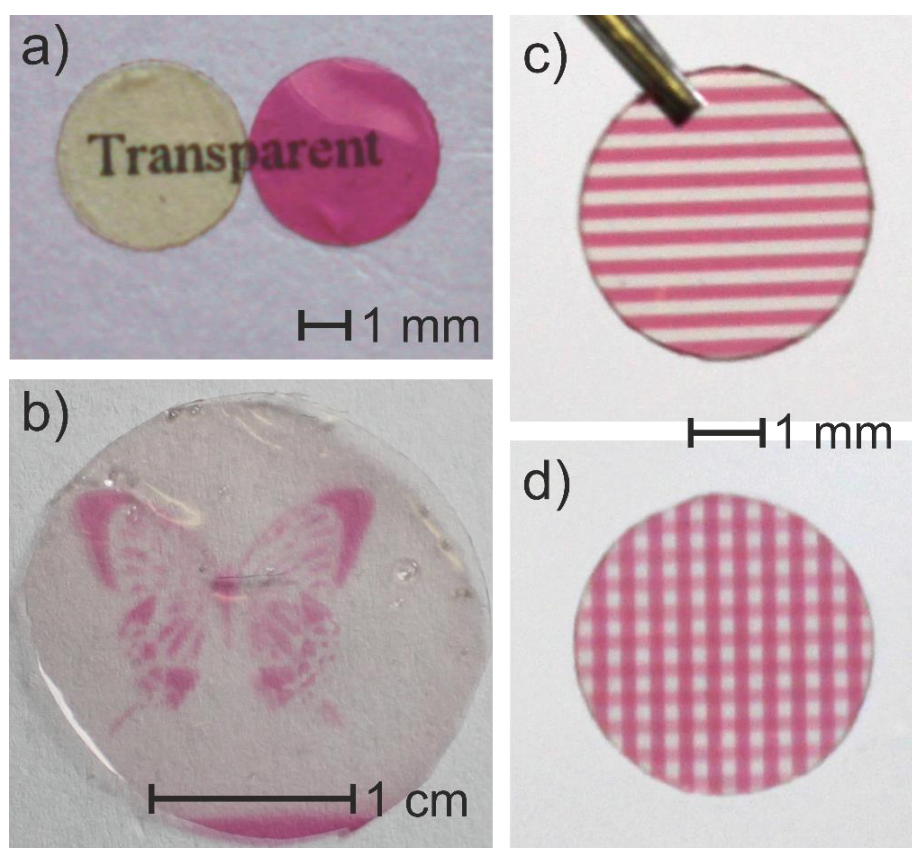


Figure 6.6.2. SF films doped with DTE. a) Photographs of 4 mm diameter SF pads doped with DTE before and after 30 s UV irradiation and placed over the printed word “Transparent” to denote the transparency of the film. It is possible to develop figures b) or regular patterns c) on the films using a suitable mask during the UV irradiation.

2.2. DTE Catalysis within the SF matrix

In the previous chapter, it was demonstrated that DTE can be catalysed by HRP in presence of H_2O_2 . The reaction is isomer-selective and it is only happening when the DTE molecule is in the closed form since the redox potential gap existing between the two isomers precludes the oxidation of the open form by the peroxidase. All these factors made DTE a photo-inducible enzymatic mediator. For instance, in a doped SF matrix, the DTE available to be catalysed by the HRP is then determined by the UV irradiation parameters (area and time). This fact permits to compare between non-irradiated (reference) and irradiated (sensing) areas or even design a color gradient that would disappear distinctively depending on the analyte concentration in the sample.

The DTE reactivity with H_2O_2 by HRP catalysis may not be interesting per se but it may be very useful in biosensing applications as H_2O_2 is the by-product of many enzymatic reactions. Good examples are the glucose, ethanol, cholesterol or lactate oxidations by the specific oxidases. By the use of colorimetric mediators like TMB or ABTS, which are oxidized as well by the HRP in presence of H_2O_2 changing their color, it would be possible to detect and even quantify the amount of initial analyte.

Those common mediators have been substituted by DTE and co-immobilized together with GOx and HRP within the SF matrix in order to build a glucose optical biosensor. The still liquid SF solution was doped with GOx and HRP (25 and 60 u ml^{-1} , respectively) additionally to the DTE and casted films were obtained following the same protocol explained before. 4 mm circular pads were cut from the SF films and were exposed to 300 nm light during 30 s using a mask with a periodic pattern of 200 μm (**Figure 6.6.2c, 6.6.3a**). The SF pad is immersed in a PBS solution with different glucose concentrations (0, 4 and 8 mM) for 1 min (**Figure 6.6.3b**) and, after excess of liquid removal, it was exposed again 30 s to UV irradiation, rotating the pad to develop the same pattern 90° respect to the previous one (**Figure 6.6.3c**). This procedure is done for several reasons. First, the fact that after the immersion in PBS and the second UV irradiation, the non-colored area became colored revealed that DTE leakage from the SF matrix to the solution was negligible. Indeed, when irradiated, immersed in PBS without glucose and secondly irradiated (**Figure 6.6.3d-3f**), the measured absorbance spectrum of the once-irradiated areas (before and after immersion) revealed essentially the same intensity at 530 nm. Second, as no DTE leakage from the SF matrix is observed, the area irradiated after the immersion serves as reference to the area irradiated before the immersion.

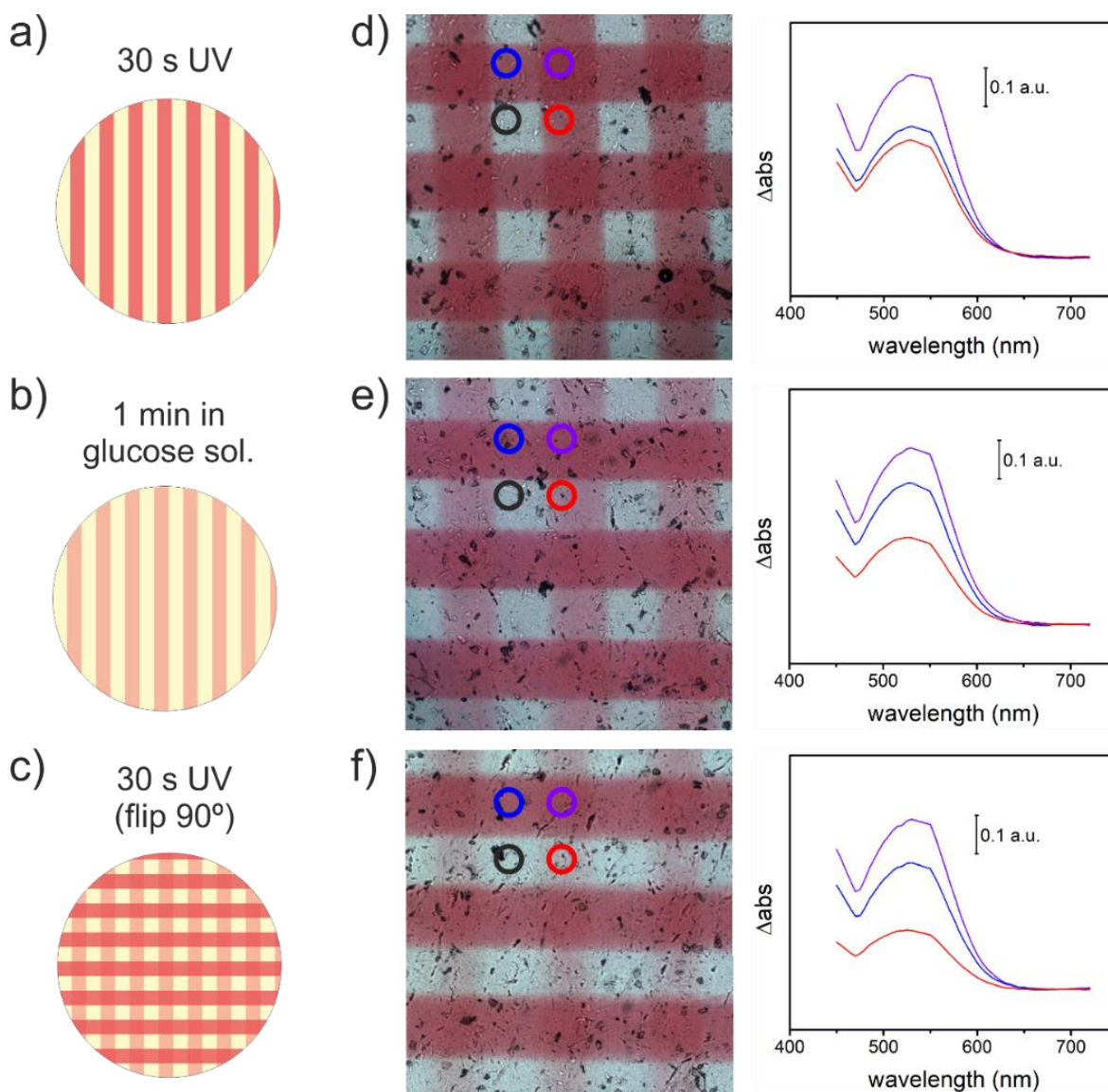


Figure 6.6.3. Glucose detection using patterned SF films doped with DTE, GOx and HRP. a) First, a doped SF pad of 4 mm diameter is irradiated with UV for 30 seconds, using an aluminum mask to generate patterns of 200 μm . b) The pad is then immersed in a PBS solution with glucose. c) Finally, the pad is removed from the solution, dried and irradiated using the same mask forming a 90° angle respect to the previous pattern. d) 0 mM, e) 4 mM and f) 8 mM glucose PBS solution lead to different color decay within the film. By image spectral analysis, is possible to quantify the decay in different areas of the film: never irradiated area (black), irradiated area before immersion (red), irradiated area after the immersion (blue) and irradiated area before and after the immersion (purple).

In case of glucose presence in the PBS solution, a decay in the color intensity as well as in the absorption band could be appreciated. This color loss was a consequence of the previously described enzymatic reaction: the GOx oxidized glucose in presence of O_2 to glucono-1,5-lactone and H_2O_2 and, afterwards, the H_2O_2 was used by the HRP to

oxidize the closed DTE. The color loss was related to the glucose concentration in the PBS solutions. Actually, when bleached either by the reaction or by visible light irradiation, the SF pads could be reused for a second analysis.

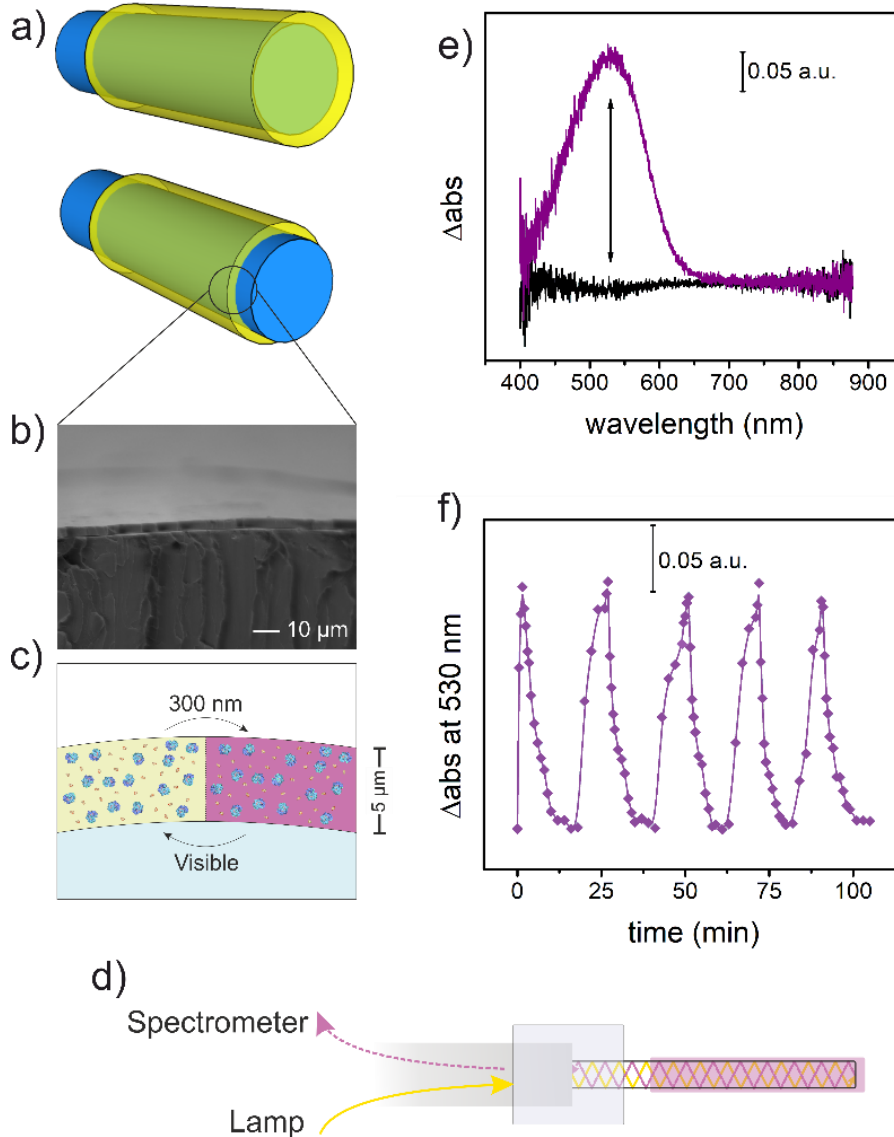


Figure 6.6.4. PMMA-SF optical fiber doped with DTE. a) Scheme of a PMMA filament dip coated with a doped SF solution. The filament is coated 4 times at 0.6 mm s^{-1} using a linear actuator. b) Cross section image of a PMMA-SF optical fiber obtained by SEM and c) scheme of the cross-section including the immobilized enzymes within the SF matrix and the two color situations of the cladding. The measurements are performed in a reflection mode following the scheme in d) and using a bifurcated probe to guide the light from the halogen lamp to the PMMA filament and back to the spectrometer. The PMMA filament is coupled to the optic probe using a PDMS adapter. e) Absorbance spectrum of the doped SF cladding after UV irradiation and f) absorbance evolution at 530 nm during consecutive cycles of coloration and bleaching upon UV and visible light irradiation respectively.

2.3. PMMA filaments coated with DTE and enzymes doped SF

Besides the SF films casting, the doped SF precursor, including DTE and enzymes, was also used for the cladding fabrication of a PMMA-SF optical fiber by dip coating of the PMMA filaments (**Figure 6.6.4a**). The obtained functional bio-cladding revealed to have a thickness of 5 μm measured by SEM imaging of a cut optical fiber (**Figure 6.6.4b**) after the water annealing process. In order to check the isomerization of the DTE within the SF cladding and the following color change (**Figure 6.6.4c**), the PMMA-SF optical fibers were coupled to an optical probe to measure in reflectance (**Figure 6.6.4d**). In this configuration, the light was confined from a halogen lamp into the PMMA filament and interacted with the DTE doped SF cladding. The back-reflected light was collected by the probe and guided to the spectrometer. Reversibly, the DTE could be closed and opened within the SF bio-cladding as in the SF films by UV and visible light irradiations and measured by absorbance (**Figure 6.6.4e, 6.6.4f**). Color changes could be appreciated even with the bare eye.

2.4. Glucose detection and optical biosensor regeneration

These PMMA-SF optical fibers were then employed in glucose determination by a fast immersion in a liquid sample. The annealed PMMA-SF optical fibers were coupled to the optical probe and this was, at the same time, attached to the linear actuator to precisely control the immersion time of the fibers in PBS solutions with different glucose concentrations (**Figure 6.6.5a**). Specifically, the optical fibers were irradiated with UV light until the absorption band peak of DTE at 530 nm reached an intensity of 0.4 a.u. by the spectrometer (set as 100 % of signal). Then, the fibers were immersed during 8 s in the glucose PBS solution and extracted. The absorbance spectrum before and after the immersion was compared and the absorption decrease was evaluated among different glucose concentrations (**Figure 6.6.5b-5e**), being more pronounced for higher ones. After a detection cycle, the PMMA-SF optical fiber was irradiated again with UV light until 0.4. a.u. (100 % signal) value was registered at 530 nm. Then, a subsequent immersion was carried out and a second absorbance decay measured. The same measuring protocol was done 7 times, obtaining a repetitive response of the optical biosensor (**Figure 6.6.5f**). The fall percentage respect to the initial absorbance value was used for the biosensor calibration (**Figure 6.6.5g**).

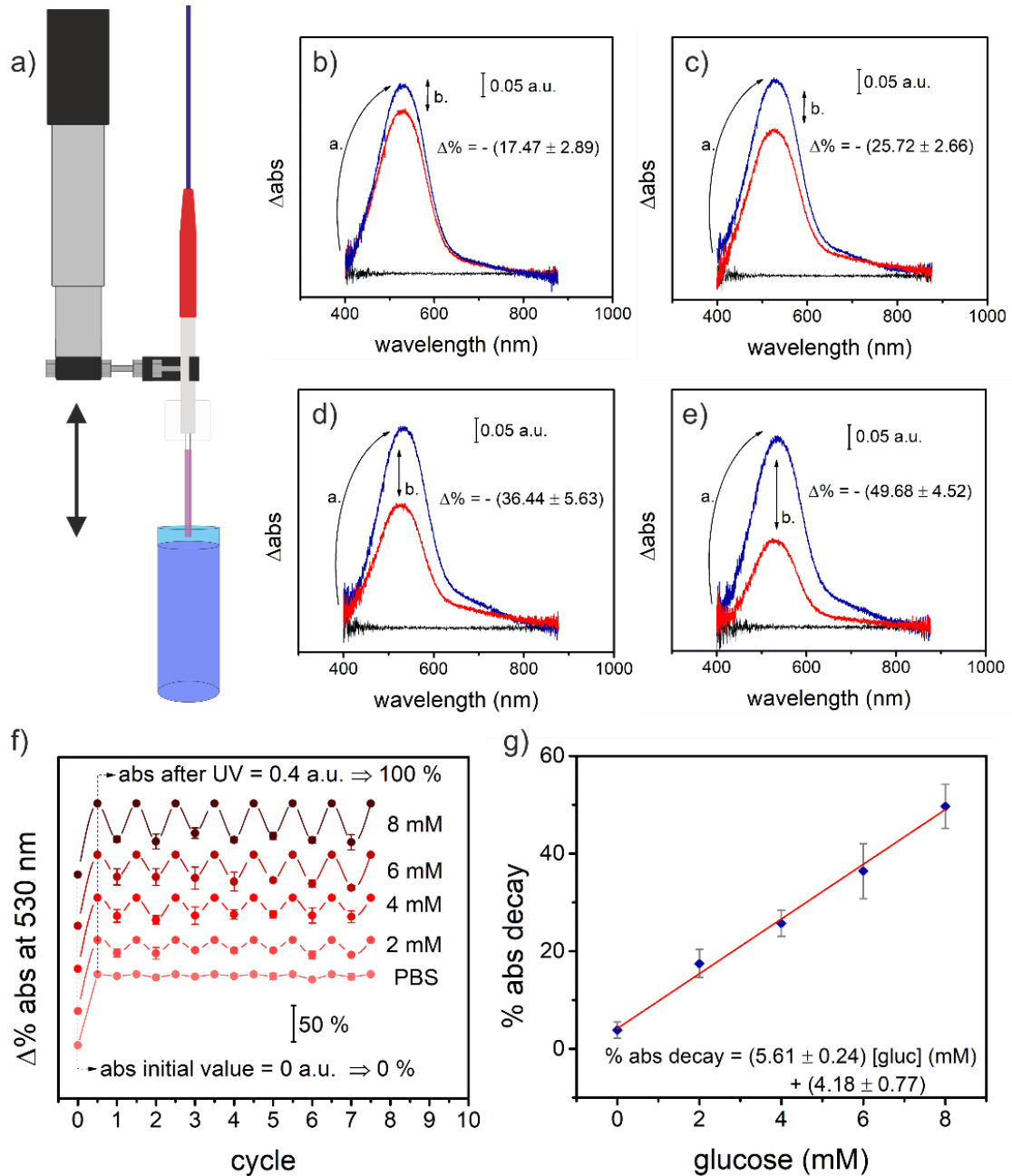


Figure 6.6.5. Glucose cyclic detection with DTE doped PMMA-SF optical fibers.

a) Used setup for fibers measurement. The optic probe was attached to a linear actuator and the PMMA-SF optical fiber was joined to the probe using a PDMS mold for a proper light coupling. After UV irradiation of the filament, it was immersed for 10 seconds in a PBS solution with glucose and an absorbance fall was observed related to the glucose concentration: b) 2 mM, c) 4 mM, d) 6 mM and e) 8 mM. f) Consecutive cycles of UV irradiation and glucose detection by fiber immersion in PBS with glucose solutions. Initially, the coated filament was irradiated with the UV lamp until the absorbance value at 530 nm reached 0.4 a.u. Then, the fiber was immersed during 10 s in a PBS solution with glucose and the abs value decayed at 530 nm. Once the signal was stable, the same process was repeated. b) Calibration curve for different glucose concentration based on the absorbance decay at 530 nm. n=5.

Doped SF has been used recently as bio-cladding for glucose determination in single-use PMMA-SF optical fibers, where besides the HRP and GOx, ABTS mediator was co-immobilized. One of the main advantages of the system was the capability of direct whole blood analysis by the filtering properties of the bio-cladding: the doped cladding changed its color by the presence of the analyte and, after a fast washing step, the strong absorbance signal from the blood is removed. In the present chapter, a new photochromic peroxidase substrate is incorporated in the bio-cladding of this type of optical fiber biosensors that permits to reuse of the sensing part by a fast light pulse, in contrast to the common colorimetric disposable biosensors.

Furthermore, it has demonstrated a linear response between 0 and 8 mM glucose concentrations, useful for diabetes detection, when values of no more than 6 mM are expected in fasting conditions for healthy patients.

3. Conclusions

The homogeneous immobilization of the poorly water-soluble photoelectrochromic DTE within the SF was achieved by the combination of water-ethanol mixtures of the DTE and SF solutions before deposition and a fast solvent evaporation to obtain transparent films rather than gels. The capability of the molecule to undergo reversible isomerization in the solid SF composites was demonstrated by UV induced coloration of the material, with no evidence of particle aggregation according to the transparency and homogeneous color change of the films. Additionally to the SF film fabrication, the doped SF precursor was also employed for PMMA filaments dip coating, obtaining a PMMA-SF optical fiber with an active bio-cladding that also responded reversibly to alternative UV and visible light irradiation cycles. Afterwards, both GOx and HRP enzymes were co-immobilized with the DTE inside the SF bulk. Closed (colored) DTE, which has demonstrated previously to be sensitive to HRP catalysis in presence of H₂O₂, lost its color when the doped SF was immersed in glucose solutions. This fact has been used for the development of an optical biosensor, both in the film and in the fiber optics bio-cladding configuration, which could be regenerated after a detection cycle by 300 nm UV light irradiation. The presented system, with a linear response to glucose concentrations between 0 and 8 mM, would permit the glucose monitoring in diabetic patients using the same biosensor and regenerating the system by a fast light pulse.

7. General Discussion

In this chapter, the obtained and presented results in section 6 are discussed and compared among them, evaluating the suitability of every one of them depending on the conditions.

As the main objective, the presented thesis attempts to move forward in the development of new biosensors for classical, but also future, affections such as diabetes. The thesis pretends to develop a new generation of monitoring systems where the principal limitation of traditional biosensors, which is the stability and durability of the biological recognition element, is here amended. For this purpose, two different biomaterials in combination with two different sensing strategies have been taken as cornerstones for the presented study: alginate hydrogel for electrochemical biosensors and SF for optical biosensors. Both types of biosensors present, in common, the use of enzymatic oxidase-peroxidase systems for the detection of glucose and lactate, in combination with electrochromic and photoelectrochromic mediators. Additionally, alginate and silk-fibroin provide the enzymes a highly-hydrated and physiological environment where they should remain stable for long time periods, expanding the lifetime of the biosensor.

In a sensing field where the available commercial devices are predominantly based on amperometric detections using disposable screen-printed electrodes,¹⁷³ the discussed strategies for biosensing glucose, and also lactate, present several novelties and advantages respect to the established ones.

First, in contrast to the disposable test strips, electrochemical biosensors based on electrodeposable alginate have demonstrated to be reusable by simply eliminating the alginate membrane with innocuous Ca^{2+} chelating compounds (i.e. PBS) and generating a second membrane for a succeeding analysis (**Chapter 6.1**). At optimal electrodeposition conditions, identical biocatalytic membranes are obtained, which provide comparable responses to the analyte thus avoiding additional re-calibration steps. Furthermore, the alginate hydrogel has demonstrated to protect the metal surface of the electrode, preventing biofouling effects caused by the complex matrices of real samples like whole blood. All these properties have been checked using a commercial screen-printed gold electrode, characterized for being inexpensive. Nevertheless, the developed biosensor has demonstrated good sensitivity ($-0.27 \mu\text{A cm}^{-2} \text{mM}^{-1}$), low LOD (0.126 mM), low CV (10 %) and a linear response between 0 and 12 mM for glucose determination, which is valid to detect hyperglycaemia levels in humans. Hence, when modified with this biocatalytic membrane, it is possible to determine the analyte concentration in whole blood samples and without requiring additional dilution or pre-treatment protocols.

Besides cost reductions, the reusability of the alginate based electrochemical biosensor is very convenient, because makes it possible to select the analyte of interest by simply changing the recognition elements (enzymes) in the membrane. This fact has been demonstrated for the co-detection of glucose and lactate using a four electrodes array integrated in a Si chip fabricated in the Clean Room of IMB-CNM (**Chapter 6.2**). By the use of fast prototyping techniques, a PMMA-PDMS structure was design for the chip encapsulation and fluidics management, what permits the injection of hydrogel precursors and samples in the electrodes chamber, where the alginate is electrodeposited and the analytes are detected. After the detection, a washing step with PBS restore the system for subsequent analysis. The possibility to change the membrane content is not only useful for changing the analyte to be detected but also to adapt the system to different concentration ranges of the same analyte. For example, using the same device glucose and lactate from healthy human and control and diabetic induced (STZ) mice were detected. Concentrations in the samples were notably different, especially in case of glucose, where human present normal values around 3-6 mM while control mice presents 10-20 mM and diabetic up to 60 mM. Adapting the concentration of enzymes in the membrane, a higher or lower response was obtained for a certain concentration of analyte. Furthermore, due to its precise fabrication, the system is characterized for being highly precise and repetitive, so the response is stable between different measurements once calibrated, if the conditions of the membrane remain unaltered. The alginate based biosensor integrated in the present system (optimized) still shows good sensitivity ($-0.24 \mu\text{A cm}^{-2} \text{mM}^{-1}$ for glucose and $-0.54 \mu\text{A cm}^{-2} \text{mM}^{-1}$ for lactate), low LOD (0.175 mM for glucose and 0.100 mM for lactate), low CV (11 % for glucose and 13 % for lactate) besides the adequate and adaptable linear response.

Although alginate has demonstrated strong points such as reusability and versatility for it application in biosensors, it is true that requires special conditions for the precursor storage (low temperature and asepsis), as well as an additional equipment (potentiostat) for the membrane fabrication and electrochemical detection. Besides, alginate membrane, once generated, present high storage restriction since, when dehydrated, they do not recover their initial state. For these reasons, SF has been employed as matrix for a second type of (optical) biosensors.

In case of SF, these drawbacks are overcome. First, doped SF films are fabricated in a green and water-based process, respectful with doping biomolecules, that ends in a

dry and crystalline structure that preserves the enzymatic activity and the biosensor response unaltered during, at least, 40 weeks without requiring refrigeration or humidity (**Chapter 6.3**). These doped SF films, transparent in the visible range, are integrated in a PMMA structure where, by capillary pumping, interacts with the liquid fraction of whole blood samples. Thanks to its nanometric porosity, SF present filtering capacity and the colour change of the mediators included in the SF can be detected with a negligible interference from blood haemoglobin. This colour change can be measured not only spectroscopically, but also by image analysis or even with the bare eye, what solves the instrumentation issue that presented alginate hydrogels as it could be done with a smartphone camera and a dedicated application. In comparison with the alginate biosensor, despite the LOD is higher (0.800 mM), the CV is still low (11 %).

The blood filtration capability of SF was corroborated in a second disposition of this membrane used as bio-cladding of PMMA fibers (**Chapter 6.4**). This bio-cladding also changed its color when the PMMA-SF optical fiber was immersed in whole blood by the presence of glucose in the sample. While the haemoglobin signal is removed by a washing step, the characteristic purple color of the SF is maintained due to the covalent bonding of the ABTS radical (produced in the detection reaction) to the tyrosine amino acids present in the SF structure. In optical fiber setup, the LOD and sensitivity improved respect to the film (0.652 mM and 0.12 a.u. mM⁻¹ versus 0.800 mM and 0.1 a.u. mM⁻¹, respectively), although the CV was incremented in one point (from 11 to 12 %).

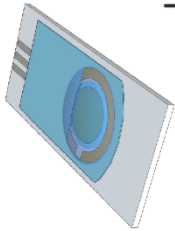
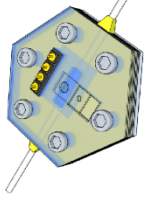
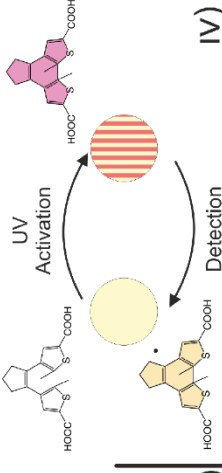
Despite SF-based biosensors bring measurement system simplicity and long biosensor lifetime, some advantages of alginate membranes are not fulfilled in this case: reusability and versatility. The second is not applicable to SF because in case of alginate, the electrochemical transducer is maintained and, it is the in-situ membrane generation possibility and the precursor selection capability by the user what makes the system versatile. In case of SF, the doped films or bio-claddings are not susceptible for any further change after the water annealing process. Nevertheless, reusability was approached by the use of DTE, a photoelectrochromic compound that become colored by UV irradiation and has demonstrated to be catalytically reduced by the peroxidase in presence of H₂O₂, losing the color (**Chapter 6.5**). In the same way used for the previous systems with TMB or ABTS, DTE catalysis was coupled to the GOx-HRP enzymatic cascade system and the color loss of the compound was induced by the presence of glucose. The catalysis by HRP has demonstrated to be selective for the closed form of

DTE (colored) due to the redox potential difference with the open form (non-colored). This fact permitted to “activate” the biosensor by UV light pulse, regardless the presence of analyte.

Although the solubility in water of DTE, in contrast to ABTS, is negligible, a new protocol combining DTE dissolved in ethanol with SF aqueous solutions permitted the fabrication of transparent DTE doped films and bio-claddings, also incorporating GOx and HRP (**Chapter 6.6**). The immobilization within the SF matrix permitted the glucose optical biosensing in two steps: i) DTE coloration by UV light pulse and ii) color lose by DTE catalysis in presence of glucose. The reusability comes by a subsequent UV light pulse that close a second amount of DTE molecules, which are then susceptible of being catalysed if the biosensor is exposed to glucose again. Analytically, the biosensor using DTE shows a lower performance that may be improbable with higher LOD (1.3 mM) and CV (17 %) and a shorter linear response (0 to 8 mM) although still useful in diabetes application.

In comparison (see **Results Table**), the electrochemical biosensor based on alginate, characterized in **Chapter 6.1** and developed in **Chapter 6.2**, offers the most powerful sensing capabilities in the frame of this thesis in terms of sensibility, linear range, detection time and multi-parametric analysis capacity. Some parameters are matched by the non-reversible SF based colorimetric biosensors, like CV, LOD or whole blood analysis capability (**Chapter 6.3 and Chapter 6.4**), which also have long durability and need simpler equipment to perform the analysis. The reusability was achieved in the optical biosensor by the substitution of the colorimetric mediator (**Chapter 6.5**) by a photoelectrochromic molecule (DTE) with low success in analytical parameters (**Chapter 6.6**).

Thus, the selection of the type of biosensor must be based on the type of application, being more accurate the electrochemical based on alginate than the optical based on SF but at the same time, needing special conditions for the precursor storage and additional equipment (potentiostat) to carry out the detections.

	 I)	 II)	 III)	 IV)
Detection	Electrochemical	Electrochemical	Optical	Optical
Reusability	Yes	Yes	No	Yes
Measurement Range	0 - 12 mM	0 - 12 mM 10 - 70 mM	0 - 12 mM	0 - 8 mM
Durability	n/a	n/a	40 weeks	40 weeks*
Limit of Detection	0.126 mM	0.175 mM	0.800 mM (film) 0.652 mM (fiber)	1.3 mM (fiber)
Sensitivity	$-0.27 \mu\text{A cm}^{-2} \text{mM}^{-1}$	$-0.24 \mu\text{A cm}^{-2} \text{mM}^{-1}$	0.1 a.u. mM^{-1} (film) 0.12 a.u. mM^{-1} (fiber)	$-0.022 \text{ a.u. mM}^{-1}$ (fiber)
Variation coefficient	10 %	11 %	11 %	17 % (fiber)
Whole blood analysis	Yes	Yes	Yes	Yes*
Multiparametric	No	Yes	No	No
Detection Time	4 min	4 min	9 min (film) 5 min (fiber)	2 min (film) 5 min (fiber)

Results Table. Summary of the developed electrochemical (I and II) and optical (III and IV) biosensors with their main characteristics for glucose analysis. *Durability and blood filtering are not measured specifically but expected from results in III.

8. Conclusions

8. Conclusions

The results presented in this thesis confirms the suitability of using alginate hydrogels and SF as matrices in the development of new biosensors based on natural biomaterials.

According to the stated objectives:

1. Alginate hydrogel has demonstrated the capability of actuate as a size-exclusion filter, allowing the direct electrochemical detection of glucose in whole blood samples, protecting the electrode from biofouling effects.
2. The use of electrodepositable hydrogel in combination with a Pt electrodes array, fabricated by planar technology, within a PMMA-based fluidic structure permitted the fabrication of a reusable multiparametric point-of-care device. The system offers the possibility of selecting the analytes and concentration range to be detected, by changing the composition of the alginate precursor.
3. SF has demonstrated to maintain the enzymatic activity through long periods of time and also to be useful in the whole blood analysis, filtering the sample with the help of a miniaturized PMMA structure by capillary pumping. Likewise, it can be incorporated to optical fiber fabrication as a bio-functional cladding.
4. The photoelectrochromic molecule DTE has demonstrated to be catalysed by HRP in presence of H_2O_2 . This fact has been employed to develop light-inducible and light-regenerable glucose optical biosensors based on DTE co-immobilized with enzymes in SF films and SF bio-functional claddings of PMMA fibers.

9. Future Scope

The aim of this final section is to discuss and propose potential improvements for the previous alginate- and SF-based biosensors, following the same researching line.

Electrodeposited alginate based biosensors are considered highly developed in this thesis (Chapters 5.1 and 5.2), from the material characterization and biosensor optimization to the integration in a lab-on-chip type device using electrodes fabricated by Si-based technologies and PMMA structures mechanized by laser ablation. Furthermore, additional instrumentation design and production (μ -potentiostat) in collaboration with electronic engineers (ICAS group from IMB-CNM) have been developed for the biosensor control and data processing. The combination of the lab-on-a-chip and the instrumentation provides a fully-functional prototype only requiring minimal modification to be adapted to the requirement of the application of interest.

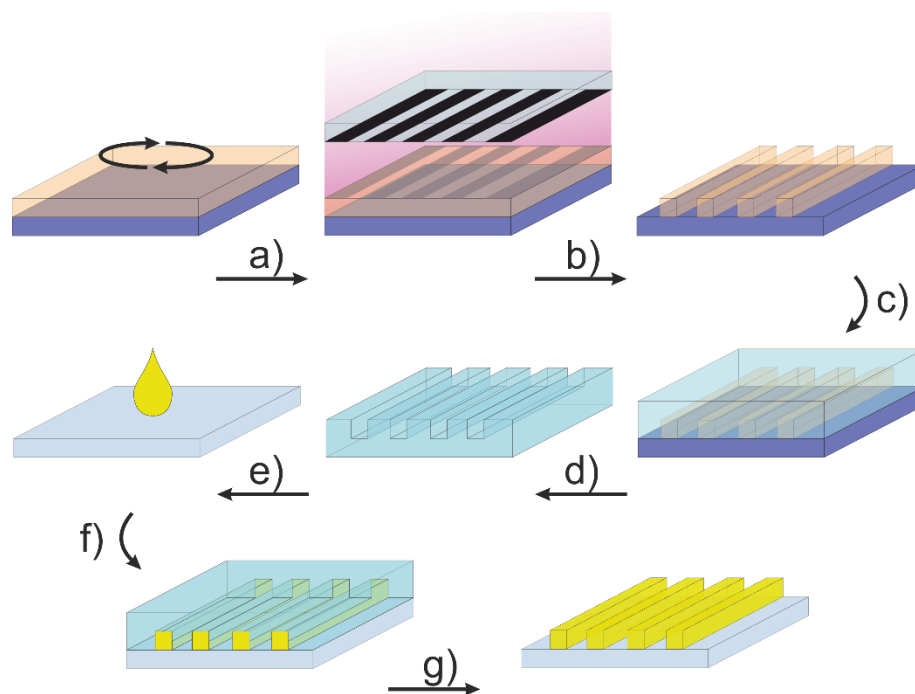


Figure 9.1. SF stamping process using PDMS moulds. SF patterning by stamping with PDMS. Previously, a layer of SU-8, deposited by spin coating (a) on a thermal oxidized Si wafer, is crosslinked by UV irradiation and developed with acetone (b). Then, a PDMS precursor is casted over the SU-8 patterns (c), cured at 80 °C and peeled off (d). A SF solution drop is casted on a glass substrate (e) and the PDMS pressed over it until the water evaporates (f). The SF patterns are finally water annealed (g).

In case of SF, also a deep study has been carried out from a macroscale point of view. It has demonstrated to be biocompatible for the immobilization of enzymes with electrochromic or photoelectrochromic compounds for the development of a glucose

optical biosensor. In fact, the first reversible optical biosensor has been developed in the framework of the present thesis based on the use of photoelectrochromic biosensors. Nevertheless, the material has been used only as plane doped films integrated in PMMA structures or as a doped cladding for PMMA filaments, either by direct casting of the precursor solution or by dip coating of the filaments (**Chapters 6.3** and **6.6**).

Following these results and as a future approach, first steps have been taken for the micropatterning of SF with the aim of integrating the material in clean room processes. In a first indirect approach, the SF has been microstructured by stamping on a glass substrate, using a PDMS negatively patterned mould. The PDMS mould is previously obtained by casting on a SU-8 structure fabricated in a photolithography process (**Figure 9.1**). Good resolutions are achieved, as it is shown in the microscope image (**Figure 9.2a**) and in the 3D reconstruction (**Figure 9.2b**).

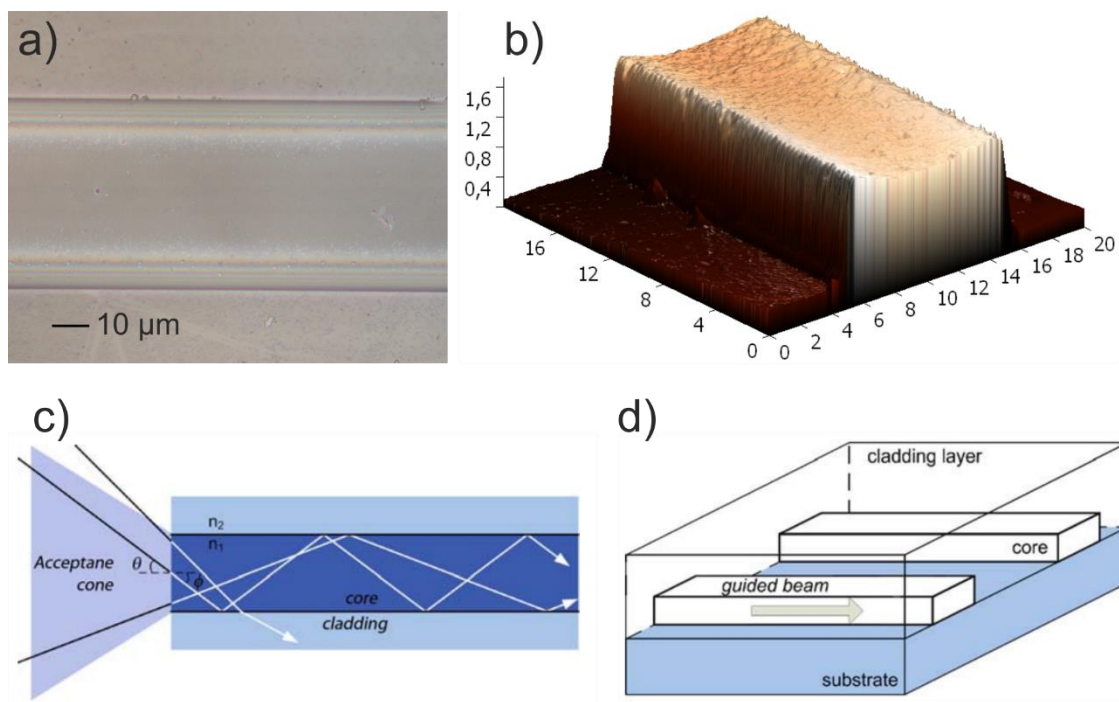


Figure 9.2. SF waveguides fabrication. a) Optical microscope image from the top and b) 3D reconstruction from AFM results of a SF waveguide fabricated by stamping (axis in μm). c) Light confinement in a waveguide and d) planar waveguides scheme on a substrate.¹⁵⁷

This protocol can be potentially used in planar waveguides fabrication due to the relatively high RI of SF (~ 1.54), what would permit an effective light coupling in the

9. Future Scope

structure (**Figure 9.2c, 9.2d**).¹⁵⁷ Furthermore, the biocompatibility of the SF patterning process drives to the possibility of doping the bulk of the waveguides with biorecognition elements and colorimetric molecules, in contrast to the extensively used planar waveguides of SiO₂ or Si₃N₄. As it has been demonstrated in this thesis, doped SF films and claddings permit the diffusion of small analytes (i.e. glucose), changing the color due to enzymatic reactions occurring within the matrix, while retaining potential interfering molecules, such as haemoglobin or the cell fraction. The same strategy can be applied to planar waveguides, where the increased optical path length compared to the thin films used in this thesis, would increase the sensibility of the biosensor.

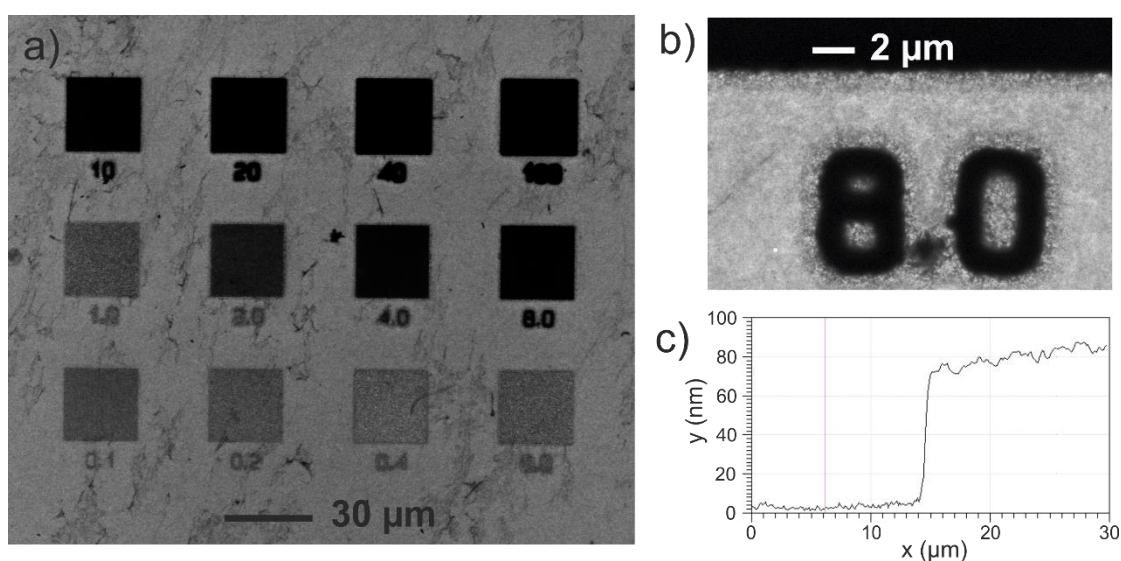


Figure 9.3. SF patterning by e-beam. a) SEM image of e-beam patterned SF layers of 200 nm thickness deposited by spin coating on a thermally oxidized Si wafer. The numbers below the squared irradiated areas indicate the factor (from 0.1 to 100) applied from a basic dose of 100 $\mu\text{C cm}^{-2}$ (0.1 factor corresponds to 10 $\mu\text{C cm}^{-2}$). b) Detail of an 800 $\mu\text{C cm}^{-2}$ irradiated area and c) respective profile measured by AFM.

Additionally to stamping patterning, also e-beam lithography has been explored as an alternative strategy to structure SF films. This method has demonstrated to pattern SF both as a positive or as a negative resist.¹⁶² If the SF is previously annealed, it can be used as a positive resist with high irradiation doses (**Figure 9.3**), while if it is not annealed, the crosslinking can be provoked by low doses of e-beam irradiation. This method is also all-water based and, therefore, compatible with biomolecules immobilization, especially when the SF is used as positive resist as no irradiation occurs over the remaining material.

The use of the presented techniques opens the possibility of SF structuring not only for light guiding and optical biosensing applications but also, for example, for highly controlled fluidic management based on the microfluidic synthetic paper concept developed by Prof. van der Wijngaart at KTH using OSTE. In this concept, the construction of micropillars enhances the capillary pumping properties of the material that, thanks to the precision of microfabrication techniques, can be highly controlled by playing with the size and distribution of the pillars.

The excellent optical properties of SF for its application in optical biosensing, demonstrated in this thesis, can be therefore improved by its microstructuration, reducing the amount of material and dopants used, miniaturizing the systems, and increasing the capillary properties to achieve faster detections.

10. Bibliography

- (1) International Diabetes Federation. IDF Diabetes Atlas, 8th Edition. 2017, pp 1–150.
- (2) Evans, J. M. M.; Newton, R. W.; Ruta, D. A.; MacDonald, T. M.; Morris, A. D. Socio-Economic Status, Obesity and Prevalence of Type 1 and Type 2 Diabetes Mellitus. *Diabet. Med.* **2000**, *17* (6), 478–480.
- (3) Fetita, L. S.; Sobngwi, E.; Serradas, P.; Calvo, F.; Gautier, J. F. Review: Consequences of Fetal Exposure to Maternal Diabetes in Offspring. *J. Clin. Endocrinol. Metab.* **2006**, *91* (10), 3718–3724.
- (4) Forouzanfar, M. H.; Afshin, A.; Alexander, L. T.; Biryukov, S.; Brauer, M.; Cercy, K.; Charlson, F. J.; Cohen, A. J.; Dandona, L.; Estep, K.; et al. Global, Regional, and National Comparative Risk Assessment of 79 Behavioural, Environmental and Occupational, and Metabolic Risks or Clusters of Risks, 1990–2015: A Systematic Analysis for the Global Burden of Disease Study 2015. *Lancet* **2016**, *388* (10053), 1659–1724.
- (5) Beagley, J.; Guariguata, L.; Weil, C.; Motala, A. A. Global Estimates of Undiagnosed Diabetes in Adults. *Diabetes Res. Clin. Pract.* **2014**, *103* (2), 150–160.
- (6) Nagel, B.; Dellweg, H.; Gierasch, L. M. Glossary for Chemists of Terms Used in Biotechnology. *Pure App. Chem* **1992**, *64* (1), 143–168.
- (7) Liu, J.; Cao, Z.; Lu, Y. *Functional Nucleic Acid Sensors*; 2009; Vol. 109.
- (8) Wei, H.; Wang, E. Nanomaterials with Enzyme-like Characteristics (Nanozymes): Next-Generation Artificial Enzymes. *Chem. Soc. Rev* **2013**, *42* (14), 6060.
- (9) Muyldermans, S. Nanobodies: Natural Single-Domain Antibodies. *Annu. Rev. Biochem.* **2013**, *82* (1), 775–797.
- (10) Lakard, B.; Herlem, G.; Lakard, S.; Antoniou, A.; Fahys, B. Urea Potentiometric Biosensor Based on Modified Electrodes with Urease Immobilized on Polyethylenimine Films. *Biosens. Bioelectron.* **2004**, *19* (12), 1641–1647.
- (11) Shamsipur, M.; Asgari, M.; Maragheh, M. G.; Moosavi-Movahedi, A. A. A Novel Impedimetric Nanobiosensor for Low Level Determination of Hydrogen Peroxide Based on Biocatalysis of Catalase. *Bioelectrochemistry* **2012**, *83* (1), 31–37.
- (12) Wang, H.; Ohnuki, H.; Endo, H.; Izumi, M. Impedimetric and Amperometric Bifunctional Glucose Biosensor Based on Hybrid Organic-Inorganic Thin Films. *Bioelectrochemistry* **2015**, *101*, 1–7.
- (13) Leland C. Clark, J.; Lyons, C. Electrode Systems for Continous Monitoring in Cardiovascular Surgery. *Ann. NY Acad. Sci.* **1962**, *102* (29).
- (14) Updike, S.; Hicks, G. The Enzyme Electrode. *Nature* **1967**, *214* (5092), 986–988.
- (15) Guilbault, G.; Lubrano, G. An Enzyme Electrode for the Amperometric Detection of Glucose. *Anal. Chim. Acta* **1973**, *64*, 439–455.
- (16) Foulds, N. C.; Lowe, C. R. Enzyme Entrapment in Electrically Conducting Polymers. *J. Chem. Soc.* **1986**, *82*, 1259–1264.
- (17) Harrison, D. J.; Turner, R. F. B.; Tg, C.; Baltes, H. P. Characterization of Perfluorosulfonic Acid Polymer Coated Enzyme Electrodes and a Miniaturized Integrated Potentiostat for Glucose Analysis in Whole Blood. *Anal. Chem.* **1988**, *60*, 2002–2007.
- (18) Karyakin, A. A.; Gitelmacher, O. V; Karyakina, E. E. Prussian Blue-Based First-Generation Biosensor . A Sensitive Amperometric Electrode for Glucose. *Anal. Chem.* **1995**, *67* (14), 2419–2423.
- (19) Wang, J.; Liu, J.; Chen, L.; Lu, F. Highly Selective Membrane-Free, Mediator-Free Glucose Biosensor. *Anal. Chem.* **1994**, *66* (21), 3600–3603.
- (20) Wang, J.; Fang, L.; Lopez, D.; Tobias, H. Highly Selective and Sensitive Amperometric Biosensing of Glucose at Ruthenium-Dispersed Carbon Paste Enzyme Electrodes. *Anal. Lett.* **1993**, *26* (9), 1819–1830.

10. Bibliography

- (21) Gough, D. A.; Lucisano, J. Y.; Tse, P. H. H. Two-Dimensional Enzyme Electrode Sensor for Glucose. *Anal. Biochem.* **1985**, *57* (12), 2351–2357.
- (22) Armour, J. C.; Lucisano, J. Y.; Mckean, B. D.; Gough, D. A. Application of Chronic Intravascular Blood Glucose Sensor in Dogs. *Diabetes* **1990**, *39* (December), 1519–1526.
- (23) Cass, A. E. G.; Davis, G.; Francis, G. D.; Hill, H. A. O.; Aston, W. J.; Higgins, I. J.; Plotkin, E. V.; Scott, L. D. L.; Turner, A. P. F. Ferrocene-Mediated Enzyme Electrode for Amperometric Determination of Glucose. *Anal. Chem.* **1984**, *56* (4), 667–671.
- (24) Wilson, R.; Turner, A. P. F. Glucose Oxidase: An Ideal Enzyme. *Biosens. Bioelectron.* **1992**, *7*, 165–185.
- (25) Linke, B.; Kerner, W.; Kiwit, M.; Pishko, M.; Heller, A. Amperometric Biosensor for in Vivo Glucose Sensing Based on Glucose Oxidase Immobilized in a Redox Hydrogel. *Biosens. Bioelectron.* **1994**, *9*, 151–158.
- (26) Ohara, T. J.; Rajagopalan, R.; Heller, A. Glucose Electrodes Based on Cross-Linked [Os(Bpy)₂Cl]⁺²⁺ Complexed Poly (1-Vinylimidazole) Films. *Anal. Chem.* **1993**, *65*, 3512–3517.
- (27) Degani, Y.; Heller, A. Direct Electrical Communication between Chemically Modified Enzymes and Metal Electrodes. Electron Transfer from Glucose Oxidase to Metal Electrodes via Electron Relays, Bound Covalently to the Enzyme. *J. Phys. Chem.* **1987**, *91* (6), 1285–1289.
- (28) Peng Si; Ding, S.; Yuan, J.; Lou, X. W. (David); Kim, D.-H. Hierarchically Structured One-Dimensional TiO₂ for Protein Immobilization, Direct Electrochemistry, and Mediator-Free Glucose Sensing. *ACS Nano* **2011**, *5* (9), 7617–7626.
- (29) Deng, S.; Jian, G.; Lei, J.; Hu, Z.; Ju, H. A Glucose Biosensor Based on Direct Electrochemistry of Glucose Oxidase Immobilized on Nitrogen-Doped Carbon Nanotubes. *Biosens. Bioelectron.* **2009**, *25* (2), 373–377.
- (30) Gao, R.; Zheng, J. Amine-Terminated Ionic Liquid Functionalized Carbon Nanotube-Gold Nanoparticles for Investigating the Direct Electron Transfer of Glucose Oxidase. *Electrochem. commun.* **2009**, *11* (3), 608–611.
- (31) Luo, Z.; Yuwen, L.; Han, Y.; Tian, J.; Zhu, X.; Weng, L.; Wang, L. Reduced Graphene Oxide/PAMAM-Silver Nanoparticles Nanocomposite Modified Electrode for Direct Electrochemistry of Glucose Oxidase and Glucose Sensing. *Biosens. Bioelectron.* **2012**, *36* (1), 179–185.
- (32) Mani, V.; Devadas, B.; Chen, S. M. Direct Electrochemistry of Glucose Oxidase at Electrochemically Reduced Graphene Oxide-Multiwalled Carbon Nanotubes Hybrid Material Modified Electrode for Glucose Biosensor. *Biosens. Bioelectron.* **2013**, *41* (1), 309–315.
- (33) Rafighi, P.; Tavahodi, M.; Haghighi, B. Chemical Fabrication of a Third-Generation Glucose Biosensor Using Graphene-Polyethyleneimine-Gold Nanoparticles Hybrid. *Sensors Actuators B. Chem.* **2016**, *232*, 454–461.
- (34) Wang, J. Electrochemical Glucose Biosensors. *Chem. Rev.* **2008**, *108* (2), 814–825.
- (35) Chen, C.; Xie, Q.; Yang, D.; Xiao, H.; Yingchun. Recent Advances in Electrochemical Glucose Biosensors : A Review. *RSC Adv.* **2013**, *3*, 4473–4491.
- (36) Gharsallah, Z.; Najjar, M.; Suthar, B.; Janyani, V. High Sensitivity and Ultra-Compact Optical Biosensor for Detection of UREA Concentration. *Opt. Quantum Electron.* **2018**, *50*, 249.
- (37) Tavousi, A.; Rakhshani, M. R.; Mansouri-Birjandi, M. A. High Sensitivity Label-Free Refractometer Based Biosensor Applicable to Glycated Hemoglobin Detection in Human Blood Using All-Circular Photonic Crystal Ring Resonators. *Opt. Commun.* **2018**, *429*, 166–174.
- (38) Nabok, A.; Al-Rubaye, A. G.; Al-Jawdah, A. M.; Tsargorodska, A.; Marty, J. L.; Catanante, G.; Szekacs, A.; Takacs, E. Novel Optical Biosensing Technologies for Detection of Mycotoxins. *Opt. Laser Technol.* **2019**, *109*, 212–221.
- (39) Engvall, E.; Perlmann, P. Enzyme-Linked Immunosorbent Assay (ELISA) Quantitative Assay of

- Immunoglobulin G. *Immunochemistry* **1971**, *8*, 871–874.
- (40) Bandi, Z. L.; Schoen, I.; Delara, M. Enzyme-Linked Immunosorbent Urine Pregnancy Tests. *Clin. Specif. Stud.* **1986**, *87*, 236–242.
- (41) Vamvakaki, V.; Chaniotakis, N. A. Pesticide Detection with a Liposome-Based Nano-Biosensor. *Biosens. Bioelectron.* **2007**, *22*, 2848–2853.
- (42) Hossain, S. M. Z.; Luckham, R. E.; Smith, A. M.; Lebert, J. M.; Davies, L. M.; Pelton, R. H.; Filipe, C. D. M.; Brennan, J. D. Development of a Bioactive Paper Sensor for Detection of Neurotoxins Using Piezoelectric Inkjet Printing of Sol - Gel-Derived Bioinks. *Anal. Chem.* **2009**, *81* (13), 5474–5483.
- (43) Zhao, W.; Chiunan, W.; Lam, J. C. F.; Mcmanus, S. A.; Chen, W.; Cui, Y.; Pelton, R.; Brook, M. A.; Li, Y. DNA Aptamer Folding on Gold Nanoparticles: From Colloid Chemistry to Biosensors. *J. Am. Chem. Soc.* **2008**, *130*, 3610–3618.
- (44) Link, S.; El-Sayed, M. A. Spectral Properties and Relaxation Dynamics of Surface Plasmon Electronic Oscillations in Gold and Silver Nanodots and Nanorods. *J. Phys. Chem. B* **1999**, *103*, 8410–8426.
- (45) Wang, Y.; Yang, F.; Yang, X. Biosensors and Bioelectronics Colorimetric Biosensing of Mercury (II) Ion Using Unmodified Gold Nanoparticle Probes and Thrombin-Binding Aptamer. *Biosens. Bioelectron.* **2010**, *25* (8), 1994–1998.
- (46) Li, B.; Du, Y.; Dong, S. Analytica Chimica Acta DNA Based Gold Nanoparticles Colorimetric Sensors for Sensitive and Selective Detection of Ag(I) Ions. *Anal. Chim. Acta* **2009**, *644*, 78–82.
- (47) Seok, Y.; Hyun, J.; Ae, I.; Jin, S.; Jurng, J.; Bock, M. A Novel Colorimetric Aptasensor Using Gold Nanoparticle for a Highly Sensitive and Specific Detection of Oxytetracycline. *Biosens. Bioelectron.* **2010**, *26* (4), 1644–1649.
- (48) Miranda, O. R.; Li, X.; Garcia-gonzalez, L.; Zhu, Z.; Yan, B.; Bunz, U. H. F.; Rotello, V. M. Colorimetric Bacteria Sensing Using a Supramolecular Enzyme-Nanoparticle Biosensor. *J. Am. Chem. Soc.* **2011**, *133*, 9650–9653.
- (49) Uni, V.; Liu, J.; Lu, Y. A Colorimetric Lead Biosensor Using DNAzyme-Directed Assembly of Gold Nanoparticles. *J. Am. Chem. Soc.* **2003**, *125*, 6642–6643.
- (50) Chen, X.; Chen, J.; Wang, F.; Xiang, X.; Luo, M.; Ji, X.; He, Z. Determination of Glucose and Uric Acid with Bienzyme Colorimetry on Microfluidic Paper-Based Analysis Devices. *Biosens. Bioelectron.* **2012**, *35* (1), 363–368.
- (51) Yu, C.; Lin, C.; Liu, C.; Cheng, T.; Tseng, W. Synthesis of Poly(Diallyldimethylammonium Chloride)-Coated Fe₃O₄ Nanoparticles for Colorimetric Sensing of Glucose and Selective Extraction of Thiol. *Biosens. Bioelectron.* **2010**, *26* (2), 913–917.
- (52) Li, R.; Zhen, M.; Guan, M.; Chen, D.; Zhang, G.; Ge, J.; Gong, P.; Wang, C.; Shu, C. A Novel Glucose Colorimetric Sensor Based on Intrinsic Peroxidase-like Activity of C60-Carboxyfullerenes. *Biosens. Bioelectron.* **2013**, *47*, 502–507.
- (53) Su, L.; Qin, W.; Zhang, H.; Ur, Z.; Ren, C.; Ma, S. The Peroxidase/Catalase-like Activities of MFe₂O₄ (M = Mg , Ni , Cu) MNPs and Their Application in Colorimetric Biosensing of Glucose. *Biosens. Bioelectron.* **2015**, *63*, 384–391.
- (54) Liu, Q.; Yang, Y.; Li, H.; Zhu, R.; Shao, Q.; Yang, S.; Xu, J. NiO Nanoparticles Modified with 5,10,15,20-Tetrakis(4-Carboxyl Pheyl)-Porphyrin: Promising Peroxidase Mimetics for H₂O₂ and Glucose Detection. *Biosens. Bioelectron.* **2015**, *64*, 147–153.
- (55) Liu, Q.; Yang, Y.; Lv, X.; Ding, Y.; Zhang, Y.; Jing, J. Chemical One-Step Synthesis of Uniform Nanoparticles of Porphyrin Functionalized Ceria with Promising Peroxidase Mimetics for H₂O₂ and Glucose Colorimetric Detection. *Sensors Actuators B Chem.* **2017**, *240*, 726–734.
- (56) Jin, L.; Meng, Z.; Zhang, Y.; Cai, S.; Zhang, Z.; Li, C.; Shang, L. Ultrasmall Pt Nanoclusters as Robust Peroxidase Mimics for Colorimetric Detection of Glucose in Human Serum. *Appl. Mater. Interfaces* **2017**, *9*, 10027–10033.

10. Bibliography

- (57) Zhang, H.; Liang, X.; Han, L.; Li, F. “Non-Naked” Gold with Glucose Oxidase-Like Activity: A Nanozyme for Tandem Catalysis. *Small* **2018**, *14*, 1–8.
- (58) Wang, Q.; Zhang, L.; Shang, C.; Zhang, Z.; Dong, S. Triple-Enzyme Mimetic Activity of Nickel–Palladium Hollow Nanoparticles and Their Application in Colorimetric Biosensing of Glucose. *Chem. Commun.* **2016**, *52*, 5410–5413.
- (59) Su, L.; Feng, J.; Zhou, X.; Ren, C.; Li, H.; Chen, X. Colorimetric Detection of Urine Glucose Based ZnFe₂O₄ Magnetic Nanoparticles. *Anal. Chem.* **2012**, *84*, 5753–5758.
- (60) Fl, E.; Gabriel, M.; Garcia, P. T.; Lopes, F. M.; Karlos, W.; Coltro, T. Paper-Based Colorimetric Biosensor for Tear Glucose Measurements. *Micromachines* **2017**, *8*, 1–9.
- (61) Socorro-Lerános, A. B.; Santano, D.; Del Villar, I.; Matias, I. R. Trends in the Design of Wavelength-Based Optical Fibre Biosensors (2008–2018). *Biosens. Bioelectron. X* **2019**, *1* (February), 100015.
- (62) Vaiano, P.; Carotenuto, B.; Pisco, M.; Ricciardi, A.; Quero, G.; Consales, M.; Crescitelli, A.; Esposito, E.; Cusano, A. Lab on Fiber Technology for Biological Sensing Applications. *Laser Photonics Rev.* **2016**, *10*, 922–961.
- (63) Tierney, S.; Hasle Falch, B. M.; Hjelme, D. R.; Stokke, B. T. Determination of Glucose Levels Using a Functionalized Hydrogel-Optical Fiber Biosensor: Toward Continuous Monitoring of Blood Glucose in Vivo. *Anal. Chem.* **2009**, *81*, 3630–3636.
- (64) Wang, X.; Li, Q.; Guan, Y.; Zhang, Y. Glucose Oxidase-Incorporated Hydrogel Thin Film for Fast Optical Glucose Detecting under Physiological Conditions. *Mater. Today Chem.* **2016**, *1–2*, 7–14.
- (65) Srivastava, S. K.; Arora, V.; Sapra, S.; Gupta, B. D. Localized Surface Plasmon Resonance-Based Fiber Optic U-Shaped Biosensor for the Detection of Blood Glucose. *Plasmonics* **2012**, *7*, 261–268.
- (66) Shukla, S. K.; Demir, M. M.; Govender, P. P.; Tiwari, A.; Shukla, S. K. Optical Fibre Based Non-Enzymatic Glucose Sensing over Cu²⁺-Doped Polyaniline Hybrid Matrix. *Sensors Actuators, B Chem.* **2017**, *242*, 522–528.
- (67) Jiang, B.; Zhou, K.; Wang, C.; Sun, Q.; Yin, G.; Tai, Z.; Wilson, K.; Zhao, J.; Zhang, L. Label-Free Glucose Biosensor Based on Enzymatic Graphene Oxide-Functionalized Tilted Fiber Grating. *Sensors Actuators, B Chem.* **2018**, *254*, 1033–1039.
- (68) Sassolas, A.; Blum, L. J.; Leca-Bouvier, B. D. Immobilization Strategies to Develop Enzymatic Biosensors. *Biotechnol. Adv.* **2012**, *30* (3), 489–511.
- (69) Vert, M.; Doi, Y.; Hellwich, K. H.; Hess, M.; Hodge, P.; Kubisa, P.; Rinaudo, M.; Schué, F. Terminology for Biorelated Polymers and Applications (IUPAC Recommendations 2012). *Pure Appl. Chem.* **2012**, *84* (2), 377–410.
- (70) Palanisamy, S.; Ramaraj, S. K.; Chen, S. M.; Yang, T. C. K.; Pan, Y. F.; Chen, T. W.; Velusamy, V.; Selvam, S. A Novel Laccase Biosensor Based on Laccase Immobilized Graphene–Cellulose Microfiber Composite Modified Screen-Printed Carbon Electrode for Sensitive Determination of Catechol. *Sci. Rep.* **2017**, *7* (1), 1–12.
- (71) Weishaupt, R.; Siqueira, G.; Schubert, M.; Kämpf, M. M.; Zimmermann, T.; Maniura-Weber, K.; Faccio, G. A Protein-Nanocellulose Paper for Sensing Copper Ions at the Nano- to Micromolar Level. *Adv. Funct. Mater.* **2017**, *27* (4).
- (72) Yang, M. H.; Jeong, S. W.; Chang, S. J.; Kim, K. H.; Jang, M.; Kim, C. H.; Bae, N. H.; Sim, G. S.; Kang, T.; Lee, S. J.; et al. Flexible and Disposable Sensing Platforms Based on Newspaper. *ACS Appl. Mater. Interfaces* **2016**, *8* (51), 34978–34984.
- (73) Yang, Y.; Ozsoz, M.; Liu, G. Gold Nanocage-Based Lateral Flow Immunoassay for Immunoglobulin G. *Microchim. Acta* **2017**, *184* (7), 2023–2029.
- (74) Dai, G.; Hu, J.; Zhao, X.; Wang, P. A Colorimetric Paper Sensor for Lactate Assay Using a Cellulose-Binding Recombinant Enzyme. *Sensors Actuators, B Chem.* **2017**, *238*, 138–144.

- (75) Li, D.; Frey, M. W.; Baeumner, A. J. Electrospun Polylactic Acid Nanofiber Membranes as Substrates for Biosensor Assemblies. *J. Memb. Sci.* **2006**, *279* (1–2), 354–363.
- (76) Sun, C.; Niu, Y.; Yang, X.; Liu, M.; Yang, X.; Huang, X.; Zhao, W. Preparation of Hemocompatible Poly(Lactic-Co-Glycolic Acid)-F127 Nanospheres and Their Application to Biosensor for Analysis of Whole Blood. *J. Nanosci. Nanotechnol.* **2015**, *15* (1), 105–111.
- (77) Pandey, C. M.; Sharma, A.; Sumana, G.; Tiwari, I.; Malhotra, B. D. Cationic Poly(Lactic-Co-Glycolic Acid) Iron Oxide Microspheres for Nucleic Acid Detection. *Nanoscale* **2013**, *5* (9), 3800–3807.
- (78) Nanda, S. S.; An, S. S. A.; Yi, D. K. Measurement of Creatinine in Human Plasma Using a Functional Porous Polymer Structure Sensing Motif. *Int. J. Nanomedicine* **2015**, *10*, 93–99.
- (79) Shan, C.; Yang, H.; Han, D.; Zhang, Q.; Ivaska, A.; Niu, L. Graphene/AuNPs/Chitosan Nanocomposites Film for Glucose Biosensing. *Biosens. Bioelectron.* **2010**, *25* (5), 1070–1074.
- (80) Zhang, M.; Smith, A.; Gorski, W. Carbon Nanotube-Chitosan System for Electrochemical Sensing Based on Dehydrogenase Enzymes. *Anal. Chem.* **2004**, *76* (17), 5045–5050.
- (81) Kang, X.; Wang, J.; Wu, H.; Aksay, I. A.; Liu, J.; Lin, Y. Glucose Oxidase-Graphene-Chitosan Modified Electrode for Direct Electrochemistry and Glucose Sensing. *Biosens. Bioelectron.* **2009**, *25* (4), 901–905.
- (82) Shan, C.; Yang, H.; Han, D.; Zhang, Q.; Ivaska, A.; Niu, L. Electrochemical Determination of NADH and Ethanol Based on Ionic Liquid-Functionalized Graphene. *Biosens. Bioelectron.* **2010**, *25* (6), 1504–1508.
- (83) Tan, X.; Li, M.; Cai, P.; Luo, L.; Zou, X. An Amperometric Cholesterol Biosensor Based on Multiwalled Carbon Nanotubes and Organically Modified Sol-Gel/Chitosan Hybrid Composite Film. *Anal. Biochem.* **2005**, *337* (1), 111–120.
- (84) Li, J.; Liu, Q.; Liu, Y.; Liu, S.; Yao, S. DNA Biosensor Based on Chitosan Film Doped with Carbon Nanotubes. *Anal. Biochem.* **2005**, *346* (1), 107–114.
- (85) Wu, W.; Shen, J.; Banerjee, P.; Zhou, S. Chitosan-Based Responsive Hybrid Nanogels for Integration of Optical PH-Sensing, Tumor Cell Imaging and Controlled Drug Delivery. *Biomaterials* **2010**, *31* (32), 8371–8381.
- (86) Sun, X.; Wang, X. Acetylcholinesterase Biosensor Based on Prussian Blue-Modified Electrode for Detecting Organophosphorous Pesticides. *Biosens. Bioelectron.* **2010**, *25* (12), 2611–2614.
- (87) Kaushik, A.; Solanki, P. R.; Ansari, A. A.; Sumana, G.; Ahmad, S.; Malhotra, B. D. Iron Oxide-Chitosan Nanobiocomposite for Urea Sensor. *Sensors Actuators, B Chem.* **2009**, *138* (2), 572–580.
- (88) Guo, L.; Li, Z.; Chen, H.; Wu, Y.; Chen, L.; Song, Z.; Lin, T. Colorimetric Biosensor for the Assay of Paraoxon in Environmental Water Samples Based on the Iodine-Starch Color Reaction. *Anal. Chim. Acta* **2017**, *967*, 59–63.
- (89) Zhang, R.; Jin, Z.; Zhang, C.; Yang, R.; Sun, M.; Wong, C. P. An Ultrasensitive Biosensor Based on Electroactive Nanoparticles Self-Assembled from 3-Thiophenecarboxylic Acid-Modified Starch. *Colloid Polym. Sci.* **2018**, *296* (8), 1365–1372.
- (90) Vasileva, P.; Donkova, B.; Karadjova, I.; Dushkin, C. Synthesis of Starch-Stabilized Silver Nanoparticles and Their Application as a Surface Plasmon Resonance-Based Sensor of Hydrogen Peroxide. *Colloids Surfaces A Physicochem. Eng. Asp.* **2011**, *382* (1–3), 203–210.
- (91) Liu, X.; Pan, Z.; Dong, Z.; Lu, Y.; Sun, Q.; Wu, T.; Bao, N.; He, H.; Gu, H. Amperometric Oxygen Biosensor Based on Hemoglobin Encapsulated in Nanosized Grafted Starch Particles. *Microchim. Acta* **2016**, *183* (1), 353–359.
- (92) Matharu, Z.; Enomoto, J.; Revzin, A. Miniature Enzyme-Based Electrodes for Detection of Hydrogen Peroxide Release from Alcohol-Injured Hepatocytes. *Anal. Chem.* **2013**, *85* (2), 932–939.
- (93) Pallela, R.; Chandra, P.; Noh, H. B.; Shim, Y. B. An Amperometric Nanobiosensor Using a

10. Bibliography

- Biocompatible Conjugate for Early Detection of Metastatic Cancer Cells in Biological Fluid. *Biosens. Bioelectron.* **2016**, *85*, 883–890.
- (94) Jiang, D.; Ji, J.; an, lu; Sun, X.; Zhang, Y.; Zhang, G.; Tang, L. Mast Cell-Based Electrochemical Biosensor for Quantification of the Major Shrimp Allergen Pen a 1 (Tropomyosin). *Biosens. Bioelectron.* **2013**, *50*, 150–156.
- (95) Xia, S.; Zhu, P.; Pi, F.; Zhang, Y.; Li, Y.; Wang, J.; Sun, X. Development of a Simple and Convenient Cell-Based Electrochemical Biosensor for Evaluating the Individual and Combined Toxicity of DON, ZEN, and AFB1. *Biosens. Bioelectron.* **2017**, *97* (May), 345–351.
- (96) Liu, X.; Huang, R.; Su, R.; Qi, W.; Wang, L.; He, Z. Grafting Hyaluronic Acid onto Gold Surface to Achieve Low Protein Fouling in Surface Plasmon Resonance Biosensors. *ACS Appl. Mater. Interfaces* **2014**, *6* (15), 13034–13042.
- (97) Šefčovičová, J.; Filip, J.; Tomčík, P.; Gemeiner, P.; Bučko, M.; Magdolen, P.; Tkac, J. A Biopolymer-Based Carbon Nanotube Interface Integrated with a Redox Shuttle and a D-Sorbitol Dehydrogenase for Robust Monitoring of D-Sorbitol. *Microchim. Acta* **2011**, *175* (1–2), 21–30.
- (98) Lee, K. Y.; Mooney, D. J. Alginate: Properties and Biomedical Applications. *Prog. Polym. Sci.* **2012**, *37* (1), 106–126.
- (99) Clark, D. E.; Green, H. C. Alginic Acid and Process of Making Same, 1936.
- (100) Remminghorst, U.; Rehm, B. H. A. Bacterial Alginates: From Biosynthesis to Applications. *Biotechnol. Lett.* **2006**, *28* (21), 1701–1712.
- (101) Bruchet, M.; Melman, A. Fabrication of Patterned Calcium Cross-Linked Alginate Hydrogel Films and Coatings through Reductive Cation Exchange. *Carbohydr. Polym.* **2015**, *131*, 57–64.
- (102) Cheng, Y.; Luo, X.; Betz, J.; Payne, G. F.; Bentley, W. E.; Rubloff, G. W. Mechanism of Anodic Electrodeposition of Calcium Alginate. *Soft Matter* **2011**, *7* (12), 5677.
- (103) Maiti, S.; Singha, K.; Ray, S.; Dey, P.; Sa, B. Adipic Acid Dihydrazide Treated Partially Oxidized Alginate Beads for Sustained Oral Delivery of Flurbiprofen Oxidized Alginate Beads of Flurbiprofen S. Maiti et Al. *Pharm. Dev. Technol.* **2009**, *14* (5), 461–470.
- (104) Wiegand, C.; Heinze, T.; Hipler, U. C. Comparative in Vitro Study on Cytotoxicity, Antimicrobial Activity, and Binding Capacity for Pathophysiological Factors in Chronic Wounds of Alginate and Silver-Containing Alginate. *Wound Repair Regen.* **2009**, *17* (4), 511–521.
- (105) Kreeger, P. K.; Deck, J. W.; Woodruff, T. K.; Shea, L. D. The in Vitro Regulation of Ovarian Follicle Development Using Alginate-Extracellular Matrix Gels. *Biomaterials* **2006**, *27* (5), 714–723.
- (106) Hill, E.; Boontheekul, T.; Mooney, D. J. Regulating Activation of Transplanted Cells Controls Tissue Regeneration. *Proc. Natl. Acad. Sci. U. S. A.* **2006**, *103* (8), 2494–2499.
- (107) Chen, X.; Yan, H.; Shi, Z.; Feng, Y.; Li, J.; Lin, Q.; Wang, X.; Sun, W. A Novel Biosensor Based on Electro-Co-Deposition of Sodium Alginate-Fe₃O₄-Graphene Composite on the Carbon Ionic Liquid Electrode for the Direct Electrochemistry and Electrocatalysis of Myoglobin. *Polym. Bull.* **2017**, *74* (1), 75–90.
- (108) Buk, V.; Emregul, E.; Emregul, K. C. Alginate Copper Oxide Nano-Biocomposite as a Novel Material for Amperometric Glucose Biosensing. *Mater. Sci. Eng. C* **2017**, *74*, 307–314.
- (109) Ge, Q.; Ge, P.; Jiang, D.; Du, N.; Chen, J.; Yuan, L.; Yu, H.; Xu, X.; Wu, M.; Zhang, W.; et al. A Novel and Simple Cell-Based Electrochemical Biosensor for Evaluating the Antioxidant Capacity of Lactobacillus Plantarum Strains Isolated from Chinese Dry-Cured Ham. *Biosens. Bioelectron.* **2018**, *99* (June 2017), 555–563.
- (110) Lee, S. M.; Han, N.; Lee, R.; Choi, I. H.; Park, Y. B.; Shin, J. S.; Yoo, K. H. Real-Time Monitoring of 3D Cell Culture Using a 3D Capacitance Biosensor. *Biosens. Bioelectron.* **2016**, *77*, 56–61.
- (111) Biswas, A.; Bornhoeft, L. R.; Banerjee, S.; You, Y. H.; McShane, M. J. Composite Hydrogels Containing Bioactive Microreactors for Optical Enzymatic Lactate Sensing. *ACS Sensors* **2017**, *2*

- (11), 1584–1588.
- (112) Li, P.; Müller, M.; Chang, M. W.; Frettlöh, M.; Schönherr, H. Encapsulation of Autoinducer Sensing Reporter Bacteria in Reinforced Alginate-Based Microbeads. *ACS Appl. Mater. Interfaces* **2017**, *9* (27), 22321–22331.
- (113) Cevenini, L.; Lopreside, A.; Calabretta, M. M.; D’Elia, M.; Simoni, P.; Michelini, E.; Roda, A. A Novel Bioluminescent NanoLuc Yeast-Estrogen Screen Biosensor (NanoYES) with a Compact Wireless Camera for Effect-Based Detection of Endocrine-Disrupting Chemicals. *Anal. Bioanal. Chem.* **2018**, *410* (4), 1237–1246.
- (114) Gaddes, D.; Reeves, W. B.; Tadigadapa, S. Calorimetric Biosensing System for Quantification of Urinary Creatinine. *ACS Sensors* **2017**, *2* (6), 796–802.
- (115) Taura, J. R. S. Mechanism of Silk Processing in Insects and Spiders. *Nature* **2003**, *926* (2002), 1057–1061.
- (116) Murphy, A. R.; Kaplan, D. L. Biomedical Applications of Chemically-Modified Silk Fibroin. *J. Mater. Chem.* **2009**, *19* (36), 6443–6450.
- (117) Inoue, S.; Tanaka, K.; Arisaka, F.; Kimura, S.; Ohtomo, K.; Mizuno, S. Silk Fibroin of Bombyx Mori Is Secreted, Assembling a High Molecular Mass Elementary Unit Consisting of H-Chain, L-Chain, and P25, with a 6:6:1 Molar Ratio. *J. Biol. Chem.* **2000**, *275* (51), 40517–40528.
- (118) Zhou, C. Z.; Confalonieri, F.; Jacquet, M.; Perasso, R.; Li, Z. G.; Janin, J. Silk Fibroin: Structural Implications of a Remarkable Amino Acid Sequence. *Proteins Struct. Funct. Genet.* **2001**, *44* (2), 119–122.
- (119) Foo, C. W. P.; Bini, E.; Hensman, J.; Knight, D. P.; Lewis, R. V.; Kaplan, D. L. Role of PH and Charge on Silk Protein Assembly in Insects and Spiders. *Appl. Phys. A Mater. Sci. Process.* **2006**, *82* (2), 223–233.
- (120) Lu, S.; Wang, X.; Lv, Q.; Hu, X.; Uppal, N.; Kaplan, D. L. Stabilization of Enzymes in Silk Films. *Biomacromolecules* **2009**, *10* (5), 1032–1042.
- (121) Tao, H.; Brenckle, M. A.; Yang, M.; Zhang, J.; Liu, M.; Siebert, S. M.; Averitt, R. D.; Mannoor, M. S.; McAlpine, M. C.; Rogers, J. A.; et al. Silk-Based Conformal , Adhesive , Edible Food Sensors. **2012**, 1067–1072.
- (122) Amsden, B. J. J.; Domachuk, P.; Gopinath, A.; White, R. D.; Negro, L. D.; Kaplan, D. L.; Omenetto, F. G. Rapid Nanoimprinting of Silk Fibroin Films for Biophotonic Applications. **2010**, 1746–1749.
- (123) Park, J.; Lee, S.-G.; Marelli, B.; Lee, M.; Kim, T.; Oh, H.-K.; Jeon, H.; Omenetto, F. G.; Kim, S. Eco-Friendly Photolithography Using Water-Developable Pure Silk Fibroin. *RSC Adv.* **2016**, *6* (45), 39330–39334.
- (124) Burrs, S. L.; Vanegas, D. C.; Bhargava, M.; Mechulan, N.; Hendershot, P.; Yamaguchi, H.; Gomes, C.; McLamore, E. S. A Comparative Study of Graphene-Hydrogel Hybrid Bionanocomposites for Biosensing. *Analyst* **2015**, *140* (5), 1466–1476.
- (125) Pal, R. K.; Farghaly, A. A.; Wang, C.; Collinson, M. M.; Kundu, S. C.; Yadavalli, V. K. Conducting Polymer-Silk Biocomposites for Flexible and Biodegradable Electrochemical Sensors. *Biosens. Bioelectron.* **2016**, *81*, 294–302.
- (126) Yin, H.; Zhou, Y.; Xu, J.; Ai, S.; Cui, L.; Zhu, L. Amperometric Biosensor Based on Tyrosinase Immobilized onto Multiwalled Carbon Nanotubes-Cobalt Phthalocyanine-Silk Fibroin Film and Its Application to Determine Bisphenol A. *Anal. Chim. Acta* **2010**, *659* (1–2), 144–150.
- (127) Yin, H.; Ai, S.; Xu, J.; Shi, W.; Zhu, L. Amperometric Biosensor Based on Immobilized Acetylcholinesterase on Gold Nanoparticles and Silk Fibroin Modified Platinum Electrode for Detection of Methyl Paraoxon, Carbofuran and Phoxim. *J. Electroanal. Chem.* **2009**, *637* (1–2), 21–27.
- (128) Burke, K. A.; Brenckle, M. A.; Kaplan, D. L.; Omenetto, F. G. Evaluation of the Spectral Response of Functionalized Silk Inverse Opals as Colorimetric Immunosensors. *ACS Appl. Mater. Interfaces*

10. Bibliography

- 2016, 8 (25), 16218–16226.
- (129) Koh, L. D.; Cheng, Y.; Teng, C. P.; Khin, Y. W.; Loh, X. J.; Tee, S. Y.; Low, M.; Ye, E.; Yu, H. D.; Zhang, Y. W.; et al. Structures, Mechanical Properties and Applications of Silk Fibroin Materials. *Prog. Polym. Sci.* **2015**, 46 (November 2017), 86–110.
- (130) Kishimoto, Y.; Morikawa, H.; Yamanaka, S.; Tamada, Y. Electrospinning of Silk Fibroin from Aqueous Solution at Low Concentration. *Mater. Sci. Eng. C* **2017**, 73, 498–506.
- (131) Zhu, M.; Wang, K.; Mei, J.; Li, C.; Zhang, J.; Zheng, W.; An, D.; Xiao, N.; Zhao, Q.; Kong, D.; et al. Fabrication of Highly Interconnected Porous Silk Fibroin Scaffolds for Potential Use as Vascular Grafts. *Acta Biomater.* **2014**, 10 (5), 2014–2023.
- (132) Bosio, V. E.; Brown, J.; Rodriguez, M. J.; Kaplan, D. L. Biodegradable Porous Silk Microtubes for Tissue Vascularization. *J. Mater. Chem. B* **2017**, 5 (6), 1227–1235.
- (133) Eng, J. T.; Med, R.; Mueller, D.; Tascher, G.; Ursula, M.; Knobloch, D.; Nuessler, A. K. In-Depth Physiological Characterization of Primary Human Hepatocytes in a 3D Hollow-Fiber Bioreactor. *J. Tissue Eng. Regen. Med.* **2011**, No. January, 349–355.
- (134) Luo, K.; Yang, Y.; Shao, Z. Physically Crosslinked Biocompatible Silk-Fibroin-Based Hydrogels with High Mechanical Performance. *Adv. Funct. Mater.* **2016**, 26 (6), 872–880.
- (135) Guo, J. Smartphone-Powered Electrochemical Dongle for Point-of-Care Monitoring of Blood β -Ketone. *Anal. Chem.* **2017**, 89 (17), 8609–8613.
- (136) Fu, Y.; Guo, J. Blood Cholesterol Monitoring with Smartphone as Miniaturized Electrochemical Analyzer for Cardiovascular Disease Prevention. *IEEE Trans. Biomed. Circuits Syst.* **2018**, 12 (4), 784–790.
- (137) Min, J.; Nothing, M.; Coble, B.; Zheng, H.; Park, J.; Im, H.; Weber, G. F.; Castro, C. M.; Swirski, F. K.; Weissleder, R.; et al. Integrated Biosensor for Rapid and Point-of-Care Sepsis Diagnosis. *ACS Nano* **2018**, 12 (4), 3378–3384.
- (138) Drey, L. L.; Graber, M. C.; Bieschke, J. Counting Unstained, Confluent Cells by Modified Bright-Field Microscopy. *Biotechniques* **2013**, 55 (1), 28–33.
- (139) Kanakasabapathy, M. K.; Pandya, H. J.; Draz, M. S.; Chug, M. K.; Sadasivam, M.; Kumar, S.; Etemad, B.; Yogesh, V.; Safavieh, M.; Asghar, W.; et al. Rapid, Label-Free CD4 Testing Using a Smartphone Compatible Device. *Lab Chip* **2017**, 17 (17), 2910–2919.
- (140) Kanakasabapathy, M. K.; Sadasivam, M.; Singh, A.; Preston, C.; Thirumalaraju, P.; Venkataraman, M.; Bormann, C. L.; Draz, M. S.; Petrozza, J. C.; Shafiee, H. An Automated Smartphone-Based Diagnostic Assay for Point-of-Care Semen Analysis. *Sci. Transl. Med.* **2017**, 9 (382), 1–14.
- (141) McCracken, K. E.; Yoon, J. Y. Recent Approaches for Optical Smartphone Sensing in Resource-Limited Settings: A Brief Review. *Anal. Methods* **2016**, 8 (36), 6591–6601.
- (142) Brangel, P.; Sobarzo, A.; Parolo, C.; Miller, B. S.; Howes, P. D.; Gelkop, S.; Lutwama, J. J.; Dye, J. M.; McKendry, R. A.; Lobel, L.; et al. A Serological Point-of-Care Test for the Detection of IgG Antibodies against Ebola Virus in Human Survivors. *ACS Nano* **2018**, 12 (1), 63–73.
- (143) Kim, S. C.; Jalal, U. M.; Im, S. B.; Ko, S.; Shim, J. S. A Smartphone-Based Optical Platform for Colorimetric Analysis of Microfluidic Device. *Sensors Actuators, B Chem.* **2017**, 239, 52–59.
- (144) De Cortina, S. H.; Bristow, C. C.; Humphries, R.; Vargas, S. K.; Konda, K. A.; Caceres, C. F.; Klausner, J. D. Laboratory Evaluation of a Smartphone-Based Electronic Reader of Rapid Dual Point-of-Care Tests for Antibodies to Human Immunodeficiency Virus and *Treponema Pallidum* Infections. *Sex. Transm. Dis.* **2017**, 44 (7), 412–416.
- (145) Lee, N.; Wang, C.; Park, J. User-Friendly Point-of-Care Detection of Influenza A (H1N1) Virus Using Light Guide in Three-Dimensional Photonic Crystal. *RSC Adv.* **2018**, 8 (41), 22991–22997.
- (146) Yetisen, A. K.; Martinez-Hurtado, J. L.; Garcia-Melendrez, A.; Da Cruz Vasconcellos, F.; Lowe, C. R. A Smartphone Algorithm with Inter-Phone Repeatability for the Analysis of Colorimetric Tests. *Sensors Actuators, B Chem.* **2014**, 196, 156–160.

- (147) Chun, H. J.; Park, Y. M.; Han, Y. D.; Jang, Y. H.; Yoon, H. C. Paper-Based Glucose Biosensing System Utilizing a Smartphone as a Signal Reader. *Biochip J.* **2014**, *8* (3), 218–226.
- (148) Hong, J. Il; Chang, B. Y. Development of the Smartphone-Based Colorimetry for Multi-Analyte Sensing Arrays. *Lab Chip* **2014**, *14* (10), 1725–1732.
- (149) Choi, S.; Kim, S. K.; Lee, G. J.; Park, H. K. Paper-Based 3D Microfluidic Device for Multiple Bioassays. *Sensors Actuators, B Chem.* **2015**, *219*, 245–250.
- (150) Wang, X.; Li, F.; Cai, Z.; Liu, K.; Li, J.; Zhang, B.; He, J. Sensitive Colorimetric Assay for Uric Acid and Glucose Detection Based on Multilayer-Modified Paper with Smartphone as Signal Readout. *Anal. Bioanal. Chem.* **2018**, *410* (10), 2647–2655.
- (151) Zhang, H.; Smith, E.; Zhang, W.; Zhou, A. Inkjet Printed Microfluidic Paper-Based Analytical Device (MPAD) for Glucose Colorimetric Detection in Artificial Urine. *Biomed. Microdevices* **2019**, *21* (3).
- (152) Koh, A.; Kang, D.; Xue, Y.; Lee, S.; Pielak, R. M.; Kim, J.; Hwang, T.; Min, S.; Banks, A.; Bastien, P.; et al. A Soft, Wearable Microfluidic Device for the Capture, Storage, and Colorimetric Sensing of Sweat. *Sci. Transl. Med.* **2016**, *8* (366), 1–14.
- (153) Sun, K.; Yang, Y.; Zhou, H.; Yin, S.; Qin, W.; Yu, J.; Chiu, D. T.; Yuan, Z.; Zhang, X.; Wu, C. Ultrabright Polymer-Dot Transducer Enabled Wireless Glucose Monitoring via a Smartphone. *ACS Nano* **2018**, *12* (6), 5176–5184.
- (154) Yetisen, A. K.; Moreddu, R.; Seifi, S.; Jiang, N.; Vega, K.; Dong, X.; Dong, J.; Butt, H.; Jakobi, M.; Elsner, M.; et al. Dermal Tattoo Biosensors for Colorimetric Metabolite Detection. *Angew. Chemie Int. Ed.* **2019**, *58* (31), 10506–10513.
- (155) Gao, W.; Emaminejad, S.; Nyein, H. Y. Y.; Challa, S.; Chen, K.; Peck, A.; Fahad, H. M.; Ota, H.; Shiraki, H.; Kiriya, D.; et al. Fully Integrated Wearable Sensor Arrays for Multiplexed in Situ Perspiration Analysis. *Nature* **2016**, *529* (7587), 509–514.
- (156) Ji, D.; Liu, L.; Li, S.; Chen, C.; Lu, Y.; Wu, J.; Liu, Q. Smartphone-Based Cyclic Voltammetry System with Graphene Modified Screen Printed Electrodes for Glucose Detection. *Biosens. Bioelectron.* **2017**, *98* (March), 449–456.
- (157) Lin, C. Oxidation (of Silicon). In *Encyclopedia of Microfluidics and Nanofluidics*; 2008; pp 1513–1591.
- (158) Lam, M. Photoresist of Photolithography https://commons.wikimedia.org/wiki/File:Photoresist_of_Photolithography.png.
- (159) Lokhande, A. C.; Chalapathy, R. B. V.; He, M.; Jo, E.; Gang, M.; Pawar, S. A.; Lokhande, C. D.; Kim, J. H. Development of Cu₂SnS₃ (CTS) Thin Film Solar Cells by Physical Techniques: A Status Review. *Sol. Energy Mater. Sol. Cells* **2016**, *153*, 84–107.
- (160) Perry, B. H.; Gopinath, A.; Kaplan, D. L.; Negro, L. D.; Omenetto, G. Nano- and Micropatterning of Optically Transparent, Mechanically Robust, Biocompatible Silk Fibroin Films **. *Adv. Mater.* **2008**, *20*, 3070–3072.
- (161) Kurland, N. E.; Dey, T.; Kundu, S. C.; Yadavalli, V. K. Precise Patterning of Silk Microstructures Using Photolithography. *Adv. Mater.* **2013**, *25* (43), 6207–6212.
- (162) Kim, S.; Marelli, B.; Brenckle, M. A.; Mitropoulos, A. N.; Gil, E. S.; Tsioris, K.; Tao, H.; Kaplan, D. L.; Omenetto, F. G. All-Water-Based Electron-Beam Lithography Using Silk as a Resist. *Nat. Nanotechnol.* **2014**, *9* (4), 306–310.
- (163) Guirado, G.; Coudret, C.; Hliwa, M.; Launay, J. P. Understanding Electrochromic Processes Initiated by Dithienylcyclopentene Cation-Radicals. *J. Phys. Chem. B* **2005**, *109* (37), 17445–17459.
- (164) Guirado, G.; Coudret, C.; Launay, J. P. Electrochemical Remote Control for Dithienylethene-Ferrocene Switches. *J. Phys. Chem. C* **2007**, *111* (6), 2770–2776.
- (165) Bard, A. J.; Faulkner, L. R. *Electrochemical Methods. Fundamentals and Applications*; 2001; Vol.

10. Bibliography

- 8.
- (166) Elgrishi, N.; Rountree, K. J.; McCarthy, B. D.; Rountree, E. S.; Eisenhart, T. T.; Dempsey, J. L. A Practical Beginner's Guide to Cyclic Voltammetry. *J. Chem. Educ.* **2018**, *95* (2), 197–206.
- (167) Owen, T. *Fundamentals of UV-Visible Spectroscopy*; 1996.
- (168) Orozco, J.; Suárez, G.; Fernández-Sánchez, C.; McNeil, C.; Jiménez-Jorquera, C. Characterization of Ultramicroelectrode Arrays Combining Electrochemical Techniques and Optical Microscopy Imaging. *Electrochim. Acta* **2007**, *53* (2), 729–736.
- (169) Zarkadas, G. M.; Stergiou, A.; Papanastasiou, G. Influence of Tartaric Acid on the Electrodeposition of Silver from Binary Water + Dioxane AgNO₃ solutions. *J. Appl. Electrochem.* **2001**, *31* (11), 1251–1259.
- (170) Aymerich, J.; Márquez, A.; Terés, L.; Muñoz-Berbel, X.; Jiménez, C.; Domínguez, C.; Serra-Graells, F.; Dei, M. Cost-Effective Smartphone-Based Reconfigurable Electrochemical Instrument for Alcohol Determination in Whole Blood Samples. *Biosens. Bioelectron.* **2018**, *117* (June), 736–742.
- (171) Zhang, Y.; Tsitkov, S.; Hess, H. Proximity Does Not Contribute to Activity Enhancement in the Glucose Oxidase–Horseradish Peroxidase Cascade. *Nat. Commun.* **2016**, *7*, 13982.
- (172) Vashist, S. K.; Lippa, P. B.; Yeo, L. Y.; Ozcan, A.; Luong, J. H. T. Emerging Technologies for Next-Generation Point-of-Care Testing. *Trends Biotechnol.* **2015**, *33* (11), 692–705.
- (173) Bahadir, E. B.; Sezgintürk, M. K. Applications of Commercial Biosensors in Clinical, Food, Environmental, and Biothreat/Bio warfare Analyses. *Anal. Biochem.* **2015**, *478*, 107–120.
- (174) Desmet, C.; Marquette, C. A.; Blum, L. J.; Doumouche, B. Paper Electrodes for Bioelectrochemistry: Biosensors and Biofuel Cells. *Biosens. Bioelectron.* **2015**, *76*, 145–163.
- (175) Huysal, K.; Budak, Y. U.; Demirci, H.; Önelge, M. Evaluation of CareSens POCT Devices for Glucose Testing in the Routine Hospital Setting. *J. Clin. Diagnostic Res.* **2015**, *9* (10), BC04–BC07.
- (176) Johnson, R. N.; Baker, J. R. Error Detection and Measurement in Glucose Monitors. *Clin. Chim. Acta* **2001**, *307* (1–2), 61–67.
- (177) Tonyushkina, K.; Nichols, J. H. Glucose Meters: A Review of Technical Challenges to Obtaining Accurate Results. *J. Diabetes Sci. Technol.* **2009**, *3* (4), 971–980.
- (178) Bamberg Kathleen, MacKenzie Melissa Moore, Joanna Olchesky, Sarah, R. S. Effect of Adverse Storage Conditions on Performance of Glucometer Test Strips. *Clin. Lab. Sci.* **2005**, *18* (4), 203.
- (179) Sassolas, A.; Blum, L. J.; Leca-Bouvier, B. D. Immobilization Strategies to Develop Enzymatic Biosensors. *Biotechnol. Adv.* **2012**, *30* (3), 489–511.
- (180) Mørch, Y. a.; Donati, I.; Strand, B. L. Effect of Ca²⁺, Ba²⁺, and Sr²⁺ on Alginate Microbeads. *Biomacromolecules* **2006**, *7* (5), 1471–1480.
- (181) Kuo, C. K.; Ma, P. X. Ionically Crosslinked Alginate Hydrogels as Scaffolds for Tissue Engineering: Part 1. Structure, Gelation Rate and Mechanical Properties. *Biomaterials* **2001**, *22* (6), 511–521.
- (182) Abu-rabeah, K.; Polyak, B.; Ionescu, R. E.; Cosnier, S.; Marks, R. S.; Abu-rabeah, K.; Polyak, B.; Ionescu, R. E.; Cosnier, S. Synthesis and Characterization of a Pyrrole – Alginate Conjugate and Its Application in a Biosensor Construction Synthesis and Characterization of a Pyrrole - Alginate Conjugate and Its Application in a Biosensor Construction. **2005**, 3313–3318.
- (183) Liu, C.; Guo, X.; Cui, H.; Yuan, R. An Amperometric Biosensor Fabricated from Electro-Co-Deposition of Sodium Alginate and Horseradish Peroxidase. *J. Mol. Catal. B Enzym.* **2009**, *60* (3–4), 151–156.
- (184) An, E. H.; Xia, L. I.; Ai, J. C.; Ui, H. C.; Hang, X. Z. Development of Highly Sensitive Amperometric Biosensor for Glucose Using Carbon Nanosphere / Sodium Alginate Composite

- Matrix for Enzyme Immobilization. *Anal. Sci.* **2014**, *30* (September).
- (185) Betz, J. F.; Cheng, Y.; Tsao, C.-Y.; Zargar, A.; Wu, H.-C.; Luo, X.; Payne, G. F.; Bentley, W. E.; Rubloff, G. W. Optically Clear Alginate Hydrogels for Spatially Controlled Cell Entrapment and Culture at Microfluidic Electrode Surfaces. *Lab Chip* **2013**, *13* (10), 1854–1858.
- (186) Cheng, Y.; Luo, X.; Tsao, C.-Y.; Wu, H.-C.; Betz, J.; Payne, G. F.; Bentley, W. E.; Rubloff, G. W. Biocompatible Multi-Address 3D Cell Assembly in Microfluidic Devices Using Spatially Programmable Gel Formation. *Lab Chip* **2011**, *11* (14), 2316–2318.
- (187) Hunt, N. C.; Grover, L. M. Cell Encapsulation Using Biopolymer Gels for Regenerative Medicine. *Biotechnol. Lett.* **2010**, *32* (6), 733–742.
- (188) Perullini, M.; Calcabrini, M.; Jobbágy, M.; Bilmes, S. a. Alginate/Porous Silica Matrices for the Encapsulation of Living Organisms: Tunable Properties for Biosensors, Modular Bioreactors, and Bioremediation Devices. *Mesoporous Biomater.* **2015**, *2* (1), 3–12.
- (189) Rondeau, A.; Larsson, N.; Boujtita, M.; Gorton, L.; El Murr, N. The Synergetic Effect of Redox Mediators and Peroxidase in a Bionzymatic Biosensor for Glucose Assays in FIA. *Analisis* **1999**, *27* (7), 649–656.
- (190) Wisniewski, N.; Reichert, M. Methods for Reducing Biosensor Membrane Biofouling. *Colloids Surfaces B Biointerfaces* **2000**, *18* (3–4), 197–219.
- (191) Krainer, F. W.; Glieder, A. An Updated View on Horseradish Peroxidases: Recombinant Production and Biotechnological Applications. *Appl. Microbiol. Biotechnol.* **2015**, *99* (4), 1611–1625.
- (192) Ferri, T. A Glucose Biosensor Based on Electro-Enzyme Catalyzed Oxidation of Glucose Using a HRP-GOD Layered Assembly. *Electroanalysis* **2001**, *13* (14), 1198–1202.
- (193) Silverstein, T. P.; Goodney, D. E. Enzyme-Linked Biosensors: Michaelis-Menten Kinetics Need Not Apply. *J. Chem. Educ.* **2010**, *87* (9), 905–907.
- (194) Dumitraşcu, L.; Stănciuc, N.; Bahrim, G. E.; Ciumac, A.; Aprodu, I. PH and Heat-Dependent Behaviour of Glucose Oxidase down to Single Molecule Level by Combined Fluorescence Spectroscopy and Molecular Modelling. *J. Sci. Food Agric.* **2016**, *96* (6), 1906–1914.
- (195) Gubala, V.; Harris, L. F.; Ricco, A. J.; Tan, M. X.; Williams, D. E. Point of Care Diagnostics: Status and Future. *Anal. Chem.* **2012**, *84* (2), 487–515.
- (196) Hu, J.; Wang, S. Q.; Wang, L.; Li, F.; Pingguan-Murphy, B.; Lu, T. J.; Xu, F. Advances in Paper-Based Point-of-Care Diagnostics. *Biosens. Bioelectron.* **2014**, *54*, 585–597.
- (197) Gervais, L.; De Rooij, N.; Delamarche, E. Microfluidic Chips for Point-of-Care Immunodiagnosics. *Adv. Mater.* **2011**, *23* (24).
- (198) Nayak, S.; Blumenfeld, N. R.; Laksanasopin, T.; Sia, S. K. Point-of-Care Diagnostics: Recent Developments in a Connected Age. *Anal. Chem.* **2017**, *89* (1), 102–123.
- (199) Yoo, E. H.; Lee, S. Y. Glucose Biosensors: An Overview of Use in Clinical Practice. *Sensors* **2010**, *10* (5), 4558–4576.
- (200) Lu, S.; Yu, T.; Wang, Y.; Liang, L.-G.; Chen, Y.; Xu, F.; Wang, S. Nanomaterial-Based Biosensors for Measurement of Lipids and Lipoproteins towards Point-of-Care of Cardiovascular Disease. *Analyst* **2017**, No. Idl, 3309–3321.
- (201) Hirst, J. A.; McLellan, J. H.; Price, C. P.; English, E.; Feakins, B. G.; Stevens, R. J.; Farmer, A. J. Performance of Point-of-Care HbA1c Test Devices: Implications for Use in Clinical Practice - A Systematic Review and Meta-Analysis. *Clin. Chem. Lab. Med.* **2017**, *55* (2), 167–180.
- (202) Khuroo, M. S.; Khuroo, N. S.; Khuroo, M. S. Diagnostic Accuracy of Point-of-Care Tests for Hepatitis C Virus Infection: A Systematic Review and Meta-Analysis. *PLoS One* **2015**, *10* (3), 1–22.
- (203) Shafiee, H.; Wang, S.; Inci, F.; Toy, M.; Henrich, T. J.; Kuritzkes, D. R.; Demirci, U. Emerging

10. Bibliography

- Technologies for Point-of-Care Management of HIV Infection. *Annu. Rev. Med.* **2015**, *66* (1), 387–405.
- (204) Tuttle, R.; Weick, A.; Schwarz, W. S.; Chen, X.; Obermeier, P.; Seeber, L.; Tief, F.; Muehlhans, S.; Karsch, K.; Peiser, C.; et al. Evaluation of Novel Second-Generation RSV and Influenza Rapid Tests at the Point of Care. *Diagn. Microbiol. Infect. Dis.* **2015**, *81* (3), 171–176.
- (205) Lin, C.-C.; Tseng, C.-C.; Chuang, T.-K.; Lee, D.-S.; Lee, G.-B. Urine Analysis in Microfluidic Devices. *Analyst* **2011**, *136* (13), 2669.
- (206) Sireci, A. N. Hematology Testing in Urgent Care and Resource-Poor Settings. An Overview of Point of Care and Satellite Testing. *Clin. Lab. Med.* **2015**, *35* (1), 197–207.
- (207) Lewis, J. M.; Heineck, D. P.; Heller, M. J. Detecting Cancer Biomarkers in Blood: Challenges for New Molecular Diagnostic and Point-of-Care Tests Using Cell-Free Nucleic Acids. *Expert Rev. Mol. Diagn.* **2015**, *15* (9), 1187–1200.
- (208) Shadfán, B. H.; Simmons, A. R.; Simmons, G. W.; Ho, A.; Wong, J.; Lu, K. H.; Bast, R. C.; McDevitt, J. T. A Multiplexable, Microfluidic Platform for the Rapid Quantitation of a Biomarker Panel for Early Ovarian Cancer Detection at the Point-of-Care. *Cancer Prev. Res.* **2015**, *8* (1), 37–48.
- (209) Mohammed, S. I.; Ren, W.; Flowers, L.; Rajwa, B.; Chibweshá, C. J.; Parham, G. P.; Irudayaraj, J. M. K. Point-of-Care Test for Cervical Cancer in LMICs. *Oncotarget* **2016**, *7* (14), 18787–18797.
- (210) Majors, C. E.; Smith, C. A.; Natoli, M. E.; Kundrod, K. A.; Richards-Kortum, R. Point-of-Care Diagnostics to Improve Maternal and Neonatal Health in Low-Resource Settings. *Lab Chip* **2017**, *17* (20), 3351–3387.
- (211) Perry, D. J.; Fitzmaurice, D. A.; Kitchen, S.; MacKie, I. J.; Mallett, S. Point-of-Care Testing in Haemostasis. *Br. J. Haematol.* **2010**, *150* (5), 501–514.
- (212) Mahato, K.; Maurya, P. K.; Chandra, P. Fundamentals and Commercial Aspects of Nanobiosensors in Point-of-Care Clinical Diagnostics. *3 Biotech* **2018**, *8* (3), 1–14.
- (213) Mahato, K.; Srivastava, A.; Chandra, P. Paper Based Diagnostics for Personalized Health Care: Emerging Technologies and Commercial Aspects. *Biosens. Bioelectron.* **2017**, *96* (April), 246–259.
- (214) Berhane, F.; Fite, a.; Daboul, N.; Al-Janabi, W.; Msallaty, Z.; Caruso, M.; Lewis, M. K.; Yi, Z.; Diamond, M. P.; Abou-Samra, a. B.; et al. I.27 Plasma Lactate Levels Increase during Hyperinsulinemic Euglycemic Clamp and Oral Glucose Tolerance Test. *Diabetes Res. Clin. Pract.* **2014**, *103*, S8.
- (215) Patterson, C. C.; Harjutsalo, V.; Rosenbauer, J.; Neu, A.; Cinek, O.; Skrivarhaug, T.; Rami-Merhar, B.; Soltesz, G.; Svensson, J.; Parslow, R. C.; et al. Trends and Cyclical Variation in the Incidence of Childhood Type 1 Diabetes in 26 European Centres in the 25 Year Period 1989-2013: A Multicentre Prospective Registration Study. *Diabetologia* **2018**.
- (216) Brouwers, M. C. G. J.; Ham, J. C.; Wisse, E.; Misra, S.; Landewe, S.; Rosenthal, M.; Patel, D.; Oliver, N.; Bilo, H. J. G.; Murphy, E. Elevated Lactate Levels in Patients with Poorly Regulated Type 1 Diabetes and Glycogenic Hepatopathy: A New Feature of Mauriac Syndrome. *Diabetes Care* **2015**, *38* (2), e11-2.
- (217) Silva, D. Da; Zancan, P.; Coelho, W. S.; Gomez, L. S.; Sola-Penna, M. Metformin Reverses Hexokinase and 6-Phosphofructo-1-Kinase Inhibition in Skeletal Muscle, Liver and Adipose Tissues from Streptozotocin-Induced Diabetic Mouse. *Arch. Biochem. Biophys.* **2010**, *496* (1), 53–60.
- (218) Alfaras, I.; Mitchell, S. J.; Mora, H.; Lugo, D. R.; Warren, A.; Navas-Enamorado, I.; Hoffmann, V.; Hine, C.; Mitchell, J. R.; Le Couteur, D. G.; et al. Health Benefits of Late-Onset Metformin Treatment Every Other Week in Mice. *NPJ aging Mech. Dis.* **2017**, *3* (1), 16.
- (219) Dincer, C.; Bruch, R.; Kling, A.; Dittrich, P. S.; Urban, G. A. Multiplexed Point-of-Care Testing – XPOCT. *Trends Biotechnol.* **2017**, *35* (8), 728–742.

- (220) Díaz-González, M.; Muñoz-Berbel, X.; Jiménez-Jorquera, C.; Baldi, A.; Fernández-Sánchez, C. Diagnostics Using Multiplexed Electrochemical Readout Devices. *Electroanalysis* **2014**, *26* (6), 1154–1170.
- (221) Lee, J. H.; Seo, H. S.; Kwon, J. H.; Kim, H. T.; Kwon, K. C.; Sim, S. J.; Cha, Y. J.; Lee, J. Multiplex Diagnosis of Viral Infectious Diseases (AIDS, Hepatitis C, and Hepatitis A) Based on Point of Care Lateral Flow Assay Using Engineered Proteinticles. *Biosens. Bioelectron.* **2015**, *69*, 213–225.
- (222) Shen, F.; Du, W.; Davydova, E. K.; Karymov, M. A.; Pandey, J.; Ismagilov, R. F. Nanoliter Multiplex Pcr Arrays on a Slipchip. *Anal. Chem.* **2010**, *82* (11), 4606–4612.
- (223) Tian, T.; Wei, X.; Jia, S.; Zhang, R.; Li, J.; Zhu, Z.; Zhang, H.; Ma, Y.; Lin, Z.; Yang, C. J. Integration of Target Responsive Hydrogel with Cascaded Enzymatic Reactions and Microfluidic Paper-Based Analytic Devices (MPADs) for Point-of-Care Testing (POCT). *Biosens. Bioelectron.* **2016**, *77*, 537–542.
- (224) Wang, Y.; Wang, W.; Yu, L.; Tu, L.; Feng, Y.; Klein, T.; Wang, J. P. Giant Magnetoresistive-Based Biosensing Probe Station System for Multiplex Protein Assays. *Biosens. Bioelectron.* **2015**, *70*, 61–68.
- (225) Gu, H.; Zhou, T.; Yu, Y.; Yang, Y.; Shi, G. Size-Tunable Pt Nanoparticles Assembled on Functionalized Ordered Mesoporous Carbon for the Simultaneous and on-Line Detection of Glucose and L-Lactate in Brain Microdialysate. *Biosens. Bioelectron.* **2013**, *41*, 511–518.
- (226) Vasylieva, N.; Marinesco, S.; Barbier, D.; Sabac, A. Silicon/SU8 Multi-Electrode Micro-Needle for in Vivo Neurochemical Monitoring. *Biosens. Bioelectron.* **2015**, *72*, 148–155.
- (227) Li, X.; Zang, J.; Liu, Y.; Lu, Z.; Li, Q.; Li, C. M. Simultaneous Detection of Lactate and Glucose by Integrated Printed Circuit Board Based Array Sensing Chip. *Anal. Chim. Acta* **2013**, *771*, 102–107.
- (228) Márquez, A.; Jiménez-Jorquera, C.; Domínguez, C.; Muñoz-Berbel, X. Electrodepositable Alginate Membranes for Enzymatic Sensors: An Amperometric Glucose Biosensor for Whole Blood Analysis. *Biosens. Bioelectron.* **2017**, *97* (February), 136–142.
- (229) Márquez-Maqueda, A.; Ríos-Gallardo, J. M.; Vigués, N.; Pujol, F.; Díaz-González, M.; Mas, J.; Jiménez-Jorquera, C.; Domínguez, C.; Muñoz-Berbel, X. Enzymatic Biosensors Based on Electrodeposited Alginate Hydrogels. *Procedia Eng.* **2016**, *168*, 622–625.
- (230) Lee, S. M.; An, W. S. New Clinical Criteria for Septic Shock: Serum Lactate Level as New Emerging Vital Sign. *J. Thorac. Dis.* **2016**, *8* (7), 1388–1390.
- (231) Bjornstad, P.; Schäfer, M.; Truong, U.; Cree-Green, M.; Pyle, L.; Baumgartner, A.; Garcia Reyes, Y.; Maniatis, A.; Nayak, S.; Wadwa, R. P.; et al. Metformin Improves Insulin Sensitivity and Vascular Health in Youth With Type 1 Diabetes Mellitus. *Circulation* **2018**, *138* (25), 2895–2907.
- (232) Mora, J. I.; Vera A. Alvarez; Viviana P. Cyras; Analia Vázquez. Extraction of Cellulose and Preparation of Nanocellulose from Sisal Fibers. *Cellulose* **2008**, *15*, 149–159.
- (233) Ummartyotin, S.; Juntaro, J.; Sain, M.; Manuspiya, H. Development of Transparent Bacterial Cellulose Nanocomposite Film as Substrate for Flexible Organic Light Emitting Diode (OLED) Display. *Ind. Crops Prod.* **2012**, *35* (1), 92–97.
- (234) Peng, B. Y.; Wu, C. W.; Shen, Y. K.; Lin, Y. Microfluidic Chip Fabrication Using Hot Embossing and Thermal Bonding of Cop. *Polym. Adv. Technol.* **2010**, *21* (7), 457–466.
- (235) Hansson, J.; Yasuga, H.; Haraldsson, T.; Wijngaart, W. Van Der. Synthetic Microfluidic Paper: High Surface Area and High Porosity Polymer Micropillar Arrays. *Lab Chip* **2016**, *16*, 298–304.
- (236) Hu, L.; Zheng, G.; Yao, J.; Liu, N.; Weil, B.; Eskilsson, M.; Karabulut, E.; Ruan, Z.; Fan, S.; Bloking, J. T.; et al. Transparent and Conductive Paper from Nanocellulose Fibers. *Energy Environ. Sci.* **2013**, *6* (2), 513–518.
- (237) Carlborg, C. F.; Haraldsson, T.; Oberg, K.; Malkoch, M.; Van der Wijngaart, W. Beyond PDMS : Off-Stoichiometry Thiol – Ene (OSTE) Based Soft Lithography for Rapid Prototyping of Microfluidic Devices. *Lab Chip* **2011**, *11*, 3136–3147.

10. Bibliography

- (238) Um, I. C.; Kweon, H. Y.; Park, Y. H.; Hudson, S. Structural Characteristics and Properties of the Regenerated Silk Fibroin Prepared from Formic Acid. *Int. J. Biol. Macromol.* **2001**, *29* (2), 91–97.
- (239) Koh, L. D.; Cheng, Y.; Teng, C. P.; Khin, Y. W.; Loh, X. J.; Tee, S. Y.; Low, M.; Ye, E.; Yu, H. D.; Zhang, Y. W.; et al. Structures, Mechanical Properties and Applications of Silk Fibroin Materials. *Prog. Polym. Sci.* **2015**, *46*, 86–110.
- (240) Yang, Y.; Chen, X.; Ding, F.; Zhang, P.; Liu, J.; Gu, X. Biocompatibility Evaluation of Silk Fibroin with Peripheral Nerve Tissues and Cells in Vitro. *Biomaterials* **2007**, *28* (9), 1643–1652.
- (241) Cao, Y.; Wang, B. Biodegradation of Silk Biomaterials. *Int. J. Mol. Sci.* **2009**, *10* (4), 1514–1524.
- (242) Rockwood, D. N.; Preda, R. C.; Yücel, T.; Wang, X.; Lovett, M. L.; Kaplan, D. L. Materials Fabrication from Bombyx Mori Silk Fibroin. *Nat. Protoc.* **2011**, *6* (10), 1612–1631.
- (243) Yucel, T.; Lovett, M. L.; Kaplan, D. L. Silk-Based Biomaterials for Sustained Drug Delivery. *J. Control. Release* **2014**, *190*, 381–397.
- (244) Gil, E. S.; Mandal, B. B.; Park, S. H.; Marchant, J. K.; Omenetto, F. G.; Kaplan, D. L. Helicoidal Multi-Lamellar Features of RGD-Functionalized Silk Biomaterials for Corneal Tissue Engineering. *Biomaterials* **2010**, *31* (34), 8953–8963.
- (245) Tao, H.; Brenckle, M. A.; Yang, M.; Zhang, J.; Liu, M.; Siebert, S. M.; Averitt, R. D.; Mannoor, M. S.; McAlpine, M. C.; Rogers, J. A.; et al. Silk-Based Conformal, Adhesive, Edible Food Sensors. *Adv. Mater.* **2012**, *24* (8), 1067–1072.
- (246) Capelli, R.; Amsden, J. J.; Generali, G.; Toffanin, S.; Benfenati, V.; Muccini, M.; Kaplan, D. L.; Omenetto, F. G.; Zamboni, R. Integration of Silk Protein in Organic and Light-Emitting Transistors. *Org. Electron. physics, Mater. Appl.* **2011**, *12* (7), 1146–1151.
- (247) Applegate, M. B.; Perotto, G.; Kaplan, D. L.; Omenetto, F. G. Biocompatible Silk Step-Index Optical Waveguides. *Biomed. Opt. Express* **2015**, *6* (11), 4221.
- (248) Cronin-Golomb, M.; Murphy, A. R.; Mondia, J. P.; Kaplan, D. L.; Omenetto, F. G. Optically Induced Birefringence and Holography in Silk. *J. Polym. Sci. Part B Polym. Phys.* **2012**, *50* (4), 257–262.
- (249) Parker, S. T.; Domachuk, P.; Amsden, J.; Bressner, J.; Lewis, J. A.; Kaplan, D. L.; Omenetto, F. C. Biocompatible Silk Printed Optical Waveguides. *Adv. Mater.* **2009**, *21* (23), 2411–2415.
- (250) Wang, Y.; Li, W.; Li, M.; Zhao, S.; De Ferrari, F.; Liscidini, M.; Omenetto, F. G. Biomaterial-Based “Structured Opals” with Programmable Combination of Diffractive Optical Elements and Photonic Bandgap Effects. *Adv. Mater.* **2018**, *1805312*, 1805312.
- (251) Li, A. B.; Kluge, J. A.; Guziewicz, N. A.; Omenetto, F. G.; Kaplan, D. L. Silk-Based Stabilization of Biomacromolecules. *J. Control. Release* **2015**, *219*, 416–430.
- (252) Lawrence, B. D.; Cronin-golomb, M.; Georgakoudi, I.; Kaplan, D. L.; Omenetto, F. G. Bioactive Silk Protein Biomaterial Systems for Optical Devices. *Biomacromolecules* **2008**, *9*, 1214–1220.
- (253) Liu, Y.; Liu, H.; Qian, J.; Deng, J.; Yu, T. Regenerated Silk Fibroin Membrane as Immobilization Matrix for Peroxidase and Fabrication of a Sensor for Hydrogen Peroxide Utilizing Methylene Blue as Electron Shuttle. *Anal. Chim. Acta* **1995**, *316*, 65–72.
- (254) Lu, Q.; Hu, X.; Wang, X.; Kluge, J. A.; Lu, S.; Cebe, P.; Kaplan, D. L. Water-Insoluble Silk Films with Silk I Structure. *Acta Biomater.* **2010**, *6* (4), 1380–1387.
- (255) Lawrence, B. D.; Cronin-Golomb, M.; Georgakoudi, I.; Kaplan, D. L.; Omenetto, F. G. Bioactive Silk Protein Biomaterial Systems for Optical Devices. *Biomacromolecules* **2008**, *9* (4), 1214–1220.
- (256) Park, S.; Kaplan, D. L.; Hu, X.; Shmelev, K.; Sun, L.; Gil, E.; Park, S.; Cebe, P.; Kaplan, D. L. Regulation of Silk Material Structure by Temperature-Controlled Water Vapor Annealing. **2011**, No. March, 1686–1696.
- (257) Li, M.; Tao, W.; Kuga, S.; Nishiyama, Y. Controlling Molecular Conformation of Regenerated

- Wild Silk Fibroin by Aqueous Ethanol Treatment. *Polym. Adv. Technol.* **2003**, *14* (10), 694–698.
- (258) Åkerström, B.; Maghzal, G. J.; Winterbourn, C. C.; Kettle, A. J. The Lipocalin A1-Microglobulin Has Radical Scavenging Activity. *J. Biol. Chem.* **2007**, *282* (43), 31493–31503.
- (259) Riddle, M. C.; Herman, W. H. The Cost of Diabetes Cared an Elephant in the Room. *Diabetes Care* **2018**, *41* (5), 929–932.
- (260) Park, S.; Guo, Y.; Jia, X.; Choe, H. K.; Grena, B.; Kang, J.; Park, J.; Lu, C.; Canales, A.; Chen, R.; et al. One-Step Optogenetics with Multifunctional Flexible Polymer Fibers. *Nat. Neurosci.* **2017**, *20* (4), 612–619.
- (261) Lee, J.; Ozden, I.; Song, Y. K.; Nurmikko, A. V. Transparent Intracortical Microprobe Array for Simultaneous Spatiotemporal Optical Stimulation and Multichannel Electrical Recording. *Nat. Methods* **2015**, *12* (12), 1157–1162.
- (262) Hayashi, K. Optical Chemical Sensor. *IEEJ Trans. Sensors Micromachines* **2015**, *135* (8), 299–304.
- (263) Goicoechea, J.; Zamarreño, C. R.; Matías, I. R.; Arregui, F. J. Optical Fiber PH Sensors Based on Layer-by-Layer Electrostatic Self-Assembled Neutral Red. *Sensors Actuators, B Chem.* **2008**, *132* (1), 305–311.
- (264) Sciacca, B.; François, A.; Hoffmann, P.; Monro, T. M. Multiplexing of Radiative-Surface Plasmon Resonance for the Detection of Gastric Cancer Biomarkers in a Single Optical Fiber. *Sensors Actuators, B Chem.* **2013**, *183*, 454–458.
- (265) Jang, H. S.; Park, K. N.; Kang, C. D.; Kim, J. P.; Sim, S. J.; Lee, K. S. Optical Fiber SPR Biosensor with Sandwich Assay for the Detection of Prostate Specific Antigen. *Opt. Commun.* **2009**, *282* (14), 2827–2830.
- (266) Srivastava, S. K. SPR Based Fiber Optic Sensor for the Detection of Vitellogenin: An Endocrine Disruption Biomarker in Aquatic Environments. *Biosens. J.* **2015**, *04* (01), 1–5.
- (267) Vepari, C.; Kaplan, D. L. Silk as a Biomaterial. *Prog. Polym. Sci.* **2007**, *32* (8–9), 991–1007.
- (268) Wang, X.; Wenk, E.; Matsumoto, A.; Meinel, L.; Li, C.; Kaplan, D. L. Silk Microspheres for Encapsulation and Controlled Release. *J. Control. Release* **2007**, *117*, 360–370.
- (269) Domachuk, P.; Perry, H.; Amsden, J. J.; Kaplan, D. L.; Omenetto, F. G. Bioactive “Self-Sensing” Optical Systems. *Appl. Phys. Lett.* **2009**, *95* (25).
- (270) Tao, H.; Marelli, B.; Yang, M.; An, B.; Onses, M. S.; Rogers, J. A.; Kaplan, D. L.; Omenetto, F. G. Inkjet Printing of Regenerated Silk Fibroin: From Printable Forms to Printable Functions. *Adv. Mater.* **2015**, *27* (29), 4273–4279.
- (271) Association, A. D. Standards of Medical Care in Diabetes. *Diabetes Care* **2014**, *37*, 14–80.
- (272) Barachevsky, V. A.; Butenko, V. G. Photoelectrochromic Organic Systems. *Russ. J. Gen. Chem.* **2018**, *88* (12), 2747–2772.
- (273) Baetens, R.; Jelle, B. P.; Gustavsen, A. Properties, Requirements and Possibilities of Smart Windows for Dynamic Daylight and Solar Energy Control in Buildings: A State-of-the-Art Review. *Sol. Energy Mater. Sol. Cells* **2010**, *94* (2), 87–105.
- (274) Nishi, H.; Namari, T.; Kobatake, S. Photochromic Polymers Bearing Various Diarylethene Chromophores as the Pendant: Synthesis, Optical Properties, and Multicolor Photochromism. *J. Mater. Chem.* **2011**, *21* (43), 17249–17258.
- (275) Monk, P. M. S.; Mortimer, R. J.; Rosseinsky, D. R. *Electrochromism and Electrochromic Devices*; Cambridge University Press: Cambridge, 2007.
- (276) Jarosz, T.; Gebka, K.; Stolarczyk, A.; Domagala, W. Transparent to Black Electrochromism-The “Holy Grail” of Organic Optoelectronics. *Polymers (Basel)*. **2019**, *11* (2), 1–18.
- (277) Zhang, Q.; Yue, S.; Sun, H.; Wang, X.; Hao, X.; An, S. Nondestructive Up-Conversion Readout in

10. Bibliography

- Er/Yb Co-Doped Na_{0.5}Bi_{2.5}Nb₂O₉-Based Optical Storage Materials for Optical Data Storage Device Applications. *J. Mater. Chem. C* **2017**, *5* (15), 3838–3847.
- (278) Baloukas, B.; Lamarre, J. M.; Martinu, L. Electrochromic Interference Filters Fabricated from Dense and Porous Tungsten Oxide Films. *Sol. Energy Mater. Sol. Cells* **2011**, *95* (3), 807–815.
- (279) Zou, W.; González, A.; Jampaiah, D.; Ramanathan, R.; Taha, M.; Walia, S.; Sriram, S.; Bhaskaran, M.; Dominguez-Vera, J. M.; Bansal, V. Skin Color-Specific and Spectrally-Selective Naked-Eye Dosimetry of UVA, B and C Radiations. *Nat. Commun.* **2018**, *9* (1), 1–10.
- (280) Nam, Y. S.; Yoo, I.; Yarimaga, O.; Park, I. S.; Park, D. H.; Song, S.; Kim, J. M.; Lee, C. W. Photochromic Spiropyran-Embedded PDMS for Highly Sensitive and Tunable Optochemical Gas Sensing. *Chem. Commun.* **2014**, *50* (32), 4251–4254.
- (281) Xiang, Q.; Meng, G. F.; Zhao, H. B.; Zhang, Y.; Li, H.; Ma, W. J.; Xu, J. Q. Au Nanoparticle Modified WO₃ Nanorods with Their Enhanced Properties for Photocatalysis and Gas Sensing. *J. Phys. Chem. C* **2010**, *114* (5), 2049–2055.
- (282) Tobaldi, D. M.; Leonardi, S. G.; Pullar, R. C.; Seabra, M. P.; Neri, G.; Labrincha, J. A. Sensing Properties and Photochromism of Ag-TiO₂ Nano-Heterostructures. *J. Mater. Chem. A* **2016**, *4* (24), 9600–9613.
- (283) Massaad, J.; Micheau, J. C.; Coudret, C.; Sanchez, R.; Guirado, G.; Delbaere, S. Gated Photochromism and Acidity Photomodulation of a Diacid Dithienylethene Dye. *Chem. - A Eur. J.* **2012**, *18* (21), 6568–6575.
- (284) Berglund, G. I.; Carlsson, G. H.; Smith, A. T.; Szöke, H.; Henriksen, A.; Hajdu, J. The Catalytic Pathway of Horseradish Peroxidase at High Resolution. *Nature* **2002**, *417* (6887), 463–468.
- (285) Massaad, J.; Micheau, J. C.; Coudret, C.; Serpentine, C. L.; Guirado, G. Proton Catalysis in the Redox Responsivity of a Mini-Sized Photochromic Diarylethene. *Chem. - A Eur. J.* **2013**, *19* (37), 12435–12445.
- (286) P. David Josephy; Eling, T.; Mason, R. P. The Horseradish Peroxidase-Catalyzed Oxidation of 3,5,3',5'-Tetramethylbenzidine. *J. Biol. Chem.* **1982**, *257*, 3669–3675.
- (287) Yamazaki, I. Free Radicals in Biology; Pryor, W. A., Ed.; Academic Press: New York, 1977; pp 183–218.
- (288) Piette, L. H.; Bulovv, G.; Yamazaki, I. Electron Paramagnetic Resonance Studies of the Chlorpromazine Free Radical Formed during Enzymic Oxidation by Peroxidase-Hydrogen Peroxide. *Biochim. Biophys. Acta* **1964**, *88*, 120–129.
- (289) Reuillard, B.; Gentil, S.; Carrière, M.; Le Goff, A.; Cosnier, S. Biomimetic versus Enzymatic High-Potential Electrocatalytic Reduction of Hydrogen Peroxide on a Functionalized Carbon Nanotube Electrode. *Chem. Sci.* **2015**, *6* (9), 5139–5143.
- (290) Scognamiglio, V.; Arduini, F.; Palleschi, G.; Rea, G. Biosensing Technology for Sustainable Food Safety. *TrAC - Trends Anal. Chem.* **2014**, *62*, 1–10.
- (291) Heiden, M. G. Vander; Cantley, L. C.; Thompson, C. B. Understanding the Warburg Effect: The Metabolic Requirements of Cell Proliferation. *Science* (80-.). **2009**, *324* (5930), 1029–1033.
- (292) DeBerardinis, R. J.; Lum, J. J.; Hatzivassiliou, G.; Thompson, C. B. The Biology of Cancer: Metabolic Reprogramming Fuels Cell Growth and Proliferation. *Cell Metab.* **2008**, *7* (1), 11–20.
- (293) Kim, J.; Campbell, A. S.; de Ávila, B. E. F.; Wang, J. Wearable Biosensors for Healthcare Monitoring. *Nat. Biotechnol.* **2019**, *37* (4), 389–406.
- (294) Chen, L.; Hei, W.; Chen, Y.; Mcdonald, M. W.; Melling, J.; Zhang, J. Biosensors and Bioelectronics Nanostructured Biosensor for Detecting Glucose in Tear by Applying Fluorescence Resonance Energy Transfer Quenching Mechanism. *Biosens. Bioelectron.* **2017**, *91* (October 2016), 393–399.
- (295) Cho, M.; Park, S. Sensors and Actuators B: Chemical Carbon-Dot-Based Ratiometric Fluorescence Glucose Biosensor. *Sensors Actuators B. Chem.* **2019**, *282* (July 2018), 719–729.

- (296) Liu, X.; Huang, D.; Lai, C.; Qin, L.; Zeng, G.; Xu, P.; Li, B. Peroxidase-Like Activity of Smart Nanomaterials and Their Advanced Application in Colorimetric Glucose Biosensors. *2019*, *1900133*, 1–27.
- (297) Lobry, M.; Lahem, D.; Loyez, M.; Debliquy, M.; Chah, K.; David, M.; Caucheteur, C. Non-Enzymatic D-Glucose Plasmonic Optical Fiber Grating Biosensor. *Biosens. Bioelectron.* **2019**, *142* (June), 111506.
- (298) Jiang, B.; Zhou, K.; Wang, C.; Sun, Q.; Yin, G.; Tai, Z.; Wilson, K.; Zhao, J.; Zhang, L. Sensors and Actuators B : Chemical Label-Free Glucose Biosensor Based on Enzymatic Graphene Oxide-Functionalized Tilted Fiber Grating. *Sensors Actuators B. Chem.* **2018**, *254*, 1033–1039.
- (299) Cenis, J. L.; Aznar-Cervantes, S. D.; Lozano-Pérez, A. A.; Rojo, M.; Muñoz, J.; Meseguer-Olmo, L.; Arenas, A. Silkworm Gut Fiber of Bombyx Mori as an Implantable and Biocompatible Light-Diffusing Fiber. *Int. J. Mol. Sci.* **2016**, *17* (7).
- (300) Wang, Y.; Rudym, D. D.; Walsh, A.; Abrahamsen, L.; Kim, H. J.; Kim, H. S.; Kirker-Head, C.; Kaplan, D. L. In Vivo Degradation of Three-Dimensional Silk Fibroin Scaffolds. *Biomaterials* **2008**, *29* (24–25), 3415–3428.
- (301) Tao, H.; Siebert, S. M.; Brenckle, M. A.; Averitt, R. D.; Cronin-Golomb, M.; Kaplan, D. L.; Omenetto, F. G. Gold Nanoparticle-Doped Biocompatible Silk Films as a Path to Implantable Thermo-Electrically Wireless Powering Devices. *Appl. Phys. Lett.* **2010**, *97* (12), 1–4.
- (302) Rockwood, D. N.; Preda, R. C.; Yücel, T.; Wang, X.; Lovett, M. L.; Kaplan, D. L. Materials Fabrication from Bombyx Mori Silk Fibroin. *Nat. Protoc.* **2011**, *6* (10), 1612–1631.
- (303) Chu, R.; Guan, C.; Yang, J.; Zhu, Z.; Li, P.; Shi, J.; Tian, P.; Yuan, L.; Brambilla, G. High Extinction Ratio D-Shaped Fiber Polarizers Coated by a Double Graphene/PMMA Stack. *Opt. Express* **2017**, *25* (12), 13278.